Study on Biologically Active Compounds from Brazilian Plant *Tabebuia avellanedae*

Li Zhang

September, 2014

DISSERTATION

Study on Biologically Active Compounds from Brazilian Plant *Tabebuia avellanedae*

Graduate School of
Natural Science and Technology
KANAZAWA UNIVERSITY

Major Subject: Life Sciences
Laboratory of Molecular Pharmacognosy
Course: Bioactive Substances

School Registration No.: 1123032333
Name: Li Zhang
Chief Advisor: Yohei Sasaki

Graduate School of Natural Science and Technology

Kanazawa University

To Whom It May Concern

We herely certify that this is a typical copy of the original doctoral thesis of Miss Li Zhang.

_____

Supervisor professor

Prof. Dr. Yohei Sasaki

The Official Seal of

The Graduate School of

Natural Science ＆Technology,

Kanazawa University

_____

KANOH Shigeyoshi

Dean of the Graduate School of

Natural Science and Technology,

Kanazawa University

ACKNOWLEDGEMENT

I wish to express my gratitude to Professor Yohei Sasaki. I deeply appreciated the warmly welcome and the encouragement I have received during my study.

I wish to express my gratitude to Professor Tomihisa Ohta for providing excellent, scientific and personal advice. Thanks for all that he has taught me. Thanks for his valuable comments which helped shape this work.

I wish to express my gratitude to Professor Takeshi Tadano for providing excellent, scientific and personal advice. He always supported me, always had time for questions and discussions.

Very special thanks to Dr. Takanori Tatsuno and Dr. Isao Hasegawa and other staffs and students in this laboratory. I couldn’t have done this work without a lot of support from them, both intellectually and emotionally.

Finally, I would like to thank my family, for their love, understanding, support and encouragement to reach my dreams. They deserve my deepest thanks.

CONTENTS

ABBREVIATIONS

1D	one dimensional
2D	two dimensional
Api	apiose
BAX	b-cell lymphoma 2-associated X
BCG	bacille de calmette et guérin
BCL-2	b-cell lymphoma 2
BuOH	butanol
br.d.	broad doublet
C	carbon
CC	column chromatography
$CDCl_3$	chloroform
CDI	cyclin-dependent kinase inhibitor
CDK	cyclin-dependent kinases
cont.	control
COSY	correlated spectroscopy
COX-2	cyclooxygenase-2
d	doublet
dd	double doublet
DMEM	dulbecco's modified eagle's medium
DMF	dimethylformamide
DMSO	dimethyl sulfoxide
DNA	deoxyribonucleic acid
DOX	doxorubicin
ELISA	enzyme-linked immune sorbent assay
ERK	extracellular signal-regulated kinase

EtOAc	ethyl acetate
FABMS	fast atom bombardment mass spectrometry
FACS	fluorescence assisted cell sorting
FBS	fetal bovine serum
Fr.	fraction
Fig.	frigure
g	gram
Glc	glucose
h.	hour
H	proton
HMBC	heteronuclear multiple bond connectivity
HMQC	heteronuclear multiple quantum coherence
HPLC	high performance liquid chromatography
HREIMS	high resolution electron ionization mass spectrometry
HRFABMS	high resolution fast atom bombardment mass spectrometry
Hz	hertz
IC 50	half maximal (50%) inhibitory concentration
iNOS	inducible nitric oxide synthase
IR	infrared spectroscopy
J	spin-spin coupling constant (Hz)
JAK	janus kinase
LPS	lipopolysaccharide
m	multiplet
MeOH	methanol
min.	minute
MTT	3-(4,5-dimethyl-2-thiazolyl)-2,5-diphenyl-tetrazolium bromide
m/z	mass to charge ratio
NBT	nitro blue rereazolium chloride

NF-κB	nuclear factor-kappa B
NMR	nuclear magnetic resonance
n	number
NO	nitric oxide
NOE	nuclear overhauser effect
ODS	octa decyl silyl
p	p value or calculated probabilit
P53	phosphoprotein p53
PBS	phosphate buffered saline
PGE2	prostaglandin E2
PGs	prostaglandins
ppm	parts per million
PI3K	1,2phosphatidylinositol 3-knases
PVDF	polyvinylidene fluoride
q	quartet
RNA	ribonucleic acid
ROS	reactive oxygen species
RT-PCR	reverse transcription polymerase chain reaction
s	singlet
S.D.	standard deviation
STAR	sigal transducer and activator of transcription
SDS-PAGE	sodium dodecyl sulfate-polyaclylamidegel electrophoresis,
SiO_2	silica gel
SPF	specific pathogen free
t	triplet
TLC	thin layer chromatography
UV	ultraviolet spectroscopy
RPMI	roswell park memorial institute medium

TNF-α	tumor necrosis factor-α
WBC	white blood cell
[α]	specific rotatory power
δ	chemical sift (ppm)
λ	wave length (nm)
℃	degrees celsius

1. INTRODUCTION

Tabebuia avellanedae Lorentz ex Griseb (**Fig. 1a**), which belongs to the family *Bignoniaceae*, is a popular tree distributed throughout the tropical rain forests of Central and South America. *T. avellaneda* is called “divine tree” by indigenous peoples of South America, because it is considered to be one of the most effective, economical and versatile remedies against a multitude of acute and chronic diseases for over 1000 years.[1-4] Its inner bark (**Fig. 1b**)is commonly known as “taheebo”, “lapacho”,“pau d’arco”, and “ipe roxo”, and it is widely used in local and traditional phytomedicine, usually ingested as a decoction to treat numerous conditions like bacterial and fungal infections, fever, syphilis, malaria, trypanosomiasis, aswell as stomach and bladder disorders.[4,5] As early as 1873, biomedical uses of Red Lapacho (“Pau D’Arco”) were reported.[5] In 1967 after reports in the Brazilian press it came to the light of clinicians (and the public in general).[6,7] Until now, a variety of studies have been done on *T. avellanedae* by different research teams around the world.

a. **b.**

Figure 1 *Tabebuia avellanedae* (**a.**) and the inner bark of it (**b.**)
(Pictures were from http://orienteocidente.files.wordpress.com,
http://www.superfoods-for-superhealth.com)

1.1. Pharmacodynamic and Chemical studies of *T. avellanedae*

T. avellanedae has been used for various ethnopharmacological purposes. Colombians use the bark infusion as stimulant of central nervous system [7]; Bahamians commonly use the bark decoction to prepare an energizing tonic for strength [7], and Brazilians use this plant to treat malaria, cancer, fever, stomach disorders, bacterial and fungal infections and to relief of a variety of mental and emotional states such as anxiety, poor memory, irritability and depression [1,5].

Recent pharmacological study indicated that constituents of the bark of this plant exert a number of activities, such as anti-inflammation [8], anti-infectious[9], anti-cancer [10,11], antinociceptive, anti-emetogenic [12] , anti-microbial [13,14], anti-fungal [15], anti-trypanosomal [2], anti-gastric lesions [3], anti-depressant [16,17], antiulcerogenic [3,18] and anti-angiogenic[19].

Following its popular use, the chemistry of this plant was extensively studied, and a variety of constituents have been isolated, such as furanonaphthoquinones, naphtoquinones, quinones, lignans, benzoic acid, cyclopentene dialdehyde, flavonoids, iridoids, phenolic glycosides, saponins, and coumarins.[2,11,12,14,20-24]

1.2. Anti-cancer research progress of *T. avellanedae*

T. avellanedae is utilized as a folk remedy for the treatment of cancer [1,25,26], and its anticancer activity has also been evaluated and confirmed in laboratories [12,13,22,27].

The chemistry of this plant was extensively studied and a variety of constituents have been isolated, anticancer properties have been related mainly to the presence of naphtoquinones, which also constitute the most prevalent active chemical group in the plant. Among the naphtoquinons obtained from the bark of *T. avellanedae,* lapachol and *β*-lapachone attracted the most interest of the researchers in the early

experimental studies [5]. It was reported that lapachol have potent anti-proliferative properties against various tumor cell lines [22,28-30]. However, the phase I clinical trial had to be interrupted prematurely due to the prolonged prothrombin time observed with doses required for antitumoural activity, which was associated to nausea and vomiting [31]. *β*-lapachone was proved to have a strong cytotoxic activity *in vitro* against several human and murine cell lines through arresting cell cycle progression and inducing apoptosis associated with the down-regulation of the anti-apoptotic B-cell lymphoma 2 (BCL-2) and b-cell lymphoma X (BCL-X), up-regulation of the pro-apoptotic B-cell lymphoma 2-associated X (BAX) expression, inhibition of cyclooxygenase-2 (COX-2) and human telomerase reverse transcriptase (hTERT) expression, and proteolytic activation of caspase-3 and -9 [32-35]. However, in the following studies, the increased rate of 42% in the duration of survival was observed in tumour-bearers treated with the dose of 1 mg/kg while toxicity was evident at 5mg/g with the death of 33% of treated tumour -bearers in the first 24 h after administration [36]. These negative results reduced the interest on further investigations with these compounds.

The latest studies to find more anticancer compounds from *T. avellanedae* led to the discovery of several furanonaphthoquinones based on the naphtho[2,3-b]furan-4,9-dione skeltone [11]. But the following studies mainly focused on the synthesis based on those active furanonaphthoquinones and simply tested their antiproliferative effects [20,37]. Further studies should be carried out to find more active furanonaphthoquinones as potential candidates of anticancer agents. In addition, molecular targets of efficacy, mechanisms of action of them also remain to be identified.

1.3. Anti-inflammatory research progress of *T. avellanedae*

The inner bark of *T. avellanedae* was one of the primary medicines used by the Callawaya tribe for over 1000 years. These people used it externally as a poultice or concentrated tea for treating a variety of skin inflammatory diseases including eczema, psoriasis, and fungal infections, and even skin cancers [4,22,38-41]. Despite its wide-range of pharmacological actions, relatively few studies have investigated the anti-inflammatory activity of *T. avellanedae* inner bark compounds and their effect and mechanism in treating inflammatory diseases. It's reported that prolonged intaking of *T. avellanedae* in arthritic patients reduced arthritis-induced pain and edema formation, and restored the morphological abnormality of arthritic joints, and the water extract of *T. avellanedae* may negatively modulate Prostaglandin E2 (PGE2) mediated inflammatory responses, as it clearly blocked the production of PGE2 and nitric oxide (NO), the expression of COX-II and inducible nitric oxide synthase (iNOS), and arachidonic acid-induced ear edema via blocking the phosphorylation of extracellular signal-regulated kinase (ERK) [8]. Further study proved that iridoids and phenylethanoid glycoside from the water extract of *T. avellanedae*, inhibited NO production in lipopolysaccharide (LPS) activated macrophage-like J774.1 cells [39], and cyclopentene dialdehydes from *T. impetiginosa* were also reported to have anti-inflammatory activities in the nitro blue teteazolium chloride (NBT)-activated human granular white blood cells (WBC) [42].

1.4. Aim of the study

The aim of this study was to discover more bioactive natural product skeletons from the inner bark of *T. avellanedae* as leads to novel agents especially for the treatment of cancer and inflammatory in the future.

2. RESULTS AND DISCUSSION

2.1. Compounds isolated from *T. avellanedae*

In this research, water extract and methanol extract of inner bark of *T. avellanedae* were separated, and 22 new compounds together with 10 known compounds were isolated and identified (**Scheme 1, Scheme 2, Scheme3**). The structures of **1-32** were in **Figure 2**. The 1D NMR data were listed in Table **1** to **13**. The 2D NMR correlations were shown in **Figure 1** to **31**.

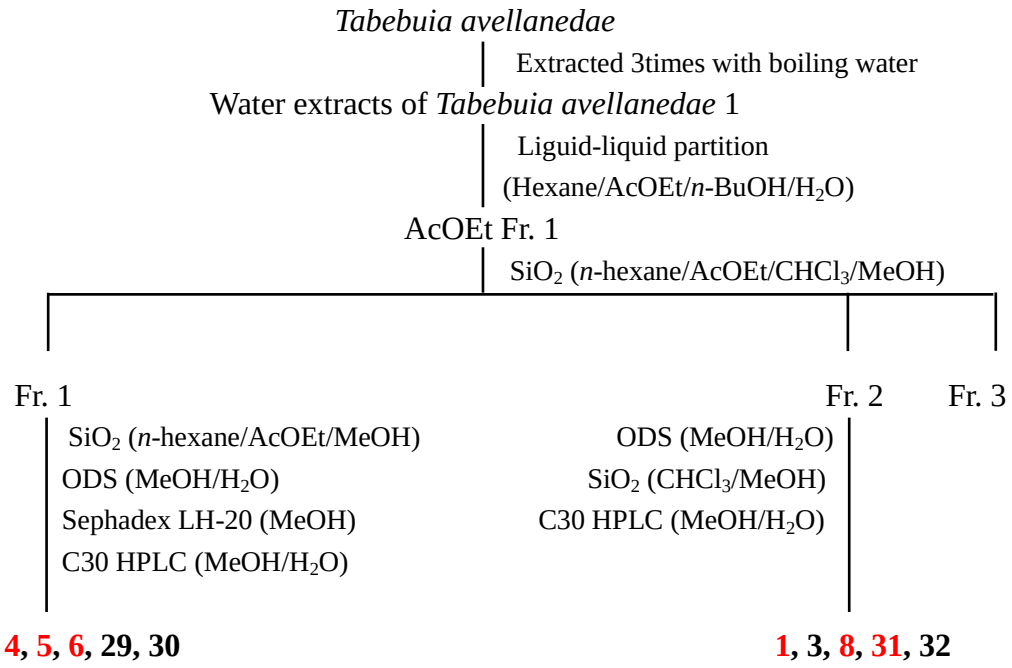

Scheme 1 Flowchart 1 of fractionation and isolation of compounds.
(■: New compounds ■: known compounds)

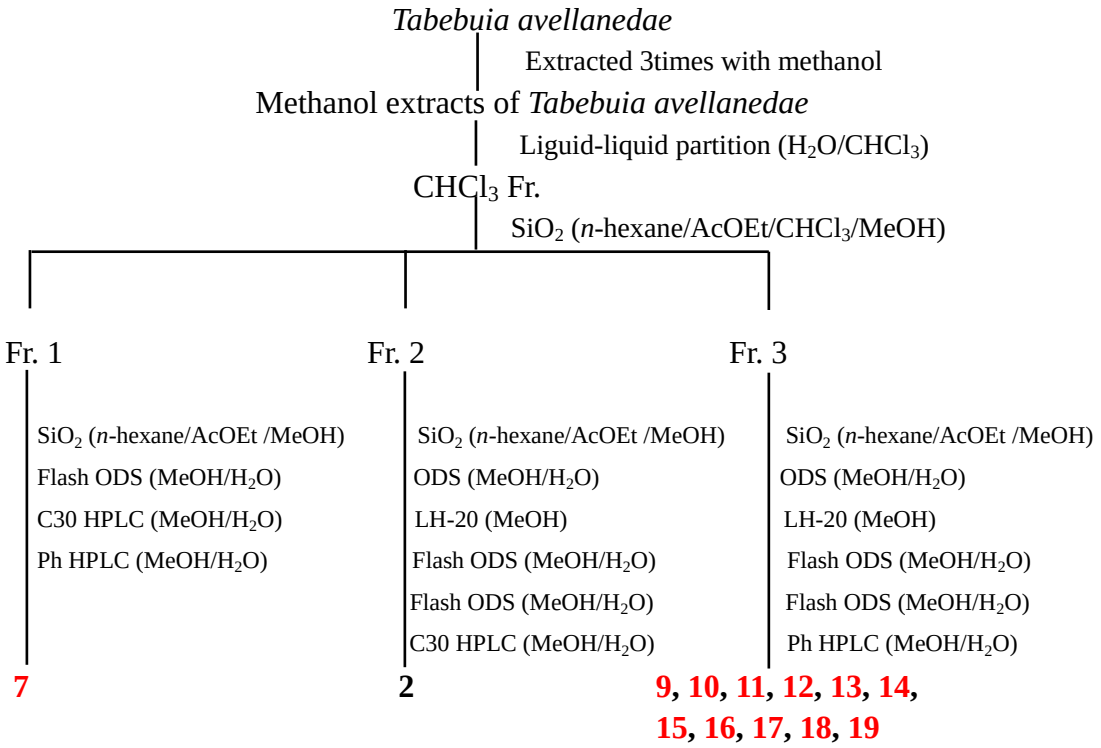

Scheme 2 Flowchart 2 of fractionation and isolation of compounds.
(■: New compounds ■: known compounds)

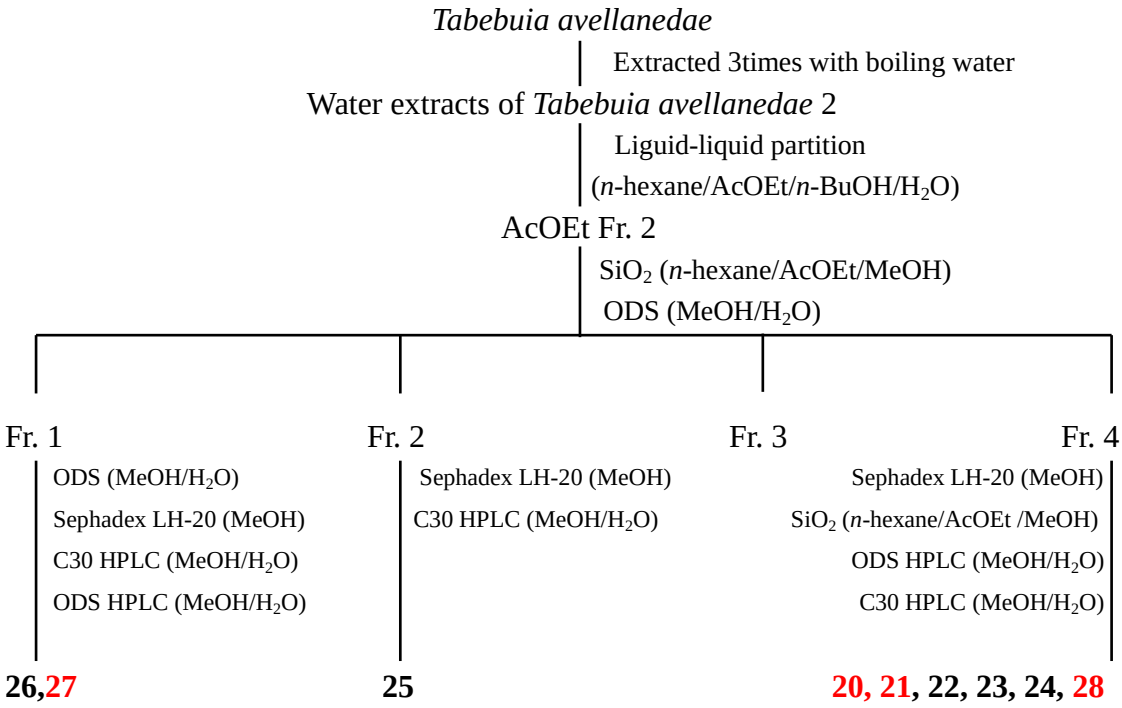

Scheme 3 Flowchart 3 of fractionation and isolation of compounds.
(■: New compounds ■: known compounds)

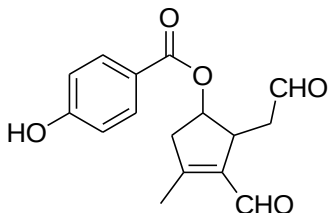
O
O
CHO
HO
CHO

1

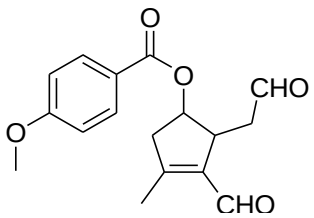
O
O
CHO
O
CHO

2

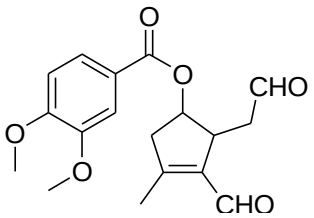
O
O
CHO
O
O
CHO

3

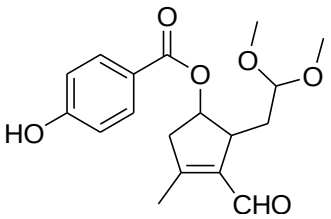
O
O
O
O
HO
CHO

4

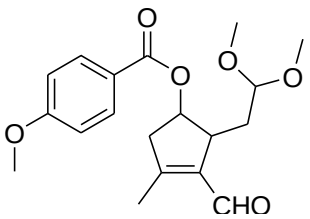
O
O
O
O
O
CHO

5

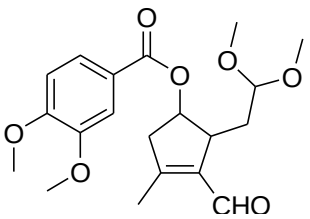
O
O
O
O
O
O
CHO

6

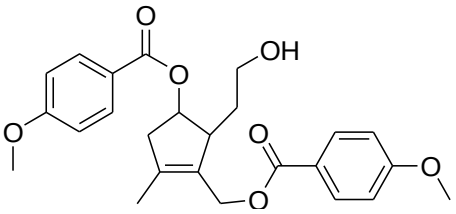
O
O
OH
O
O
O
O

7

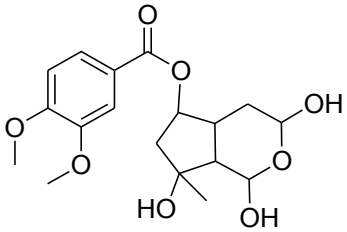
O
O
O
O
OH
O
HO
OH

8

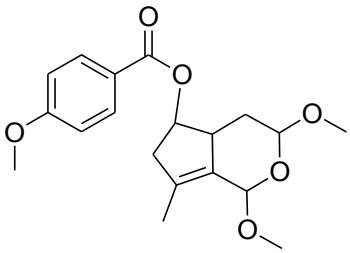
O
O
O
O
O
O

9

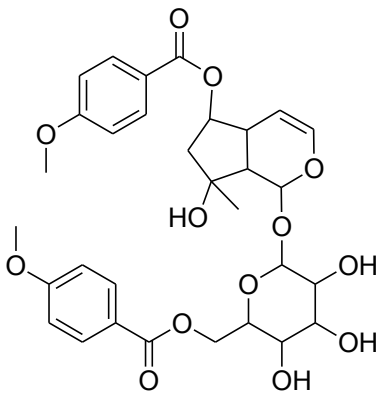

10

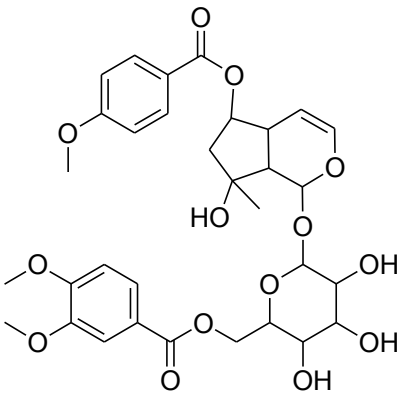

11

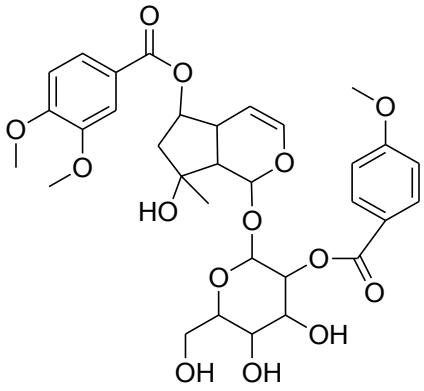

12

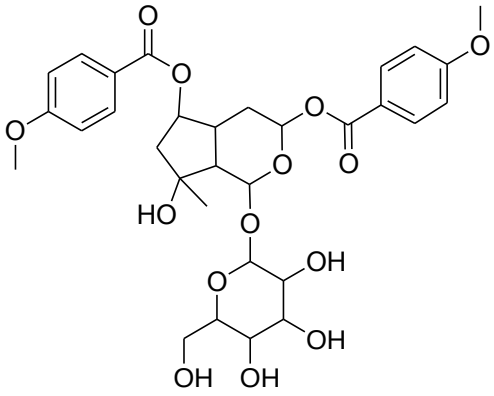

13

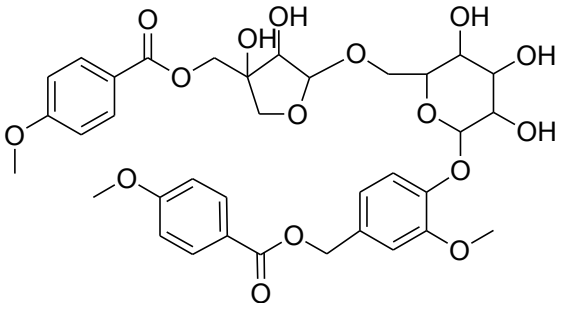

14

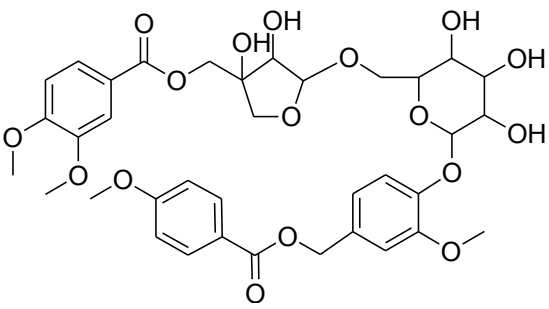

15

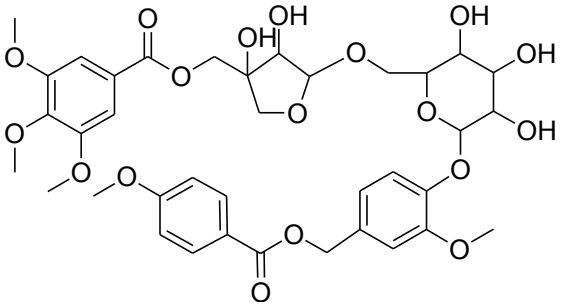

16

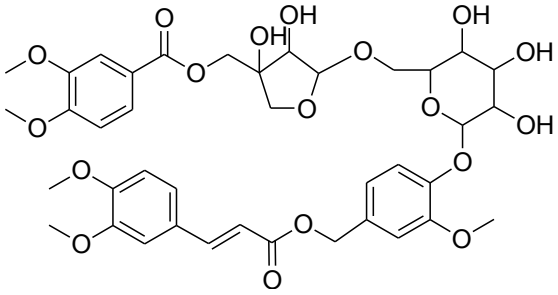

17

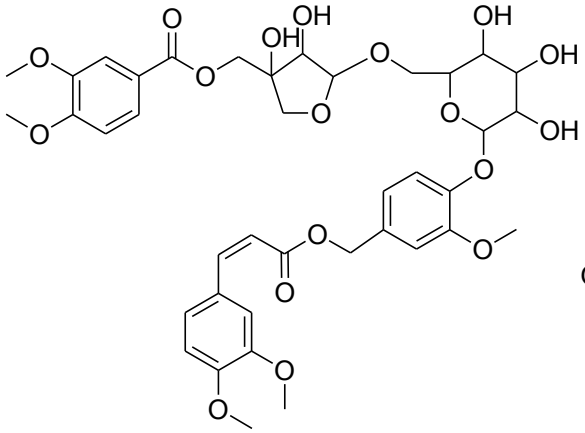

18

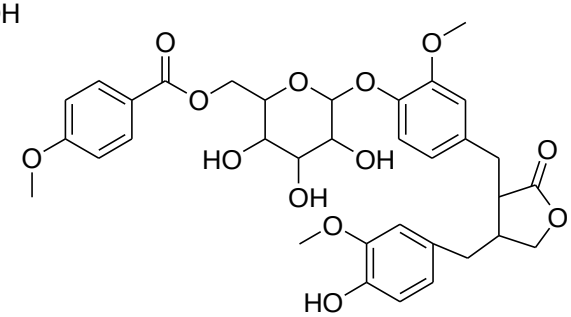

19

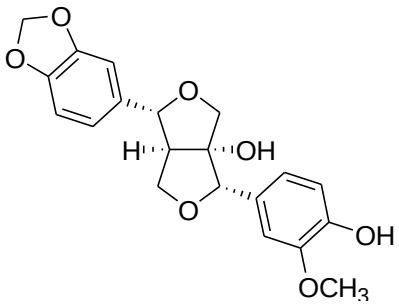

20

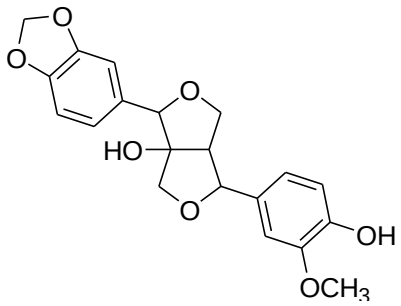

21

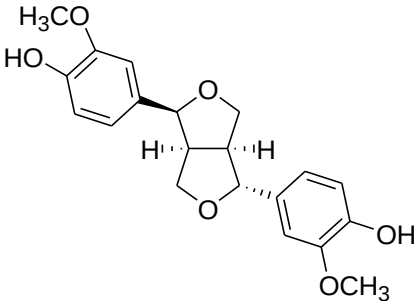

22

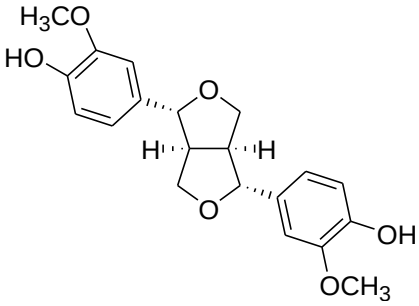

23

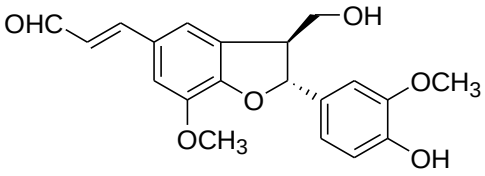

24

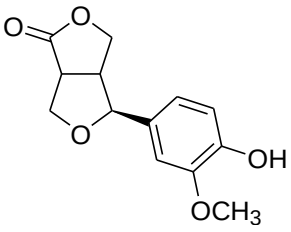

25

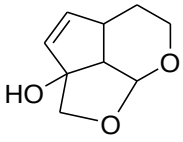

26

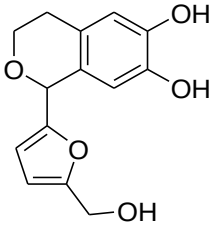

27

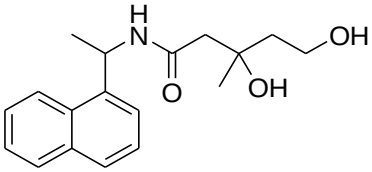

28

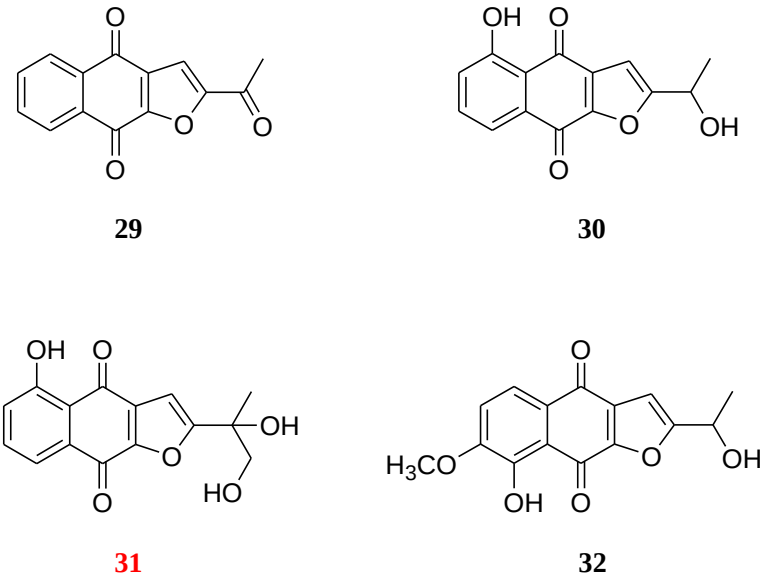

29 **30**

31 **32**

Figure 2 Isolated compounds from *Tabebuia avellanedae*.

(■: New compounds ■: known compounds)

2.2. Identification of the new compounds

2.2.1. 4-Hydroxybenzoic acid 3-formyl-4-methyl-2-(2-oxoethyl)cyclopent-3-enyl ester (**1**)

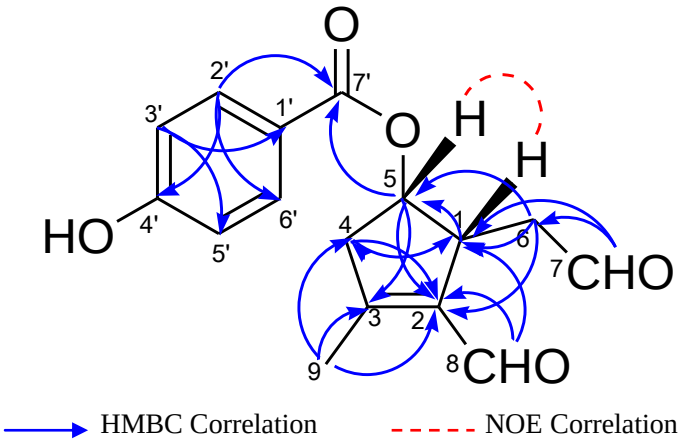

Figure 3 Key HMBC, NOE correlations of **1**

Compound **1** was obtained as yellowish solid. Its molecular formula was determined as $C_{16}H_{16}O_5$ by HRFABMS *m/z* 289.1062$[M+H]^+$ (calcd. 289.1062 for $C_{16}H_{17}O_5$). The ^{1}H NMR spectrum of two doublets δ_H 6.83 (2H, d, J = 8.9) and 7.89 (2H, d, J = 8.9) and HMBC correlations from δ_H 6.83 (H-3' and H-5') to δ_C 122.4 (C-1') and 115.2 (C-5', C-3'), from δ_H 7.89 (H-2' and H-6') to δ_C 160.0 (C-4') and 165.9 (C-7'), suggested the presence of a *p*-hydroxybenzoate carboxyl group. The ^{1}H and ^{13}C NMR spectra and HMQC correlation indicated two aldehyde (δ_H 9.97, δ_C 187.0 and δ_H 9.77, δ_C 200.0), in addition, the HMBC correlation from methyl proton δ_H 2.20 (H-9) to δ_C 45.9 (C-4), δ_C 137.3 (C-2) and δ_C 160.7 (C-3), from aldehyde proton δ_H 9.97 (H-8) to δ_C 45.9 (C-1) and δ_C 137.3 (C-2), and δ_H 3.54 (H-1) to δ_C 77.1 (C-5) and δ_C 45.9 (C-4) suggested the presence of 3-methyl-2-cyclopentene-2-carbaldehyde group with an oxidized C-5. Furthermore, HMBC correlations were observed from the other aldehyde proton δ_H 9.77 (H-7) to δ_C 44.9 (C-6) and δ_C 45.9 (C-1), and from δ_H 2.67, 2.86 (H-6a, H-6b)

to δ_C 45.9 (C-1), δ_C 137.3 (C-2) and δ_C 77.1 (C-5), indicated the presence of acetaldehyde located at C-1. Moreover, the HMBC correlation from δ_H 5.14 (H-5) to δ_C 165.9 (C-7') implied that C-5 and C-7' were connected through an oxy gen atom. Strong correlations between δ_H 5.14 (H-5) and δ_H 3.23 (H-4a), δ_H 5.14 (H-5) and δ_H 3.54 (H-1) and δ_H 5.14 (H-5), and δ_H 3.54 (H-1) and δ_H 2.86 (H-6 a) were observed in the NOE spectrum. Thus, compound **1** was determined as s hown in **Fig. 3.**

2.2.2. 4-Hydroxybenzoic acid 2-(2,2-dimethoxyethyl)-3-formyl-4-methylcyclopent-3 -enyl ester (**4**)

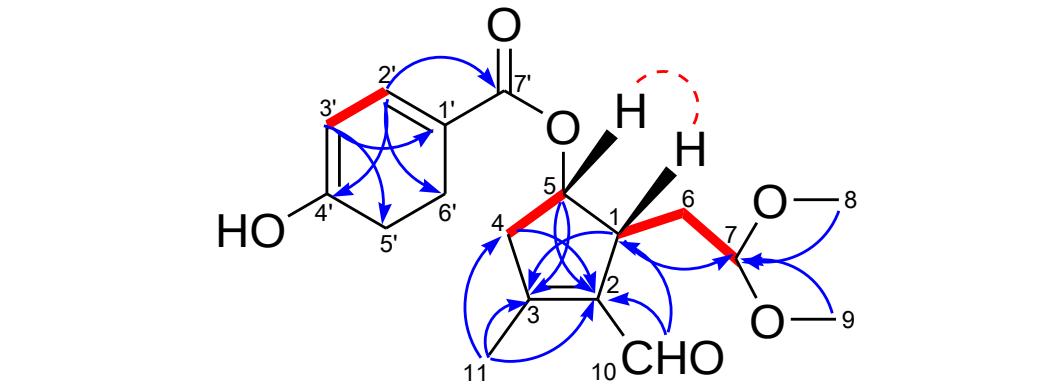

Figure 4 Key HMBC, ^{1}H-^{1}H COSY and NOE correlations of **4**

Compound **4** was obtained as brown solid. Its molecular formula was determined as $C_{18}H_{22}O_6$ by HREIMS *m/z* 334.1441 $[M]^+$ (calcd. 334.1441 for $C_{18}H_{22}O_6$). The characteristics of NMR spectra of compound **4** were very similar to those of compound **1**, indicating that they are based on the same carbon skeleton. However, compound **2** exhibited only one aldehyde signal and two more methoxy proton [δ_H 3.30 (3H, s,) and δ_H 3.31 (3H, s,)]. The HMBC correlations from the two methoxy protons δ_H 3.31 (H-8) and δ_H 3.30 (H-9) to δ_C 102.8 (C-7), from δ_H 3.25 (H-1) to δ_C 102.8 (C-7), and ^{1}H-^{1}H COSY correlations between δ_H 4.56 (H-7) and 1.56 (H-6a), δ_H 2.02 (H-6b) and 3.25 (H-1), indicated the presence of a 1,1-dimethoxyethane attached to C-1.Thus, compound

4 was determined as shown in **Fig. 4.**

2.2.3. 4-Methoxybenzoic acid 2-(2,2-dimethoxyethyl)-3-formyl-4-methylcyclopent-3-enyl ester (**5**)

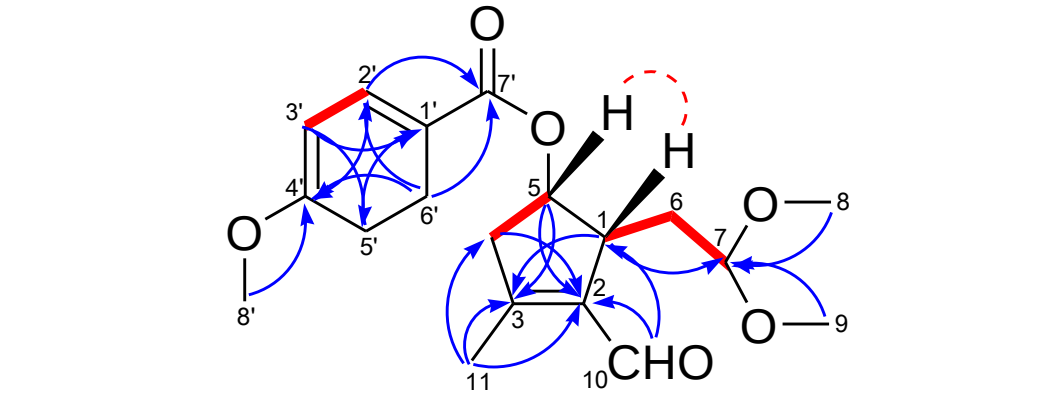

Figure 5 Key HMBC, ^{1}H-^{1}H COSY and NOE correlation of **5**

Compound **5** was obtained as a brown solid. Its molecular formula was determined as $C_{19}H_{24}O_6$ by HRFABMS *m/z* 371.1451 $[M+Na]^+$ (calcd. 371.1451 for $C_{19}H_{24}O_6$ Na). The characteristics of NMR spectra of compound **6** are very similar to those of compound **4**, indicating that they are based on the same carbon skeleton. However, compound **5** has one more singlet proton δ_H 3.83 (H-8'). In addition, the HMBC correlation was observed from δ_H 3.83 (H-8') to 163.4 (C-4'). Thus, compound **5** was determined as shown in **Fig. 5.**

2.2.4. 3,4-Dimethoxybenzoic acid 2-(2,2-dimethoxyethyl)-3-formyl-4-methyl-cyclop ent-3-enyl ester (**6**)

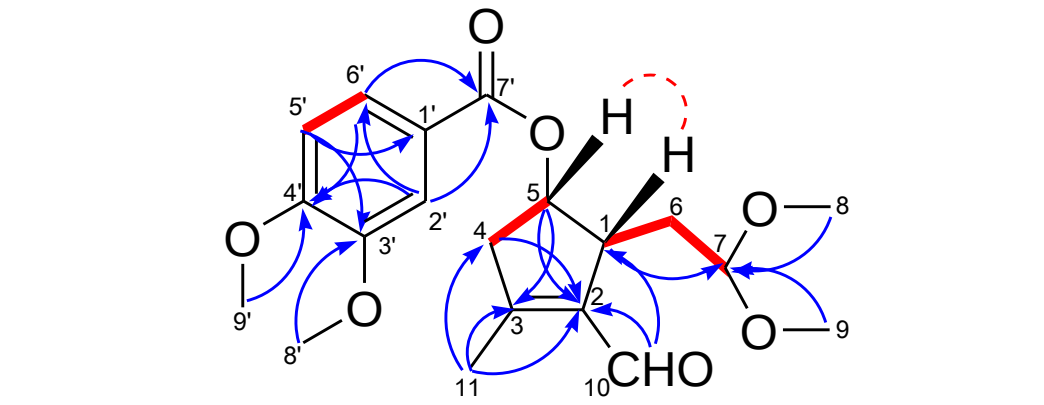

Figure 6 Key HMBC, ^{1}H-^{1}H COSY and NOE correlations of **6**

Compound **6** was obtained as a brown solid. Its molecular formula was determined as $C_{20}H_{26}O_7$ by HRFABMS *m/z* 379.1736$[M+H]^+$ (calcd. 379.1736 for $C_{20}H_{27}O_7$). The characteristics of NMR spectra of compound **6** are very similar to those of compound **4**, indicating that they are based on the same carbon skeleton. However, 1D spectra and HMQC correlations revealed the presence of one ABX system aromatic ring [δ_H 7.47 (d, J = 1.7), 6.84 (d, J = 8.5), 7.59 (dd, J = 1.7, 8.5)] instead of AABB system aromatic ring. Furthermore, compound **6** has two singlet protons δ_H 3.90 (H-8'), δ_H 3.91 (H-9'), in addition, HMBC correlations were observed from H-8' to 148.6 (C-3') and H-9' to 153.0 (C-4'). Thus, compound **6** was determined as shown in **Fig. 6.**

Table 1 ^{1}H-NMR Spectral Data of Compound **1**, **4**, **5**, **6** in $CDCl_3$

P.	^{1}H-NMR [δ_H (multi,J in Hz)]			
	1	**4**	**5**	**6**
1	3.54 (dd,6.5)	3.25 (d,8.9)	3.26 (d,8.6)	3.28 (d,8.6)
2				
3				
4α	3.23 (dd,6.9,20.3)	3.13 (dd,6.2,19.9)	3.14 (dd,6.2,19.9)	3.14 (dd,6.2,19.9)
4β	2.67 (m)	2.59 (d,19.9)	2.59 (d,19.9)	2.59 (d,19.9)
5	5.14 (dt,1.7,6.9)	5.32 (d,6.2)	5.33 (d,6.2)	5.32 (d,6.2)
6α	2.86 (ddd,1.4,4.8,16.8)	1.56 (m)	1.56 (m)	1.56 (m)
6β	2.67 (m)	2.02 (m)	2.03 (m)	2.05 (m)
7	9.77 (t,1.5)	4.56 (dd,4.0,6.5)	4.53 (dd,4.0,6.5)	4.51 (dd,4.0,6.5)
8	9.97 (s)	3.31 (s)	3.31 (s)	3.31 (s)
9	2.20 (s)	3.30 (s)	3.30 (s)	3.30 (s)
10		10.00 (s)	10.00 (s)	10.00 (s)
11		2.18 (s)	2.18 (s)	2.19 (s)
1’				
2’	7.89 (d,8.9)	7.89 (d,8.9)	7.92 (d,8.9)	7.47 (d,1.7)
3’	6.83 (d,8.9)	6.83 (d,8.9)	6.88 (d,8.9)	
4’				
5’	6.83d (8.9)	6.83 (d,8.9)	6.88 (d,8.9)	6.84 (d,8.5)
6’	7.89d (8.9)	7.89 (d,8.9)	7.92 (d,8.9)	7.59 (dd,1.7,8.5)
7’				
8’			3.83 (s)	3.90 (s)
9’				3.91 (s)

Table 2 ^{13}C-NMR Spectral Data of Compound **1**, **4**, **5**, **6** in $CDCl_3$

P.	^{13}C-NMR [δ_C]			
	1	**4**	**5**	**6**
1	45.9	47.2	47.3	47.2
2	137.3	138.9	138.9	138.9
3	160.7	159.5	159.3	159.3
4α	45.9	46.0	46.0	46.0
4β				
5	77.1	77.0	77.0	77.1
6α	44.9	33.5	33.6	33.6
6β				
7	200.0	102.8	102.8	102.8
8	187.0	53.4	53.3	53.3
9	14.4	51.9	52.0	52.0
10		187.5	187.5	187.5
11		14.4	14.4	14.2
1’	122.4	122.6	122.6	122.6
2’	132.0	161.9	131.6	111.9
3’	115.2	115.1	113.6	148.6
4’	160.0	159.9	163.4	153.0
5’	115.2	115.1	113.6	110.1
6’	132.0	131.9	131.6	123.6
7’	165.9	165.8	122.6	166.0
8’			55.4	56.0
9’				56.0

2.2.5. Compound **7**

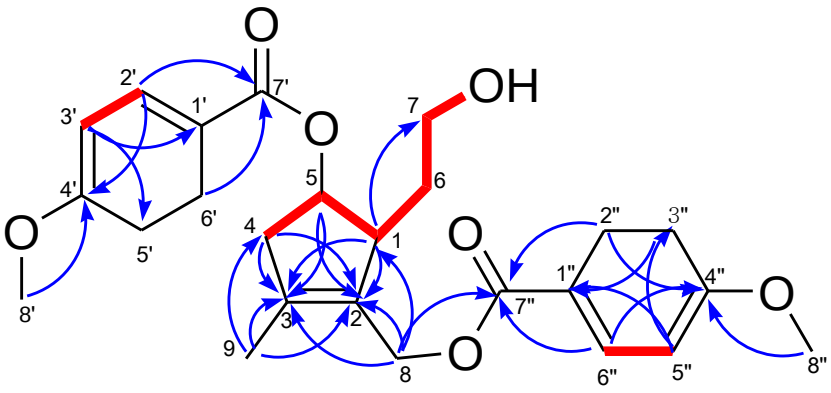

Figure 7 Key HMBC and ^{1}H-^{1}H COSY correlations of **7**

Compound **7** was obtained as a brown solid. Its molecular formula was determined as $C_{25}H_{28}O_7$ by HRFABMS *m/z* 463.1763 $[M+Na]^+$ (calcd. 463.1733 for $C_{25}H_{42}O_{17}Na$). ^{1}H-NMR and^{13}C-NMR spectra showed the presence of two AA'BB' system aromatic rings [δ_H 6.90 (2H, dt, 8.9), 6.93 (2H, dt, 8.9), 7.86 (2H, dt, 8.9), 7.91 (2H, dt, 8.9), and δ_C 114.7, 114.8, 123.6, 123.9, 132.6, 167.8, 167.9]. Furthermore, HMBC correlations from 3.34 (H-8' and H-8") to 114.8 (C-5') and 114.9 (C-5"), from δ_H 7.91 (H-2' and H-6') to 165.2 (C-4') and 167.8 (C-7'), from 7.86 (H-2" and H-6") to 165.1 (C-4") and 167.9 (C-7") indicated the presence of two *p*-hydroxybenzoate carboxyl groups. In addition, the characteristics of NMR spectra of compound **6** are very similar to those of 2-formyl-5-(3',4'-dimethoxybenzoyloxy)-3-methyl-2-cyclopentene-1-acetaldehyde [42] suggested the existence of a cyclopentenyl group. ^{1}H-^{1}H COSY correlations between H-4 and H-5, and HMBC correlations from δ_H 2.93 (H-1), 2.40, 2.93 (H-4), 5.26 (H-5) to δ_C 138.4 (C-2) and δ_C 132.7 (C-3) were observed respectively, confirming the

Table 3 ^{1}H-NMR and ^{13}C-NMR Spectral Data of Compound **7** in CD_3OD

P.	1D-NMR of **7**	
	δ_H (multi,*J* in Hz)	δ_C
1	2.93(overlap)	52.2
2		138.4
3		132.7
4*α*	2.40(d,17.8)	44.6
4*β*	2.93(overlap)	
5	5.26(dt,6.2)	79.5
6*α*	1.58(m)	34.8
6*β*	1.97(m)	
7	3.70(m)	61.3
8*α*	4.85(d,12.3)	60.2
8*β*	4.99(d,12.3)	
9	1.36(s)	14.1
1’		123.6
2’	7.91(dt,8.9)	132.6
3’	6.93(dt,8.9)	114.8
4’		165.2
5’	6.93(dt,8.9)	114.8
6’	7.91(dt,8.9)	132.6
7’		167.8
8’	3.34(s)	56.0
1”		123.9
2”	7.86(dt,8.9)	132.6
3”	6.90(dt,8.9)	114.7
4”		165.1
5”	6.90(dt,8.9)	114.9
6”	7.86(dt,8.9)	132.6
7”		167.9
8”	3.34(s)	56.0

existence of the cyclopentene skeleton. Furthermore, HMBC correlations from δ_H 1.36 (H-9) to δ_C 138.4 (C-2), 132.7 (C-3), 44.6 (C-4), and from δ_H 4.85, 4.99 (H-8) to δ_C 52.2 (C-1), 138.4 (C-2), 132.7 (C-3) revealed the existence of a methyl group attached to C-2 and a methylene group attached to C-3. In addition, the HMBC correlations from δ_H 5.26 (H-5) to δ_C 167.8 (C-7’) and from δ_H 4.85, 4.99 (H-8) to δ_C 167.9 (C-7”) indicated the locations of the two *p*-hydroxybenzoate carboxyl groups. The mass spectrum suggested the presence of one hydroxy group. In addition, a down filed shifted carbon signal 61.3 (C-7) was observed. Thus, compound **7** was determined as shown in **Fig. 7.**

2.2.6. 3,4-Dimethoxy-benzoic acid 1,3,7-trihydroxy-7-methyl-octahydro-cyclopent a[c]pyran-5-yl ester (**8**)

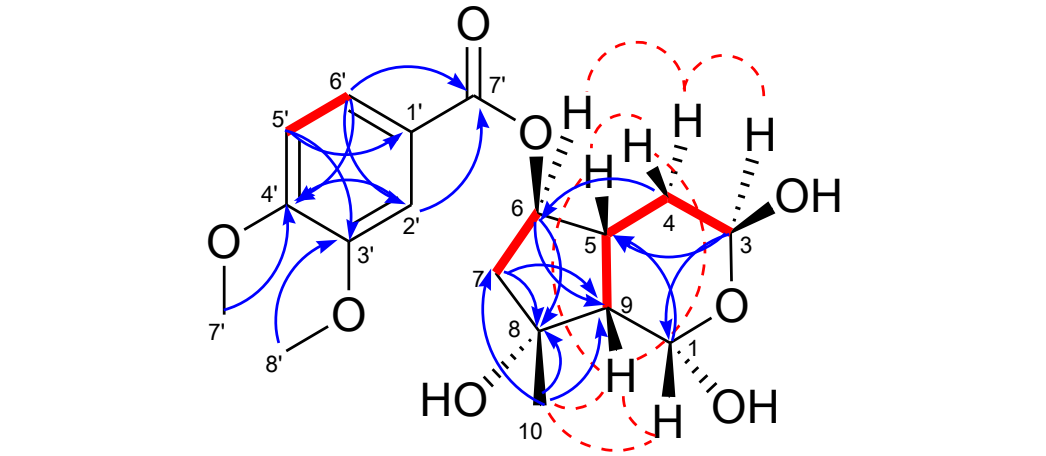

Figure 8 Key HMBC, ^{1}H-^{1}H COSY and NOE correlations of **8**

Compound **8** was obtained as a yellowish solid. Its molecular formula was determined as $C_{18}H_{24}O_8$ by HRFABMS *m/z* 391.1244 $[M+Na]^+$ (calcd. 391.1244 for $C_{18}H_{24}O_8Na$). The characteristics of NMR spectra of compound **8** are very similar to those of compound **7** [43] isolated by Garcez F R, except for the signals of the substituents located at C-1 and C-3. The signals of δ_H 5.56, δ_C 89.7 (C-1), δ_H 5.02 (H-3) and δ_C 90.8 (C-3) were observed in the NMR spectra of compound **6** instead of 4.96 (H-1), 97.7 (C-1), 4.78 (H-3) and 97.9 (C-3) in the above paper. No methoxy signal was observed in the NMR spectra of compound **6**. In addition, the mass data suggested the existence of two more hydroxyl groups compare to the compound **7** in the above paper. Therefore, two hydroxyl groups, instead of two methoxy, were located at C-1 and C-3. Thus, compound **8** was determined as shown in **Fig.8.**

2.2.7. 4-Methoxy-benzoic acid 1,3-dimethoxy-7-methyl-1,3,4,4a,5,6-hexahydro-cyclopenta[c]pyran-5-yl ester (**9**)

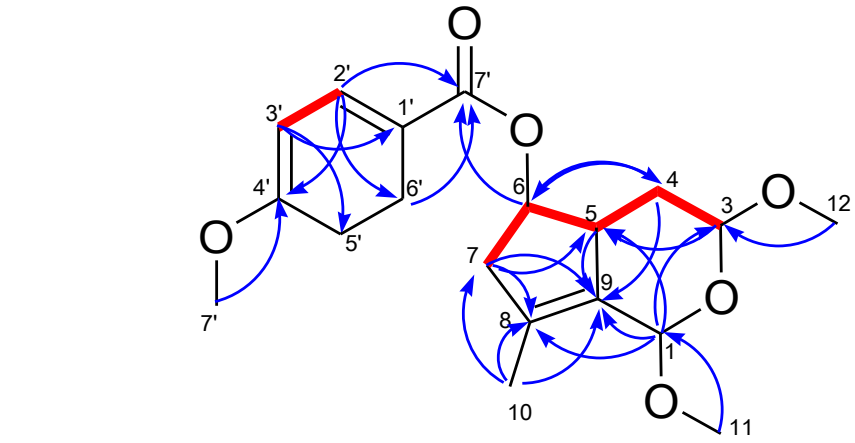

HMBC Correlation ^{1}H-^{1}H COSY Correlation NOE Correlation

Figure 9 Key HMBC, ^{1}H-^{1}H COSY and NOE correlations of **9**

Compound **9** was obtained as brown solid. The ^{1}H NMR spectrum of two doublets δ_H 6.96 (2H, d, J = 8.9) and 7.94 (2H, d, J = 8.9) and HMBC correlations from δ_H 6.96 (H-3' and H-5') to δ_C 123.6 (C-1') and 114.8 (C-5'), δ_H 7.94 (H-2' and H-6') to δ_C 165.2 (C-4') and 167.8 (C-7'), suggested the presence of a *p*-hydroxybenzoate carboxyl group. The HMBC corrections from methyl proton δ_H 1.71 (H-10) to δ_C 44.6 (C-7), δ_C 133.5 (C-8) and δ_C 130.5 (C-9) indicated the methyl was located at C-8. The ^{1}H-^{1}H COSY correlations among δ_H 2.51, 2.84 (H-7) and δ_H 5.10 (H-6), between δ_H 5.10 (H-6) and δ_H 3.08 (H-5), and the HMBC correlations from δ_H 3.08 (H-5) to δ_C 130.5 (C-9), from δ_H 2.51, 2.84 (H-7) to δ_C 48.2 (C-5), δ_C 133.5 (C-8), δ_C 130.5 (C-9) suggested the presence of cyclopentene. Furthermore, ^{1}H-^{1}H COSY correlations among δ_H 3.08 (H-5) and δ_H 2.26, 1.35 (H-4), among δ_H 2.26, 1.35 (H-4) and δ_H 4.80 (H-3), and the HMBC correlations from δ_H 5.33 (H-1) to δ_C 130.5 (C-9), 133.5 (C-8), δ_C 48.2 (C-5) and δ_C 98.2 (C-3), from δ_H 2.26, 1.35 (H-4) to δ_C 80.4 (C-6), 130.5 (C-9), from δ_H 3.45 (H-11, H-12) to δ_C 97.3 (C-1) and δ_C 98.2 (C-3) suggested the presence of the 1,3-Dimethoxy-7-methyl-1,3,4,4a,5,6-hexahydro-cyclopenta[c]pyran. Furthermore the HMBC correlation from δ_H 5.10 (H-6) to δ_C 167.8 (C-7') indicated that C-5 and C-7' was connected through a oxygen atom. Thus compound **9** was determined as shown in **Fig. 9**.

Table 4 ^{1}H-NMR and ^{13}C-NMR Spectral Data of Compound **8** (in $CDCl_3$) and **9** (in CD_3OD)

P.	**8**		**9**	
	δ_H (mult, *J* Hz)	δ_C	δ_H (mult, *J* Hz)	δ_C
1	5.56 (d,2.8)	89.7	5.33 (s)	97.3
2				
3	5.02 (d,2.4)	90.8	4.80 (dd,10.0,2.1)	98.2
4α	2.42 (ddd,2.4,10.7,13.7)	34.0	2.26 (ddd,2.1,5.5,12.4)	38.8
4β	1.72 (dd,2.4,13.7)		1.35 (dt,10.0,12.4)	
5	2.80 (dd,4.8,10.7)	35.9	3.08 (m)	48.2
6	5.08 (dd,2.4,7.2)	80.1	5.10 (dt,5.5,8.2)	80.4
7α	1.86 (dd,2.5,15.5)	47.7	2.51 (dd,5.5,16.8)	44.6
7β	2.62 (dd,7.2,15.5)		2.84 (dd,8.2,16.8)	
8		79.9		133.5
9	2.38 (m)	43.3		130.5
10	1.41(s)	23.3	1.71 (s)	13.4
11			3.45 (s)	55.0
12			3.45 (s)	56.8
1’		123.5		123.6
2’	7.49 (d,2.1)	112.0	7.94 (dt,8.9,8.9)	132.6
3’		148.7	6.96 (dt,8.9,8.9)	114.8
4’		153.1		165.2
5’	6.86 (d,8.6)	110.2	6.96 (dt,8.9,8.9)	114.8
6’	7.61 (dd,2.1,8.6)	123.5	7.94 (dt,8.9,8.9)	132.6
7’		166.0		167.8
8’	3.91 (s)	56.1	3.83 (s)	56.8
9’	3.92 (s)	56.1		

2.2.8. Compound **10**

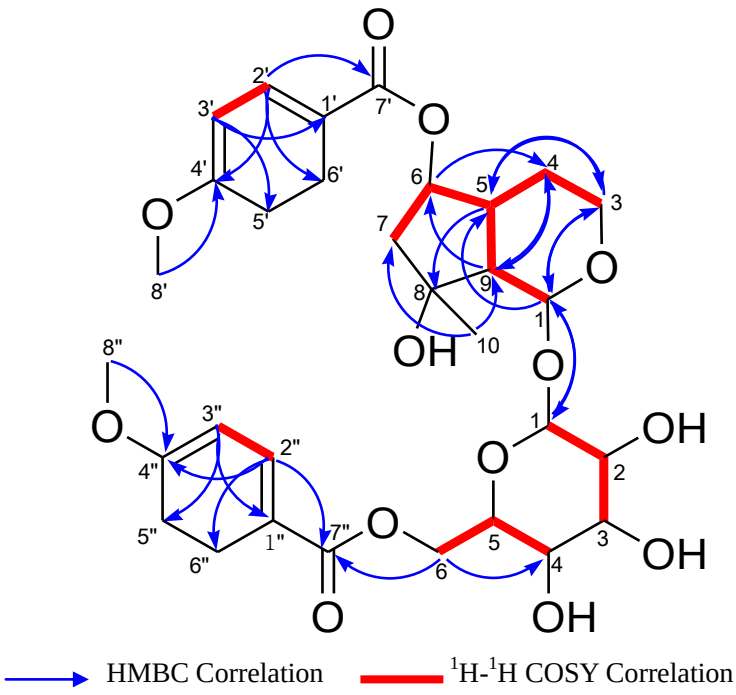

Figure 10 Key HMBC and ^{1}H-^{1}H COSY correlations of **10**

Compound **10** was obtained as a brown solid. Its molecular formula was determined as $C_{31}H_{36}O_{13}$ by HRFABMS *m/z* 639.2045 $[M+Na]^{+}$ (calcd. 639.2054 for $C_{31}H_{36}O_{13}Na$). The characteristics of NMR spectra of compound **10** are very similar to those of (1*S*,4a*R*,5*R*,7*S*,7a*S*)-1,4a,5,6,7,7a-hexahydro-7-hydroxy-5-[(4-methoxybenzoyl)oxy]-7-methylcyclopenta[*c*]pyran-1-yl-β-D-glucopyranoside [44]. However, ^{1}H-NMR and ^{13}C-NMR spectra showed the presence of two AA'**B**B' system aromatic rings [δ_H 6.96 (2H, dt, 8.9), 6.98 (2H, dt, 8.9), 7.97 (2H, dt, 8.9), 7.99 (2H, dt, 8.9), and δ_C 114.7, 114.9, 123.5, 123.8, 132.6, 132.7, 165.2, 165.3] and a glucose moiety (6 protons between δ_H 3.00-4.70 ppm and a anomeric proton at δ_H 4.71). The downfield shifted proton signal of H-Glc-6 [δ_H 4.44 (2H, dd, 5.8, 12.0)] compared with that of the literature [44], together with HMBC correlation from δ_H 4.44 (H-Glc-6) to δ_C 167.8 (C-7") revealed this is the site of gylcosylation. The HMBC correlations from 3.84 (H-8') to 165.2 (C-4'), from 3.88 (H-8") to 165.3 (C-4") revealed the locations of the methoxy. Thus, the structure of **10** was established as in **Fig. 10.**

2.2.9. Compound **11**

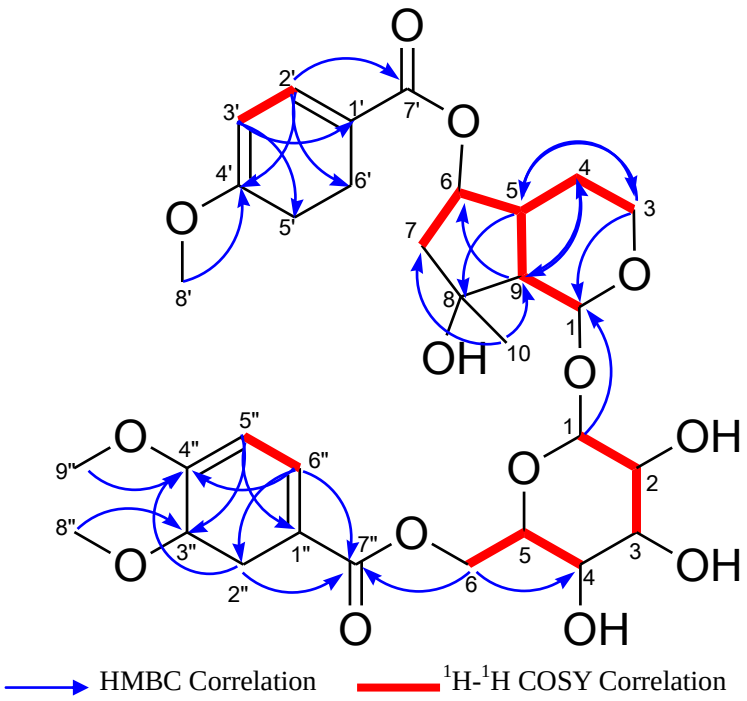

Figure 11 Key HMBC and ^{1}H-^{1}H COSY correlations of **11**

Compound **11** was obtained as a brown solid. Its molecular formula was determined as $C_{32}H_{38}O_{14}$ by HRFABMS *m/z* 669.2145 $[M+Na]^{+}$ (calcd. 669.2159 for $C_{32}H_{38}O_{14}Na$). The characteristics of NMR spectra of compound **11** are very similar to those of Compound **10**, expect for the signals of one of the aromatic rings. ^{1}H-NMR spectrum showed the presence of a AA'**B**B' system aromatic ring [δ_H 6.96 (2H, dt, 8.9), 7.97 (2H, dt, 8.9)] and a ABX system aromatic ring [δ_H 7.03 (1H, d, 8.6), 7.56 (1H, dt, 2.1), 7.69 (1H, dd, 2.1, 8.6)]. HMBC correlations from δ_H 3.86 (H-8") to 150.2 (C-3") and from δ_H 3.88 (H-9") to 154.9 (C-4") indicated the locations of these two methoxy groups. In addtion, HMBC correlation from δ_H 4.46 (H-Glc-6) to δ_C 167.8 (C-7"), indicated ABX system aromatic group was located at C-Glc-6. Thus, the structure of **11** was established as in **Fig. 11.**

2.2.10. Compound **12**

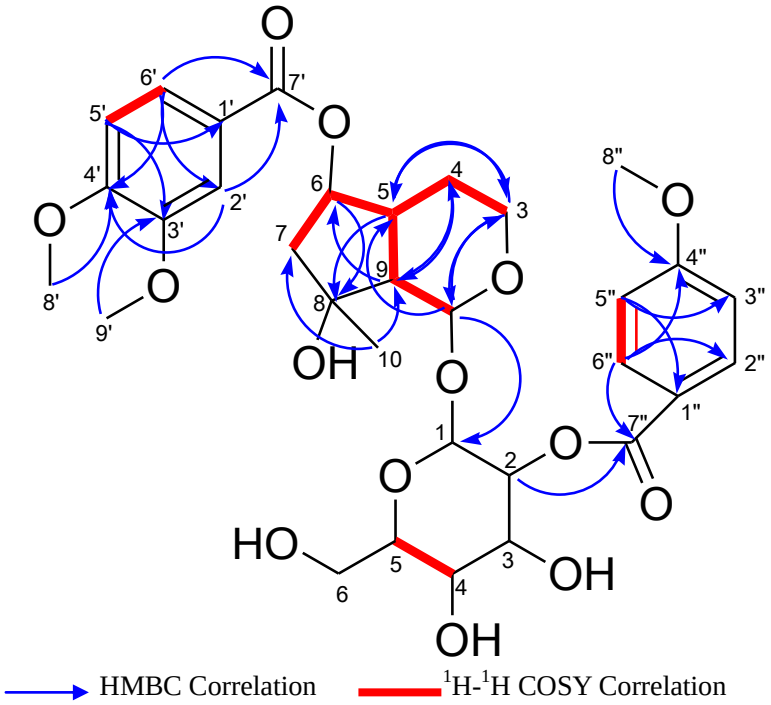

Figure 12 Key HMBC and ^{1}H-^{1}H COSY correlations of **12**

Compound **12** was obtained as a brown solid. Its molecular formula was determined as $C_{32}H_{38}O_{14}$ by HRFABMS *m/z* 669.2145 $[M+Na]^+$ (calcd. 669.2159 for $C_{32}H_{38}O_{14}Na$). The characteristics of NMR spectra of compound **12** are very similar to those of compound **10** and **11**, indicating they are based on the same skeleton. However, chemical shifts of H-Glc-2, H-Glc-6 in the ^{1}H-NMR spectra of **12** were different with **10** and **11**, indicated the site of glycosylation of **12** was different with **10** and **11**. The downfield shifted H-Glc-2 instead of H-Glc-6 and HMBC correlations from δ_H 4.92 (1H, overlap, 8.9) (H-Glc-2) to δ_C 167.3 (C-7") revealed that this was the site of glycosylation. HMBC correlations from δ_H 3.87 (H-8') to 150.1 (C-3'), from δ_H 3.89 (H-9') to 154.7 (C-4') and from δ_H 3.80 (H-8") to 165.1 (C-4") indicated the locations of the methoxy. Thus, the structure of **12** was established as in **Fig. 12.**

2.2.11. Compound **13**

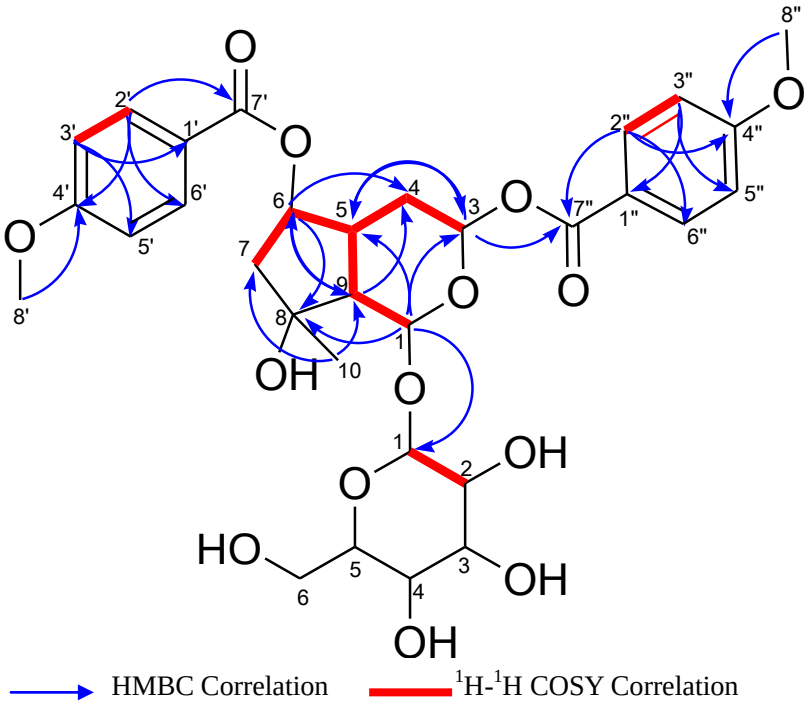

Figure 13 Key HMBC and ^{1}H-^{1}H COSY correlations of **13**

Compound **13** was obtained as a brown solid. Its molecular formula was determined as $C_{31}H_{38}O_{14}$ by HRFABMS *m/z* 657.2156 [M+Na]+ (calcd. 657.2159 for C31H38O14Na). The characteristics of NMR spectra of compound **13** are very similar to those of compound **10,** indicating they are based on the same skeleton. However, no downfield shifted proton signal except for H-Glc-1 of was found in the ^{1}H-NMR spectra of **13**, indicated that aromatic ring was not located at the glucose. Furthermore, proton signals of the double bond was not found, insteadly, δ_H 6.36 (H-3), δ_H 1.83, 2.20 (H-4) was observed. In addition, HMBC correlation from δ_H 6.36 (H-3) to δ_C 166.3 (C-7") was observed, indicated the aromatic group was located at C-3 of the iridoids moiety. Thus, the structure of **13** was established as in **Fig. 13.**

Table 5 ^{1}H-NMR Spectral Data of Compound **10, 11, 12, 13** in CD_3OD

P.	^{1}H-NMR [δ_H (multi,J in Hz)]			
	10	**11**	**12**	**13**
1	5.30 (d,3.8)	5.29 (d,3.3)	5.48 (d,1.7)	5.54 (d,3.8)
3	6.23 (dd,6.2)	6.23 (dd,6.2)	5.84 (dd,6.2)	6.36 (dd,3.4,7.2)
4	5.01 (dd,3.8,6.2)	5.02 (dd,3.1,6.2)	4.42 (dd,6.2)	1.83 (m,7.2,9.6,13.7)
				2.20 (m,7.2,9.6,13.7)
5	2.99 (m)	2.99 (m)	2.63 (d,9.3)	3.00 (m)
6	4.93 (m)	4.93 (m)	4.87 (overlap)	5.34 (m)
7	1.97 (dd,3.4,14.4)	1.96 (dd,14.4)	2.00 (dd,14.4)	2.00 (dd,3.4,15.1)
	2.18 (dd,6.5,14.4)	2.17 (dd,14.4)	2.15 (dd,14.4)	2.17 (dd,7.2,15.1)
8				
9	2.53 (dd,3.8)	2.52 (dd,3.8)	2.56 (d,9.3)	2.40 (dd,3.8)
10	1.32 (s)	1.31 (s)	1.32 (s)	1.47 (s)
Glc 1	4.71 (d,7.9)	4.72 (d,7.9)	4.95 (d,8.2)	4.84 (d,7.9)
Glc 2	3.23 (m)	3.23 (m)	4.92 (overlap)	3.23 (overlap)
Glc 3	3.41 (overlap)	3.42 (overlap)	3.70,8.9 (overlap)	3.42 (t,8.9)
Glc 4	3.43 (overlap)	3.41 (overlap)	3.40 (overlap)	3.28 (overlap)
Glc 5	3.60 (m)	3.61 (m)	3.40 (overlap)	3.21 (overlap)
Glc 6	4.44 (dd,5.8,12.0)	4.46 (dd,11.7)	3.71 (overlap)	3.60 (dd,5.8,12.0)
	4.63 (dd,2.4,12.0)	4.63 (dd,11.7)	3.96 (d,11.7)	3.74 (dd,2.4,12.0)
1’				
2’	7.97 (dt,8.9)	7.97 (dt,8.9)	7.55 (d,2.1)	8.00 (dt,8.9)
3’	6.96 (dt,8.9)	6.96 (dt,8.9)		6.98 (dt,8.9)
4’				
5’	6.96 (dt,8.9)	6.96 (dt,8.9)	7.02 (d,8.6)	6.98 (dt,8.9)
6’	7.97 (dt,8.9)	7.97 (dt,8.9)	7.66 (dd,2.1,8.6)	8.00 (dt,8.9)
7’				
8’	3.84 (s)	3.84 (s)	3.87 (s)	3.85 (s)
9’			3.89 (s)	
1”				
2”	7.99 (dt,8.9)	7.56 (d,2.1)	7.95 (dt,8.9)	8.02 (dt,8.9)
3”	6.98 (dt,8.9)		6.95 (dt,8.9)	7.02 (dt,8.9)
4”				
5”	6.98 (dt,8.9)	7.03 (d,8.6)	6.95 (dt,8.9)	7.02 (dt,8.9)
6”	7.99 (dt,8.9)	7.69 (dd,2.1,8.6)	7.95 (dt,8.9)	8.02 (dt,8.9)
7”				
8”	3.88 (s)	3.86 (s)	3.86 (s)	3.87 (s)
9”		3.88 (s)		

Table 6 ^{13}C-NMR Spectral Data of Compound **10, 11, 12, 13** in CD_3OD

P.	^{13}C-NMR [δ_C]			
	10	**11**	**12**	**13**
1	93.6	93.6	93.4	94.8
3	141.2	141.2	140.5	91.7
4	104.7	104.7	104.9	29.7
5	40.4	40.4	39.1	41.4
6	80.9	81.0	81.2	80.0
7	47.4	47.4	48.0	47.8
8	79.4	79.4	78.7	79.4
9	51.2	51.9	51.5	52.0
10	26.1	26.1	26.1	27.5
Glc 1	99.3	99.2	97.3	98.7
Glc 2	74.8	74.8	75.2	75.1
Glc 3	77.9	77.9	75.9	78.2
Glc 4	71.8	71.9	71.8	71.7
Glc 5	75.7	75.7	78.5	78.2
Glc 6	64.7	64.8	62.7	62.6
1’	123.8	123.8	124.0	123.8
2’	132.7	132.7	113.5	132.7
3’	114.7	114.7	150.1	114.8
4’	165.2	165.2	154.7	165.3
5’	114.7	114.7	111.8	114.8
6’	132.7	132.7	125.0	132.7
7’	167.7	167.7	167.6	167.8
8’	56.0	56.0	56.5	56.0
9’			56.5	
1”	123.5	123.6	123.9	123.0
2”	132.7	113.4	132.9	133.0
3”	114.9	150.2	114.5	115.0
4”	165.3	154.9	165.1	165.6
5”	114.9	112.0	114.5	115.0
6”	132.7	125.0	132.9	133.0
7”	167.8	167.8	167.3	166.3
8”	56.0	56.5	56.0	56.0
9”		56.5		

2.2.12. Compound **14**

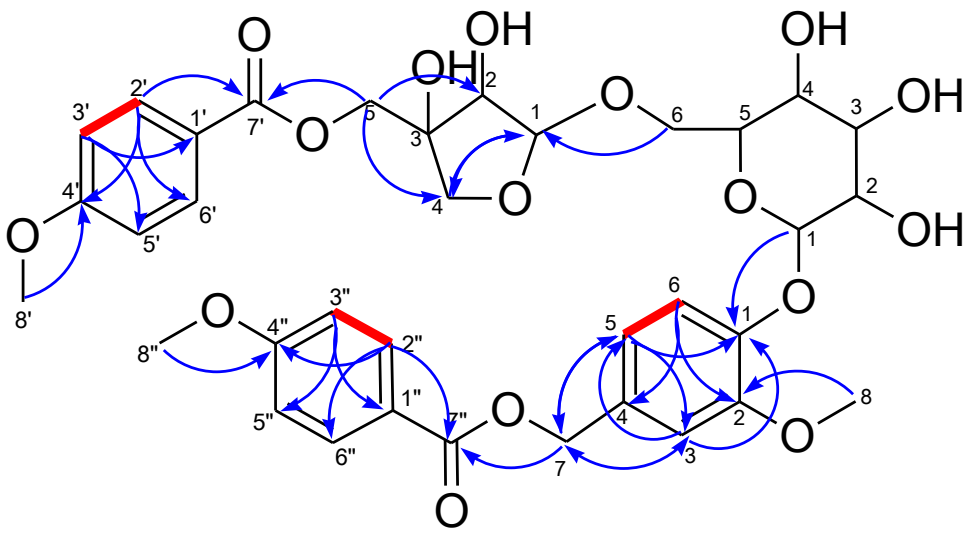

Figure 14 Key HMBC and ^{1}H-^{1}H COSY correlations of **14**

Compound **14** was obtained as a brown solid. Its molecular formula was determined as $C_{36}H_{42}O_{17}$ by HRFABMS *m/z* 739.2207 $[M+Na]^{+}$ (calcd. 739.739. 2214 for $C_{35}H_{40}O_{16}Na$). The characteristics of NMR spectra of compound **14** are similar to those of 4-[[(4-methoxybenzoyl)oxy]methyl]-2-methoxyphenyl 1-O b-D-[5-O-(4-hydroxybenzoyl)]-apiofuranosyl-(1→6)- β-Dglucopyranoside [45]. Howe ver, ^{1}H-NMR spectrum of **14** showed the presence of two AA'BB' system aro matic ring [δ_H 6.93 (2H, dt, 8.9), 6.95 (2H, dt, 8.9), 7.94 (2H, dt, 8.9), 7.97 (2H, dt, 8.9)], HMBC correlations from δ_H 7.97 (H-2') to δ_C 167.7 (C-7'), fro m δ_H 4.31 (H-Api-5) to δ_C 78.6 (C-Api-2), 75.1 (C-Api-4) and 167.7 (C-7'), i ndicated one aromatic group was located at C-Api-5. In addition, HMBC correl ations from δ_H 3.81 (H-8' and H-8") to δ_C 165.3 (C-4') and 165.2 (C-4") indi cated the locations of the methoxy groups. Thus, the structure of **14** was estab lished as in **Fig. 14**.

2.2.13. Compound **15**

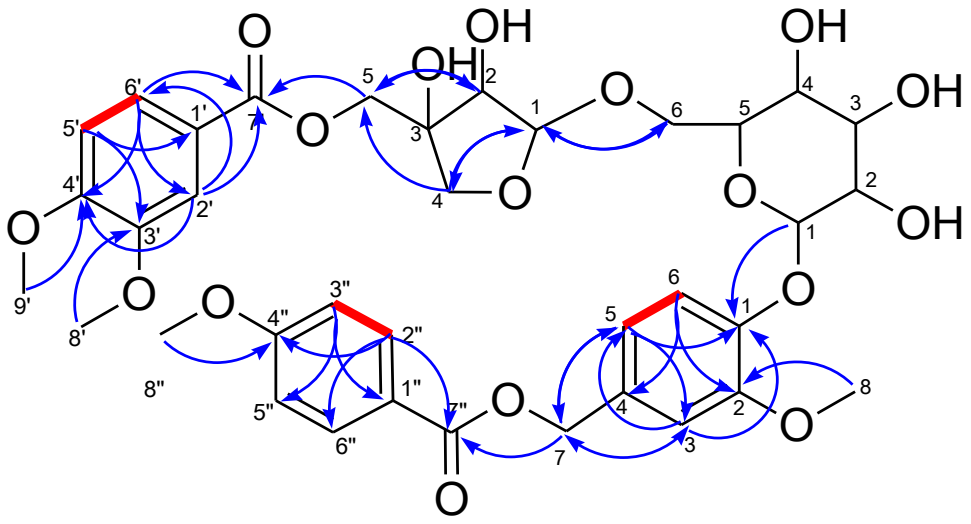

Figure 15 Key HMBC and ^{1}H-^{1}H COSY correlations of **15**

Compound **15** was obtained as a brown solid. Its molecular formula was determined as $C_{36}H_{40}O_{16}$ by HRFABMS *m/z* 769.2330 $[M+Na]^{+}$ (calcd. 769.2320 for $C_{36}H_{42}O_{17}Na$). The characteristics of NMR spectra of compound **10** are very similar to those of 4-[[(4-methoxybenzoyl)oxy]methyl]-2-methoxyphenyl 1-O b-D-[5-O-(4-hydroxybenzoyl)]-apiofuranosyl-(1→6)-b-Dglucopyranoside [45]. However, ^{1}H-NMR spectrum of **15** showed the presence of a ABX system aromatic ring [δ_H 6.93 (1H, d, 8.2), 7.50 (1H, d, 2.1), 7.66 (1H, dd, 2.1, 8.2)]. HMBC correlations from δ_H 3.77 (H-8') to δ_C 150.1 (C-3') and 3.83 (H-9') to 154.9 (C-4') indicated the locations of the methoxy groups. In addition, HMBC correlation from δ_H 7.66 (H-6') to δ_C 167.7 (C-7'), from δ_H 4.31 (H-Api-5) to 78.6 (C-Api-2) and 167.7 (C-7') indicated this ABX system aromatic group was located at C-Api-5. Thus, the structure of **15** was established as in **Fig. 15.**

2.2.14. Compound **16**

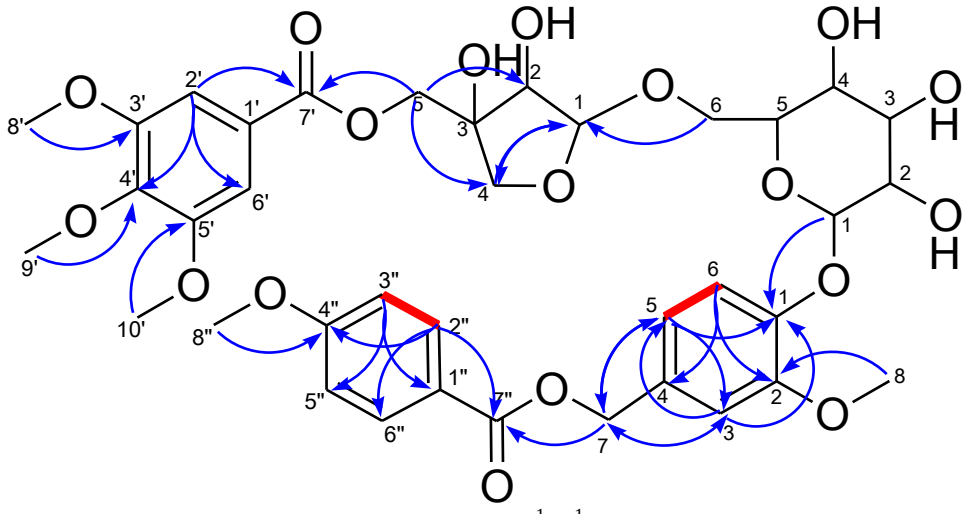

Figure 16 Key HMBC and ^{1}H-^{1}H COSY correlations of 1**6**

Compound **16** was obtained as a brown solid. Its molecular formula was determined as $C_{37}H_{44}O_{18}$ by HRFABMS *m/z* 799.2425 $[M+Na]^{+}$ (calcd. 799.242 5 for $C_{37}H_{44}O_{18}Na$). The characteristics of NMR spectra of compound **16** are v ery similar to those of 4-[[(4-methoxybenzoyl)oxy]methyl]-2-methoxyphenyl 1-O b-D-[5-O-(4-hydroxybenzoyl)]-apiofuranosyl-(1→6)-b-Dglucopyranoside [45]. Howev er, ^{1}H-NMR spectrum of **16** showed the presence of two aromatic protons [δ_H 7.31 (4H, s), 6.95 (2H, dt, 8.9), 7.94 (2H, dt, 8.9)]. HMBC correlations from δ_H 3.81 (H-8'and H-10') to δ_C 154.4 (C-3' and C-5'), 3.79 (H-9') to 143.7 (C -4'), and from 7.31 (H-2' or H-6') to 143.7 (C-4'), 167.3 (C-7') indicated the existence of the 3,4,5 - trimethoxy - benzoyl group. In addition, HMBC correl ation from δ_H 4.32 (H-Api-5) to δ_C 75 (C-Api-4) and 167.3 (C-7'), indicated t his aromatic group was located at C-Api-5. Thus, the structure of **16** was esta blished as in **Fig. 16.**

2.2.15. Compound **17**

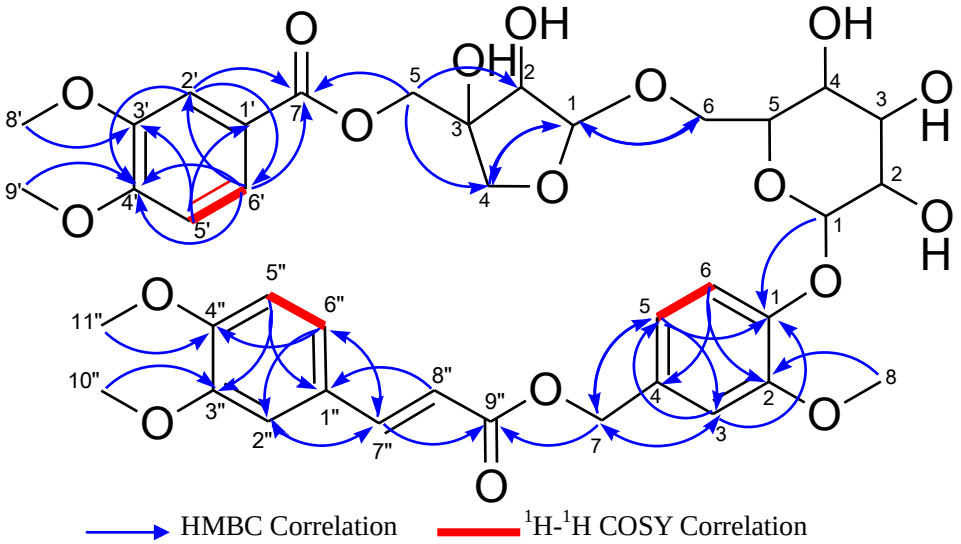

Figure 17 Key HMBC and ^{1}H-^{1}H COSY correlations of **17**

Compound **17** was obtained as a brown solid. Its molecular formula was determined as $C_{39}H_{46}O_{18}$ by HRFABMS *m/z* 825.2572 $[M+Na]^+$ (calcd. 825.2582 for $C_{39}H_{46}O_{18}Na$). The characteristics of NMR spectra of compound **17** are very similar to compound **15**. However, ^{1}H-NMR spectrum of **15** showed the presence of three ABX system aromatic rings [δ_H 6.94 (1H, d, 8.6), δ_H 6.96 (1H, d, 8.6), δ_H 7.10 (1H, d, 8.2), 7.00 (1H, d, 2.1), 7.20 (1H, d, 2.1), 7.52 (1H, d, 2.1), 6.84 (1H, dd, 2.1, 8.2), 7.14 (1H, dd, 2.1, 8.6), 7.68 (1H, dd, 2.1, 8.6)] and a *trans*-double bond [δ_H 6.41 (1H, d, 16.2), δ_H 7.61 (1H, d, 16.2)]. HMBC correlations from δ_H 3.79 (H-8') to δ_C 150.1 (C-3'), from 3.84 (H-8 and H-10") to 150.8 (C-2) and 154.4 (C-3"), from 3.85 (H-9' and C-11") to 154.4 (C-4') and 152.8 (C-4"), revealed the positions of the methoxy. HMBC correlations between 7.20 (H-2"), 7.14 (H-6") to 146.6 (C-7"), from 6.41 (H-8") to 128.8 (C-1"), from 7.61 (H-7"), 5.04 (H-7) to 168.8 (C-9") indicated the existence of a 3 - (3,4 - dimethoxy - phenyl) - propylene carboxyl group located at C-7. Thus, the structure of **17** was established as in **Fig. 17.**

2.2.16. Compound **18**

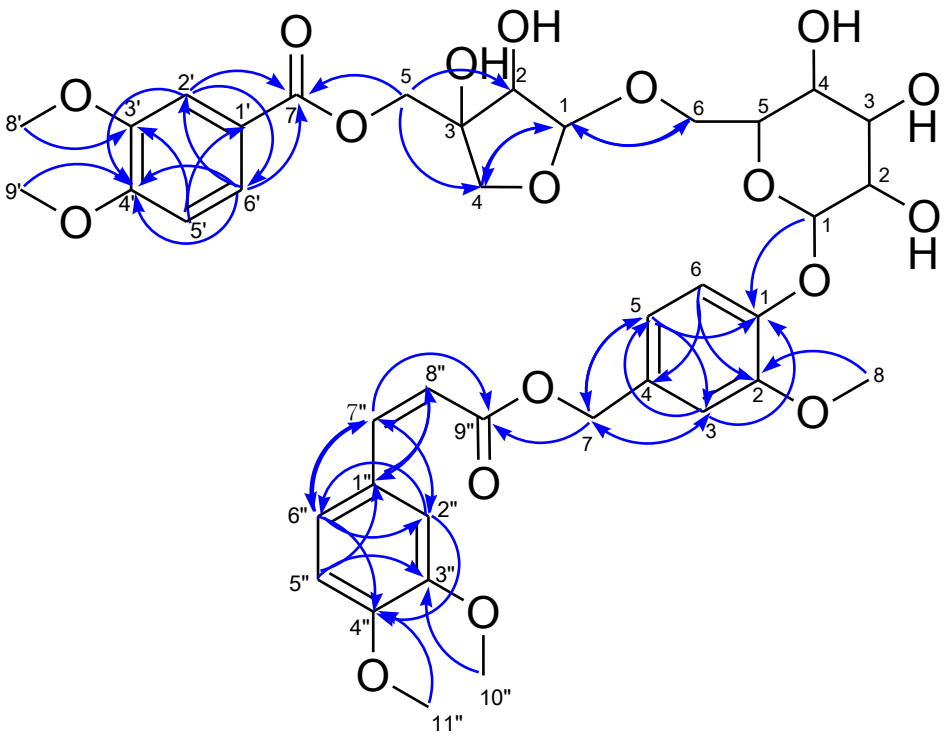

Figure 18 Key HMBC correlations of **18**

Compound **18** was obtained as a brown solid. Its molecular formula was determined as $C_{39}H_{46}O_{18}$ by HRFABMS *m/z* 825.2569 $[M+Na]^+$ (calcd. 825.2582 for $C_{39}H_{46}O_{18}Na$). The characteristics of NMR spectra of compound **18** are almost the same with compound **17**, expect for the configuration of the double bond. ^{1}H-NMR spectrum of **15** showed the presence of a *sis*-double bond [δ_H 5.83 (1H, d, 12.7), δ_H 5.86 (1H, d, 12.7)]. Thus, the structure of **18** was established as in **Fig. 18.**

Table 7 ^{1}H-NMR Spectral Data of Compound **14, 15, 16, 17, 18** in CD_3OD

P.	δ_H(multi,*J* in Hz)				
	14	**15**	**16**	**17**	**18**
1					
2					
3	7.04 (d,1.7)	7.01 (d,2.1)	7.03 (d,1.7)	7.00 (d,2.1)	6.90 (d,2.1)
4					
5	6.89 (dd,1.7,8.2)	6.87 (dd,2.1,8.2)	6.88 (dd,1.7,8.2)	6.84 (dd,2.1,8.2)	6.78 (dd,2.1,8.2)
6	7.12 (d,8.2)	7.10 (d,8.2)	7.10 (d,8.2)	7.10 (d,8.2)	7.06 (d,8.2)
7	5.14 (s)	5.10 (s)	5.13 (s)	5.04 (s)	4.99 (s)
8	3.83 (s)	3.81 (s)	3.83 (s)	3.84 (s)	3.77 (s)
Glc 1	4.84 (d,7.6)	4.83 (d,7.6)	4.82 (d,7.6)	4.82 (d,7.6)	4.82 (d,7.6)
Glc 2	3.49 (dd,7.6,8.9)	3.50(dd,7.6,9.0)	3.48 (dd,7.6,8.9)	3.49 (dd,7.6,8.9)	3.48 (dd,7.6,8.9)
Glc 3	3.44 (t,8.9)	3.44 (t,9.0)	3.43 (t,8.9)	3.43 (t,8.9)	3.43 (t,8.9)
Glc 4	3.32 (overlap)	3.32 (overlap,9.0)	3.29 (overlap)	3.29 (overlap)	3.32 (overlap)
Glc 5	3.58 (overlap)	3.57 (overlap)	3.57 (overlap)	3.57 (overlap)	3.57 (overlap)
Glc 6	3.58 (overlap)	3.59 (overlap)	3.60 (overlap)	3.60 (overlap)	3.60 (overlap)
	4.04 (d,9.6)	4.01 (d,9.6)	4.02 (d,9.6)	4.03 (d,9.6)	4.03 (d,9.6)
Api 1	4.99 (d,2.1)	5.00 (d,2.1)	5.00 (d,2.1)	4.99 (d,2.1)	4.99 (overlap)
Api 2	3.99 (d,2.1)	4.00 (d,2.1)	4.00 (d,2.1)	4.00 (d,2.1)	3.99 (d,2.1)
Api 4	3.86 (overlap)	3.85 (overlap)	3.84 (overlap)	3.84 (overlap)	3.84 (overlap)
	4.04 (overlap)	4.06 (d,9.6)	4.07 (d,9.6)	4.06 (d,9.6)	4.06 (d,9.6)
Api 5	4.31 (d,11.3)	4.31 (d,11.3)	4.32 (d,11.3)	4.31 (d,11.3)	4.32 (d,11.3)
	4.35 (d,11.3)	4.36 (d,11.3)	4.40 (d,11.3)	4.37 (d,11.3)	4.36 (d,11.3)
1’					
2’	7.97 (dt,8.9)	7.50 (d,2.1)	7.31 (s)	7.52 (d,2.1)	7.53 (d,2.1)
3’	6.93 (dt,8.9)				
4’					
5’	6.93 (dt,8.9)	6.93 (d,8.2)		6.96 (d,8.2)	6.97 (d,8.2)
6’	7.97 (dt,8.9)	7.66 (dd,2.1,8.2)	7.31 (s)	7.68 (dd, 2.1,8.2)	7.68 (dd, 2.1,8.2)
7’					
8’	3.81 (s)	3.77 (s)	3.81 (s)	3.79 (s)	3.80 (s)
9’		3.83 (s)	3.79 (s)	3.85 (s)	3.85 (s)
10’			3.81 (s)		
1”					
2”	7.94 (dt,8.9)	7.91 (dt,8.9)	7.94 (dt,8.9)	7.20 (d,2.1)	7.51 (d,2.1)
3”	6.95 (dt,8.9)	6.91 (dt,8.9)	6.95 (dt,8.9)		
4”					
5”	6.95 (dt,8.9)	6.91 (dt,8.9)	6.95 (dt,8.9)	6.94 (d,8.2)	6.83 (d,8.2)
6”	7.94 (dt,8.9)	7.91 (dt,8.9)	7.94 (dt,8.9)	7.14 (dd,2.1,8.2)	7.07 (dd,2.1,8.2)
7”				7.61 (d,16.2)	5.86 (d,12.7)
8”	3.84 (s)	3.81 (s)	3.83 (s)	6.41(d,16.2)	5.83 (d,12.7)
9”					
10”				3.84 (s)	3.72 (s)
11”				3.85 (s)	3.83 (s)

Table 8 ^{13}C-NMR Spectral Data of Compound **14, 15, 16, 17, 18** in CD_3OD

P.	δ_C				
	14	**15**	**16**	**17**	**18**
1	147.9	147.9	147.9	147.8	147.9
2	150.8	150.7	150.8	150.8	150.7
3	113.8	113.8	113.8	113.8	113.8
4	132.6	132.4	132.4	132.1	132.1
5	122.4	122.3	122.2	122.3	122.4
6	117.9	117.8	117.8	117.9	117.6
7	67.5	67.3	67.3	67.1	67
8	56	55.9	56.7	56.5	56.6
Glc 1	102.7	102.6	102.6	102.6	102.5
Glc 2	74.9	74.8	74.8	74.9	74.8
Glc 3	77.9	77.8	77.9	77.9	77.9
Glc 4	71.8	71.7	71.8	71.9	71.8
Glc 5	77	77	77	77	77
Glc 6	68.8	68.9	69	69	68.9
Api 1	110.8	110.9	111	111	110.9
Api 2	78.6	78.6	78.7	78.7	78.6
Api 3	56	79	78.9	79	79
Api 4	75.1	75	75	75.1	75.1
Api 5	67.4	67.5	67.9	67.5	67.5
1’	123.2	123.5	126.3	123.4	123.4
2’	132.9	113.5	108.2	113.5	113.5
3’	114.9	150.1	154.4	150.1	150.2
4’	165.3	154.9	143.7	154.9	154.9
5’	114.9	111.9	154.4	111.9	111.9
6’	132.9	125.1	108.2	125.1	125.1
7’	167.7	167.6	167.3	167.6	167.6
8’	56	56.7	56.7	56.5	56.3
9’		56.4	61.2	56.5	56.5
10’			56.7		
1”	123.5	123.4	123.6	128.8	129.2
2”	132.7	132.6	132.7	111.4	114.5
3”	114.9	114.8	114.8	150.7	149.6
4”	165.2	165.1	165.2	152.8	151.6
5”	114.9	114.8	114.8	112.5	111.9
6”	132.7	132.6	132.7	124.1	125.8
7”	167.5	167.7	167.7	146.6	144.4
8”	56	56.7	56	116.4	117.8
9”				168.8	168.1
10”				56.6	56.3
11”				56.6	56.6

2.2.17. Compound **19**

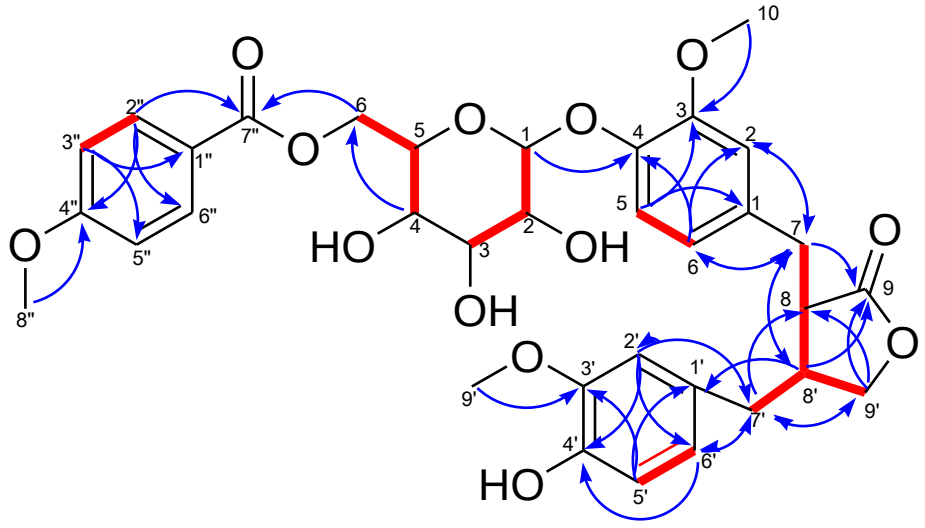

Figure 19 Key HMBC and ^{1}H-^{1}H COSY correlations of **19**

Compound **19** was obtained as a brown solid. Its molecular formula was determined as $C_{34}H_{38}O_{13}$ by HRFABMS *m/z* 677.2200 $[M+Na]^{+}$ (calcd. 677.2210 for $C_{34}H_{38}O_{13}Na$). ^{1}H-NMR spectrum showed the presence of a AA'BB' system aromatic ring [δ_H 7.00 (4H, dt, 8.9), 7.97 (2H, dt, 8.9)], two ABX system aromatic rings [δ_H 6.96 (1H, d, 8.2), 6.63 (1H, d), 6.62 (1H, d), 6.37 (1H, d), 6.40 (1H, dd) 7.41 (1H, dd)] and three methoxy [δ_H 3.66 (3H, s) , 3.75 (3H, s) and 3.87 (3H, s)]. The six proton signals between 3 ppm and 4 ppm and the a anomeric proton signal of δ_H 4.87 indicated the presence of a glucose. ^{1}H-^{1}H COSY spectrum in **Fig. 19** revealed the connections among C-7, C-8, C-7', C-8' and C-9'. HMBC correlations from δ_H 3.75 (H-10) to δ_C 150.5 (C-3), from δ_H 3.66 (H-9') to δ_C 149.0 (C-3') and from δ_H 3.87 (H-8") to 165.3 (C-4") indicated the locations of the methoxy groups. In addition, HMBC correlations from δ_H 2.75, 2.83 (H-7), 2.36 (H-8'), 3.94, 4.21 (H-9'), to δ_C 181.4 (C-9) revealed the existence of a γ-butyrolactone group. The HMBC correlations from the anomeric proton of δ_H 4.87 to δ_C 146.5 (C-4), from 4.39 (H-Glu-6) to δ_C 167.6 (C-7"), from δ_H 2.75, 2.83 (H-7) to δ_C 114.6 (C-2), δ_C 122.7 (C-6), and from δ_H 2.45, 2.52 (H-7') to δ_C 113.0 (C-2'), δ_C 122.3 (C-6') were observed, therefore the structure of **19** was established as in **Fig. 19.**

Table 9 ^{1}H-NMR and ^{13}C-NMR Spectral Data of Compound **19** in CD_3OD

19					
P.	δ_H (multi,*J* in Hz)	δ_C	P.	δ_H (multi,*J* in Hz)	δ_C
1		134.1	Glc 1	4.87 (overlap)	102.4
2	6.62 (d)	114.6	Glc 2	3.51 (overlap)	77.8
3		150.5	Glc 3	3.53 (overlap)	74.8
4		146.5	Glc 4	3.41 (overlap)	72.1
5	6.96 (d,8.2)	117.4	Glc 5	3.77 (m)	75.5
6	6.40 (dd)	122.7	Glc 6	4.39 (dd,11.7)	65.1
7	2.75 (dd,13.7)	35.4		4.63 (dd,11.7)	
	2.83 (dd,13.7)		1”		123.5
8	2.59 (m)	47.6	2”	7.97 (dt,8.9)	132.8
9		181.4	3”	7.00 (dt,8.9)	114.9
10	3.57 (s)	56.6	4”		165.3
1’		131.1	5”	7.00 (dt,8.9)	114.9
2’	6.37 (d)	113	6”	7.97 (dt,8.9)	132.8
3’		149	7”		167.6
4’		146.1	8”	3.87 (s)	56.1
5’	6.63 (d)	116.1			
6’	6.41 (dd)	122.3			
7’	2.45 (dd,7.6,13.7)	39			
	2.52 (dd,7.6,13.7)				
8’	2.36 (m)	42.2			
9’	3.94 (dd,8.9)	73			
	4.21 (dd,8.9)				
10’	3.66 (s)	56.3			

2.2.18. Compound **20**

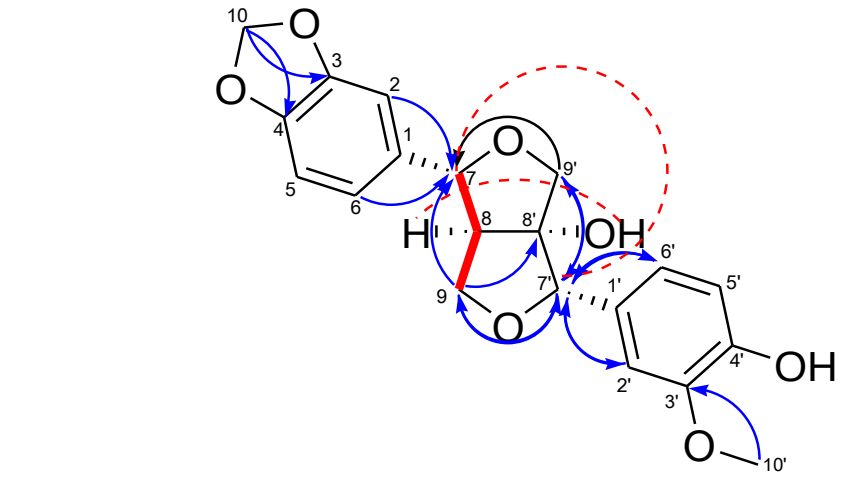

HMBC Correlation ^{1}H-^{1}H COSY Correlation NOE Correlation

Figure 20 Key HMBC, ^{1}H-^{1}H COSY and NOE correlations of **20**

Compound **20** was obtained as colorless oil. Its molecular formula was det ermined as $C_{20}H_{20}O_7$ by HRFABMS *m/z* 371.1129 [M-H]-. The 1D NMR spec tra and HMQC spectrum showed the presence of two ABX system aromatic ri ngs [δ_H 6.95 (d, *J* = 1.7), 6.79 (d, *J* = 8.5), 6.90 (dd, *J* = 1.7, 8.5) and 7.03 (d, *J* = 1.7), 6.77 (d, *J* = 8.5), 6.84 (dd, *J* = 1.7,8.5)], one methylenedioxy g roup [δ_H 5.93 (2H, s) and δ_C 102.4] and one methoxy group [δ_H 3.86 (3H, s) and δ_C 56.4]; the presence of two doublets [δ_H 4.04 (d, *J* = 9.3), 3.84 (d, *J* = 9.3) and δ_C 76.1], and an apparent triplet and a double doublets [δ_H 4.45 (t, *J* = 8.9), 3.77 (dd, *J* = 5.8,8.9) and δ_C 72.0] for nonequivalent geminal methyl ene protons at C-9' and C-9, respectively, together with one double triplet [δ_H 3.00 (dt, *J* = 5.8, 8.9) and δ_C 62.6], one doublet [δ_H 4.84 (d, *J* = 5.8) and δ_C 87.6], and one singlet [δ_H 4.66 (s) and δ_C 89.2] suggested a structure of fura nofuran lignan with two ABX aromatic rings. It has the similar spectra with (1*S**,2*R**,5*R**,6*S**)-6-(4-hydroxy-3- methoxyphenyl)-2-(3,4-methylenedioxyphenyl)-3,7-dioxabicyclo[3.3.0]-oactan-1-ol reported by S. Yamauchi *et al.*,[12] expect for the positions of the two ABX system aromatic rings. In Figure 2**,** HMBC corr elations observed from δ_H 5.93(H-10) to δ_C 149.4 (C-3), δ_C 148.7 (C-4), from

δ_H 6.90 (H-6) to δ_C 107.8 (C-2), δ_C 148.7 (C-4) and δ_C 87.6 (C-7), from δ_H 6. 95 (H-2) to δ_C 148.7 (C-4), δ_C 121.0 (C-6) and δ_C 87.6 (C-7), together with 1 H-1H COSY correlations between δ_H 4.84 (H-7) and δH 3.00 (H-8), and amon g δ_H 4.45(H-9α), δ_H 3.77 (H-9β) and δ_H 3.00 (H-8), supported the methylenedi oxy-substituted phenyl group is located at C-7 (not C-7') of furanofuran group. In addition, the NOE correlations (measured in DMSO) were observed betwee n H-8 and H-8'-OH, from H-8 to H-9β, from H-7 to H-7'α, and from H-7 to H-9α. Thus, the structure of **20** was established as in **Fig. 20.**

2.2.19. Compound **21**

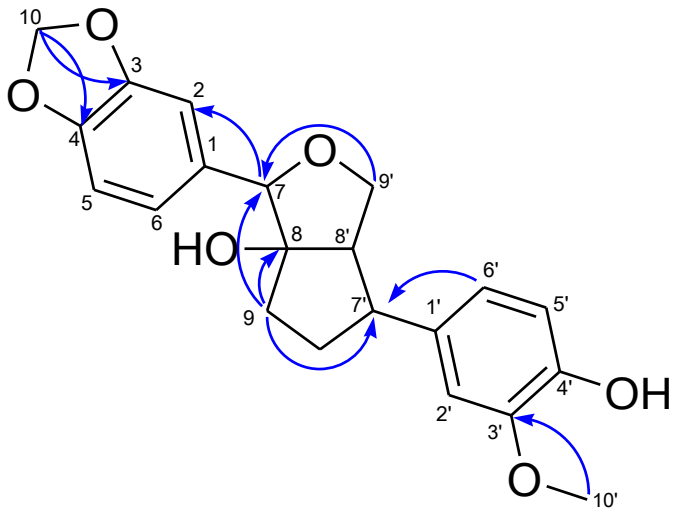

HMBC Correlation

Figure 21 Key HMBC correlations of **21**

Compound **21** was obtained as colorless oil. Its molecular formula was determined as $C_{20}H_{20}O_7$ by HRESIMS *m/z* 371.1122 $[M-H]^-$. The characteristics of the NMR spectra of compound **4** is very similar to that of compound **3**, expect for the HMBC correlations from H-7 to C-2 and from H-2' to C-7', suggested that compound **4** has an opposite positions of C-7, C-8, C-9 and C-7', C-8', C-9' with that of compound **3** . Thus the structure of **21** was established as in **Fig. 21**.

Table10. ^{13}C NMR and ^{1}H NMR Spectral Data of Compounds **20** and **21** in CD_3OD.

P.	**20**		**21**	
	δ_H (mult, *J* in Hz)	δ_C	δ_H (mult, *J* in Hz)	δ_C
1		136.4		133.5
2	6.95 (d,1.7)	107.8	6.94 (d,1.4)	109.3
3		149.4		149.1
4		148.7		148.9
5	6.79 (d,8.5)	109.0	6.77 (d,8.2)	116.0
6	6.90 (dd,1.7,8.5)	121.0	6.87 (dd,1.4,8.2)	122.0
7	4.84 (d,5.8)	87.6	4.68 (s)	89.1
8	3.00 (dt,5.8,8.9)	62.6		92.9
9α	3.77 (dd,5.8,8.9)	72.0	4.02 (d,9.3)	76.1
9β	4.45 (t,8.9)		3.85 (d,9.3)	
1'		129.0		131.7
2'	7.03 (d,1.7)	112.7	7.03 (d,1.7)	111.2
3'		148.7		149.0
4'		147.5		147.3
5'	6.77 (d,8.5)	115.7	6.78 (d,8.2)	108.6
6'	6.84 (dd,1.7,8.5)	121.6	6.85 (dd,1.7,8.2)	120.4
7'	4.66 (s)	89.2	4.83 (overlap)	87.7
8'		92.8	3.02 (dt,5.8,8.9)	62.3
9'α	4.04 (d,9.3)	76.1	3.75 (d,6.2,8.9)	72.0
9'β	3.84 (d,9.3)		4.44 (t,8.9)	
-OCH_3	3.86 (s)	56.3	3.85 (s)	56.39
-OCH_2O-	5.93 (s)	102.4	5.92 (s)	102.3

2.2.20. Compound **27**

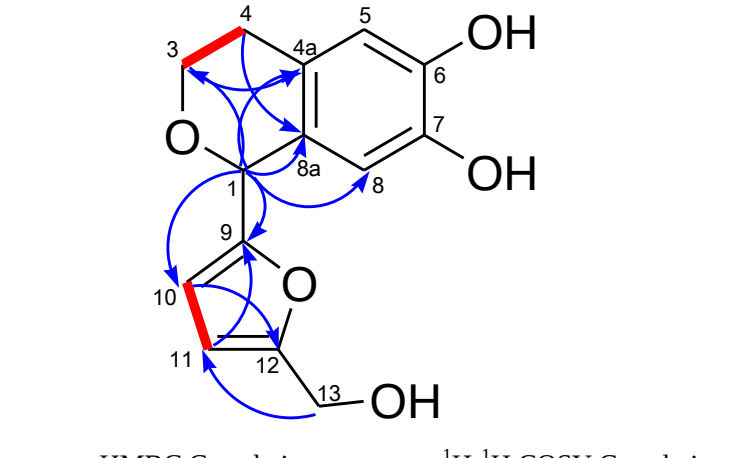

Figure 22 Key HMBC, ^{1}H-^{1}H COSY and NOE correlations of **22**

Compound **27** was obtained as yellow powder. Its molecular formula was determined as $C_{14}H_{14}O_5$ by HRFABMS m/z 261.0759 [M-H]-. The 1H NMR spectrum of two singlet δ_H 6.55 (s) and 6.35 (s), and HMBC correlations from δH 6.55 (H-5) to δ_C 126.1 (C-8a) and δ_C 144.7 (C-7), from δH 6.35 (H-8) to δ_C 126.3 (C-4a) and δ_C 145.8 (C-6) suggested the presence of a aromatic ring. The ^{1}H NMR spectrum of four multiplet at δ_H 2.68 (m), 2.72 (m), 3.96 (m) and 3.80(m), together with ^{1}H-^{1}H COSY correlations between δ_H 3.96 (H-3α) and δ_H 2.68(H-4α), from δH 3.80 (H-3β) to δ_H 2.72 (H-4β), suggested the presence of one oxidized ethyl group, and the HMBC correlations from δ_H 6.55 (H-5) to δC 28.7 (C-4), from δ_H 2.72 (H-4β) to 126.1 (C-8a), and from δ_H 3.80 (H-3β) to δC 126.3 (C-4a) indicated that the oxidized methylene group is located at C-4a of the aromatic ring. The ^{1}H NMR spectrum of a singlet at δ_H 5.66 (s) suggested the presence of one oxidized methine group, and the HMBC correlations from δ_H 5.66 (H-1) to δ_C 114.0 (C-8) and 126.3 (C-4a), indicated that the oxidized methine group is located at C-8a of the aromatic ring. Furthermore, the HMBC correlations from δ_H 5.66 (C-1) to δ_C 63.0 (C-3) confirmed the presence of one isochroman group. The ^{1}H NMR spectrum of one singlet at δ_H 4.47 (2H, s) revealed the presence of one hydroxymethyl group. The remaining signals of two doublet at δ_H 6.08 (d, J = 3.4) and 6.23 (d, J = 3.4) in the ^{1}H NMR spectrum, the ^{1}H-^{1}H COSY correlations between δ_H 6.08 and δ_H 6.23 and the

HMBC correlations from δ_H 6.08 (H-10) to δ_C 156.3 (C-12), from δ_H 6.23 (H-11) to δ_C 156.1 (C-9) were noted. Furthermore, its molecular formula was determined as $C_{14}H_{14}O_5$, indicated the presence of one furyl group. In addition, the HMBC correlations from δ_H 4.47 (H-13) to δ_C 108.9 (C-11) proved that the hydroxymethyl group is located at the C-12 of the furyl group. The HMBC correlations from δ_H 5.66 (H-1) to δ_C 111.7 (C-10) and 156.1 (C-9), indicted the furyl group is located at C-1 of the isochroman group. Thus, compound **27** was determined as shown in **Fig. 22.**

Table11. ^{1}H NMR and ^{13}C NMR Spectral Data of Compounds **27** in CD_3OD.

27					
P.	δ_H (mult, *J* in Hz)	δ_C	P.	δ_H (mult, *J* in Hz)	δ_C
1	5.66 (s)	72.6	7		144.7
3*α*	3.96 (m)	63.0	8	6.35 (s)	114.1
3*β*	3.80 (m)		8a		126.1
4*α*	2.68 (m)	28.7	9		156.1
4*β*	2.72 (m)		10	6.08 (d,3.4)	111.7
4a		126.3	11	6.23 (d,3.4)	108.9
5	6.55 (s)	116.0	12		156.3
6		145.8	13	4.47 (2H,s)	57.5

2.2.21. Compound **28**

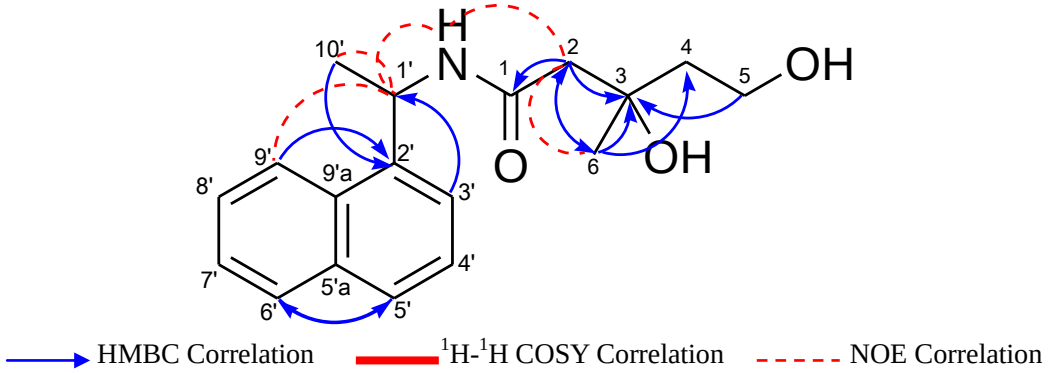

Figure 23 Key HMBC, ^{1}H-^{1}H COSY and NOE correlations of **23**

Compound **28** was obtained as yellow amorphous powder. It was synthesized by K. Mori and K. Okada in 1984 [46] but NMR data was not showed. The 1D NMR spectra of seven protons [δ_H 7.49 (m), 7.44 (dd, J = 7.6, 7.9) , 7.86 (d, J = 7.9) , 7.80 (d, J = 8.3) , 7.55 (m), 7.51 (m), 8.07 (d, J = 8.6)] and carbon signals [δ_C 137.7, 126.7, 125.2, 128.9, 133.2, 128.6, 126.0, 122.6, 123.2, 130.9], suggested the existence of more than one aromatic rings. Correlations observed in HMBC spectrum, from δ_H 8.07 (H-9') to δ_C 126.0 (C-7'), δ_C 133.9 (C-5'a) and δC 137.7(C-2'), from δ_H 7.51 (H-8') to δ_C 130.9 (C-9'a) and δ_C 128.6 (C-6'), from δ_H 7.80 (H-6') to δ_C 122.6 (C-8'), δ_C 130.9 (C-9'a) and δ_C 128.9 (C-5'), from δ_H 7.86 (H-5') to δ_C 128.6 (C-6'), δ_C 130.9 (C-9'a) and δ_C 126.7 (C-3'), from δ_H 7.44 (H-4') to δC 133.9 (C-5'a) and δ_C 137.7 (C-2'), from δ_H 7.49 (H-3') to δ_C 128.9 (C-5') and δ_C 130.9 (C-9'a) revealed presence of one naphthyl group. The 1D NMR spectra and HMQC spectrum revealed the presence of two methyl groups [δ_H 1.27 (3H, s), δC 26.9 and 1.68 (3H, d, J = 6.5), δ_C 20.7], two methylene groups [δ_H 2.46 (m), 2.20 (m), δ_C 46.5, and δ_H 1.77 (m), 1.64 (m), δ_C 42.1], one hydroxymethyl group [δ_H 3.86 (m), 3.76 (m) and δ_C 59.6], one oxidized quaternary carbon [δ_C 72.5], one downfield-shifted methine group and one carbonyl group [δ_C 171.2]. Furthermore, the HMBC correlations from δ_H 1.68 (H-10') to δ_C 137.7 (C-2') and δ_C 44.6 (C-1') and from δ_H 7.49 (H-3') to δ_C 44.6 (C-1') revealed C-1' is located at C-2' of naphthyl group. The HMBC correlations from δ_H 2.46 (H-2α) to δ_C 171.2 (C-1), δ_C 72.5 (C-3) and δ_C 26.9 (C-6), from δ_H 1.27 (H-6) to δ_C 46.5 (C-2), δ_C 72.5 (C-3) and δ_C 42.1 (C-4) and from δ_H 3.86 (H-5α), δ_H 3.76 (H-5β)

to δ_C 72.5 (C-3) indicated the presence of 3,5-dihydroxy-3-methylpentanyl group. In addition, its molecular formula was determined as $C_{18}H_{23}NO_3$ by HRFABMS *m/z* 300.1606 $[M-H]^-$, confirmed the presence of nitrogen. The NOE correlations from δ_H 5.95 (H-1') to δ_H 8.07 (H-9'), 1.68 (H-10') and 6.17 (-NH-), from δ_H 2.46 (H-2α), 2.20 (H-2β) to δ_H 6.17 (-NH-) and 1.27 (H-6) revealed the imino group is located to C-1' and C-1with amido bond. Thus, the structure of **28** was established as in **Fig. 23.**

Table12. ^{1}H NMR and ^{13}C NMR Spectral Data of Compounds **28** in $CDCl_3$.

28					
P.	δ_H (mult, *J* in Hz)	δ_C	P.	δ_H (mult, *J* in Hz)	δ_C
1		171.2	1'	5.95 (m)	44.6
2α	2.46 (d,15.4)	46.5	2'		137.7
2β	2.20 (d,15.4)		3'	7.49 (m)	126.7
3		72.5	4'	7.44 (dd,7.6,7.9)	125.2
4α	1.77 (m)	42.1	5'	7.86 (d,7.9)	128.9
4β	1.64 (m)		5'a		133.9
5α	3.86 (m)	59.6	6'	7.80 (d,8.3)	128.6
5β	3.76 (m)		7'	7.55 (m)	126.0
6	1.27(s)	26.9	8'	7.51 (m)	122.6
-NH-	6.17 (d,7.9)		9'	8.07 (d,8.6)	123.2
10'	1.68(d,6.5)	20.7	9'a		130.9

2.2.22. Compound **31**

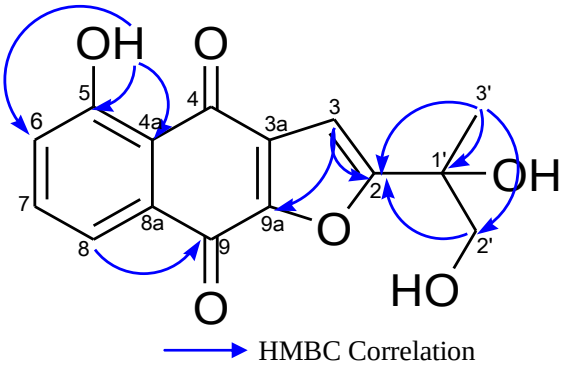

Figure 24 Key HMBC correlations of **24**

Compound **31** was obtained as yellow needles. The IR spectrum showed strong absorptions for hydroxy (3450 cm-1) and carbonyl (1645 cm-1) functionalities; and it's UV spectrum, with absorptions at 249 and 296 nm, indicated that it was a naphthoquinone derivative [26,47]. The 13C NMR spectrum showed two carbonyl signals at δ_C 186.5 and 172.6. The ^{1}H NMR spectrum in CDCl3 showed proton signals at δ_H 12.15 (1H, s) and 7.72 (1H, dd, J = 0.7; 7.2 Hz), 7.59 (1H, t, J = 7.2; 8.3 Hz), 7.25 (1H, dd, J = 0.7; 8.3 Hz) and 6.93 (1H, s). The data given above indicate that it is furanonaphthoquinone containing a peri-hydroxyl group **[3]**. The HMBC correlations from δ_H 7.72 (1H, dd, J = 0.7; 7.2 Hz) (H-8) to δ_C 125.3 (C-6), 115.2 (C-4a), from δ_H 7.59 (1H, t, J = 7.2; 8.3 Hz) (H-7) to δ_C 162.3 (C-5), 131.9 (C-8a), from δ_H 7.25 (1H, dd, J = 0.7; 8.3 Hz) (H-6) to δ_C 120.0 (C-8), 115.2 (C-4a) confirmed the presence of a aromatic ring. The HMBC correlations from δ_H 12.15 (1H, s) (-OH) to δ_C 125.3 (C-6), 115.2 (C-4a), 162.3 (C-5) indicated that the hydroxyl group is located at C-5 of the aromatic ring. The 1H NMR spectrum of a singlet at δ_H 1.59 (3H, s) and two doublets at δ_H 4.04 (1H, d, J =11.0 Hz), δ_H 3.73 (1H, d, J =11.0 Hz), together with HMBC correlations from δ_H 1.59 (3H, s) (H-3') to δ_C 165.9 (C-2), 72.5 (C-1'), 68.7 (C-2'), from δ_H 3.73 (1H, d, J =11.0 Hz) (H-2') to δ_C 165.9 (C-2), indicated the presence of 1,2-dihydroxypropyl group. Furthermore, the HMBC correlations from δ_H 6.93 (1H, s) (H-3) to δ_C 165.9 (C-2), 152.1 (C-9a), from δ_H 7.72 (1H, dd, J = 0.7; 7.2 Hz) (H-8) to δ_C 172.6 (C-9) indicated the structure of compound 3 (Fig. 1). In addition, its molecular formula which was determined as $C_{15}H_{12}O_6$ by

HREIMS m/z 288.0635, confirmed its structure in **Fig. 24.**

Table13. ^{1}H NMR and ^{13}C NMR Spectral Data of Compounds **31** in $CDCl_3$.

31		
Position	δ_H mult (*J* Hz)	δ_C
2		165.9
3	6.93 s	104.7
3a		132.7
4		186.5
4a		115.2
5		162.3
6	7.25 dd (0.7, 8.3)	125.3
7	7.59 dd (7.2, 8.3)	136.3
8	7.72 dd (0.7, 7.2)	120.0
8a		131.9
9		172.6
9a		152.1
1'		72.5
2'α	4.04 d (11.0)	68.7
2'β	3.73 d (11.0)	
3'	1.59 s	23.6
5-OH	12.15 s	

2.3. Identification of the known compounds

The 11 known compounds, 2-formyl-5-(4'-methoxybenzoyl- oxy)-3-methyl-2-cyc lopentene-1-acetaldehyde (**2**) [42], 2-formyl-5-(3',4'-dimethoxybenzoyloxy)-3-methyl -2-cyclopentene-1-acetaldehyde(**3**) [42], epipinoresinol (**22**) [48], pinoresinol (**23**) [48], (+)-balanoponin (**24**) [49], salicifoliol (**25**) [50], and 3-deoxy-artselaenin (**26**) [51], 2-a cetyl-naphtho[2,3-b]furan-4,9-dione (**29**) [52], 5-hydroxy-2-(1-hydroxy-ethyl)-naphth o[2,3-b]furan-4,9-dione (**30**) [26], 8-hydroxy-2-(1-hydroxy-ethyl)-7-methoxy-naphtho [2,3-b]furan-4,9-dione (**32**) [52] were identified by comparing their spectroscopic data with those in the previous report.

2.4. Furanonaphthoquinones from *T. avellanedae* induce cell cycle arrest and apoptosis in the human non-small cell lung cancer cell line A549

2.4.1. Cytotoxic effects of compounds (**29**-**32**) on A549, MCF-7 and SiHa cells

To determine the cytotoxic effects of the compounds (**29**-**32**) isolated from *T. avellanedae*, we first evaluated their effects on cell growth of A549, MCF-7 and SiHa cells. Results showed that compounds **29**, **30** and **31** caused dose-dependent decreases in cell viability in all the cell lines; whereas the cells used in this study did not die significantly even at the highest concentration (13.5 μM) of compound **32**. IC_{50} values (μM) of compounds (**29**-**32**) on A549, MCF-7 and SiHa cells assessed by MTT assay are presented in **Table 14**. Furthermore, results indicated that the presence of a phenolic hydroxyl group at C-5 seems to play an important role in increasing anti-proliferative effect, which has been supported by the previous report [20].

Table14. IC_{50} (μM) values for compounds (**29**-**32**) on A549, MCF-7 and SiHa cell lines (mean ± S.D., n=3)

	cell line		
	A549	MCF-7	SiHa
DOX	0.07±0.004	0.62±0.06	0.27±0.01
29	1.95±0.31	2.97±0.41	3.40±0.60
30	0.50±0.06	0.89±0.11	1.16±0.32
31	1.12±0.13	1.89±0.40	2.01±0.40
32	10.16±0.36	>13.50	>13.50

2.4.2. Effects of compounds (**30**, **31**) on cell cycle and cell cycle-associated proteins.

Cell cycle plays an important part in the processes of cell proliferation and growth as well as of cell division. It typically divided into four phases. The period

associated with DNA synthesis (S phase) and mitosis (M phase) are separated by gaps of varying length (G1 phase and G2 phase) [53]. It governs the transition from quiescence to cell proliferation, and through its checkpoints, ensures the fidelity of the genetic transcript. One of the hallmarks of cancer is the malfunction within the regulation of cell cycle, such that injured or mutated cells which are normally killed are allowed to progress the cell cycle [54]. Moreover, unlike normal cells that rely on the G1 checkpoint to protect against DNA damage, cancer cells are more dependent on the G2 checkpoint for DNA damage repair [55]. Cell cycle arrest is an important way to inhibit the proliferation of cancer cells except for apoptosis, and is considered as a potential approach for cancer treatment [56]. Therefore, cell cycle was evaluated after treatment of compounds (**30**, **31**). **Fig. 26** showed that exposure of A549 to compound **30** or compound **31** resulted in significant increased distributions in the G2/M phase and S phase accompanied by a decreased distribution in the G1 phase time-dependently. The cell percentages of G2/M phase and S phase increased by 2.5-fold and 2.8-fold, respectively, after 48h treatment of compound **30**, and increased by 3.3-fold and 1.9-fold, respectively, after 48h treatment of compound **31**, while the cell percentage of G1 phase decreased by 3.3-fold after 48h treatment of compound **30** and decreased by 2.5-fold after 48h treatment of compound **31**.

The cell cycle progression depends on a cascade of enzymes by sequential activation and inactivation of cyclins, cyclin-dependent kinases (CDK) and cyclin-dependent kinase inhibitors (CDIs) [57]. The controlled function of these cell cycle regulatory proteins is an important means of inhibition of cancer cell growth and division [57]. During late S phase and throughout G2 phase, cells prepare for mitosis by increasing levels of cyclins A and B, whereas for cell to exit mitosis, cyclins A and B must be degraded [53,57]. Progression from G1 to S phase in mammalian cells is promoted by the accumulation of cyclins D, E and A which bind to and activate different CDK catalytic subunits [57]. Therefore, effects of compounds (**30**, **31**) on cell cycle regulatory molecular, including cyclins A, B and D were determined subsequently. **Fig. 27** showed that the protein expression of cyclin A and cyclin B1 in A549 cells was significantly down-regulated after 24 h of exposure and maintained at

an extremely low level after 30 h of exposure. In addition, decreased D1 protein level was also observed after 36 h of exposure.

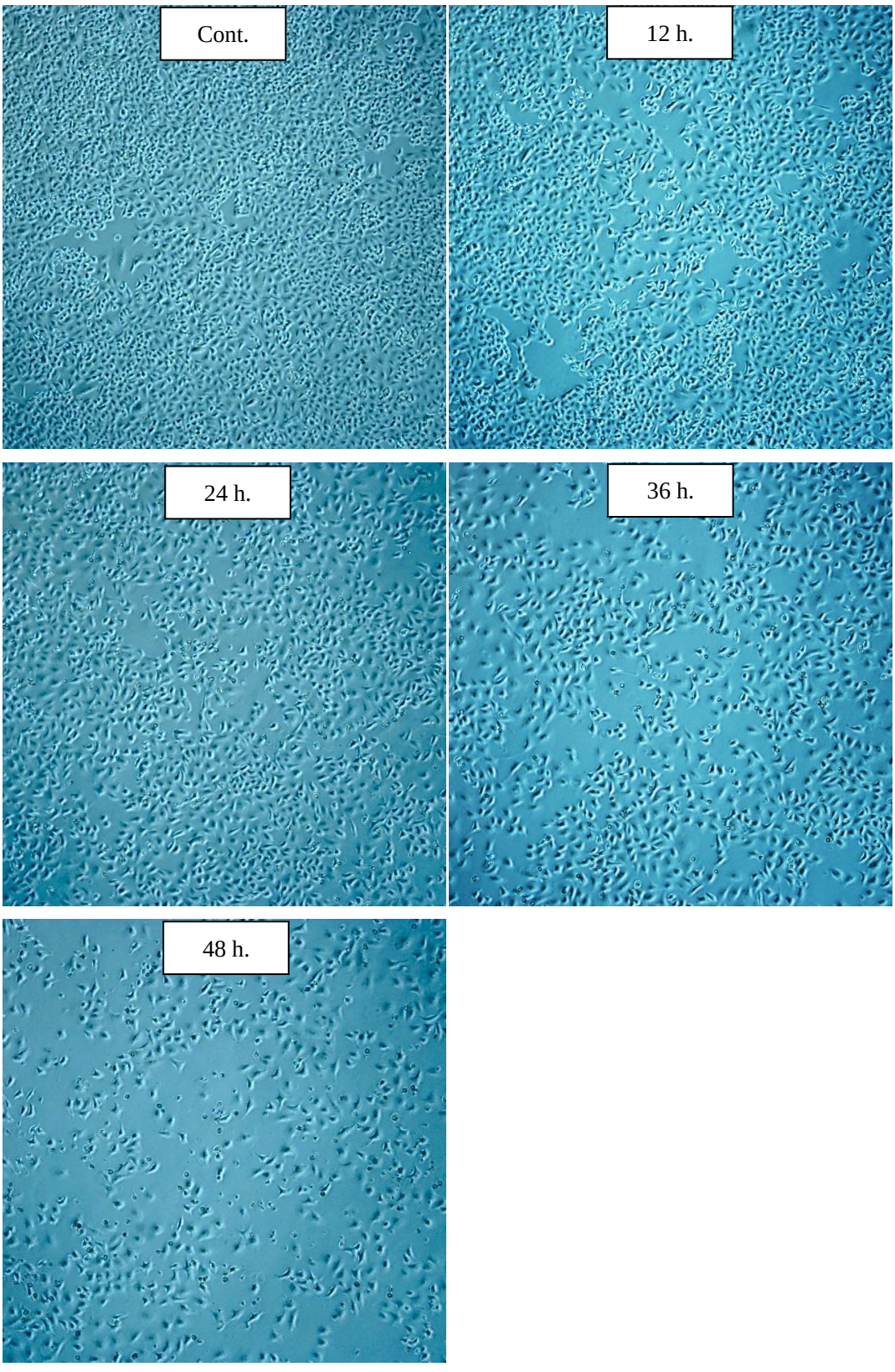

Figure 25. The cell morphology of A549 cells after treatment with compound **31**

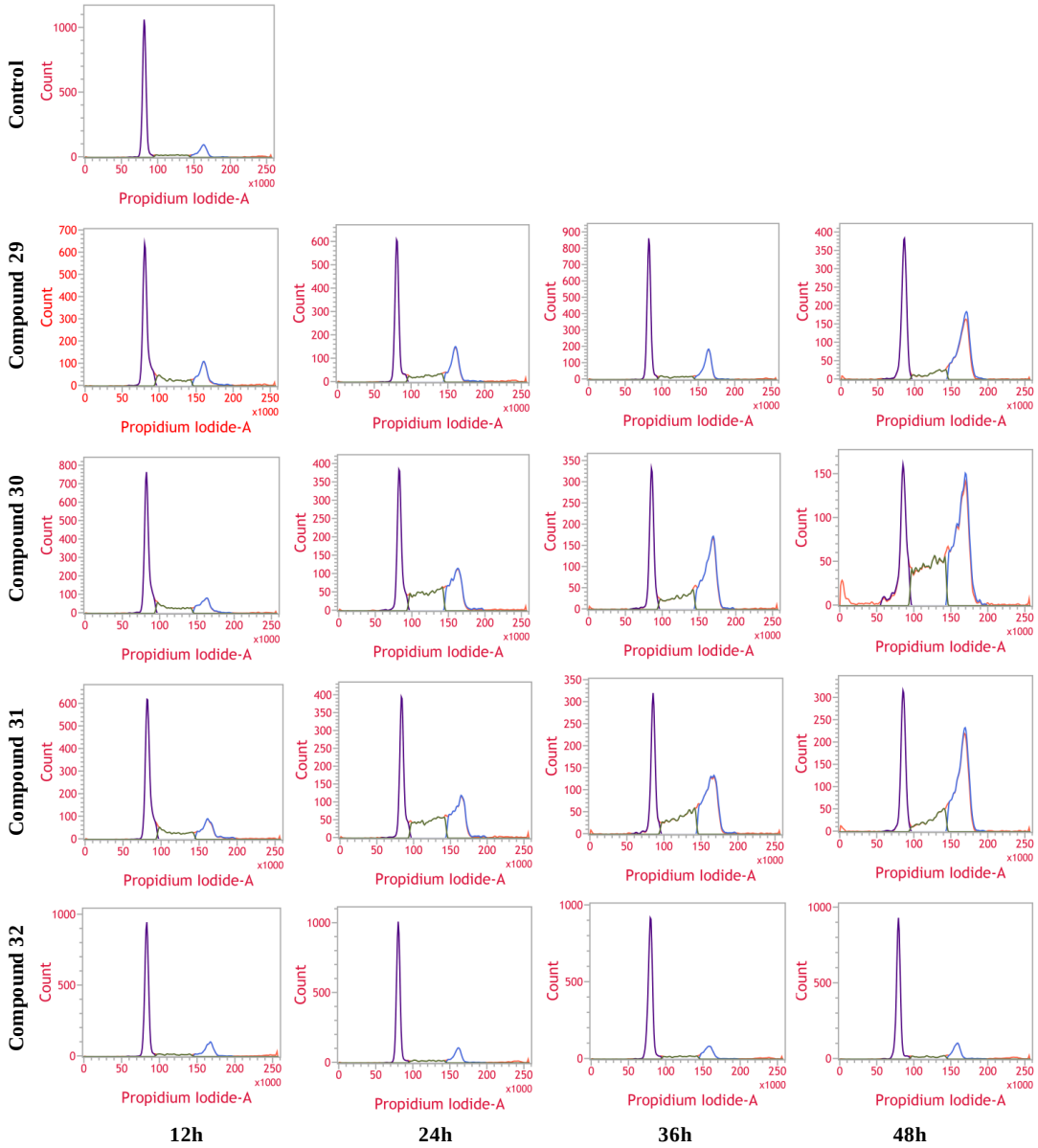

Figure 26. Induction of S and G2/M cell cycle arrest of A549 cells by compounds (**29**-**32**) from *Tabebuia avellanedae* (mean ± S.D., n=3). Significance: * $p<0.05$ versus the control (0h); ** $p<0.01$ versus the control (0h).

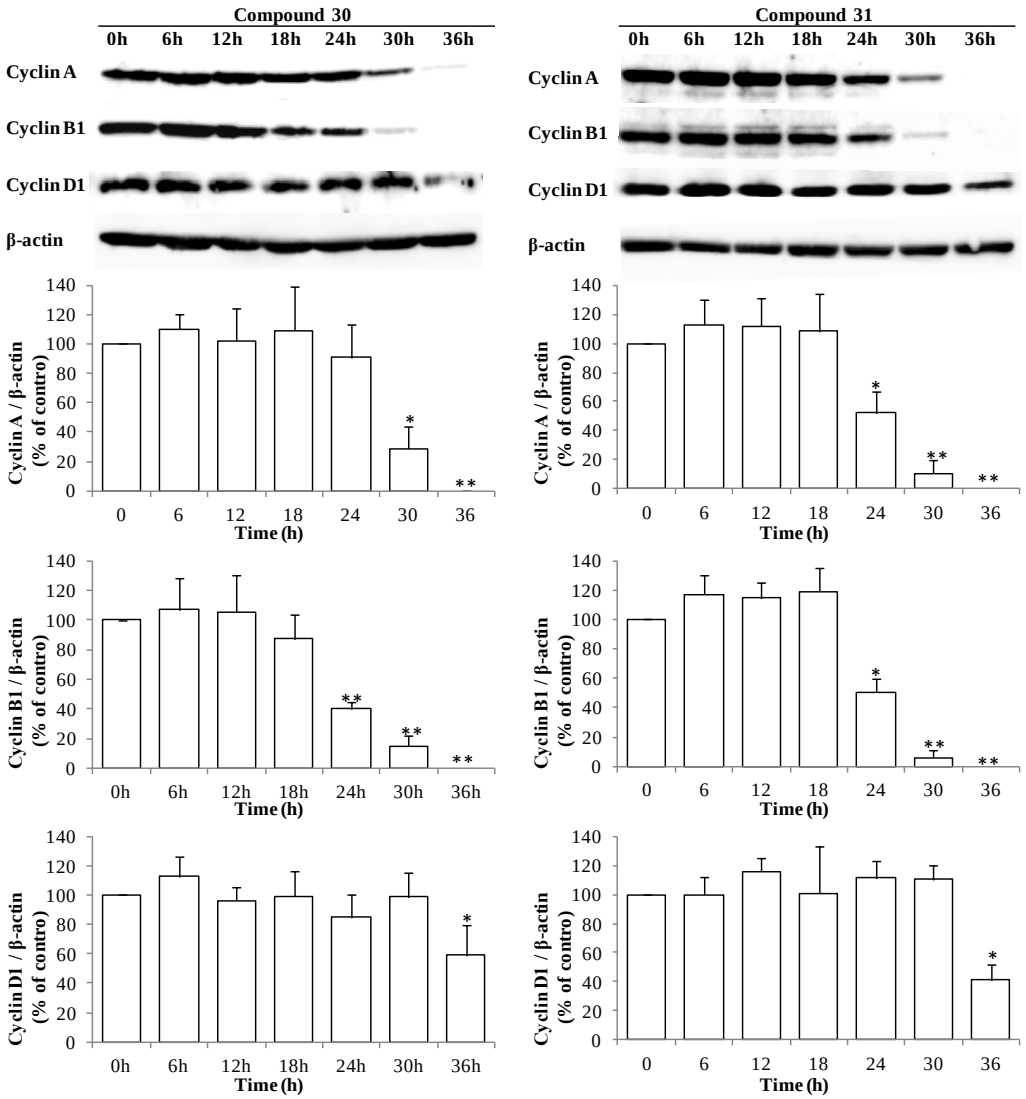

Figure 27. Down-regulation of cell cycle-associated protein expression in A549 cells treated with compounds (**30**, **31**) from *Tabebuia avellanedae* (mean ± S.D., n=3). Significance: * $p<0.05$ versus the control (0h); ** $p<0.01$ versus the control (0h).

2.4.3. Effects of compounds (**30**, **31**) on apoptosis and apoptotic markers

Apoptosis (programmed cell death) is the essential mechanism in the development and homeostasis of multi-cellular organisms to eliminate unwanted cells [58]. In addition, apoptosis can prevent carcinogenesis by eliminating damaged cell or inhibiting abnormal cell development. Therefore, the induction of apoptosis of cancer cells plays crucial roles in the anticancer properties of many anticancer agents. We invested whether the inhibited cell viability induced by compounds (**30**, **31**) was associated with apoptosis via double staining of PI and annexin V-FITC. As shown in **Fig. 28**, compound **30** and compound **31** induced apoptosis in a time-dependent manner. The quantitative analysis showed the apoptosis rates (early and late) of compound **30** and compound **31** were 17.0% and 5.0% after 36h of treatment, and 22.8% and 26.6% after 48h of treatment, respectively.

Apoptosis is controlled by a large number of genes acting as death switches. To further elucidate the underlying mechanisms; we then detected some apoptotic markers in A549 cells treated with compounds (**30**, **31**). Tumor suppressor P53 plays a crucial role in cell cycle progression, DNA repair and apoptosis [59]. Tumor cells in which P53 is inactive can bypass the G1/S checkpoint and fail to arrest and repair their damaged DNA [57]. P53 can also suppress G2/M transition as a primary component of the G2 check point. Moreover, P53 can regulate the balance of BCL-2 family members, which are considered to be the key regulators of apoptosis [60,61]. The BCL-2 family includes both pro-apoptotic (e.g. BAX) as well as anti-apoptotic (e.g. BCL-2) molecules, and they seem to spend most of their time simply to block each other's next move. The balance between their competing activities is a major checkpoint in the common portion of the mammalian cell death pathway and determines cell fate: survival or death.[62] Downstream of this checkpoint are two major execution programs: the caspase pathway and mitochondrial dysfunction. Mitochondrial dysfunction includes a change in the mitochondrial membrane potential, production of reactive oxygen species, opening of the permeability transition pore and the release of the inter-membrane space protein, cytochrome *c*.

Released cytochrome *c* activates Apaf-1, which in turn activates a downstream caspase program. Activated caspases can also affect the function of mitochondria. Caspases could be activated through Apaf-1/cytochrome *c* or directly by activation of cell surface death receptors. [63] Caspase activation serves as a final common channel for both pathways of apoptosis [64]. The activated caspase (e.g. caspase-3) cleaves death substrates, which ultimately leads to cell death [65]. **Fig. 29** demonstrated that compound **30** and compound **31** induced rapid increases in P53 mRNA level from about 6-12 h after treatment, followed by apparent up-regulation of BAX at 36 h after treatment with no effect on BCL-2. **Fig. 30** showed that both compound **30** and compound **31** induced the activities of caspase-3 in a time-dependent way.

In conclusion, compound **30** and compound **31** inhibited the cell viability of all three cell lines, with cell cycle arrest at G2/M and S phase through the down-regulation of cell cycle dependent proteins such as cyclins A, B1, D1, along with induction of apoptosis through the up-regulation of P53 and BAX, and activation of caspase-3. These furanonaphthoquinones isolated from *T. avellanedae* are promising leads for potential anticancer drugs.

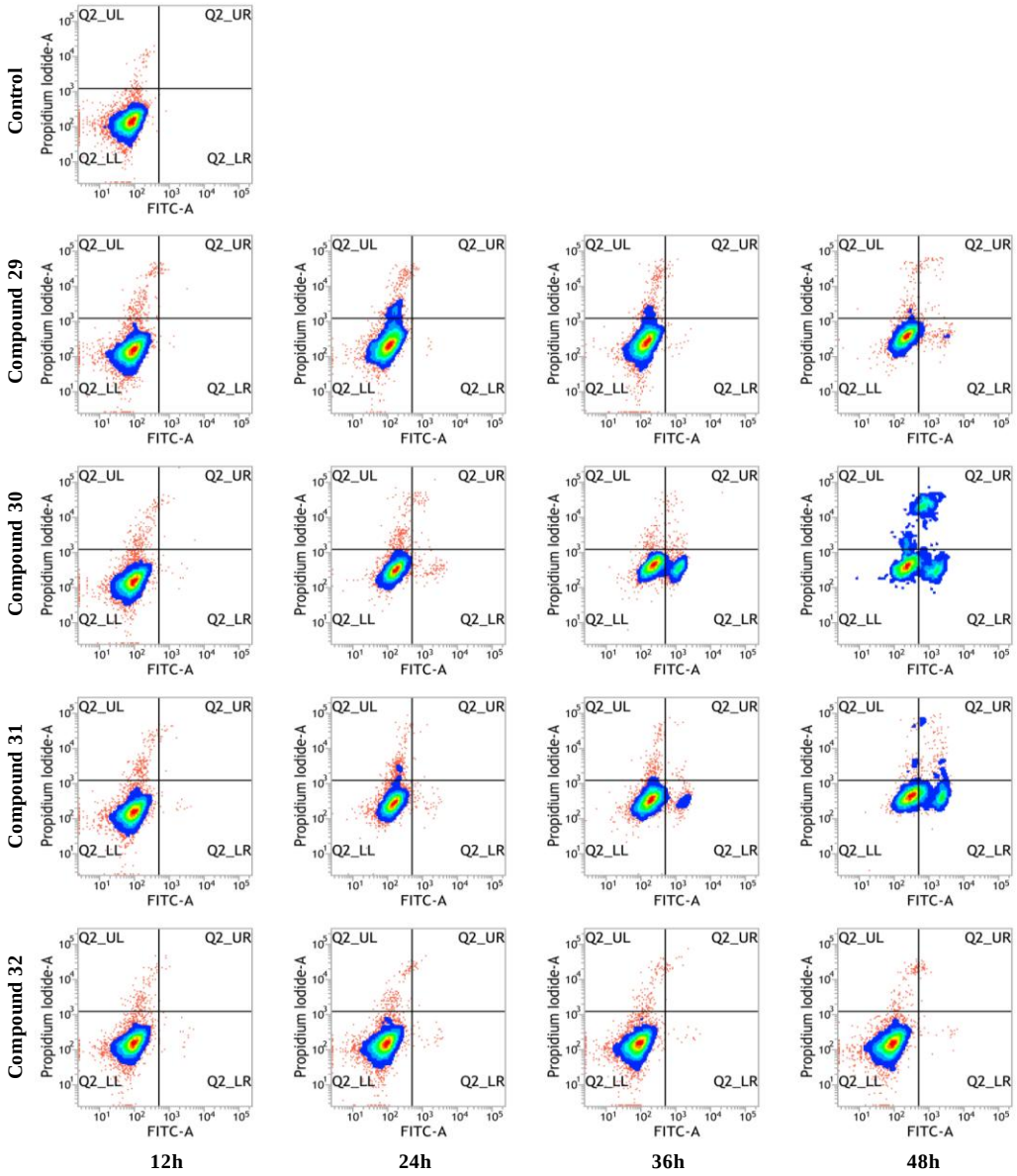

Figure 28. Induction of apoptosis of A549 cells by compounds (**29**-**32**) from *Tabebuia avellanedae* (mean ± S.D., n=3). Significance: * $p<0.05$ versus the control (0h); ** $p<0.01$ versus the control (0h).

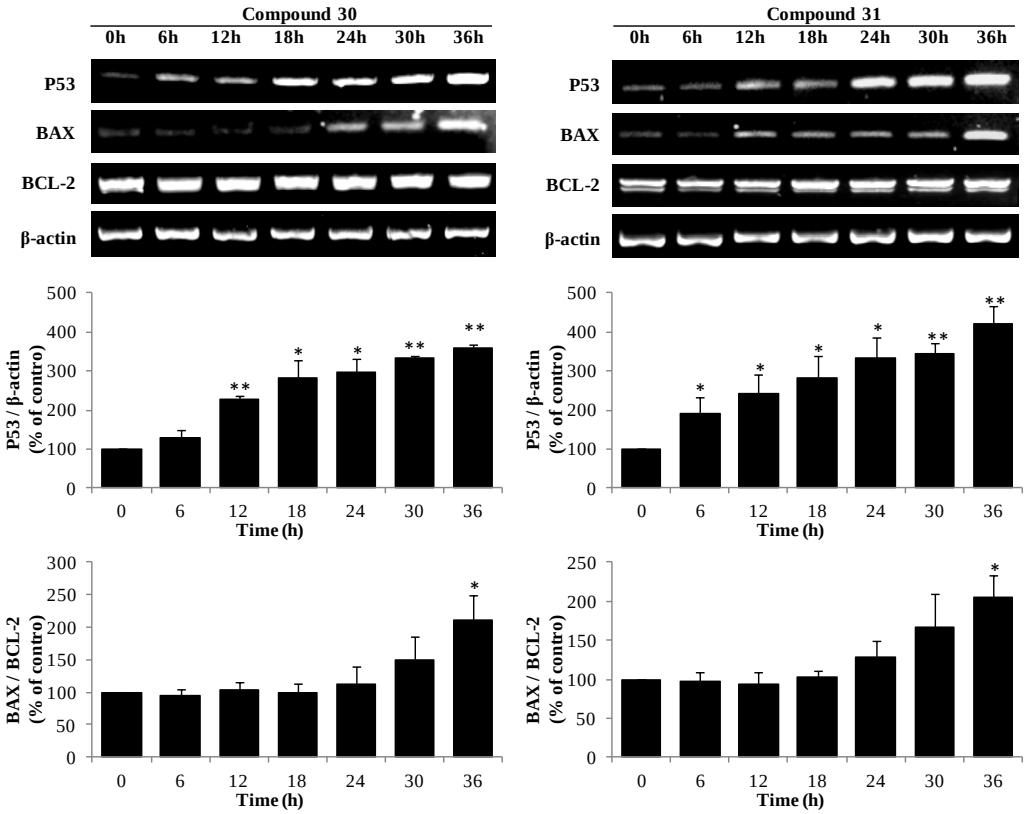

Figure 29. Alterations in mRNA expression of apoptosis-related genes P53, BAX and BCL-2 in A549 cells treated with compounds (**30**, **31**) from *Tabebuia avellanedae* (mean ± S.D., n=3). Significance: * $p<0.05$ versus the control (0h); ** $p<0.01$ versus the control (0h).

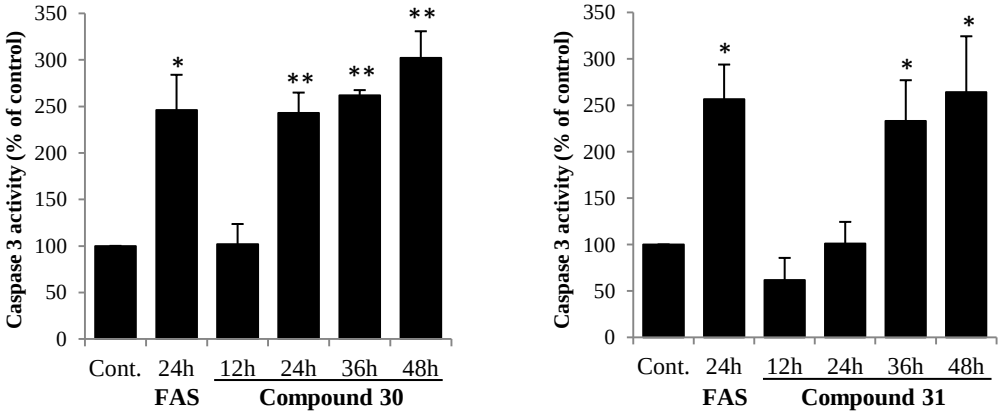

Figure 30. Activation of caspase-3 enzyme of A549 cells by compounds (**30**, **31**) from *Tabebuia avellanedae* (mean ± S.D., n=3). Significance: * $p<0.05$ versus the control (0h); ** $p<0.01$ versus the control (0h).

2.5. Compounds from *T. avellanedae* suppress inflammatory productions in the LPS-activated mouse leukaemic monocyte macrophage cell line RAW 264.7 as well as on the LPS-activated macrophages from BCG infected C3H/HeN mouse

Inflammation is one example of a group of host-defensive mechanisms known as innate immunity. This mechanism is an immunological response following bacterial and viral infection, and is primarily mediated by phagocytic macrophages, which are a type of differentiated tissue cells arising from blood monocytes. The inflammatory response involves the activation of several immune cells such as monocytes and macrophages which secrete a series of pro-inflammatory mediators such as enzymes, cytokines, chemokines as well as signalling proteins at the site of infected tissues and cells. During inflammatory responses, numerous intracellular and extracellular signals, antigen receptors and pro-inflammatory cytokines activate janus kinase (JAK)/signal transducer and activator of transcription (STAT), phosphatidylinositol 3- kinases (PI3K)/Akt, mitogen-activated protein kinases3 and nuclear factor-kappa B (NF-kB) signaling pathways. [66-69] Although these signaling pathways are important to regulate physiological functions under normal condition, their aberrant activation is associated with a wide range of inflammatory and immune disorders, and cancer. [68,70,71] Therefore, the effective blockade of the production of inflammatory mediators in macrophages is regarded as an important therapeutic target.

Macrophages are known to play a key role in host defense mechanism, and activated by exposure to interferon-γ, pro-inflammatory cytokines, and bacterial lipopolysaccharides (LPSs). [72,73] The favorite model used to study induced inflammation both in vitro and in vivo is the stimulation of macrophages by LPS obtained from Gram-negative bacteria[74-76]. In case of activation, they become potent secretory cells that release a cluster of mediators, including pro-inflammatory and cytotoxic cytokines and growth factors, bioactive lipids, hydrolytic enzymes, reactive oxygen species (ROS), and nitric oxide (NO), all of which have been implicated in the

pathogenesis of tissue injury [77]. In this research, two kind of LPS-activated macrophages were used to investigate the anti-inflammatory effects of compounds from *T. avellanedae.*

2.5.1. Effects of compounds on inflammatory factors of NO, PGE_2 and TNF- α in the RAW 264.7 cell line

Inflammation is an essential aspect of the host's response to infection and injury to maintain a healthy state. However, excessive or aberrant inflammation leads to the up-regulation of several kinds of pro-inflammatory enzymes such as nitric oxide synthase (NOS) and cyclooxygenase (COX) as mediators of inflammation in affected inflammatory cells. NOSs are comprised of three members, including endothelial NOS (eNOS), neuronal NOS (nNOS), and inducible NOS (iNOS), which makes NO from L-arginine, and COX exists as two isozymes, COX-1 and COX-2, converting arachidonic acid into prostaglandins (PGs). Among them, iNOS and COX-2 are highly expressed in response to inflammatory inducers, and are responsible for the production of a huge amount of NO and prostaglandin E2 (PGE2), respectively [78-80] It has been hypothesized that inhibition of excessive NO and PGE2 in macrophages could serve as the basis for potential drug development against inflammatory diseases. [81-83] The anti-inflammatory properties of compounds were investigated on the RAW 264.7 cell line. Results showed that LPS triggered macrophage activation and induced the rise in the production of inflammatory mediators of NO and PGE2, and all of the compounds exclude compound **1** can down-regulate the NO in a dose-dependent manner, while all of the compounds exclude compound **3** and **10** can down-regulate the PGE2 weakly, and 50 μg/ml of compound **3** and **10** can down-regulate the PGE2 strongly (**Fig. 31, 32**).

The inflammatory response is also well characterized by the abundant production of pro-inflammatory cytokines, such as interleukin-1β (IL-1β) and tumor necrotic factor-α (TNF-α). They are also mainly produced in activated macrophages by inflammatory inducers. In particular, TNF-α exhibited its pro-inflammatory activity

by regulating several intercellular and vascular cell-adhesion molecules, resulting in the recruitment of leukocytes to sites of inflammation [84,85]. TNF-α is also important for stimulating the secretion of other inflammatory cytokines, which, in turn, causes many clinical problems associated with autoimmune disorders [84,85]. In addition, TNF-α is a multi-functional cytokine involved in the signaling pathways implicated in inflammation, immunity, cell survival, and even tumorigenesis. Such findings suggest that the inhibition of TNF-α production could be a useful approach as a treatment strategy for various inflammatory diseases. In the current investigation, the concentrations of TNF-α were markedly increased after treatment with LPS in RAW 264.7 macrophages, but all these compounds used in this research had no effect on the TNF-α lever (**Fig. 33**). In addition, all tested compounds showed no cytotoxic effects on RAW 264.7 macrophages (**Fig. 34**).

2.5.2. Effects of compounds on inflammatory factors of NO, PGE_2 and TNF- α in the LPS-activated macrophages from BCG infected mouse.

The activation of murine macrophages by Bacille Calmette Guerin (BCG) has been particularly well studied [86]. The anti-inflammatory properties of compounds were also investigated in LPS-activated macrophages from BCG infected mouse. We found that LPS triggered macrophage activation and induced the rise in the production of inflammatory mediators of NO and PGE2 and TNF-α. In the current investigation, all of the compounds exclude compound **1** can down-regulate the NO in a dose-dependent manner, and all of the compounds can down-regulate the PGE2 in a dose-dependent manner (**Fig. 35, 36**), but almost all these compounds used in this research had no effects on the TNF-α lever (**Fig. 37**). The 12.5 μg/ml of compound **20** decreased the lever of TNF-α, but it seems to because of suppression of the cell viability (**Fig. 32**). In addition, 50 μg/ml of **6**, **8** and **13** showed cytotoxic effects on LPS-activated macrophages from BCG infected mouse (**Fig. 38**).

In conclusion, data presented in this research indicated that the tested compounds from *T. avellanedae* may negatively exert a significant anti-inflammatory effect on

LPS-mediated inflammatory responses. Most of them significantly blocked the production of NO and PGE2 but not TNF-*α* without altering cell viability (except for **6**, **8**, **13** on mcrophages from mouse). From these data, NO production seemed to be the most pharmacologically relevant target of *T. avellanedae*, as the *in vitro* inhibitory potency of them was stronger in NO production than in PGE2 production. These results suggest that *T. avellanedae*'s ethnopharmacological actions (treating inflammatory diseases) was based on the constituents which could mediated NO and other inflammatory mediators (e.g. PGE2).

The activation of murine macrophages by Bacille Calmette Guerin (BCG) has been particularly well studied [86]. The anti-inflammatory properties of compounds were also investigated in LPS-activated macrophages from BCG infected mouse. We found that LPS triggered macrophage activation and induced the rise in the production of inflammatory mediators of NO and PGE2 and TNF-*α*. In the current investigation, all of the compounds exclude compound **1** can down-regulate the NO in a dose-dependent manner, and all of the compounds can down-regulate the PGE2 in a dose-dependent manner (**Fig. 35, 36**), but almost all these compounds used in this research had no effects on the TNF-α lever (**Fig. 37**). The 12.5 μg/ml of compound **20** decreased the lever of TNF-α, but it seems to because of suppression of the cell viability (**Fig. 32**). In addition, 50 μg/ml of **6**, **8** and **13** showed cytotoxic effects on LPS-activated macrophages from BCG infected mouse (**Fig. 38**).

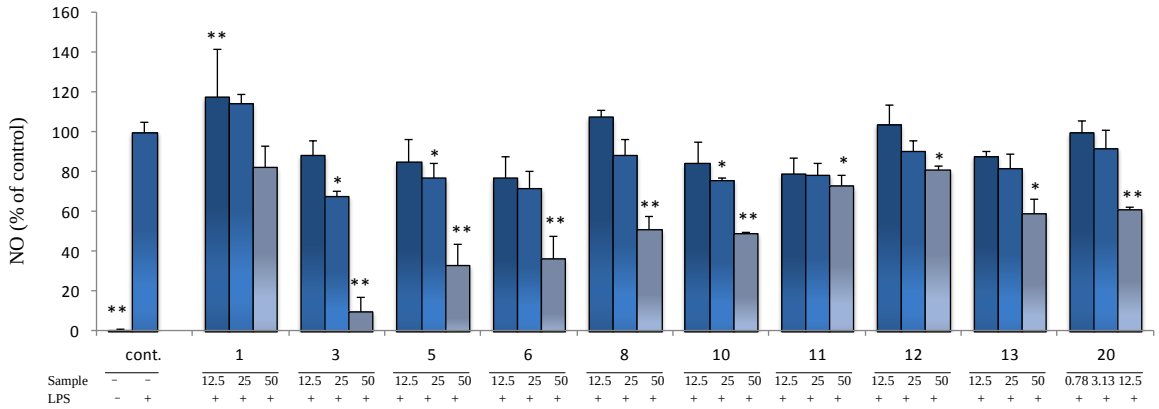

Figure 31. Effect of compounds on the production of NO in LPS-activated RAW264.7 cells (n=3). *P<0.05, **P<0.01 represents significant difference compared to LPS alone.

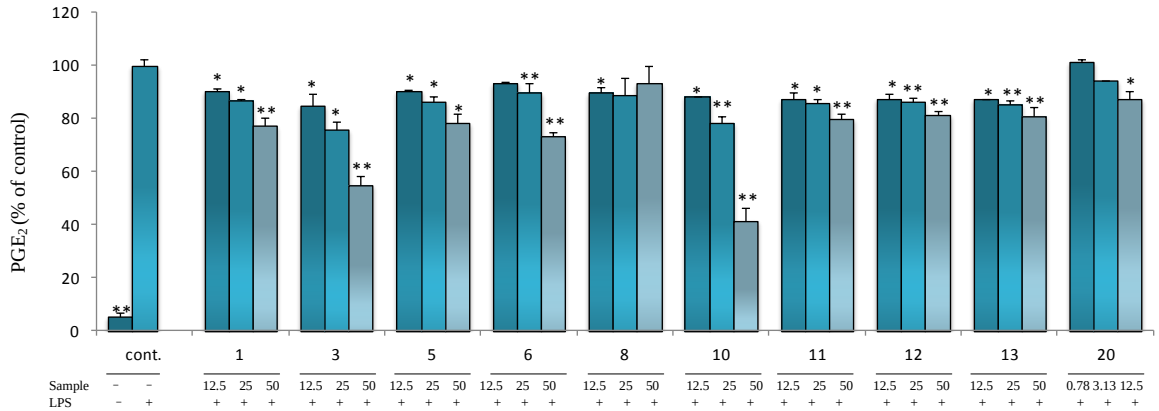

Figure 32. Effect of compounds on the production of PGE_2 in LPS-activated RAW264.7 cells (n=3). *P<0.05, **P<0.01 represents significant difference compared to LPS alone.

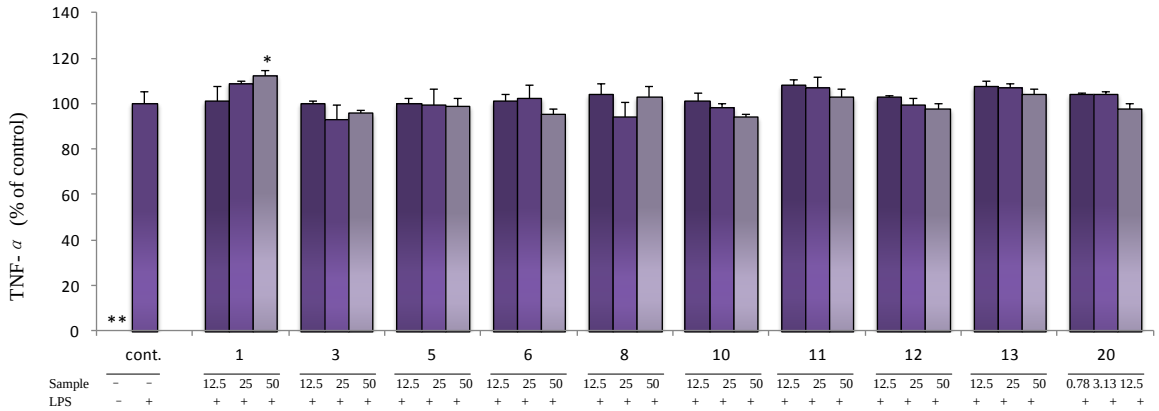

Figure 33. Effect of compounds on the production of TNF-α in LPS-activated RAW264.7 cells (n=3). *P<0.05, **P<0.01represents significant difference compared to LPS alone.

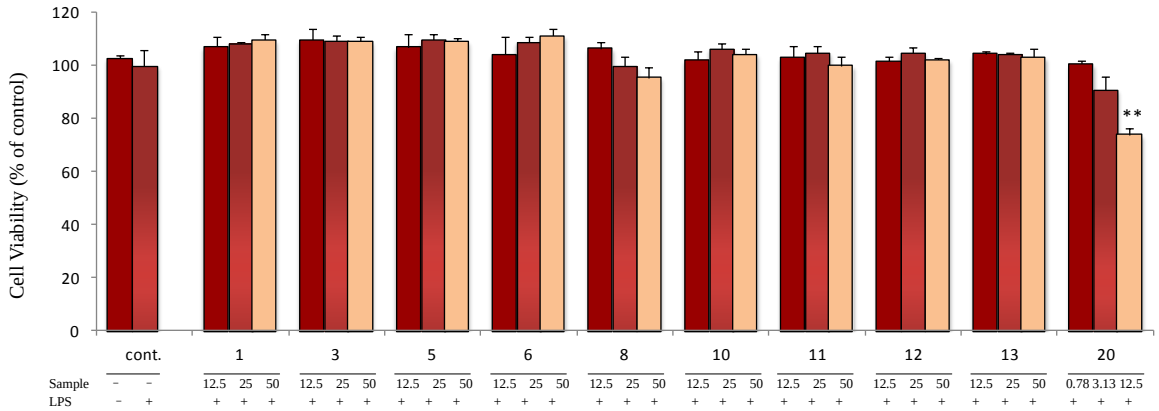

Figure 34. Effect of compounds on RAW264.7 macrophage viability (n=3). *P<0.05, **P<0.01 represents significant difference compared to LPS alone.

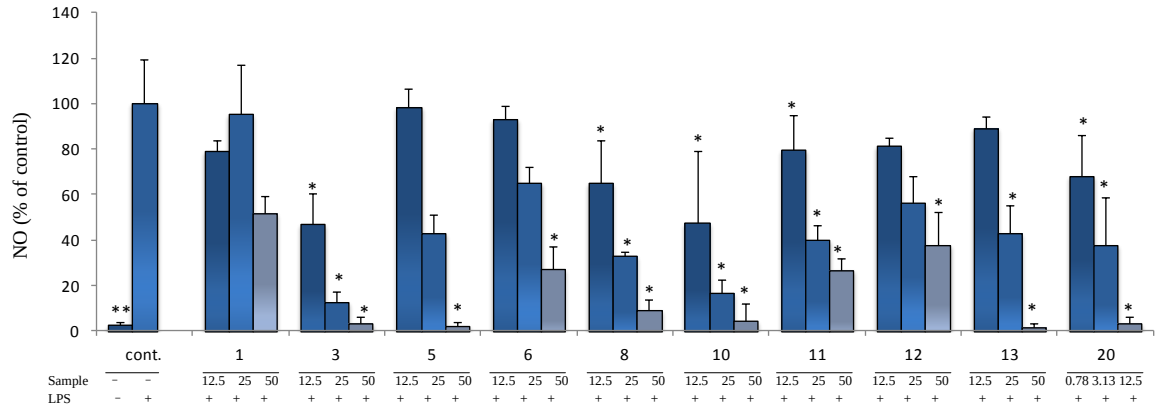

Figure 35. Effect of compounds on the production of NO in the LPS-activated macrophages from BCG infected C3H/HeN mouse (n=3). *P<0.05, **P<0.01 represents significant difference compared to LPS alone.

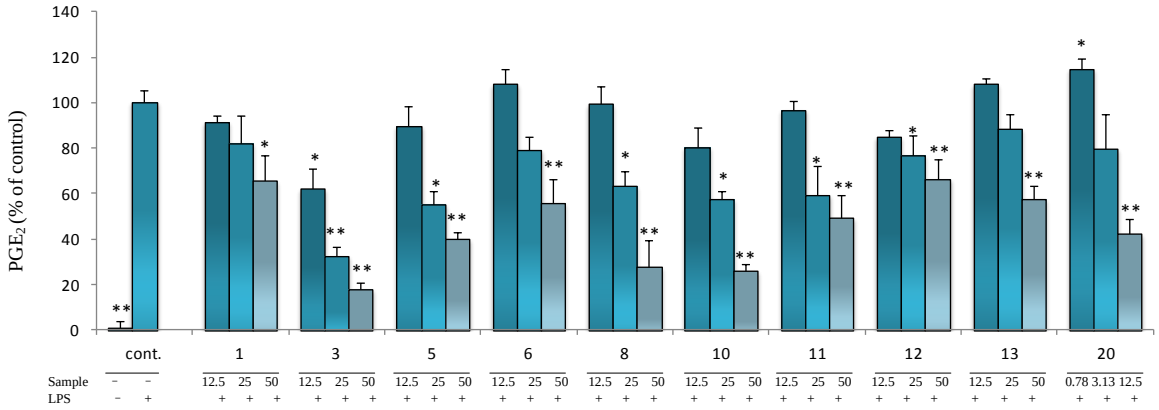

Figure 36. Effect of compounds on the production of PGE_2 in the LPS-activated macrophages from BCG infected C3H/HeN mouse (n=3). *P<0.05, **P<0.01 represents significant difference compared to LPS alone.

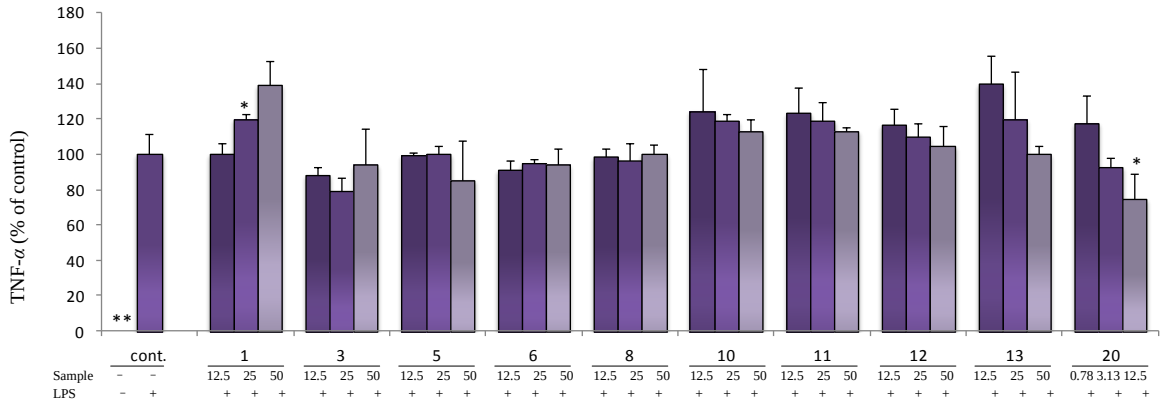

Figure 37. Effect of compounds on the production of TNF-α in the LPS-activated macrophages from BCG infected C3H/HeN mouse (n=3). *P<0.05, **P<0.01 represents significant difference compared to LPS alone.

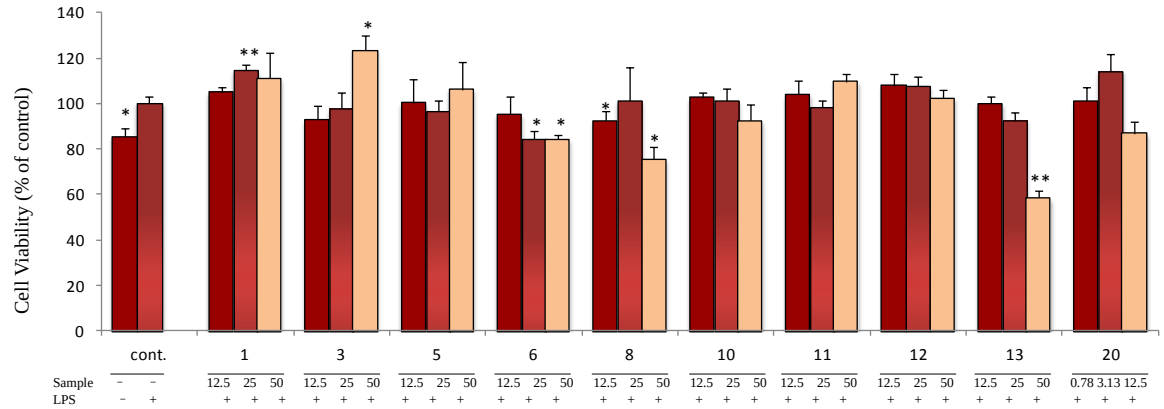

Figure 38. Effect of compounds on the viaility of macrophages from BCG infected C3H/HeN mouse (n=3). *P<0.05, **P<0.01 represents significant difference compared to LPS alone.

3. SUMMARY

In this research, 22 new compounds together with 10 known compounds were isolated from water extract and methanol extract of inner bark of *T. avellanedae*, and the chemical structures and relative configurations of the new compounds were determined by 1D, 2D NMR and MS spectroscopic analyses.

A series of furanonaphthoquinones, including a new furanonaphthoquinone and four furanonaphthoquinones, based on the naphtho[2,3-b]furan-4,9-dione skeleton were obtained from water extract of the inner bark of *T. avellanedae*. The anti-cancer activities of these four furanonaphthoquinones were investigated in this research. **30** and **31** produced cytotoxicity in A549, SiHa and MCF-7 cells at micromolar concentrations. Furthermore, cell cycle analysis was evaluated by PI staining and apoptosis was determined by annnexin-V FITC/PI staining using flow cytometry analysis, and results showed that **30** and **31** induced cell cycle arrest and apoptosis at G2/M phase in A549 cells. Investigation of the cyclin protein family members by Western blotting showed that cyclin A and cyclin B protein levels were strongly decreased with the increasing time of incubation with **30** and **31**, which may be the major factor caused G2/M phase arrest. Reverse transcription polymerase chain reaction (RT-PCR) analysis demonstrated that following the exposure of A549 cells to **30** and **31**, the level of mRNA expressions of tumor suppressor P53 and apoptotic protein BAX were down-regulated. And the caspase-3 enzyme activity was also higher in **30** and **31** exposed A549 cells. Therefore, these furanonaphthoquinones isolated from *T. avellanedae* are promising leads for potential anticancer drugs.

The anti-inflammatory effects of compounds from *T. avellanedae* were also investigated in this research. Effects of compounds (**1**, **3**, **5**, **6**, **8**, **9**, **10**, **11**, **12**, **13**) on inflammatory factors of NO, PGE_2 and TNF- α were determined on two kind of LPS-activated macrophages, including RAW264.7 macrophages and macrophages from BCG infected C3H/HeN mouse. Data presented in this research indicated that the tested compounds from *T. avellanedae* may negatively exert a significant

anti-inflammatory effect on LPS-mediated inflammatory responses. Most of them significantly blocked the production of NO and PGE2 but not TNF-α without altering cell viability (except for high dose of **6**, **8**, **13** on mcrophages from mouse). From these data, NO production seemed to be the most pharmacologically relevant target of *T. avellanedae*, as the *in vitro* inhibitory potency of them was stronger in NO production than in PGE2 production. These results suggest that *T. avellanedae*'s ethnopharmacological actions (treating inflammatory diseases) was based on the constituents which could mediated NO and other inflammatory mediators (e.g. PGE2).

4. METERIMALS AND METHODS

4.1. Cell cycle and Apoptosis

4.1.1. Reagents and antibodies

Dulbecco's Modified Eagle's Medium (DMEM), doxorubicin(DOX), MTT, and Propidium iodide (PI) were bought from Sigma-Aldrich (USA); FBS was purchased from Nichirei Biosciences (Japan); Penicillin Streptomycin was bought from Gibco (USA); RNase A and Phosphate Buffered Salts (PBS) were bought from Takara (Japan); Annexin V-FITC kit system for detection of apoptosis was purchased from Beckman Coulter (France); Coomassie (Bradford) protein assay kit was purchased from Thermo scientific (USA); cOmplete EDTA free tablet was bought from Roche Applied Science (Germany); Anti-Cyclin A, Anti-Cyclin B1, Anti-Cyclin D1, Anti-beta Actin rabbit polyclonal antibody and Goat anti-rabbit IgG HRP-conjugated antibody were purchased from Abcam (UK); Western ECL substrate kit was obtained from BIO-RAD (Australia); Protein ladder was purchased from Fermentas Life Sciences (Canada); Polyvinylidene fluoride (PVDF) membranes were from Millipore Corporation (USA); RNeasy mini kit was purchased from QIAGEN (Germany); Primers were bought from Eurofins MWG Operon (USA); SuperScript Ⅲ first-strand synthesis system and Tracklt 100 bp DNA ladder for RT-PCR were purchased from Invitrogen Life Technologies (USA); Takara Ex Taq was bought from Takara (Japan); Anti-human Fas antibody was from Medical and Biological Laboratories Co., Ltd, (Japan); CaspACE assay system colorimetric kit was bought from Promega (USA). Organic solvents and other chemicals were of the highest analytical grade.

4.1.2. Cell lines and Cell culture

Human lung carcinoma cell line (A549), human cervical carcinoma cell line

(SiHa), human breast adenocarcinoma cell line (MCF-7) were obtained from the American Type Culture Collection (ATCC; Manassas, VA, USA). All the cell lines were maintained in the DMEM medium supplemented with 10% fetal bovine serum, 100 units/ml penicillin and 100 ug/ml streptomycin. Cells were kept at 37 °C in a humidified atmosphere of 95% air and 5% CO_2, and maintained in exponential and asynchronous phase of growth by repeated trypsinization and reseeding prior to reaching subconfluency.

4.1.3. Cell viability assay (MTT)

Cell viability was assessed by3-(4,5-dimethylthiozol-2-yl)-2,5-diphenyltetrazolium bromide (MTT) assays to determine IC_{50} of the studied compounds (**29**, **30**, **31**, **32**). A549 (4×10^3 cells/ml), SiHa (6×10^3 cells/ml), MCF-7 (2×10^4 cells/ml) were incubated in 96-well microtiter plates for 24 h. Following the addition of 0.5 μM, 1.5 μM, 4.5 μM, 13.5 μM of test compounds (**29**, **30**, **31**, **32**), doxorubicin or only medium, the plates were incubated for an additional 72 h. Three replicate wells were used at each point in the experiments. After incubation, medium was abandoned and 100 μl of MTT solution (final concentration 0.5 mg/ml, freshly diluted in DMEM immediately before treatment) was added and incubated for another 4 h. The formazan product was dissolved in 150 μl of stop solution (SDS 40 g, 0.01 N HCl 200 ml, DMF 200 ml) for 18 h to solubilize the formazan. The amount of formazan was determined by measuring the absorbance at 570 nm with a microplate reader (BioTek, Japan). The IC_{50} values of the samples were determined using IDBS XL fit5.

4.1.4. Cell cycle analysis

A549 (3×10^4 cells/ml) was seeded in 6 cm petri dishes and allowed to attach for 24 h, and then treated with 4.0 μM of compound **29**, 1.0 μM of compound **30**, 2.2 μM of compound **31** or 20.0 μM of compound **32** for 12 h, 24 h, 36 h and 48 h. Prepare

negative controls using untreated cells. Cells were collected (including attached and detached cells) after incubation, washed with ice-cold PBS and fixed with -20℃ 70% ethanol and kept at -20 ℃ overnight. Cells were washed twice with PBS and incubated in 1ml PBS containing 200 μg/ml RNase A at 37 ℃ for 30 min. After further centrifugation, cells were resuspended in 1 ml of PBS containing 250 μg/ml of PI and incubated for 15 min. The percentage of cell distribution was determined using a BD FACSVerse flow cytometer (Becton Dickinson, San Jose, CA). At least 10,000 cells were used for each analysis. Data expressed as the mean of three independent experiments.

4.1.5. Apoptosis analysis

Cells were treated as above. After incubation, cells were harvested (including attached and detached cells) washed by ice-cold PBS and the magnitude of apoptosis was determined using an Annexin V-FITC kit system according to the manufacturer's protocol. Apoptosis was analyzed by a BD FACSVerse flow cytometer. At least 10,000 cells were used for each analysis. Data expressed as the mean of three independent experiments.

4.1.6. Western blot

A549 (3×10^4 cells/ml) was seeded in 6cm petri dishes and allowed to attach for 24 h, and then treated with 1.0 μM of compound **30** or 2.2 μM of compound **31** for 6 h, 12 h, 18 h, 30 h and 36 h. Prepare negative controls using untreated cells. After incubation, cells were lysed and protein concentration was determined using a Bradford assay. An equal amount of protein (20 μg) was separated by 10% sodium dodecyl sulphate-polyacrylamide gel electrophoresis (SDS-PAGE) using AE-6530 mPAGE system (Atto, Japan), and resolved proteins transferred to a 0.45 mm PVDF membrane via Hoefer Semiphor TE 70 semi-dry blotting apparatus (Amersham Biosciences Corp., USA). Blots were probed with a 1:1000 dilution of the desired

primary antibody overnight at 4℃, incubated with a 1:10000 diluted secondary antibody, visualized by ECL Western Blotting Detection System and images were captured by Image Quant LAS 4000 (Fujifilm, Japan). The density of each band was measured using Multi Gauge ver. 3.2 (Fuji Film, Japan). The densitometry readings of the bands were normalized to β-actin expression. Data expressed as the mean of three independent experiments.

4.1.7. RT-PCR

Cells were treated as above. After incubation, total RNA was extracted by RNeasy mini kit according to the manufacturer's instructions. Concentration of the extracted RNA was determined using BioSpec-nano Spectrophotometer (Shimadzu Biotech., Japan) and quality was determined by agarose gel electrophoresis using Mupid-2 Plus submarine electrophoresis system (Advance, Japan). The first strand c DNA was synthesized from 1 μg of total RNA by the SuperScript Ⅲ first-strand synthesis system according to the manufacturer's protocol. RT-PCR was performed by Takara Ex Taq kit with specific primers using Arktik thermal cycler (thermo scientific, USA). The sequences of the specific sets of the primer used in this study are given as in table 2. RT-PCR products were collected after 35 cycles (P53, BCL-2, β-actin) or 40 cycles (BAX) and separated in 1.5% agarose gels containing ethidium bromide and images were captured by Image Quant LAS 4000. Densitometric analysis of bands was done by Multi Gauge ver. 3.2. Expressions of selected genes were normalized to β-actin gene, which was used as an internal housekeeping control. Data expressed as the mean of three independent experiments.

4.1.8. Casepase-3 enzyme activity assay

A549 (3×10^4 cells/ml) was seeded in 6 cm petri dishes and allowed to attach for 24 h, and then treated with 1.0 μM of compound **30** or 2.2 μM of compound **31** for 12

h, 24 h, 36 h and 48 h, or treated with 250 ng/ml of anti-Fas antibody (induce apoptosis) for 24 h for a positive control. Prepare negative controls using untreated cells. After incubation, cells were washed with PBS and extracted in 100 μl of cell lysis buffer. Protein extracts (50 μg) were taken for caspase-3 activity measurements according to the protocols of CaspACE assay system kit. Reactions were incubated overnight at room temperature and free product pNA was monitored by a microplate reader at 405 nm. All procedures were performed three times.

4.1.9. Statistical Analysis

All data were processed and analyzed by KaleidaGraph version 3.6 (Synergy Software). Results are expressed as the mean ± standard deviation (S.D.). The statistical significances were evaluated by *t*-test of the software and $p < 0.05$ was considered to be significant.

4.2. Anti-inflammation

4.2.1. Reagents

Dulbecco's Modified Eagle's Medium (DMEM), RPMI-1640 Medium, MTT and Propidium iodide (PI) were bought from Sigma-Aldrich (USA); FBS was purchased from Nichirei Biosciences (Japan); Penicillin Streptomycin was bought from Gibco (USA); Phosphate Buffered Salts (PBS) were bought from Takara (Japan); Griess Reagent System kit was purchased from Promega (USA). Prostaglandin E2 Parameter Assay Kit was from R&D Systems (USA). Mouse TNF-α ELISA Ready-SET-Go kit was from eBioscience (CA). Freeze-Dried BCG Vaccine was from Japan BCG Laboratory (Japan). Organic solvents and other chemicals were of the highest analytical grade. Microplate reader was from Dainippon Pharmaceutical (Japan).

4.2.2. Mice, cell lines, cell culture and treatment

Mouse leukaemic monocyte macrophage cell line (RAW264.7) was obtaine d from the American Type Culture Collection (ATCC; Manassas, VA, USA). I t was maintained in the DMEM medium supplemented with 10% fetal bovine serum. Cells were kept at 37 °C in a humidified atmosphere of 95% air and 5% CO_2, and maintained in exponential and asynchronous phase of growth by repeated dislodging cells from the flask substrate with a cell scraper and resee ding prior to reaching subconfluency. RAW264.7 (5×10^5 cells/ml) were seeded in 96-well plates and allowed 24 hours to attach. Following the addition of LP S (final concentration: 250ng/ml) and 12.5, 25, 50 μg/ml of compounds (**1**, **3**, **5**, **6**, **8**, **9**, **10**, **11**, **12**, **13**), 0.78, 3.13, 12.5 μg/ml of compound **20** or only m edium, the plates were incubated for an additional 24 h. After that, cell culture supernatants were collected and analyzed for NO, PGE2 and TNF-α productio n, and the adherent cells were washed and checked for cell viability.

Male 4-week-old C3H/HeN Slc (SPF) mice were obtained from Sankyo Laboratory Service Co. (Japan). 1mg/mouse/200 μl of BCG was injected into C3H/HeN Slc mice. After 4 days, mice were decapitated and 4cc of cold RPMI-1640 was injected through the exposed peritoneum and withdrawn with a no. 25 needle for three times. Collected cells were washed by RPMI-1640 at 1400 rpm, resuspended in RPMI-1640 containing 5% FBS, seeded in 96-well plates at 5×10^5 cell/ml (160 μl/well). After 12 h, non-adherent cells were aspirated with a capillary pipette attached to wall suction, and 160 μl of RPMI-1640 containing 5% FBS was added. After an additional 12 h, cells were treated with LPS (final concentration: 250ng/ml) and 12.5, 25, 50 μg/ml of compounds (**1**, **3**, **5**, **6**, **8**, **9**, **10**, **11**, **12**, **13**), 0.78, 3.13, 12.5 μg/ml of compound **20** or only medium. After 48h of incubation, cell culture supernatants were collected and analyzed for NO, PGE2 and TNF-α production, and the adherent cells were washed and checked for cell viability.

4.2.3. Cell viability assay (MTT)

Three replicate wells were used at each point in the experiments. After incubation, the cell culture supernatants were collected, the adherent cells were washed and 100 μl of MTT solution (final concentration 0.5 mg/ml, freshly diluted in DMEM immediately before treatment) was added and incubated for another 4 h. The formazan product was dissolved in 150 μl of stop solution (SDS 40 g, 0.01 N HCl 200 ml, DMF 200 ml) for 18 h to solubilize the formazan. The amount of formazan was determined by measuring the absorbance at 570 nm with a microplate reader (BioTek, Japan).

4.2.4. NO, PGE_2 and TNF-α determination

Three replicate wells were used at each point in the experiments. The cell culture supernatants were collected after incubation, NO was assessed by the Promega Griess Reagent System, according to the manufacturer's instructions; PGE_2 was determined using a R&D Prostaglandin E2 Parameter Assay Kit, according to the manufacturer's instructions; TNF-α was quantified using an ELISA kit, according to the manufacturer's instructions.

4.2.5. Statistical Analysis

All data were processed and analyzed by KaleidaGraph version 3.6 (Synergy Software). Results are expressed as the mean ± standard deviation (S.D.). The statistical significances were evaluated by *t*-test of the software and $p < 0.05$ was considered to be significant.

4.3. Extraction, Separation and Isolation

4.3.1 General experiment procedures

Optical rotations were measured using a SEPA-3000 high-sensitivity polarimeter (Horiba, Japan). UV spectra were measured using a UV-1600 UV-visible spectrometer (Shimadzu, Japan). IR spectra were recorded on a IR-460 IR spectrophotometer (Shimadzu, Japan), whereas NMR spectra were obtained using the JEOL ECA-600 NMR spectrometer (JEOL, Japan) in $CDCl_3$. Chemical shifts were referenced to the residual solvent peaks (δ_H 7.24 and δ_C 77.0 for $CDCl_3$). The mass spectra were recorded on a JEOL JMS-700 mass spectrometer (JEOL, Japan) or JEOL JMS SX-102 (JEOL, Japan). Reversed-phase HPLC was carried out on C30-UG-5 (5 μm, Nomura Chemical, Japan), C18-AR-Ⅱ (5 μm, Nacalai Tesque., Japan). Silica gel (63-210 μm, Kantou Kagaku, Japan), ODS (63-212 μm, Wako Pure Chemical, Japan) and Sephadex LH-20. (Pharmacia Biotech AB, Uppsala, Sweden) were used for open-column chromatography. Thin-layer chromatography (TLC) was carried out on silica gel 60 F_{254} and RP-18 F_{254S} (Merck Co., Germany).

4.3.2. Plant material

Inner bark of *T. avellanedae* and Water extract of inner bark of *T. avellanedae* for the present investigation was for the present investigation was taxonomically identified and extracted by Taheebo Japan Corporation.

4.3.3. Extraction and isolation

4.3.3.1 Extraction and isolation 1

Water extract of inner bark of *T. avellanedae* for the present investigation was taxonomically identified and extracted by Taheebo Japan Corporation. In accordance

with their method, dried bark of *T. avellanedae* (10 kg) were extracted with boiling water (30 L) three times, and the water solutions were combined and concentrated in vacuo to get the crude extract. The water extract (350 g) was suspended in H_2O (3.5 L) and partitioned successively with *n*-hexane, EtOAc and *n*-BuOH (each 3.5 L, 3 times) to yield *n*-hexane fraction (2.3 g), EtOAc fraction (48.6 g), *n*-BuOH fraction (103.7 g) and H_2O fraction (190.0 g), respectively. The EtOAc fraction (47.0g) was chromatographed on silica gel with a gradient solvent system (*n*-hexane/EtOAc 3:2, $CHCl_3$/MeOH 50:1, 20:1, 10:1) to give 3 fractions (A1-A3). Fraction A1-3 (*n*-hexane /EtOAc =3/2, 1.3 g) was rechromatographed on ODS with gradient solvent (MeOH/ H_2O) to afford 11 fractions (B1-B11). Fraction B7 (MeOH/H_2O 3:4, 79.8mg) was subjected on sephadex LH-20 with MeOH to afford 5 fractions (C1-C5). Fraction C4 (40.0 mg) was further purified by ODS HPLC (C_{18}-AR-Ⅱ) with 57% MeOH to afford compound **29** (1.6 mg) and compound **30** (2.2 mg). Fractions B 9 and B 10 (MeOH/H_2O= 1/1, 70.5 mg) was rechromatographed on silica gel with a gradient solvent system ($CHCl_3$, $CHCl_3$/MeOH) to give 8 fractions (D1-D6). Fraction D1 ($CHCl_3$, 22 mg) was separated using C30 HPLC (C_{30}-UG-5) with 33% MeOH to afford compound **5** (2.1 mg) and compound **6** (1.7 mg). Fraction D5 ($CHCl_3$/MeOH 20:1, 113.7 mg) was separated using C30 HPLC (C_{30}-UG-5) with 50% MeOH to afford compound **4** (0.9 mg). Fraction A2 ($CHCl_3$/MeOH 50:1, 3.4 g) was rechromatographed on silica gel with a gradient solvent system (*n*-hexane/EtOAc) to give 3 fractions (E1-E3). Fraction E2 (*n*-hexane/EtOAc 1:1, 1.3 g) was rechromatographed on ODS with gradient solvent (MeOH/ H2O) to afford 8 fractions (E1-E8). E7 (MeOH/H_2O 2:1, 175 mg) was subjected on Sephadex LH-20 with MeOH to get 7 fractions (F1-F7). Fraction F3 (79.7 mg) was separated using C30 HPLC (C_{30}-UG-5) with 50% MeOH to afford compound **1** (2.5 mg), compound **3** (1.2 mg) and compound **8** (1.7 mg). Fraction F4 (73.7 mg) was separated using C30 HPLC (C_{30}-UG-5) with 52% MeOH to afford compound **31** (1.3 mg) and compound **32** (1.3 mg).

4.3.3.2 Extraction and isolation 2

Inner bark of *T. avellanedae* (8.0 kg) for the present investigation was extracted 3 times by methanol to afford 1.8 kg of MeOH extract. The MeOH extract (1.8 kg) was suspended in H_2O (1 8 L) and partitioned with $CHCl_3$ (each 18 L, 3 times) to yield $CHCl_3$ fraction (240 g) and H_2O fraction (1.5 kg). $CHCl_3$ fraction was chromatographed on silica gel with a gradient solvent system (*n*-hexane/EtOAc/ $CHCl_3$ /MeOH) to give 3 fractions (A1-A3). A1 (*n*-hexane /EtOAc =1/1, 138 g) was rechromatographed on silica gel with a gradient solvent system (*n*-hexane/EtOAc= 9:1、8:2、7:3、6:4、5:5、4:6、3:7、2:8、1:9、0:1) to give 10 fractions (B1-B10). Fractions B10 (*n*-hexane/EtOAc= 1:9) was rechromatographed on ODS with gradient solvent (60%、70%、80%、90%、100% of MeOH) to afford 5 fractions (C1-C5). Fractions C2 (70% MeOH) was separated using C-30 HPLC (C_{30}-UG-5) with 75% MeOH and Phenyl HPLC with 75% MeOH to afford compound **7** (1.2 mg). A21 (EtOAc, 53.8 g) was rechromatographed on silica gel with a gradient solvent system (*n*-hexane/EtOAc= 1:1、2:3、3:7、3:4、1:4、1:9) to give 6 fractions (D1-D6). Fractions D2 (*n*-hexane/EtOAc= 2:3) was rechromatographed on ODS with gradient solvent (20%、40%、60%、80%、100% of MeOH) to afford 5 fractions (E1-E5). Fractions E2 (40% MeOH) was rechromatographed on LH-20 and then Flash ODS with gradient solvent (40%、50%、60%、70%、100% of MeOH) to afford 5 fractions (F1-F5). Fractions F3 (60% MeOH) was separated using ODS HPLC (C18-AR-Ⅱ) with 65% MeOH and C-30 HPLC (C_{30}-UG-5) with 60% MeOH to afford compound **2** (3.5 mg). A21 ($CHCl_3$ /MeOH =1/1, 45.4 g) was rechromatographed on silica gel with a gradient solvent system ($CHCl_3$ /MeOH = 1:0、9:1、8:2、7:3、6:4、0:1) to give 6 fractions (G1-G6). Fractions G2 ($CHCl_3$ /MeOH = 9:1) was rechromatographed on ODS with gradient solvent (20%、40%、60%、80%、100% of MeOH) to afford 5 fractions (H1-H5). Fractions H4 (40% MeOH) was rechromatographed on LH-20 and then Flash ODS with gradient solvent (40%、50%、60%、70%、100% of MeOH) to afford 5 fractions (I1-I5). Fractions I3 (60% MeOH) was separated using C-30 HPLC (C_{30}-UG-5) with 65% MeOH and Phenyl HPLC with 65% MeOH to afford compound **11** (2.8 mg), **15** (26.8 mg), **17** (1.8 mg), **18** (0.9 mg), **19** (6.9 mg) and separated using

Phenyl HPLC with 65% MeOH to afford compound **10** (7.8 mg), **12** (3.5 mg), **13** (4.2 mg), **14** (3.5 mg), **16** (2.0 mg).

4.3.3.3 Extraction and isolation 3

Dried bark of *T. avellanedae* (10 kg) were extracted with boiling water (30 L) three times. The water solutions were combined and concentrated in vacuo, and the residue (100 g) was suspended in H2O (1 L) and partitioned successively with n-hexane, EtOAc and n-BuOH (each 1 L, 3times) to yield n-hexane fraction (0.57 g), EtOAc fraction (14.13 g), n-BuOH fraction (31.47 g) and H2O fraction (65.13 g), respectively. The EtOAc fraction (14g) was chromatographed on silica gel with a gradient solvent system (Hexane/EtOAc/MeOH) to give 15 fractions (A1-A15). A3 and A4 (Hexane/EtOAc =1/1, 2.3 g) was rechromatographed on ODS with gradient solvent (MeOH/ H2O) to afford 14 subfractions (B1-B14). B1 (MeOH/H2O= 0/1, 280mg) was subjected on ODS with gradient solvent (MeOH/ H2O) to afford 12 subfractions (C1-C12). C7 (MeOH/H2O= 1/4, 6.2 mg) was further separated by separative HPLC, ODS column (C18-AR-Ⅱ) with 33% MeOH to afford compound **27** (6.0 mg). B4 (MeOH/H2O= 1/4, 69 mg) was subjected on Sephadex-LH20 with MeOH to get 9 subfractions(D1-D9). D6 was further separated by separative HPLC, ODS column (C18-AR-Ⅱ) with 20% MeOH to afford compound **26** (6.0 mg). B5 (MeOH/H2O= 1/4, 119.2 mg) was subjected on Sephadex-LH20 with MeOH to get 3 subfractions (E1-E3), and E3 was further separated by separative HPLC, ODS column (C30-UG-5) with 40% MeOH to afford compound **25** (2.9 mg).B11 and B12 (MeOH/H2O= 3/4, 79.8 mg) was subjected on Sephadex-LH20 with MeOH to get 6 subfractions(F1-F6), and F4(40 mg) was subjected on silica gel with a gradient solvent system ($CHCl_3$/MeOH) to give 11 fractions (G1-G11). G4 (6.9 mg) was further separated by separative HPLC, ODS column (C18-AR-Ⅱ) with 50% MeOH and 55% MeOH to afford compound **23** (0.9 mg) and **20** (1.6 mg) and subfraction H. Subfraction H (1.8 mg) was further separated by separative HPLC, ODS column (C30-UG-5) with 52% MeOH to afford compound **22** (1.0 mg) and compound **21** (0.6

mg). G6 and G7 (3 mg) was further separated by separative HPLC, ODS column (C30-UG-5) with 50% MeOH to afford compound **24** (1.2 mg). B13(MeOH/H2O= 3/4, 100.9 mg) was subjected on Sephadex-LH20 with MeOH to get 6 subfractions(I1-I6), and I3 and I4 (85 mg) was subjected on silica gel with a gradient solvent system (Hexane/EtOAc) to give 10 fractions (J1-J10). J9 (21.2 mg) was further separated by separative HPLC, ODS column (C18-AR-Ⅱ) with 60% MeOH to afford compound **28** (1.0 mg).

Compound 1.

Yellowish oil: $[\alpha]_D^{23.8}$ -18.65 (MeOH, *c*1.00); UV (MeOH) λ_{max} (log ε) 255 (2.72), 206 (2.77) nm; IR υ_{max} (KBr) 3311, 2920, 2830 1705, 1660, 1608, 1593, 1514, 1444, 1356, 1271, 1164, 1099, 853, 758 cm^{-1}; ^1H NMR spectroscopic data (600 MHz, $CDCl_3$) and ^{13}C NMR spectroscopic data (125 MHz, $CDCl_3$) are shown in Table 1 and Table 2. HRFABMS m/z 289.1062[M+H]+ (calcd. 289.1062 for C16H17O5).

Compound 4.

Brown solid: $[\alpha]_D^{24.3}$ 6.79 (MeOH, *c*1.00); UV (MeOH) λ_{max} (log ε) 251 (3.05), 212 (3.03) nm; IR υ_{max} (KBr) 3300, 2925, 2820, 1705, 1652, 1608, 1593, 1515, 1456, 1271, 1122, 1049 cm^{-1}; ^1H NMR spectroscopic data (600 MHz, $CDCl_3$) and ^{13}C NMR spectroscopic data (125 MHz, $CDCl_3$) are shown in Table 1 and Table 2. HREIMS *m/z* 334.1441 $[M]^+$ (calcd. 334.1441 for $C_{18}H_{22}O_6$).

Compound 5

Brown solid: $[\alpha]_D^{21.8}$-7.99 (MeOH, *c*1.00). UV λ_{max} (MeOH) 210 (2.99), 251 (3.03) nm. IR υ_{max} (KBr) 2936, 2837,1714, 1666, 1606, 1512, 1258, 1169, 1103, 1030, 849, 772, 698 cm^{-1}; ^1H NMR spectroscopic data (600 MHz, $CDCl_3$) and ^{13}C NMR spectroscopic data (125 MHz, $CDCl_3$) are shown in Table 1 and Table 2. HRFABMS *m/z* 348.0780 $[M+Na]^+$ (calcd. 348.0780 for $C_{19}H_{24}O_6Na$).

Compound 6

Brown solid: $[\alpha]_D^{24.0}$-10.1 (MeOH, *c*1.00). UV λ_{max} (MeOH) 218 (3.06), 256 (3.00), 291 (2.56) nm. IR υ_{max} (KBr) 2937, 2835, 1705, 1666, 1600, 1515, 1271, 1225, 1176, 1126, 1107, 1024, 764 cm^{-1}; ^1H NMR spectroscopic data (600 MHz, $CDCl_3$) and ^{13}C NMR spectroscopic data (125 MHz, $CDCl_3$) are shown in Table 1 and Table 2. HRFABMS *m/z* 379.1736 $[M+H]^+$ (calcd. 379.1736 for $C_{20}H_{27}O_7$).

Compound 7

Brown solid: $[\alpha]_D^{21.8}$-101.4 (MeOH, *c*1.00). UV λ_{max} (MeOH) 204 (4.79), 256 (4.54) nm. ^1H NMR spectroscopic data (600 MHz, CD_3OD) and ^{13}C NMR spectroscopic

data (125 MHz, CD_3OD) are shown in Table 3. HRFABMS *m/z* 463.1763 $[M+Na]^+$ (calcd. 463.1733 for $C_{25}H_{42}O_{17}Na$).

Compound 8.

Brown solid: $[\alpha]_D^{23.2}$ -0.02 (MeOH, *c*1.00); UV (MeOH) λ_{max} (log ε) 289 (2.5945), 261 (2.9541) , 215 (3.0790) nm; IR υ_{max} (KBr) 3448, 2937, 1705, 1602, 1514, 1456, 1418, 1271, 1224, 1177, 1107, 1024, 764 cm^{-1}; ^1H NMR spectroscopic data (600 MHz, $CDCl_3$) and ^{13}C NMR spectroscopic data (125 MHz, $CDCl_3$), are shown in Table 4. HRFABMS *m/z* 391.1244 $[M+Na]^+$ (calcd. 391.1244 for $C_{18}H_{24}O_8Na$).

Compound 10

Brown solid: $[\alpha]_D^{21.8}$-77.8 (MeOH, *c*1.00). UV λ_{max} (MeOH) 203 (4.87), 257 (4.55) nm. ^1H NMR spectroscopic data (600 MHz, CD_3OD) and ^{13}C NMR spectroscopic data (125 MHz, CD_3OD) are shown in Table 5 and Table 6. HRFABMS *m/z* 639.2045 $[M+Na]^+$ (calcd. 639.2054 for $C_{31}H_{36}O_{13}Na$).

Compound 11

Brown solid: UV λ_{max} (MeOH) 203 (4.92), 258 (4.53) nm. ^1H NMR spectroscopic data (600 MHz, CD_3OD) and ^{13}C NMR spectroscopic data (125 MHz, CD_3OD) are shown in Table 5 and Table 6. $[\alpha]_D^{21.8}$-73.3 (*c* =0.10, MeOH). HRFABMS *m/z* 669.2145 $[M+Na]^+$ (calcd. 669.2159 for $C_{32}H_{38}O_{14}Na$).

Compound 12

Brown solid: $[\alpha]_D^{21.8}$-121.5 (MeOH, *c*1.00). UV λ_{max} (MeOH) 203 (4.91), 259 (4.52) nm. ^1H NMR spectroscopic data (600 MHz, CD_3OD) and ^{13}C NMR spectroscopic data (125 MHz, CD_3OD) are shown in Table 5 and Table 6. HRFABMS *m/z* 669.2145 $[M+Na]^+$ (calcd. 669.2159 for $C_{32}H_{38}O_{14}Na$).

Compound 13

Brown solid: $[\alpha]_D^{21.8}$-77.8 (MeOH, *c*1.00). UV λ_{max} (MeOH) 203 (4.87), 257 (4.55)

nm. ^{1}H NMR spectroscopic data (600 MHz, CD_3OD) and ^{13}C NMR spectroscopic data (125 MHz, CD_3OD) are shown in Table 5 and Table 6. HRFABMS *m/z* 639.2045 $[M+Na]^+$ (calcd. 639.2054 for $C_{31}H_{36}O_{13}Na$).

Compound 14

Brown solid: $[\alpha]_D^{21.8}$-47.7 (MeOH, *c*1.00). UVλ_{max} (MeOH) 203 (5.00), 257 (4.54) nm. ^{1}H NMR spectroscopic data (600 MHz, CD_3OD) and ^{13}C NMR spectroscopic data (125 MHz, CD_3OD) are shown in Table 7 and Table 8. HRFABMS *m/z* 739.2207 $[M+Na]^+$ (calcd. 739.739.2214 for $C_{35}H_{40}O_{16}Na$).

Compound 15

Brown solid: $[\alpha]_D^{21.8}$-51.4 (MeOH, *c*1.00). UVλ_{max} (MeOH) 204 (5.08), 259 (4.62) nm. ^{1}H NMR spectroscopic data (600 MHz, CD_3OD) and ^{13}C NMR spectroscopic data (125 MHz, CD_3OD) are shown in Table 7 and Table 8. HRFABMS *m/z* 769.2330 $[M+Na]^+$ (calcd. 769.2320 for $C_{36}H_{42}O_{17}Na$).

Compound 16

Brown solid: $[\alpha]_D^{21.8}$-49.8 (MeOH, *c*1.00). UV λ_{max} (MeOH) 204 (5.08), 259 (4.62) nm. ^{1}H NMR spectroscopic data (600 MHz, CD_3OD) and ^{13}C NMR spectroscopic data (125 MHz, CD_3OD) are shown in Table 7 and Table 8. HRFABMS *m/z* 769.2330 $[M+Na]^+$ (calcd. 769.2320 for $C_{36}H_{42}O_{17}Na$).

Compound 17

Brown solid: ^{1}H NMR spectroscopic data (600 MHz, CD_3OD) and ^{13}C NMR spectroscopic data (125 MHz, CD_3OD) are shown in Table 7 and Table 8. HRFABMS *m/z* 825.2572 $[M+Na]^+$ (calcd. 825.2582 for $C_{39}H_{46}O_{18}Na$).

Compound 18

Brown solid: ^{1}H NMR spectroscopic data (600 MHz, CD_3OD) and ^{13}C NMR spectroscopic data (125 MHz, CD_3OD) are shown in Table 7 and Table 8. HRFABMS

m/z 825.2569 $[M+Na]^+$ (calcd. 825.2582 for $C_{39}H_{46}O_{18}Na$).

Compound 19

Brown solid: $[\alpha]_D^{21.8}$-19.8 (MeOH, *c*1.00). UV λ_{max} (MeOH) 204 (4.98), 257 (4.31) nm. ^1H NMR spectroscopic data (600 MHz, CD_3OD) and ^{13}C NMR spectroscopic data (125 MHz, CD_3OD) are shown in Table 9. HRFABMS *m/z* 677.2200 $[M+Na]^+$ (calcd. 677.2210 for $C_{36}H_{42}O_{17}Na$).

Compound 20.

Colorless oil: $[\alpha]_D^{26.8}$ 0.71 (MeOH, *c*1.90); UV (MeOH) λ_{max} (log ε) 284.5 (1.10), 232 (1.39) nm; IR υ_{max} (KBr) 3334, 2877, 1699,1606, 1515, 1446, 1242, 1037, 931, 799, 756 cm^{-1}; ^1H NMR spectroscopic data (600 MHz, CD_3OD) and ^{13}C NMR spectroscopic data (125 MHz, CD_3OD) are shown in Table 10. HRFABMS *m/z* 371.1129 $[M-H]^-$ (calcd. for $C_{20}H_{19}O_7$, 371.1131).

Compound 21.

Colorless oil: $[\alpha]_D^{17.5}$ 1.57 (MeOH, *c*1.00); UV (MeOH) λ_{max} (log ε) 283 (0.2183), 234 (0.4883) , 205 (2.0026) nm; IR υ_{max} (KBr) 3429, 2943, 1733, 1558, 1506, 1259, 1035 cm^{-1}; ^1H NMR spectroscopic data (600 MHz, CD_3OD) and ^{13}C NMR spectroscopic data (125 MHz, CD_3OD) are shown in Table 10. HRESIMS *m/z* 371.1122 $[M-H]^-$ (calcd. for $C_{20}H_{19}O_7$, 371.1131).

Compound 27.

Yellow powder: $[\alpha]_D^{26.4}$ –0.51 (MeOH, *c*1.00); UV (MeOH) λ_{max} (log ε) 286 (1.27), 225 (1.71) nm; IR υ_{max} (KBr) 3271, 2926, 2852, 1720, 1651, 1556, 1506, 1456, 1286, 999 cm^{-1}; ^1H NMR spectroscopic data (600 MHz, CD_3OD) and ^{13}C NMR spectroscopic data (125 MHz, CD_3OD) are shown in Table 11. HRFABMS *m/z* 261.0759 $[M-H]^-$ (calcd. for $C_{14}H_{13}O_5$, 261.0763).

Compound 28.

Yellow powder: $[\alpha]_D^{22.6}$ 5.82 (MeOH, *c*1.00); UV (MeOH) λ_{max} (log ε) 292 (2.23), 281(2.38) , 271 (2.34), 226 (2.97), 212(2.95) nm; IR υ_{max} (KBr) 3308, 2972, 2932,1716, 1634, 1539, 1516, 1456, 1396, 1375, 1238, 1121, 1060, 1024, 800, 779, 756 cm^{-1}; ^{1}H NMR spectroscopic data (600 MHz, $CDCl_3$) and ^{13}C NMR spectroscopic data (125 MHz, $CDCl_3$), are shown in Table 12. HRFABMS *m/z* 300.1606 $[M-H]^-$ (calcd. for $C_{18}H_{22}NO_3$, 300.1600).

Compound 31

Yellow needles: $[\alpha]_D^{26.4}$ 3.00 (MeOH, *c*1.00); UV (MeOH) λ_{max} (log ε) 210 (2.93) , 234 (2.80), 249 (2.87) , 296 (2.34) , 394 (2.12) nm; IR υ_{max} (KBr) 3450, 1645, 1456, 1259, 1221 cm^{-1}; ^{1}H NMR spectroscopic data (600 MHz, $CDCl_3$) and ^{13}C NMR spectroscopic data (125 MHz, $CDCl_3$), are shown in Table 13. HREIMS *m/z* 288.0635 (calcd. for $C_{15}H_{12}O_6$, 288.0634).

4.3.4 NMR Spectra of new compounds.

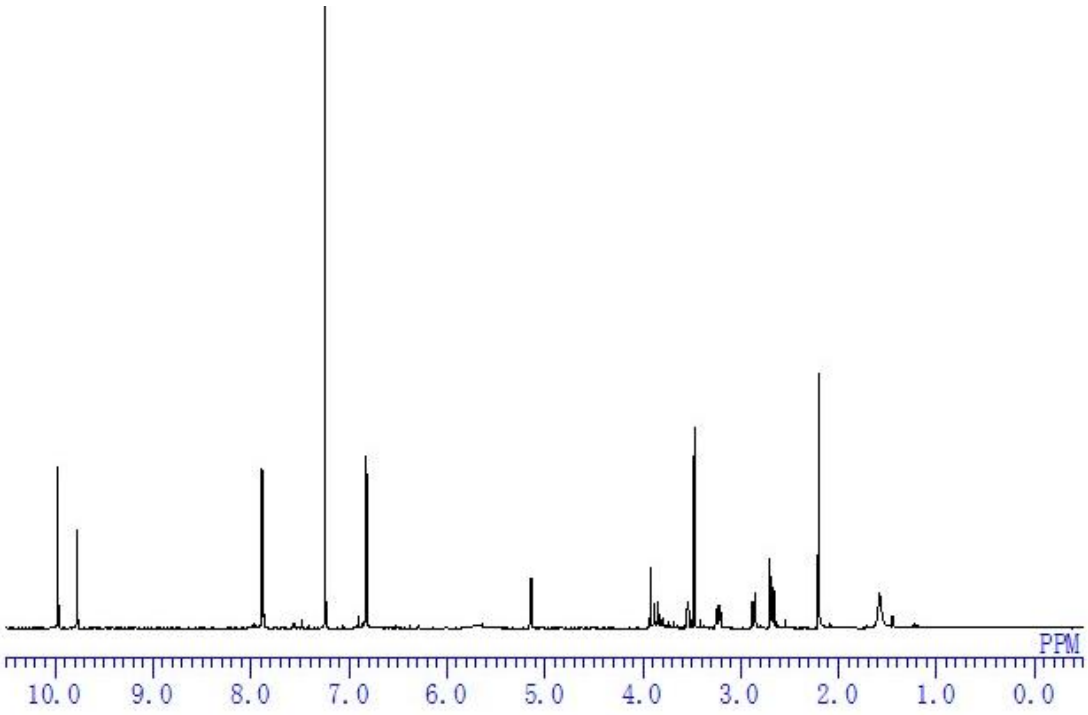

^{1}H NMR spectrum of **1** in $CDCl_3$

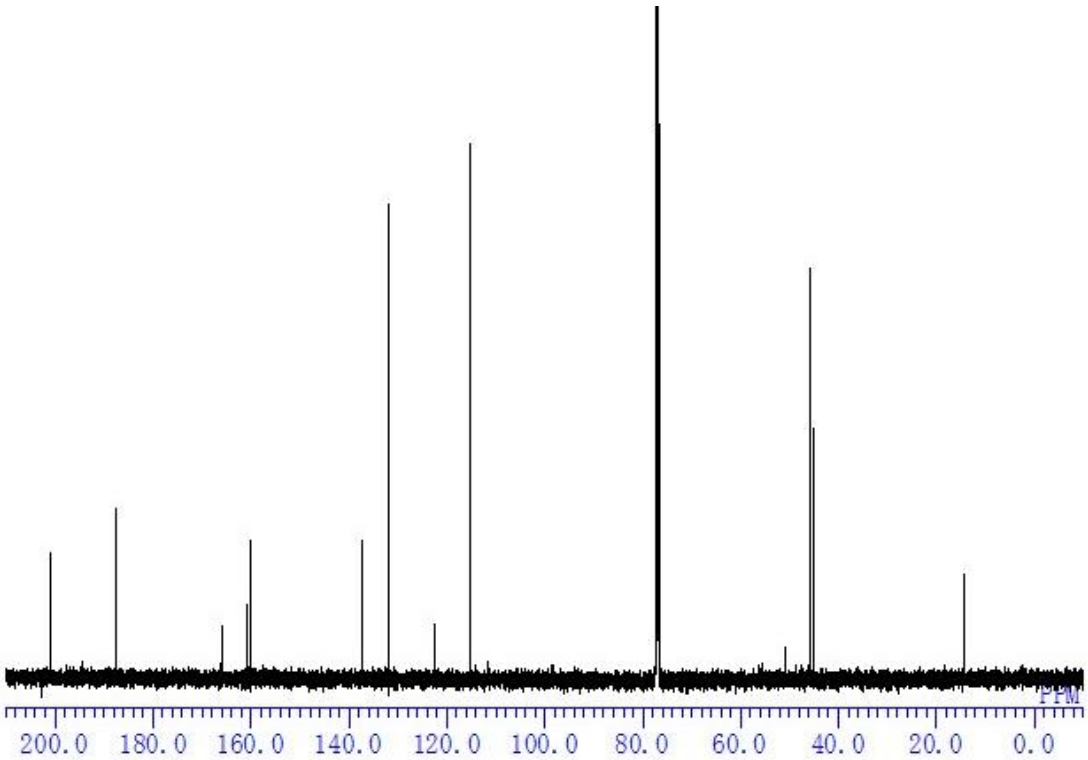

^{13}C NMR spectrum of **1** in $CDCl_3$

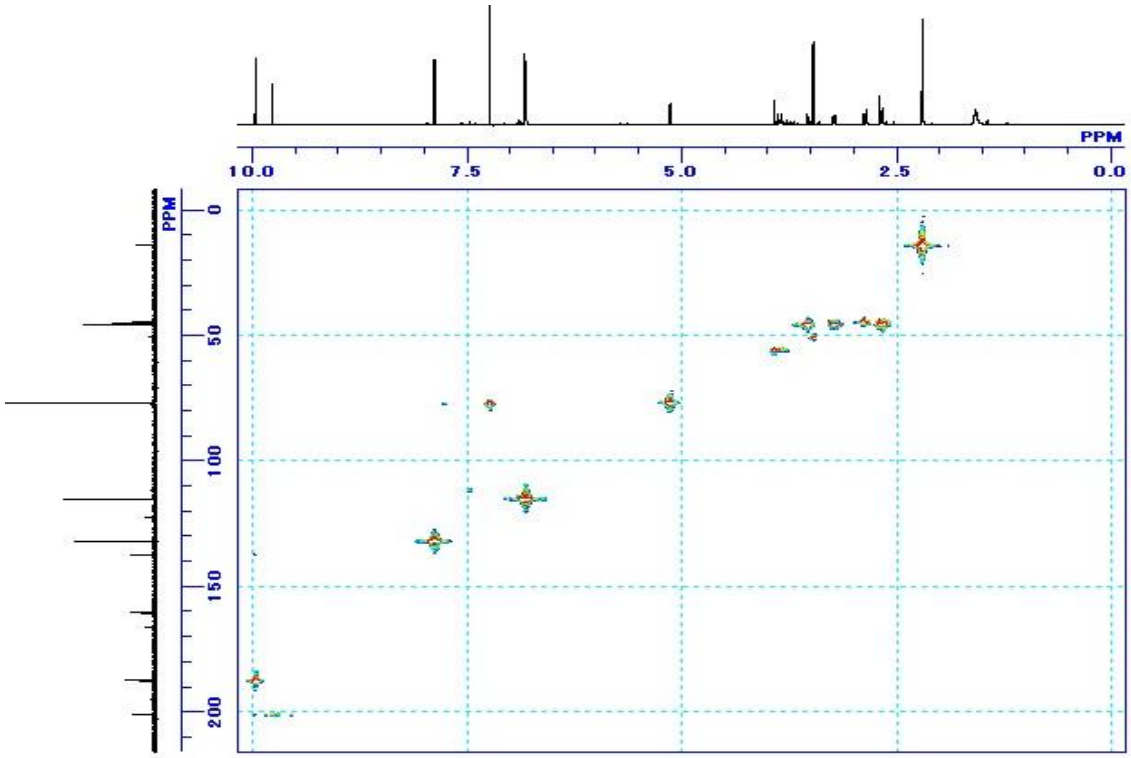

HMQC spectrum of **1** in $CDCl_3$

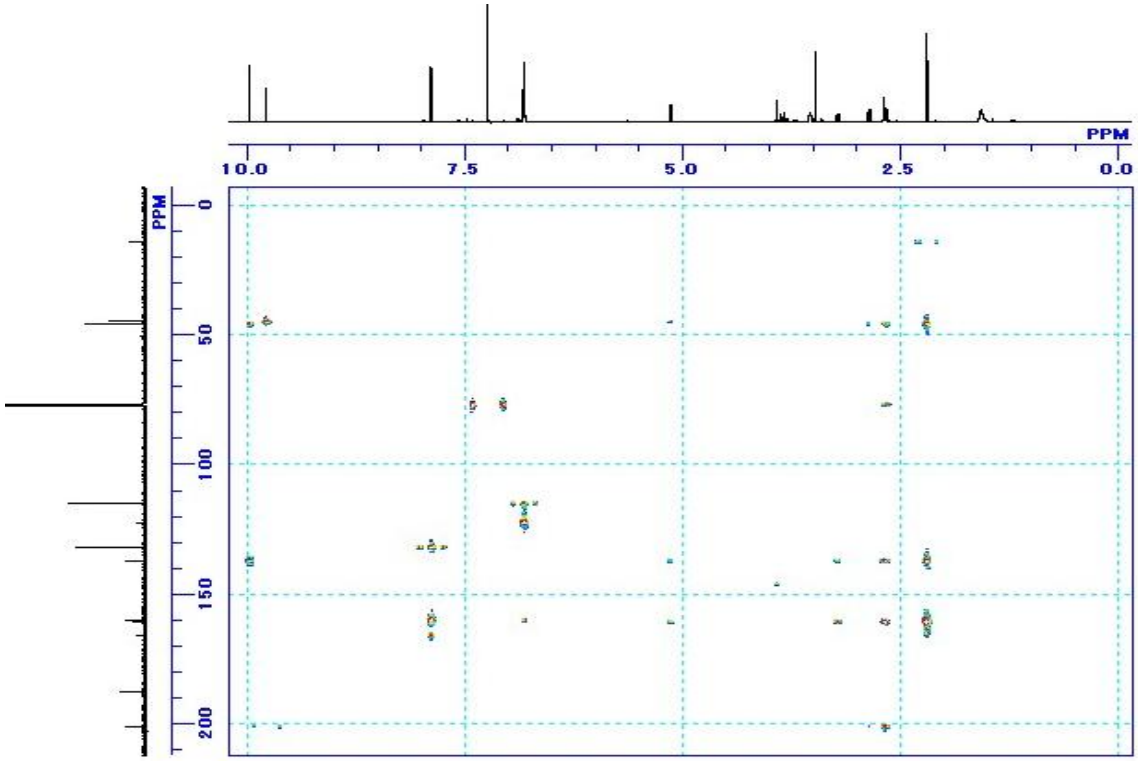

HMBC spectrum of **1** in $CDCl_3$

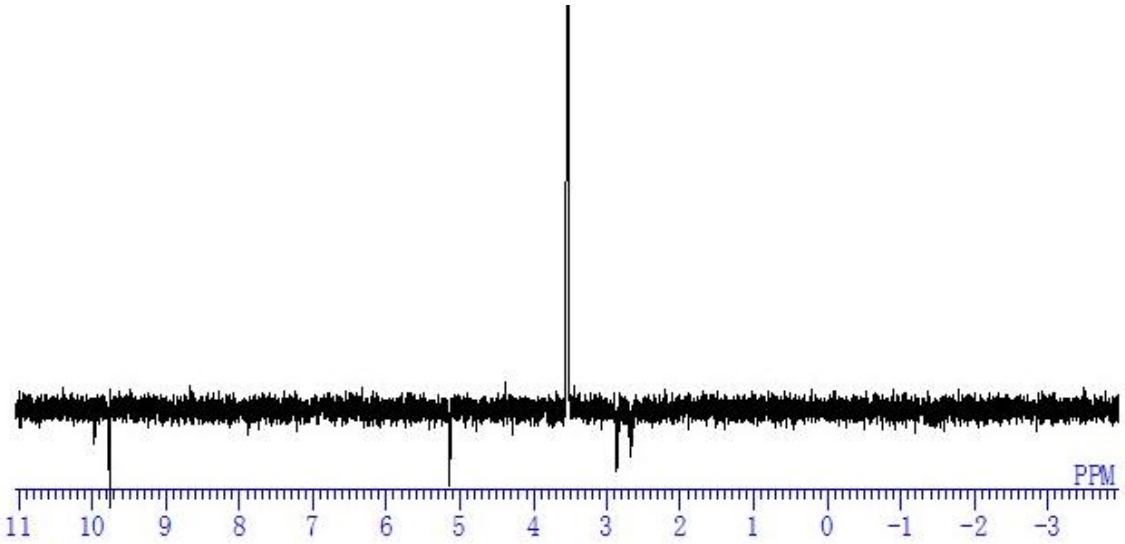

NOE spectrum of **1** in $CDCl_3$ (δ_H 3.54)

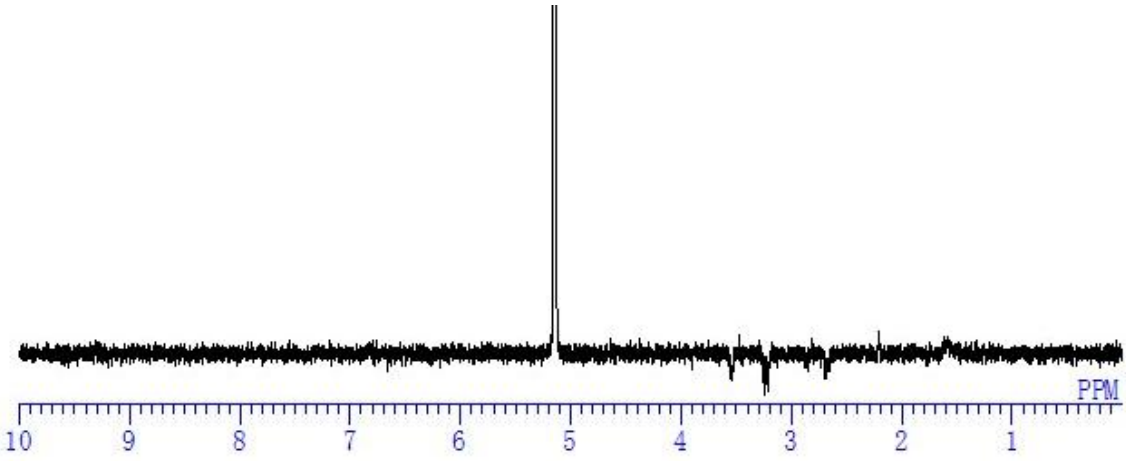

NOE spectrum of **1** in $CDCl_3$ (δ_H 5.14)

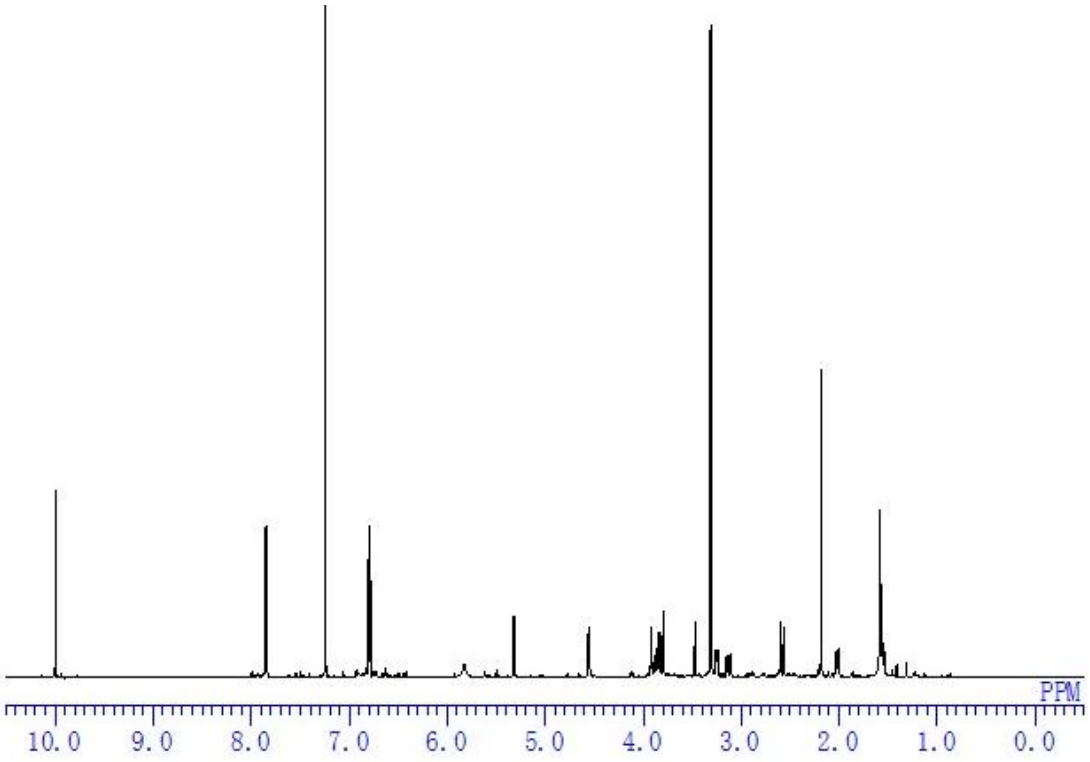

^{1}H NMR spectrum of **4** in $CDCl_3$

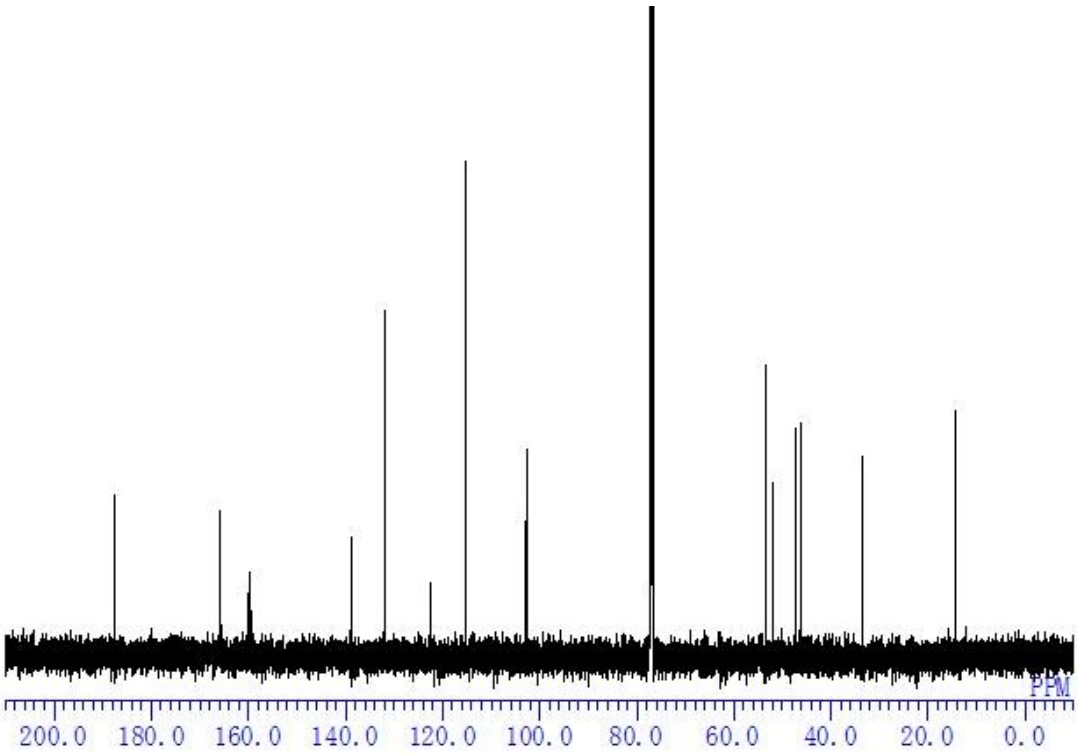

^{13}C NMR spectrum of **4** in $CDCl_3$

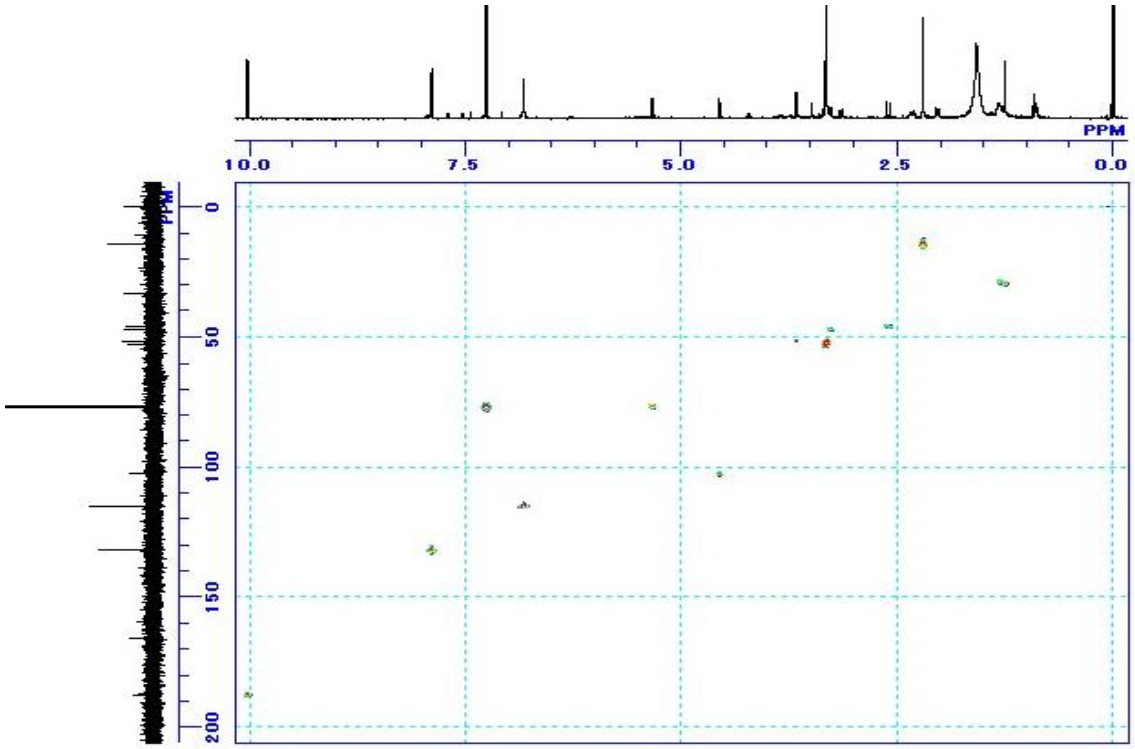

HMQC spectrum of **4** in $CDCl_3$

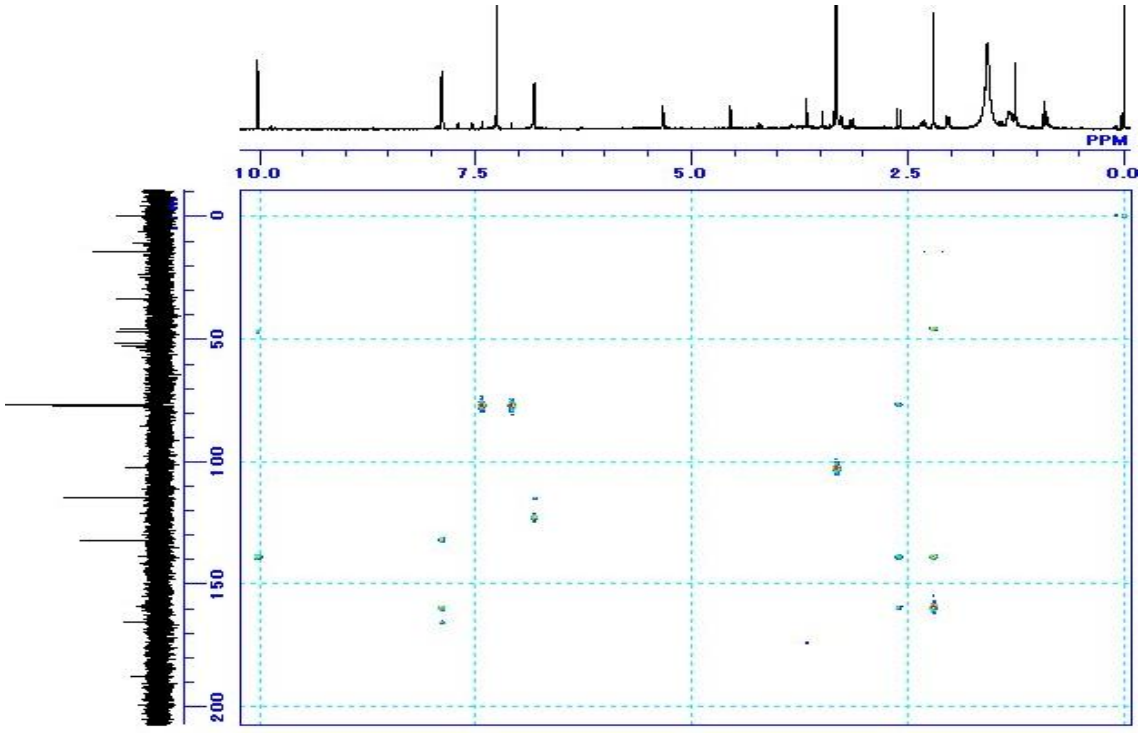

HMBC spectrum of **4** in $CDCl_3$

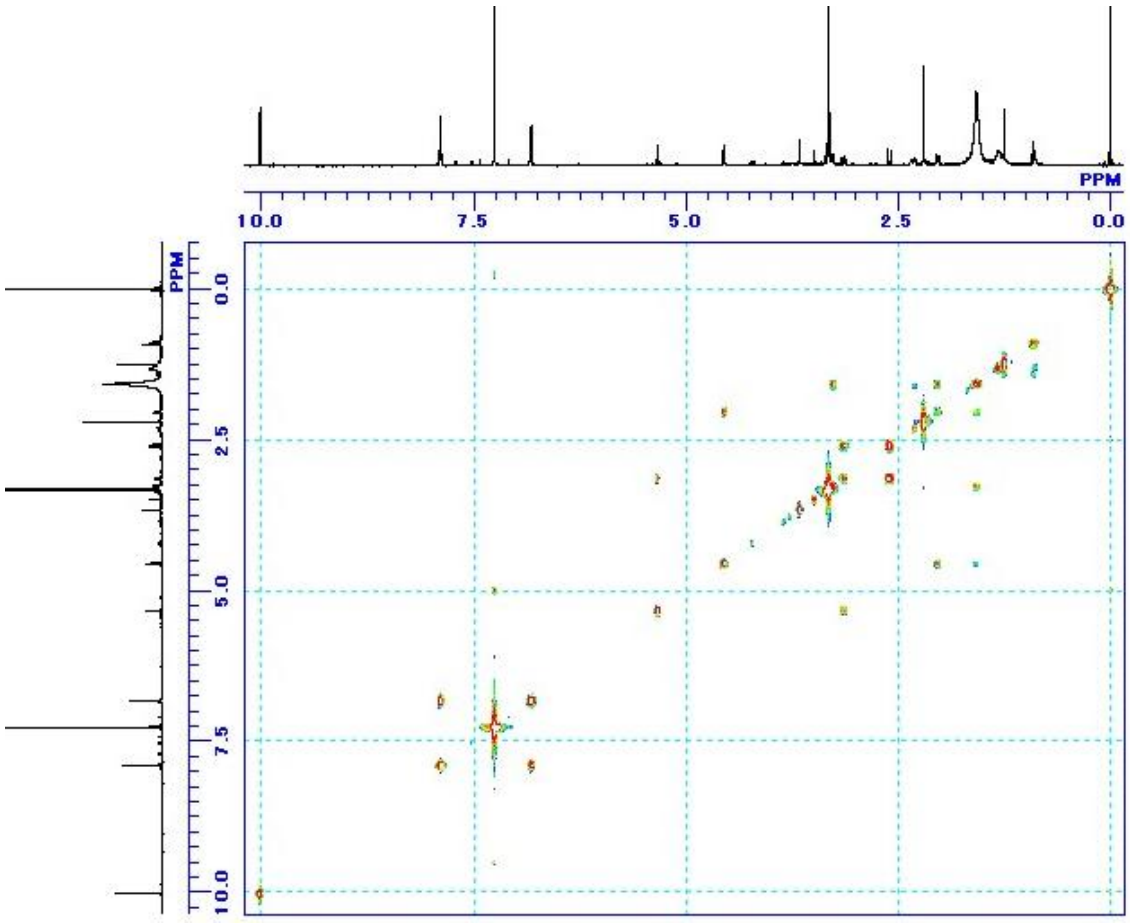

^{1}H-^{1}H COSY spectrum of **4** in $CDCl_3$

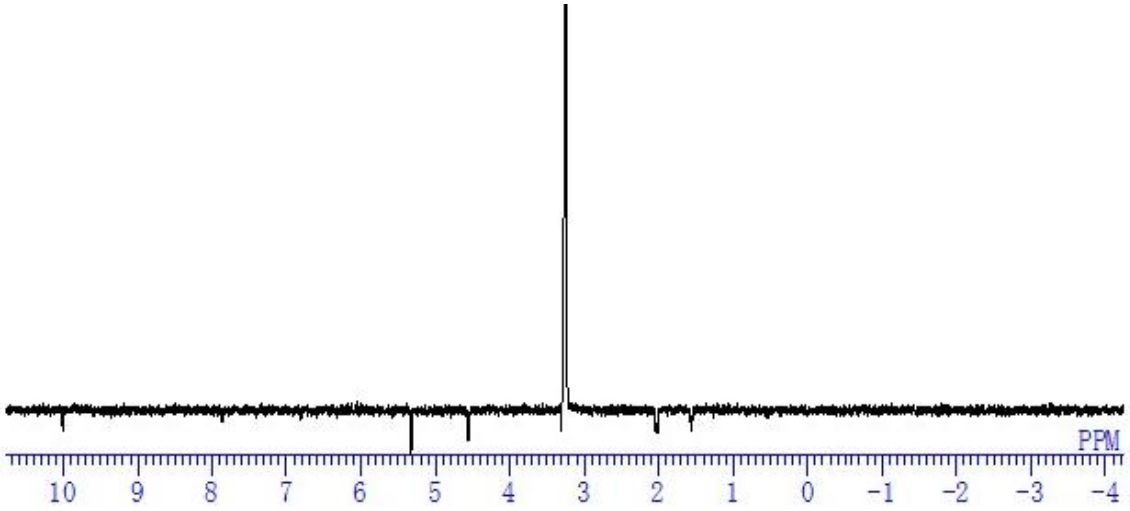

NOE spectrum of **4** in $CDCl_3$ (δ_H 3.25)

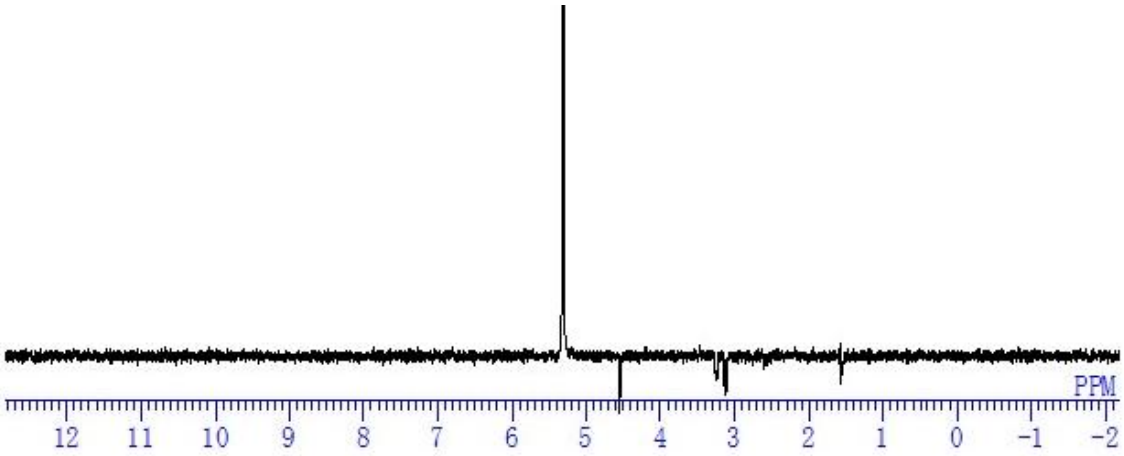

NOE spectrum of **4** in $CDCl_3$ (δ_H 5.32)

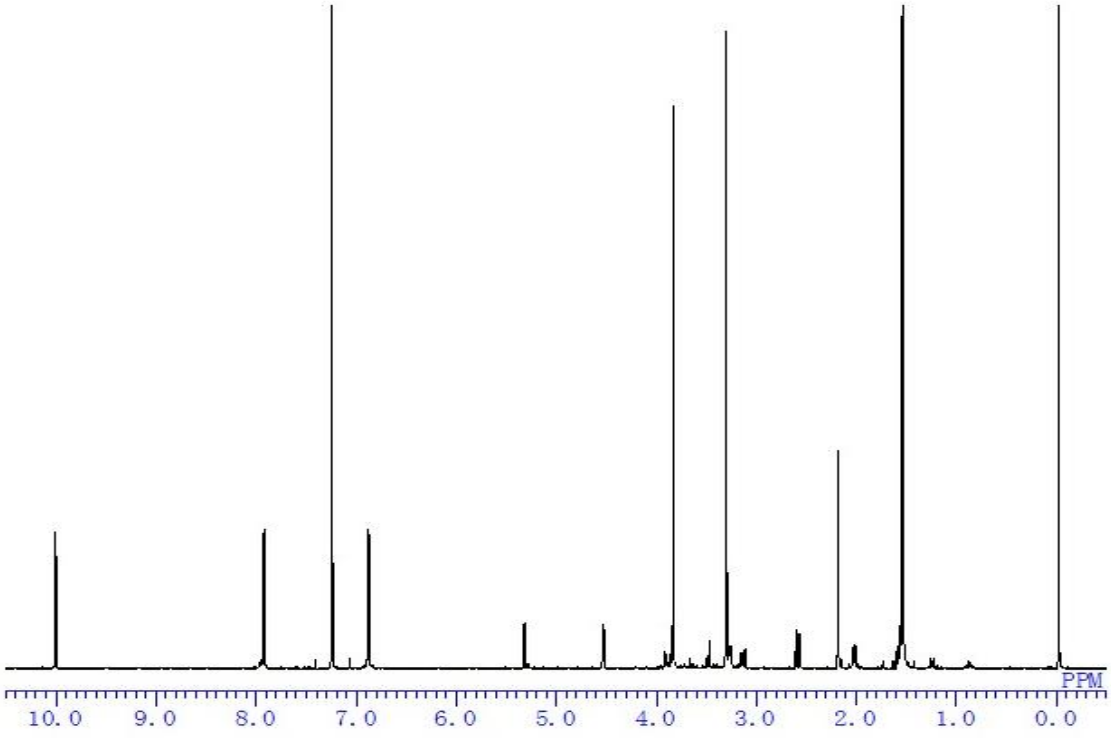

^{1}H NMR spectrum of **5** in $CDCl_3$

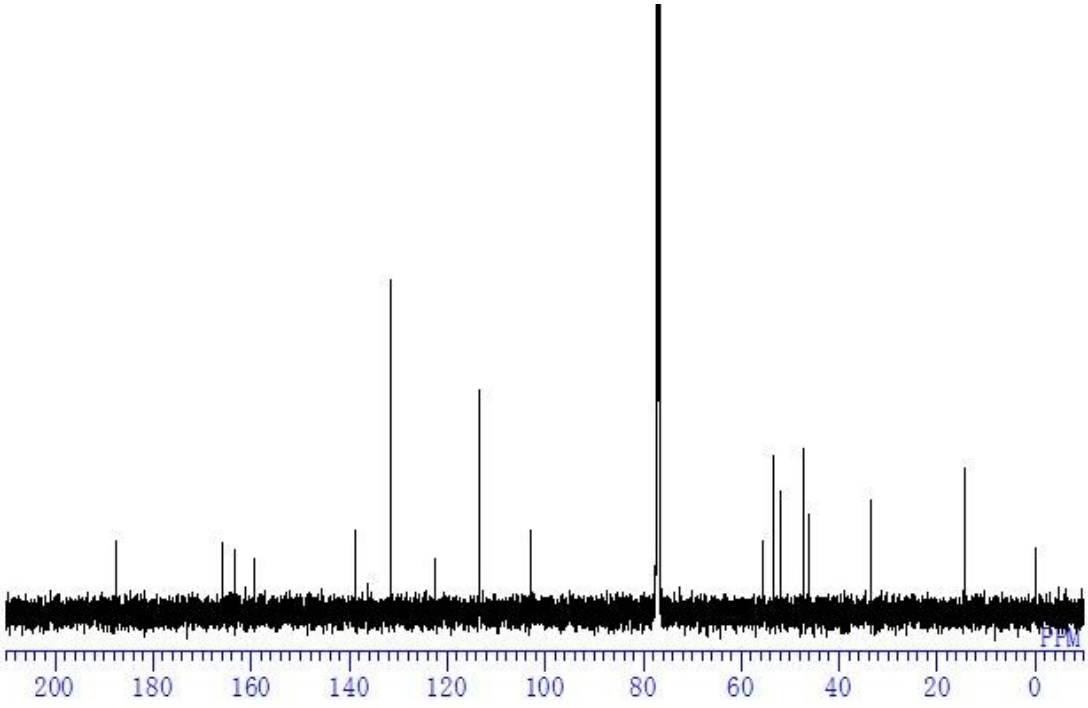

^{13}C NMR spectrum of **5** in $CDCl_3$

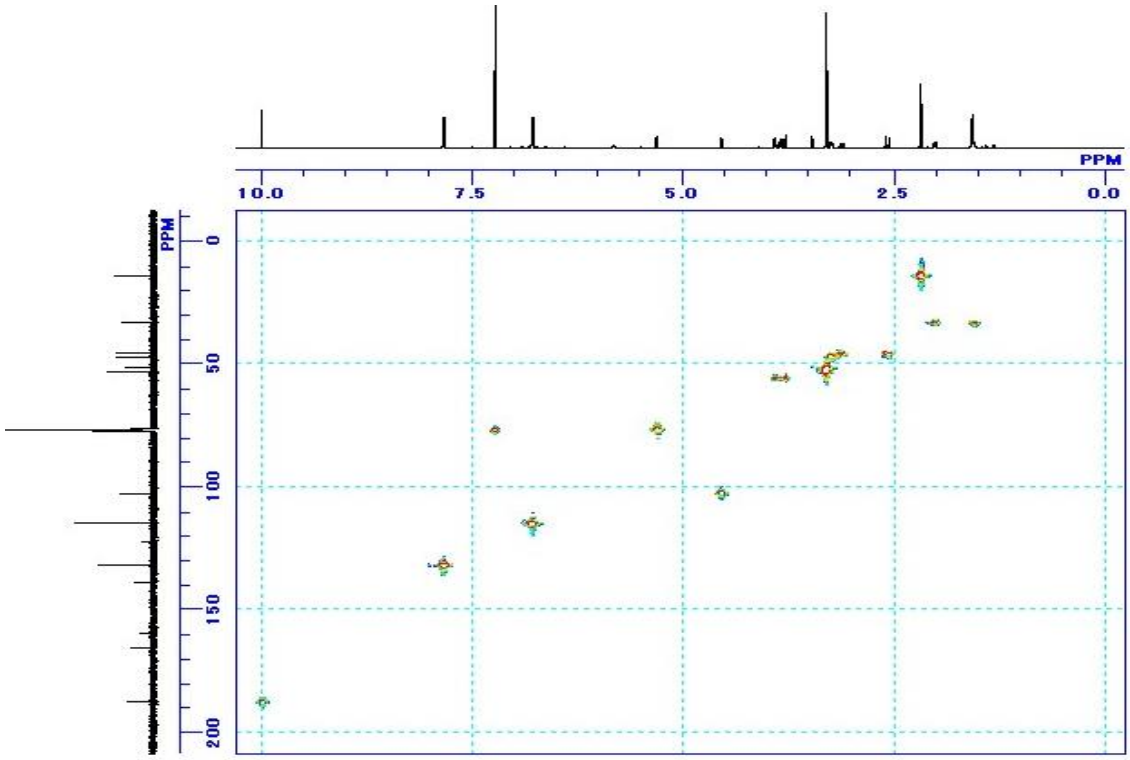

HMQC spectrum of **5** in $CDCl_3$

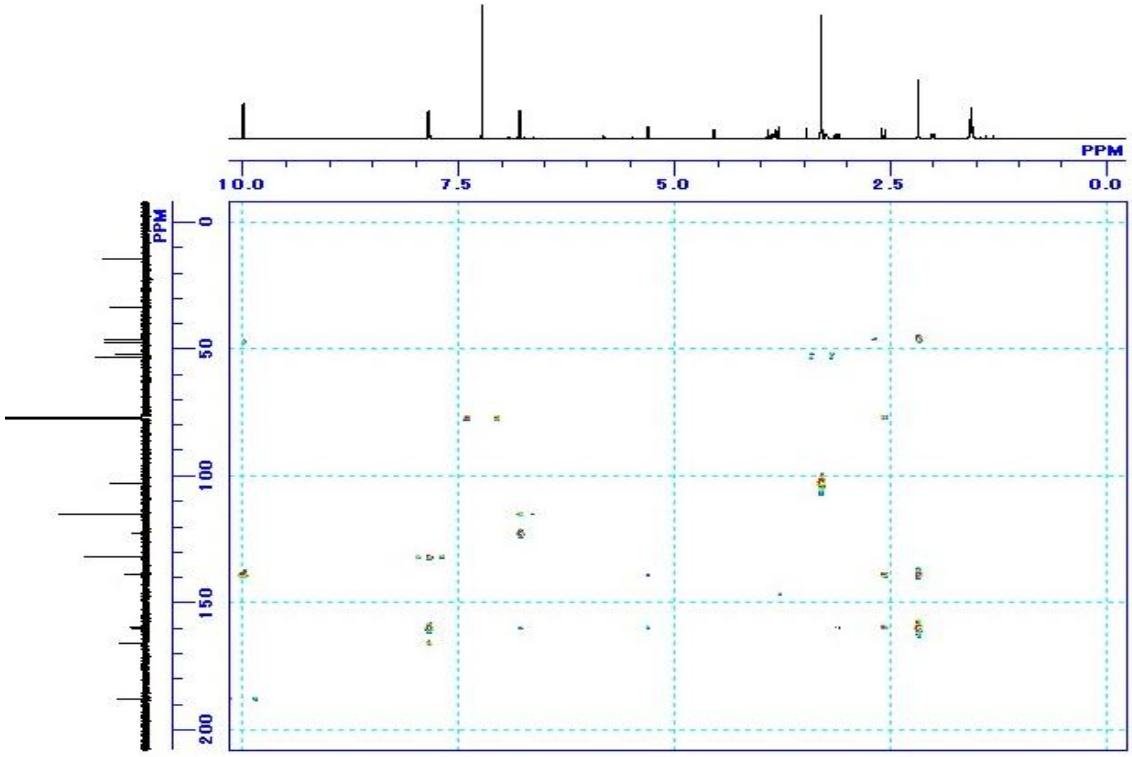

HMBC spectrum of **5** in $CDCl_3$

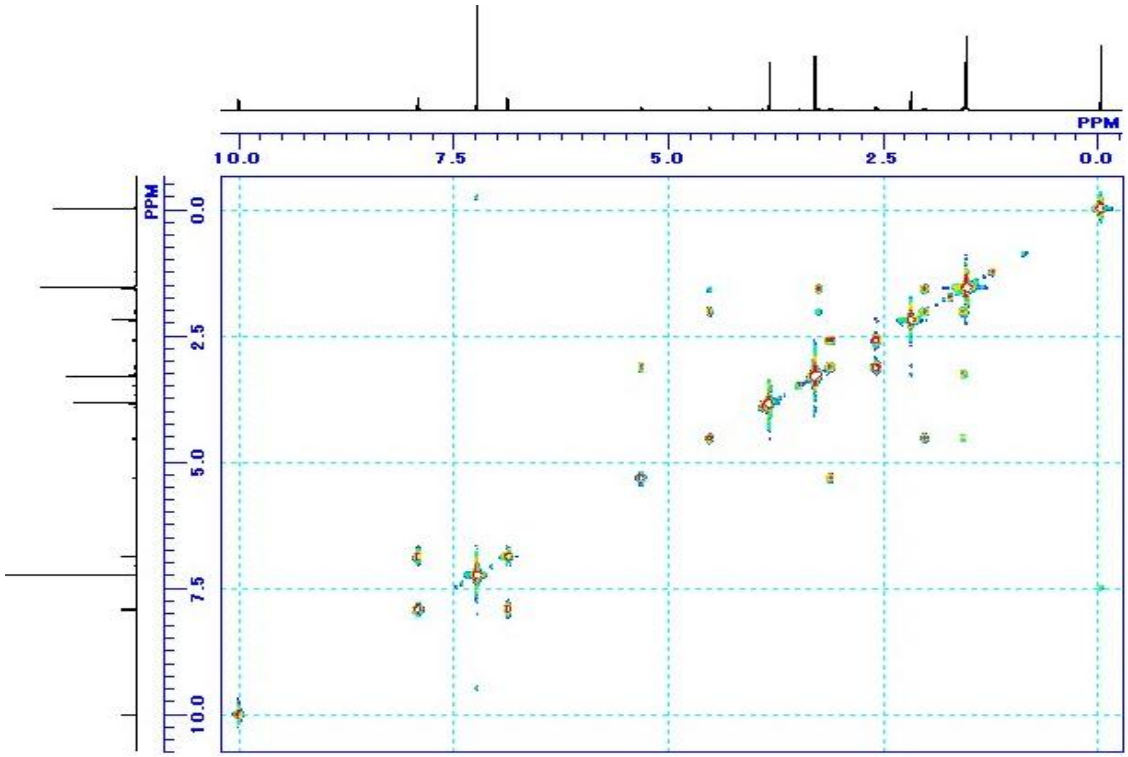

^{1}H-^{1}H COSY spectrum of **5** in $CDCl_3$

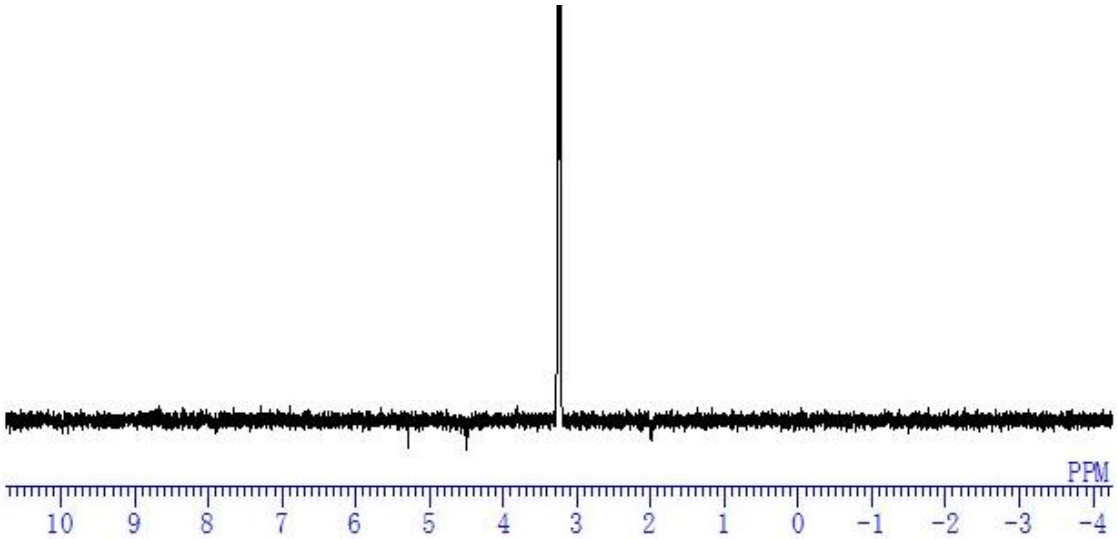

NOE spectrum of **5** in $CDCl_3$ (δ_H 3.26)

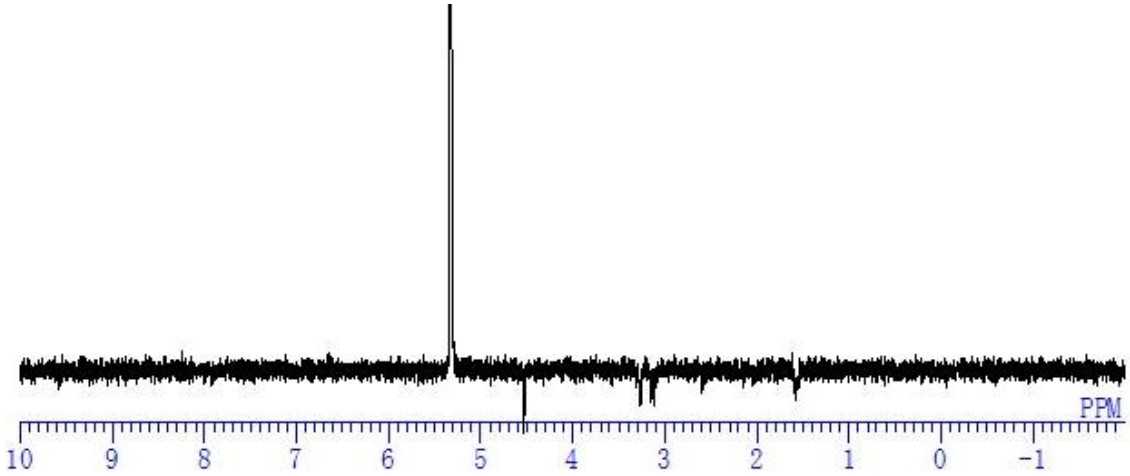

NOE spectrum of **5** in $CDCl_3$ (δ_H 5.33)

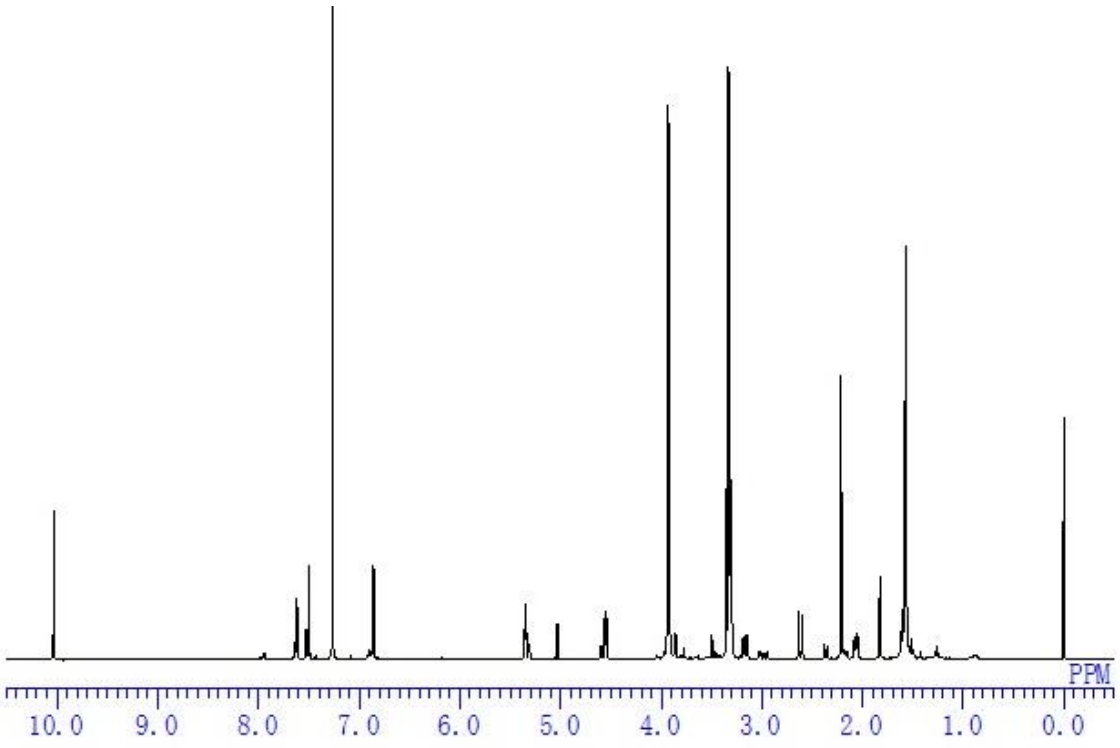

^{1}H NMR spectrum of **6** in $CDCl_3$

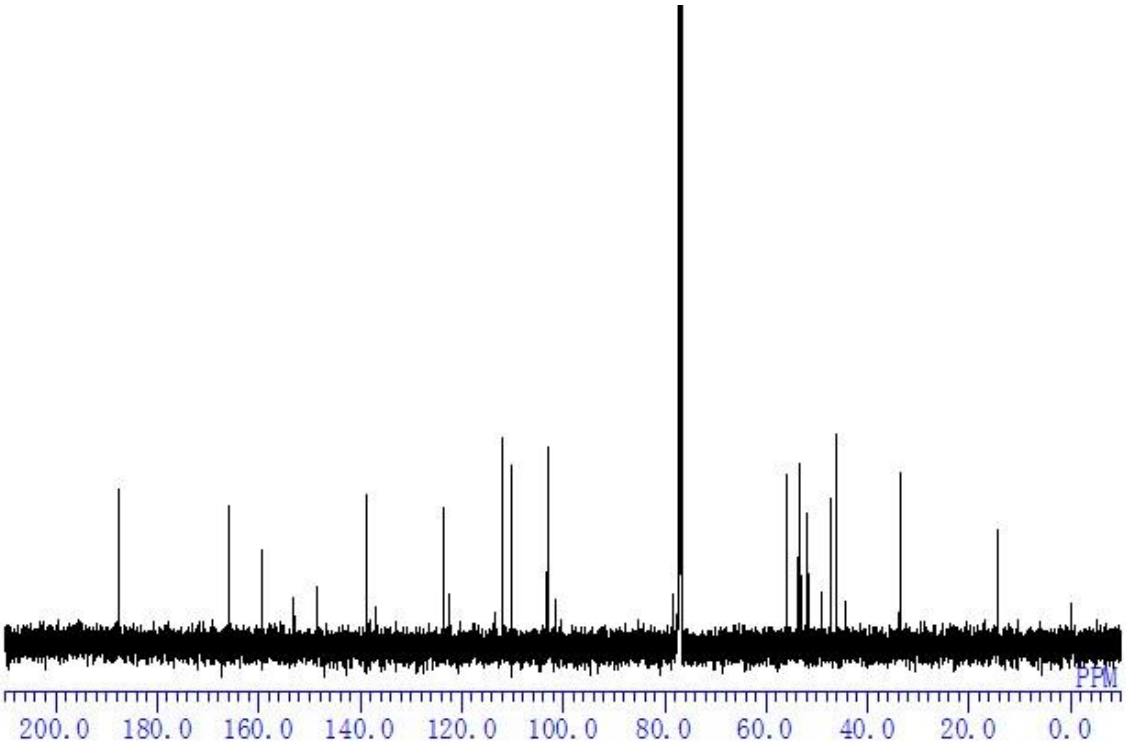

^{13}C NMR spectrum of **6** in $CDCl_3$

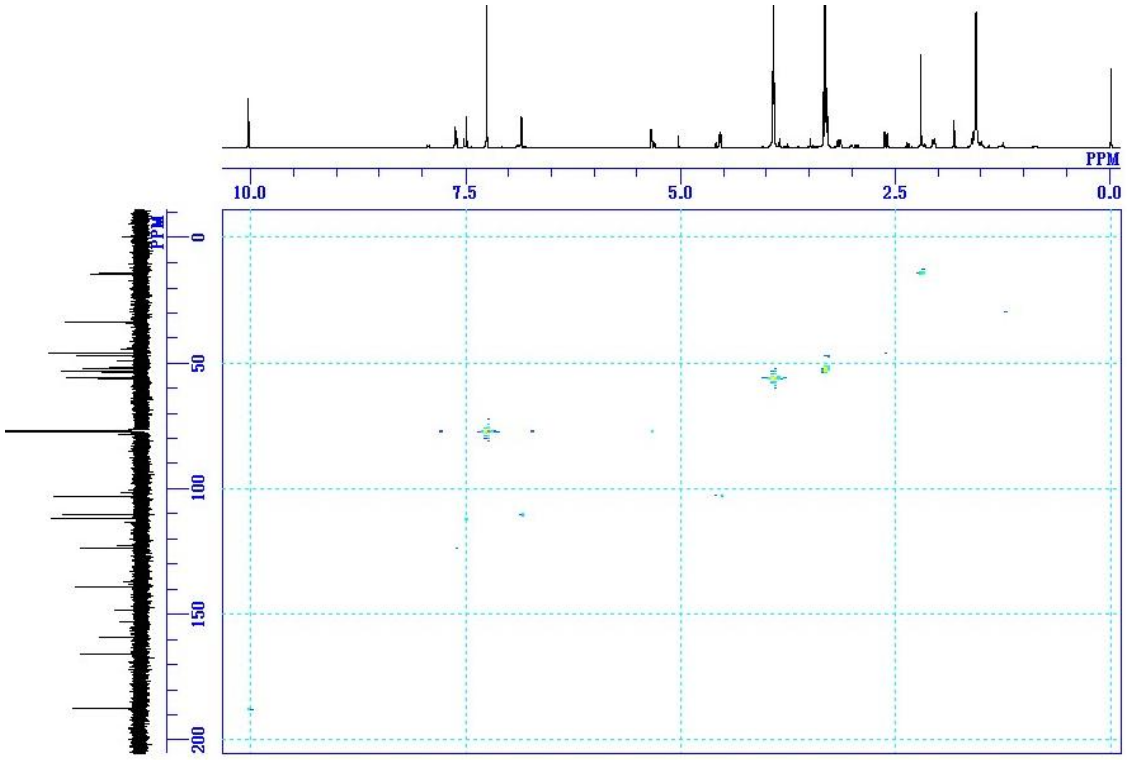

HMQC spectrum of **6** in $CDCl_3$

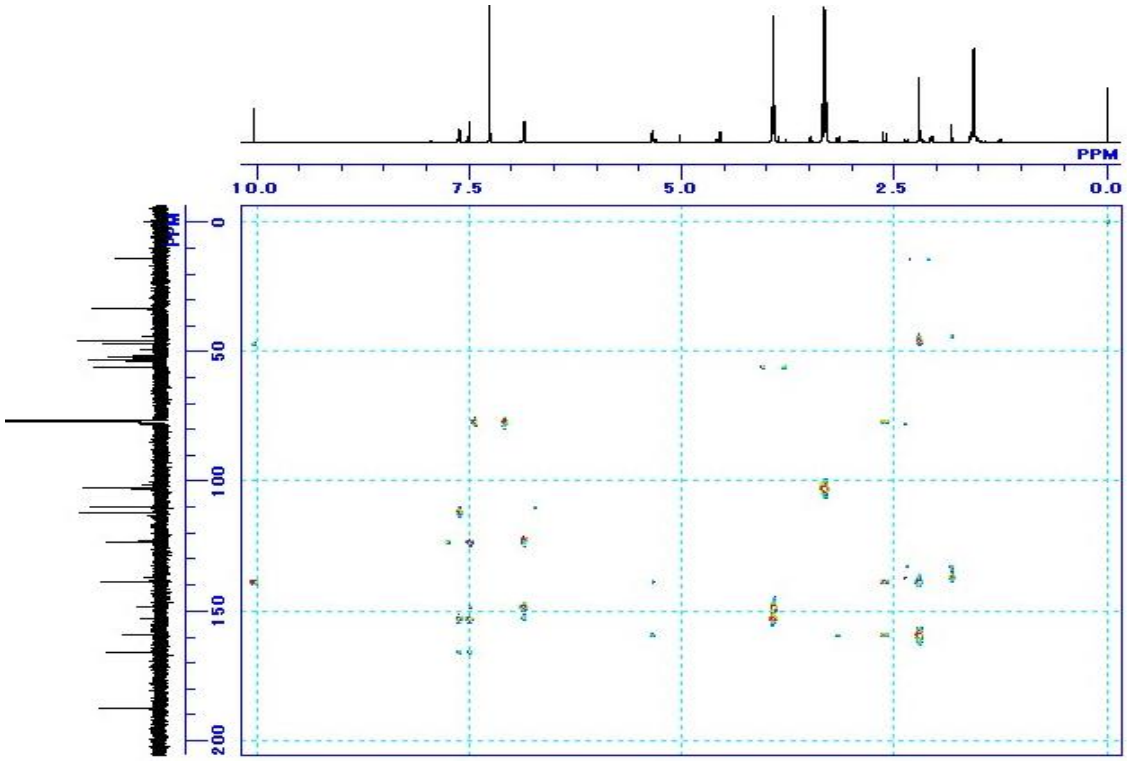

HMBC spectrum of **6** in $CDCl_3$

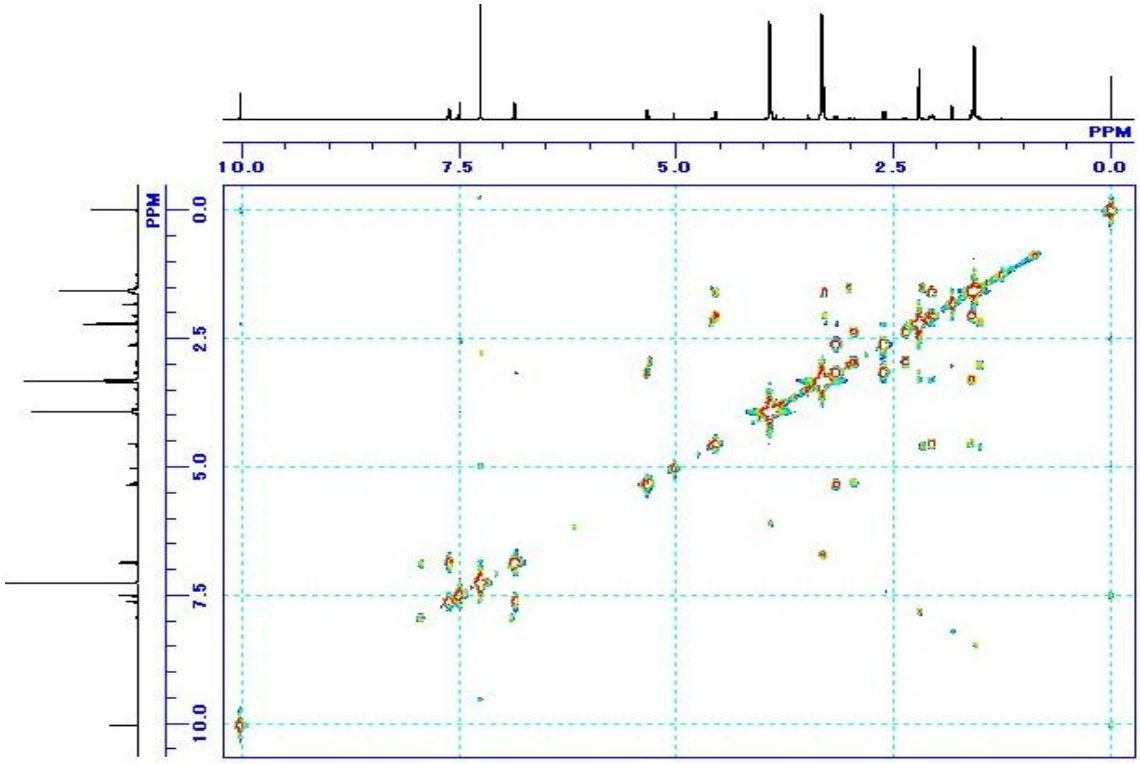

^{1}H-^{1}H COSY spectrum of **6** in $CDCl_3$

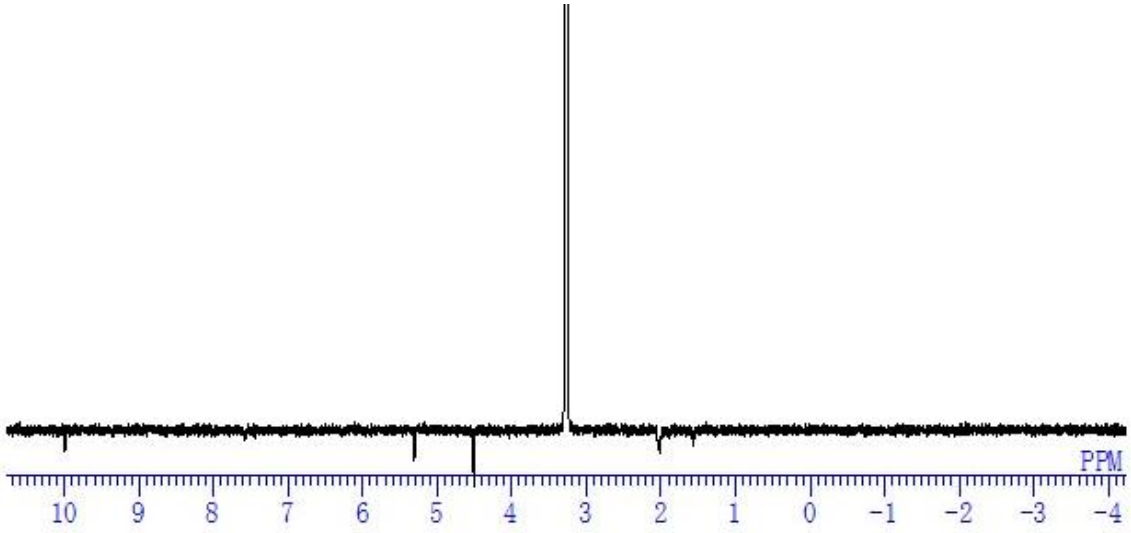

NOE spectrum of **6** in $CDCl_3$ (δ_H 3.28)

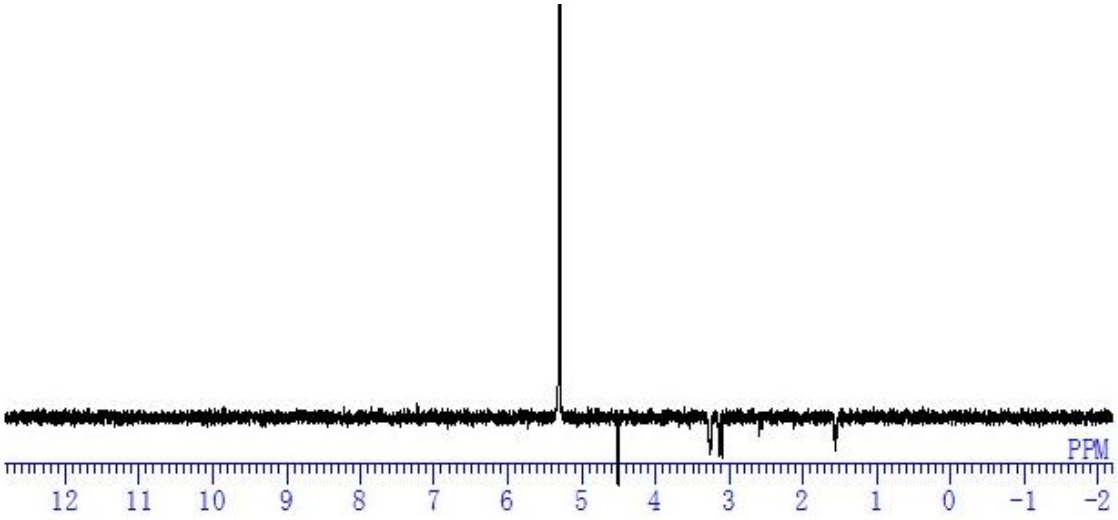

NOE spectrum of **6** in $CDCl_3$ (δ_H 5.32)

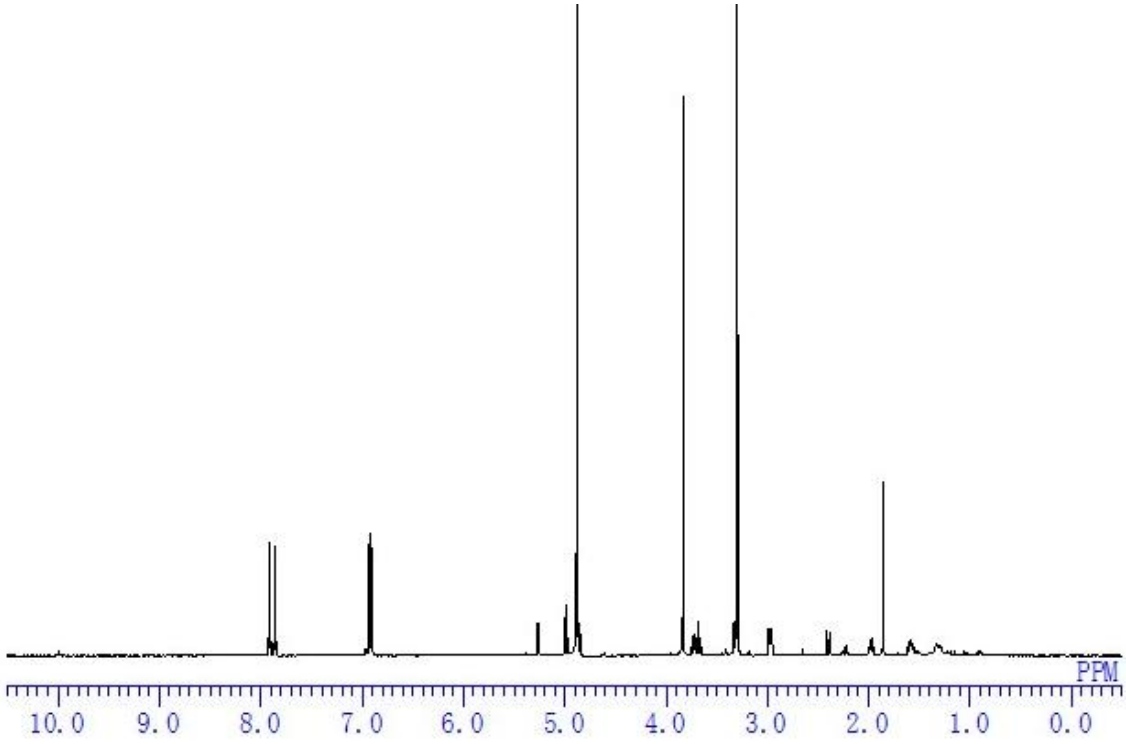

^{1}H NMR spectrum of **7** in CD_3OD

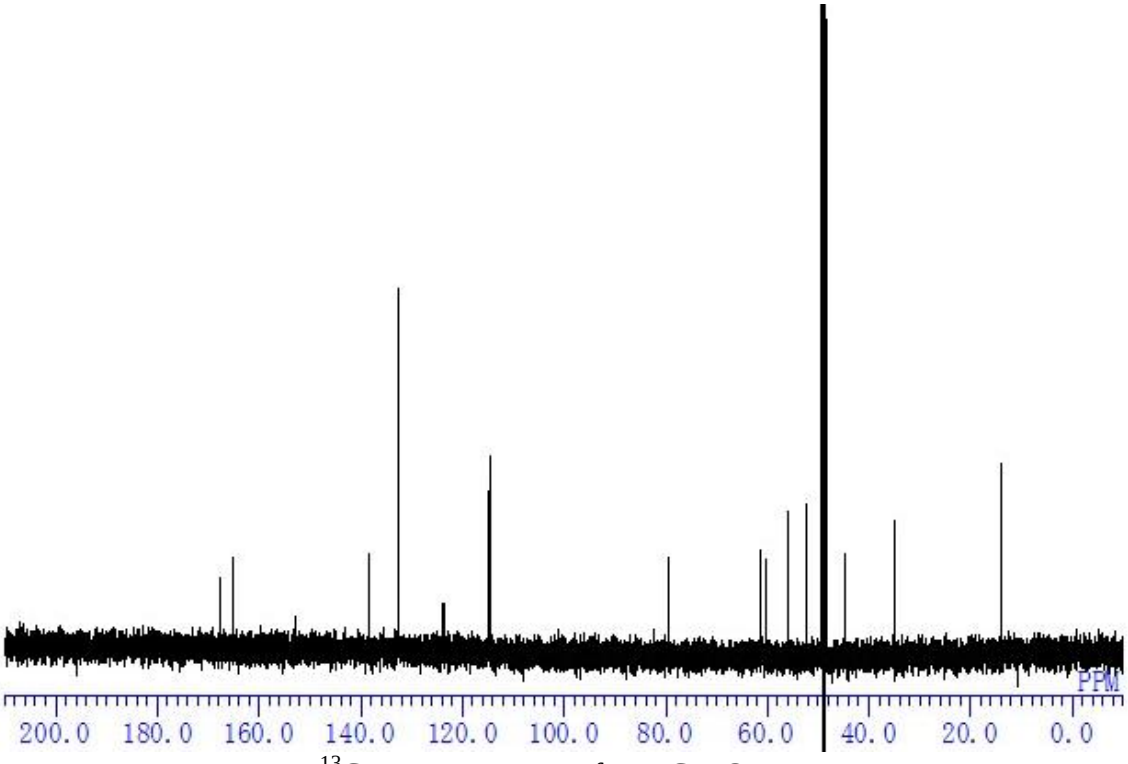

^{13}C NMR spectrum of **7** in CD_3OD

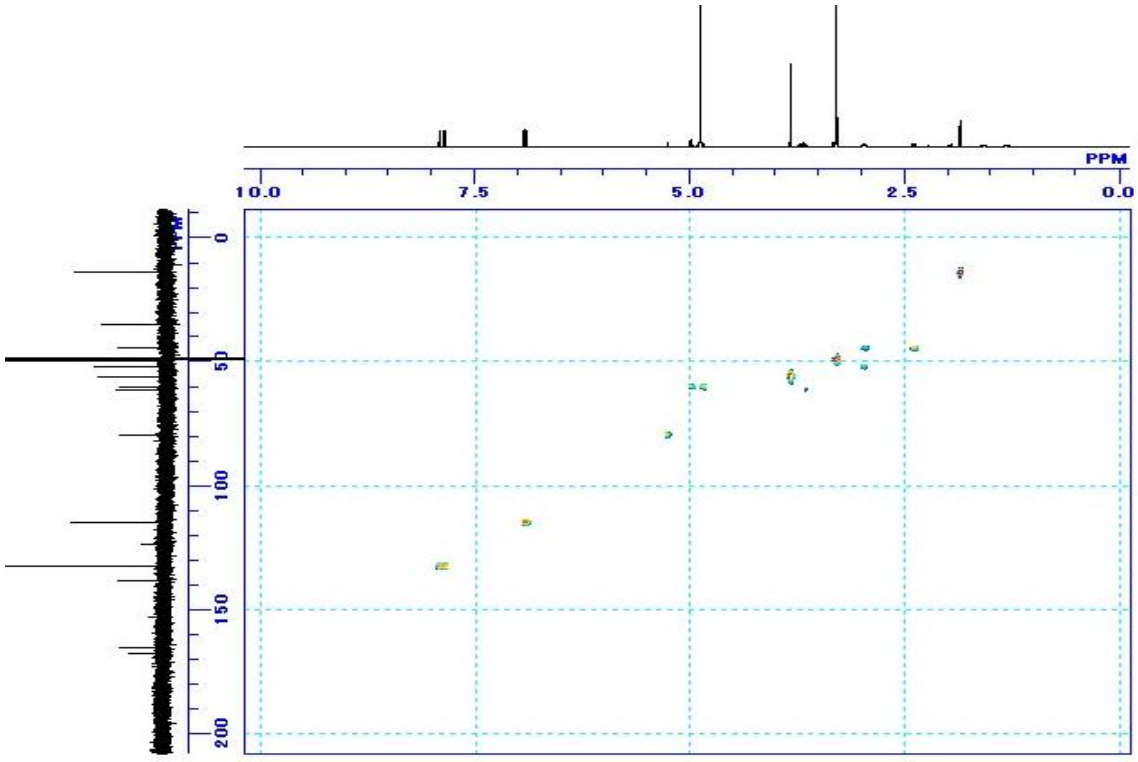

HMQC spectrum of **7** in CD_3OD

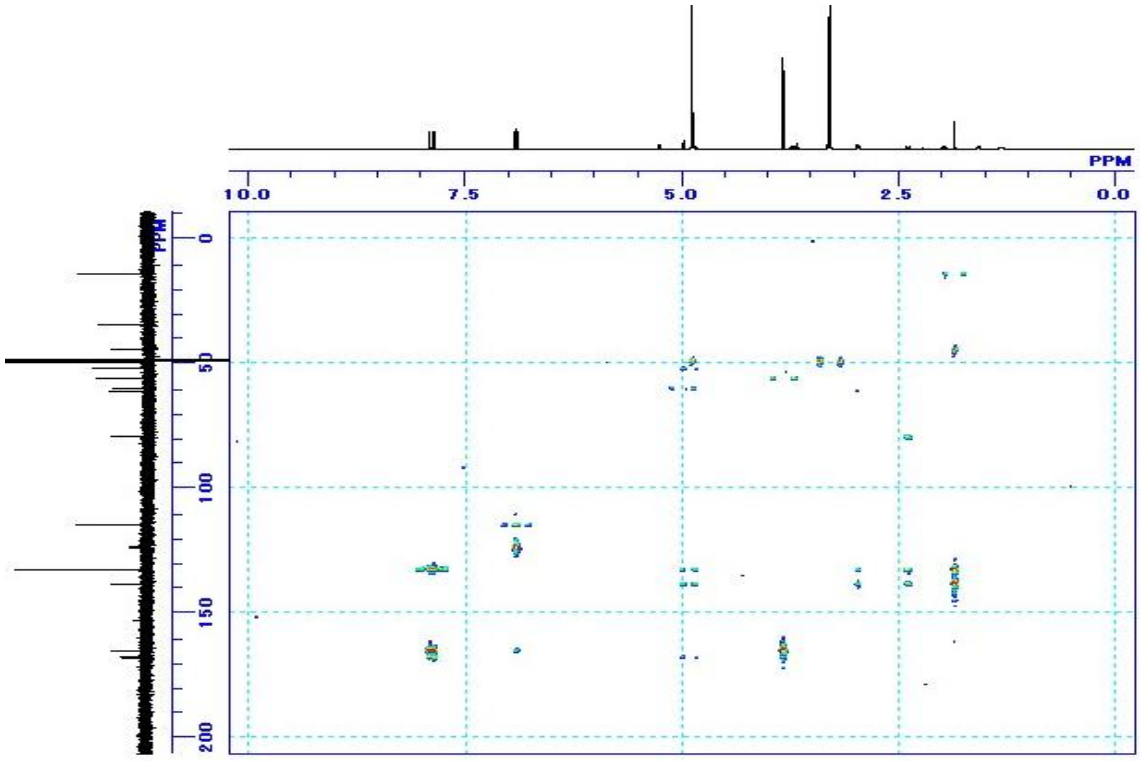

HMBC spectrum of **7** in CD_3OD

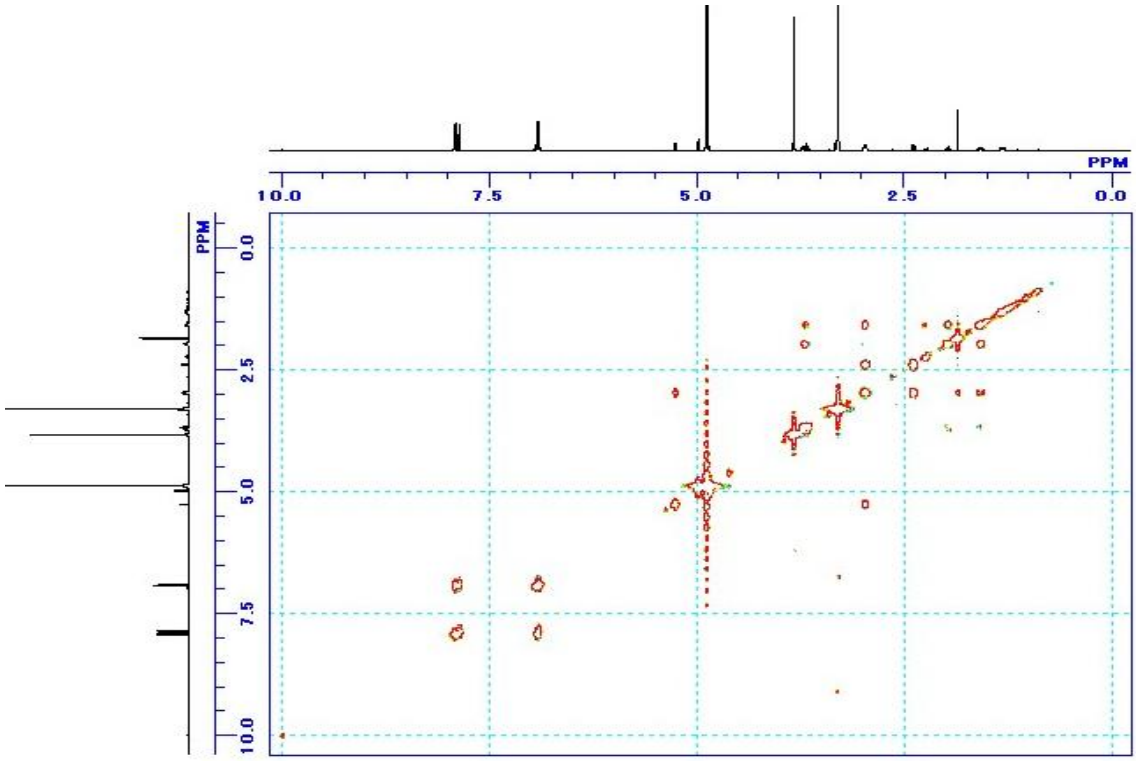

^{1}H-^{1}H COSY spectrum of **7** in CD_3OD

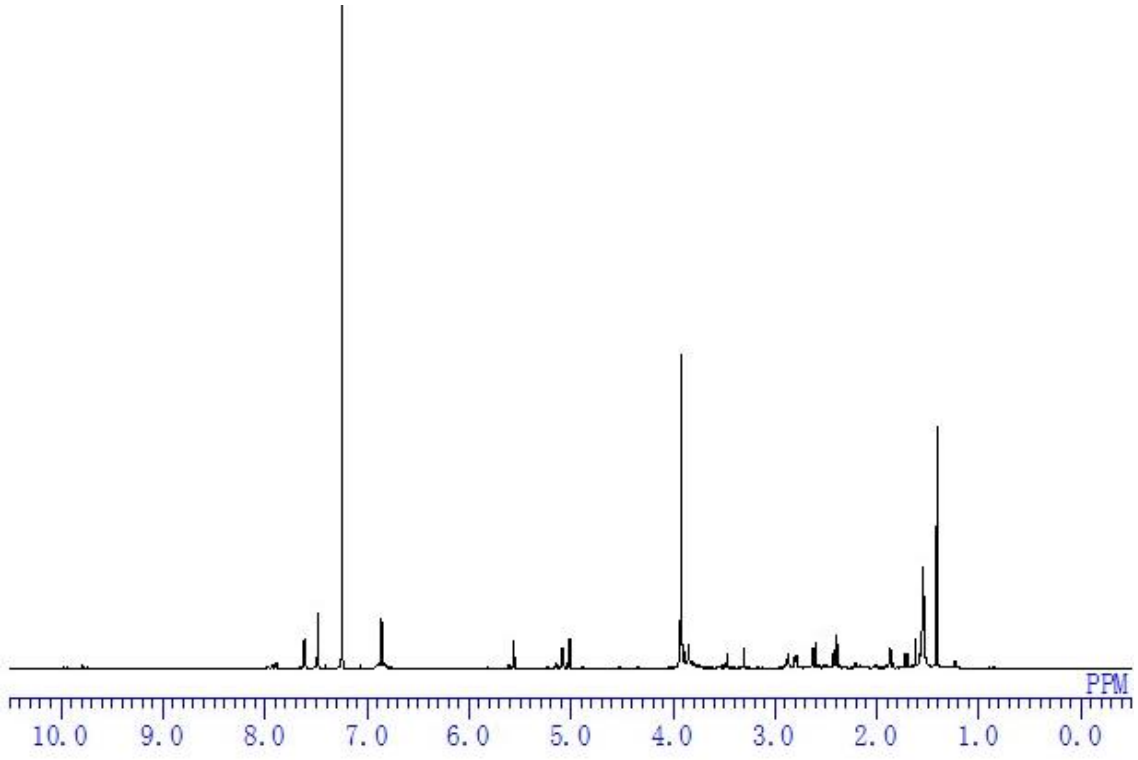

^{1}H NMR spectrum of **8** in $CDCl_3$

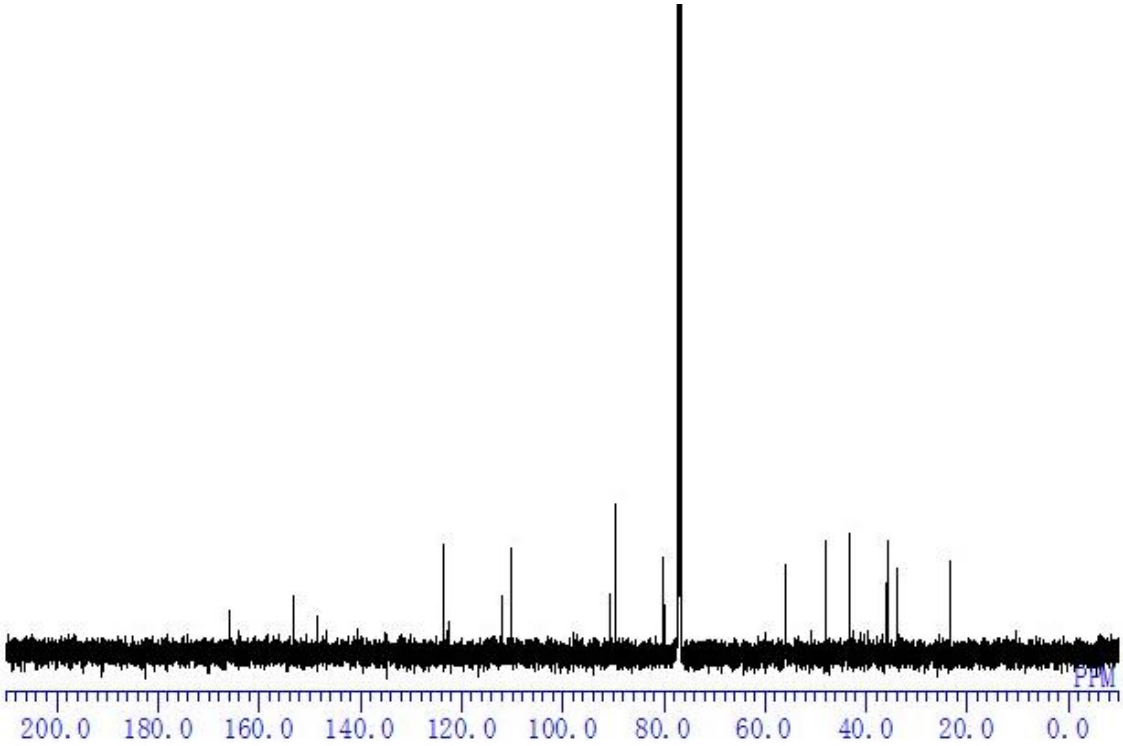

^{13}C NMR spectrum of **8** in $CDCl_3$

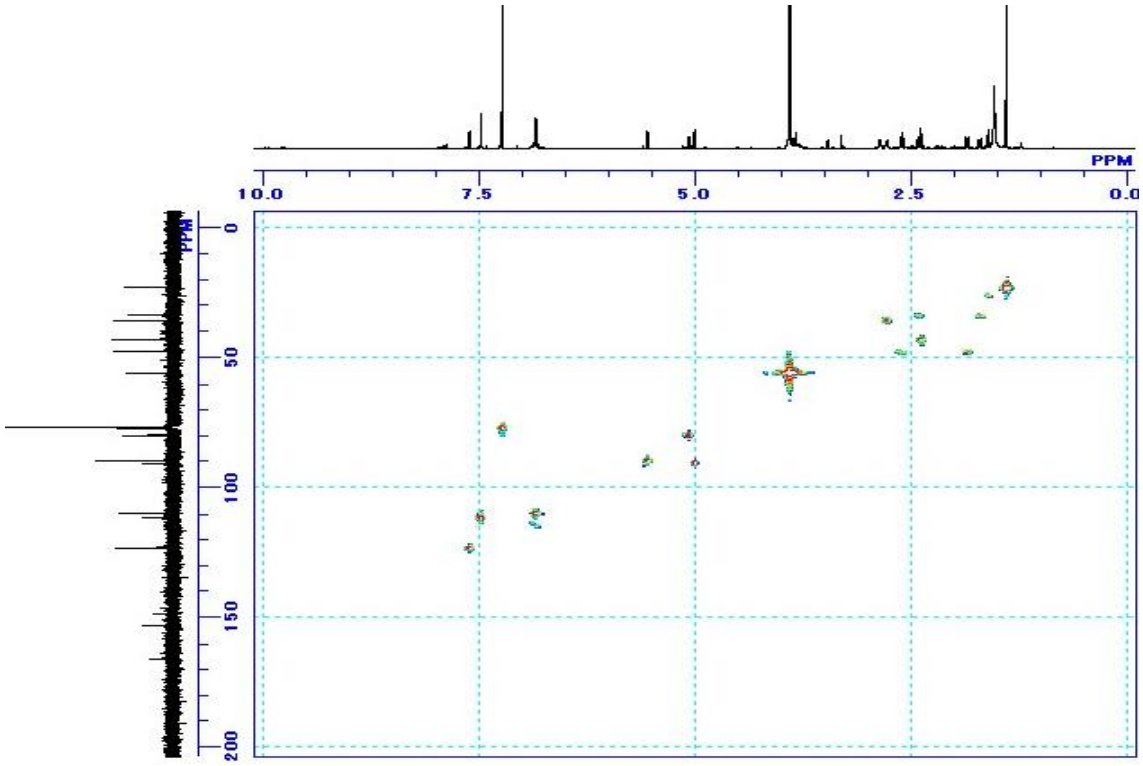

HMQC spectrum of **8** in $CDCl_3$

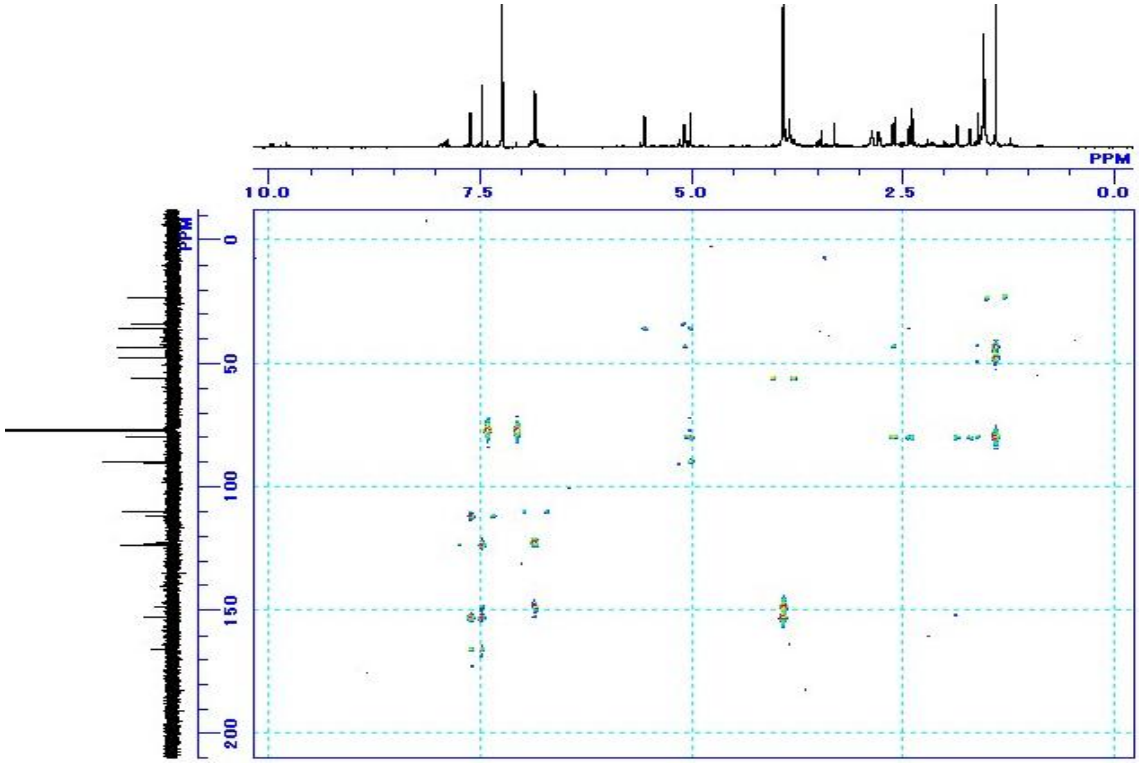

HMBC spectrum of **8** in $CDCl_3$

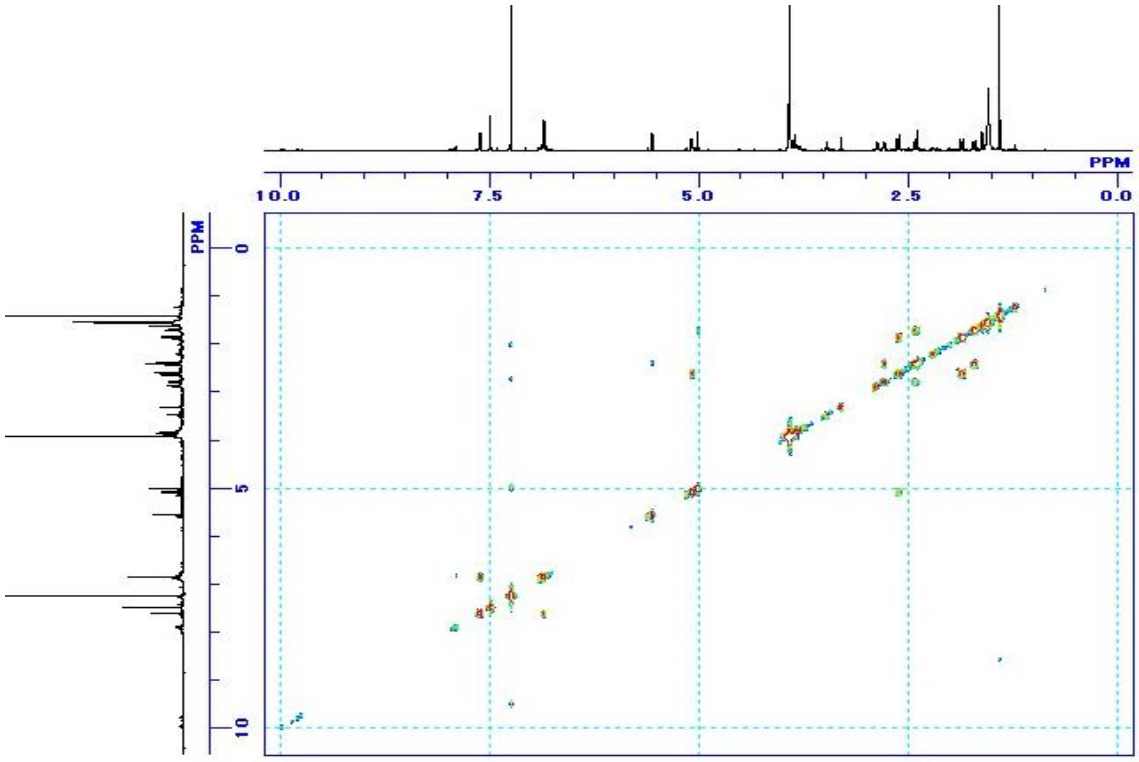

^{1}H-^{1}H COSY spectrum of **8** in $CDCl_3$

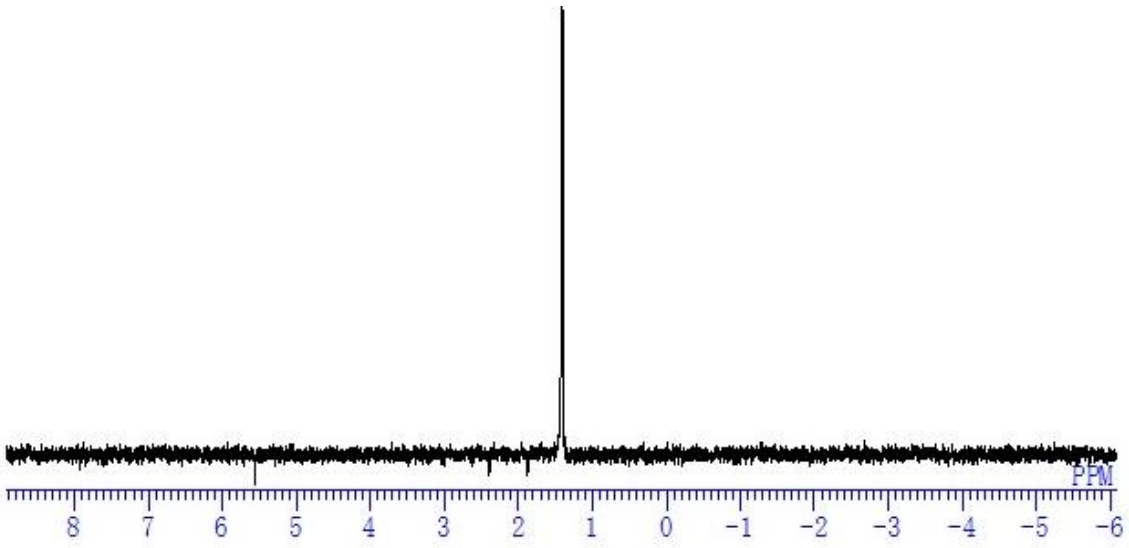

NOE spectrum of **8** in $CDCl_3$ (δ_H 1.41)

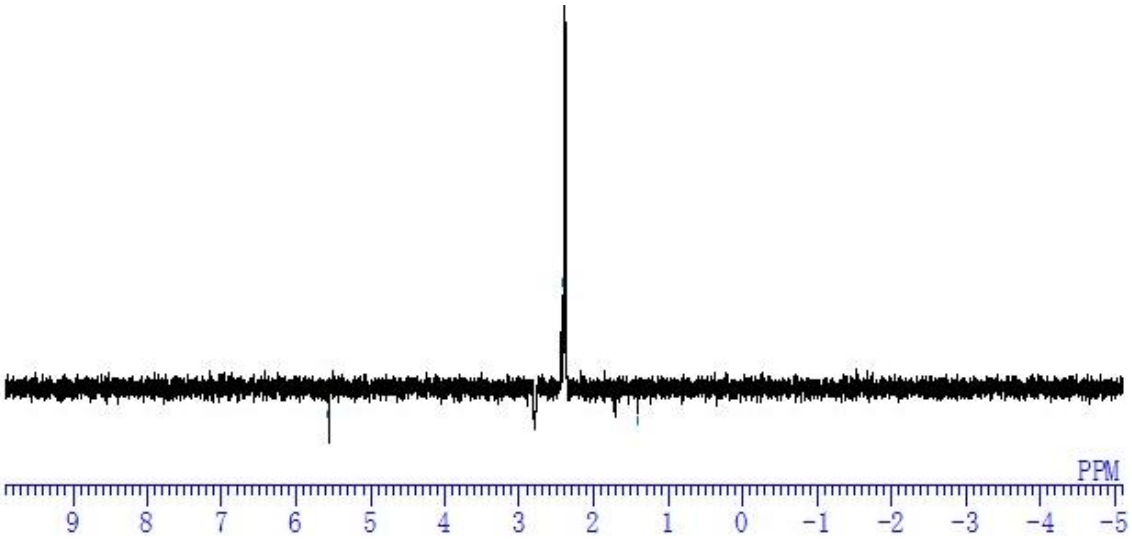

NOE spectrum of **8** in $CDCl_3$ (δ_H 2.38)

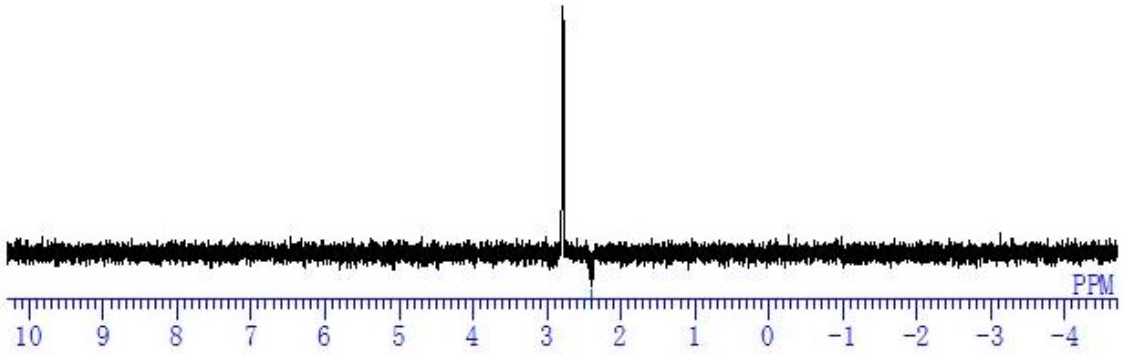

NOE spectrum of **8** in $CDCl_3$ (δ_H 2.80)

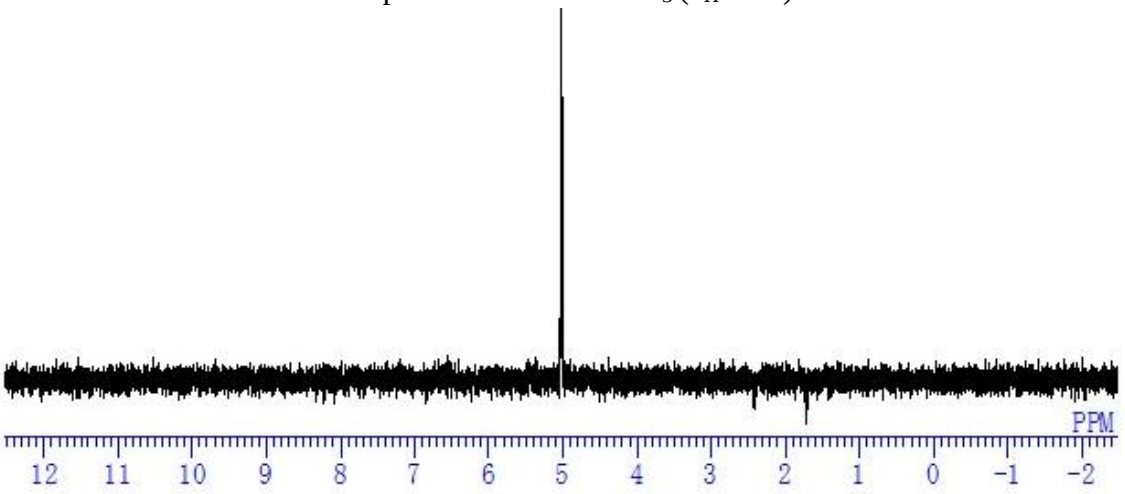

NOE spectrum of **8** in $CDCl_3$ (δ_H 5.02)

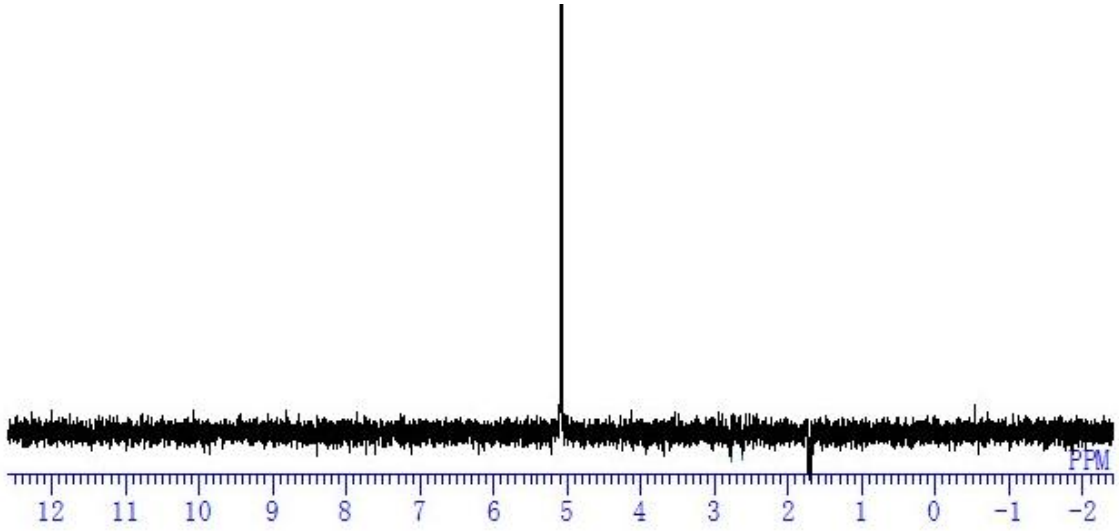

NOE spectrum of **8** in $CDCl_3$ (δ_H 5.08)

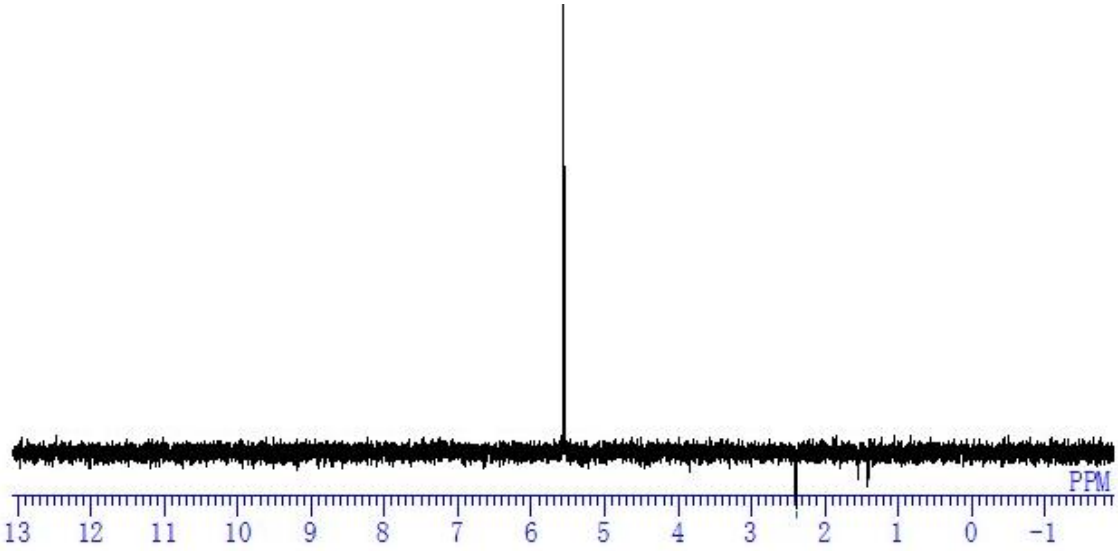

NOE spectrum of **8** in $CDCl_3$ (δ_H 5.56)

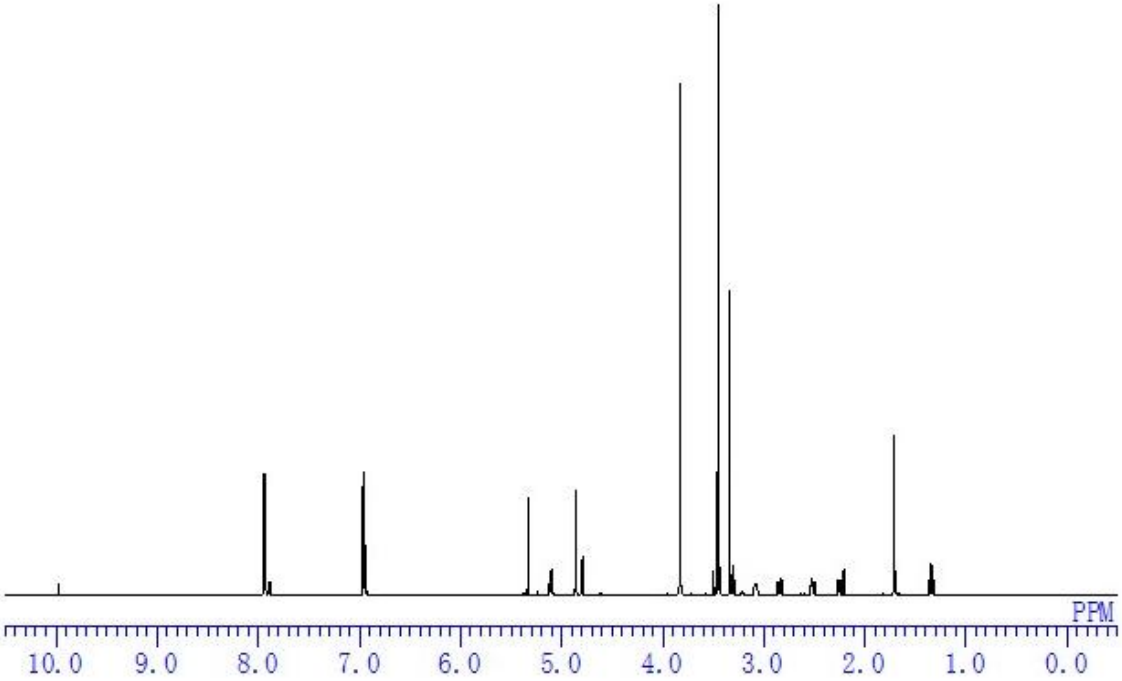

^{1}H NMR spectrum of **9** in CD_3OD

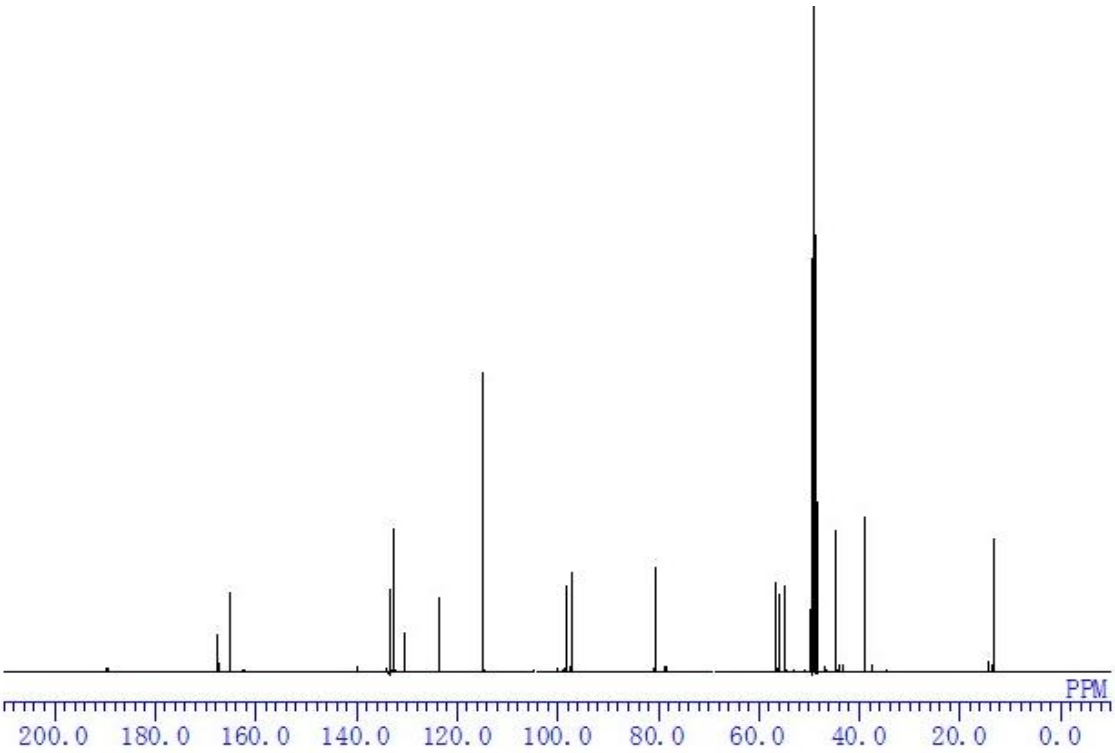

^{13}C NMR spectrum of **9** in CD_3OD

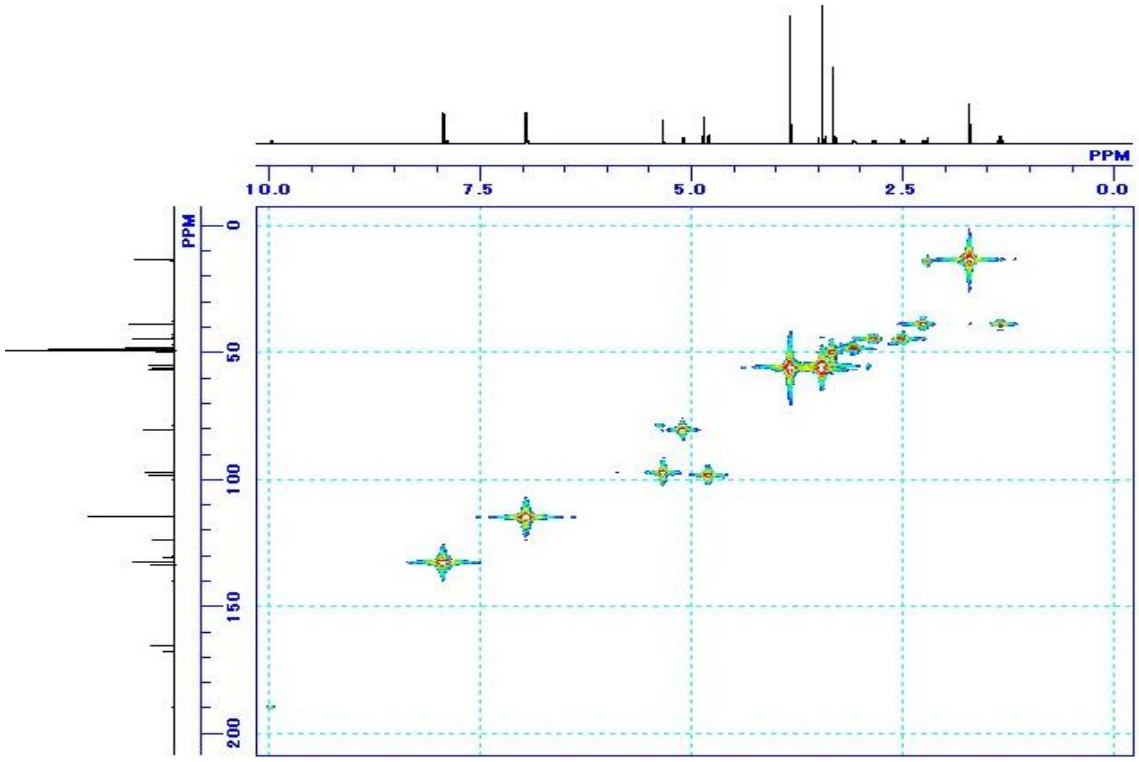

HMQC spectrum of **9** in CD_3OD

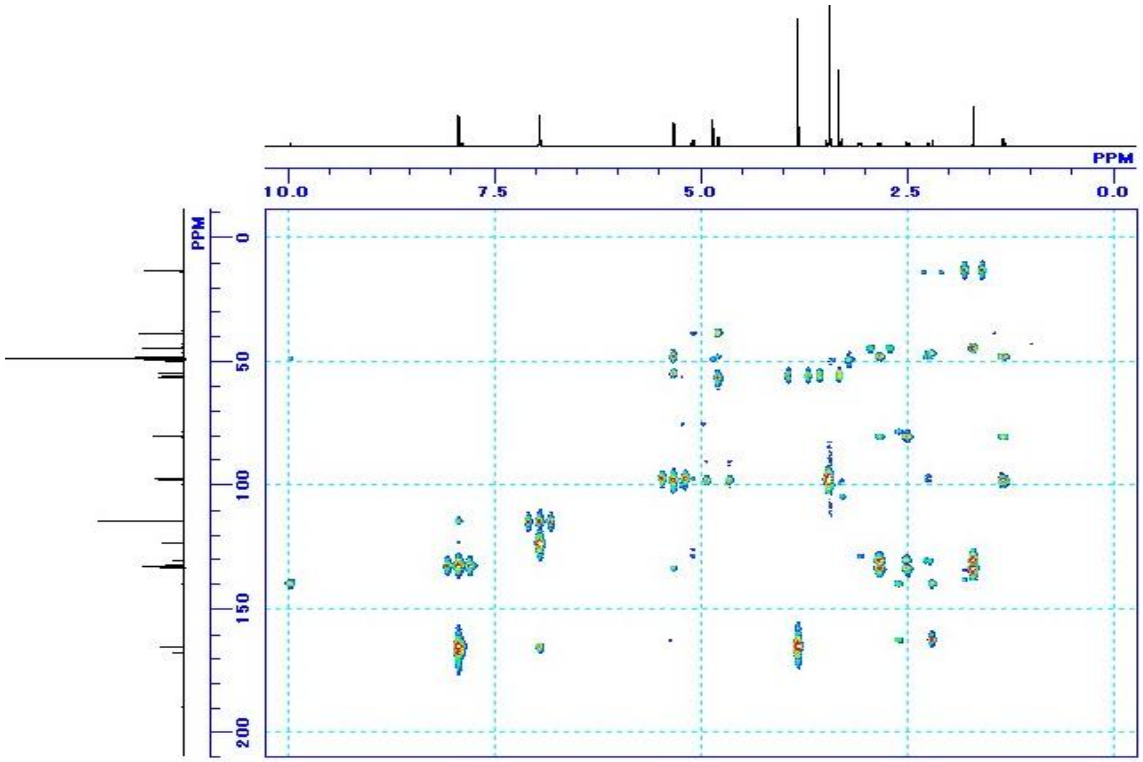

HMBC spectrum of **9** in CD_3OD

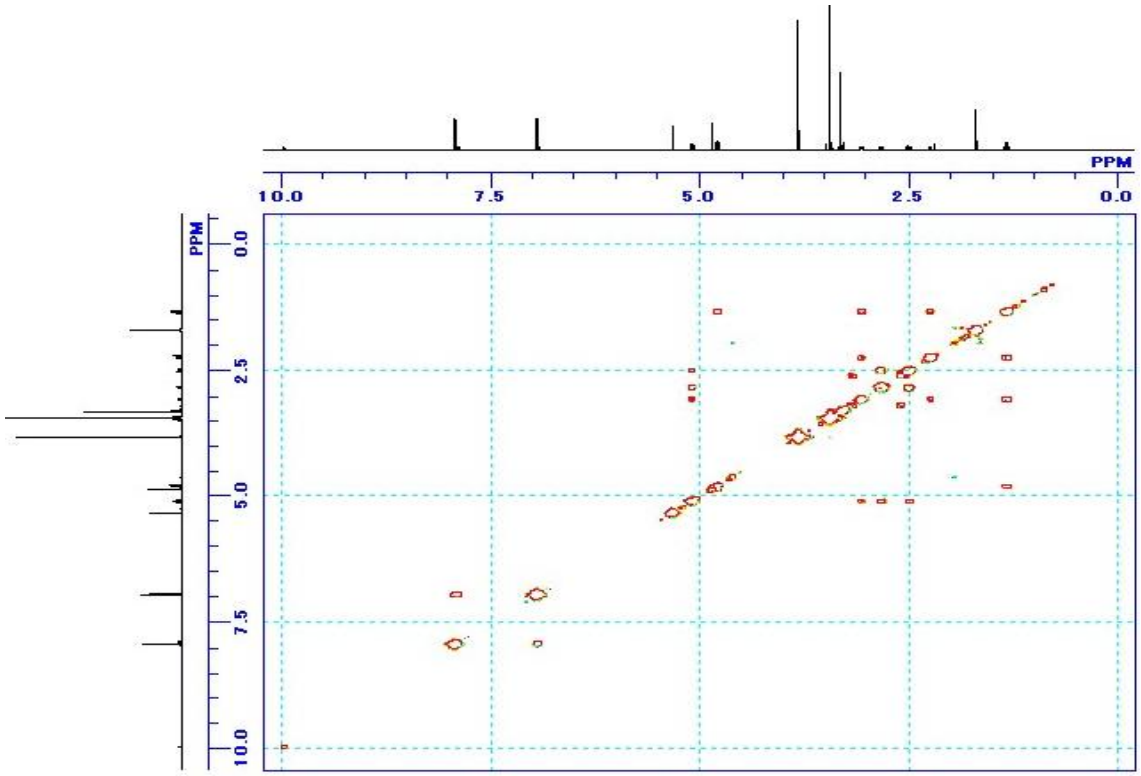

^{1}H-^{1}H COSY spectrum of **9** in CD_3OD

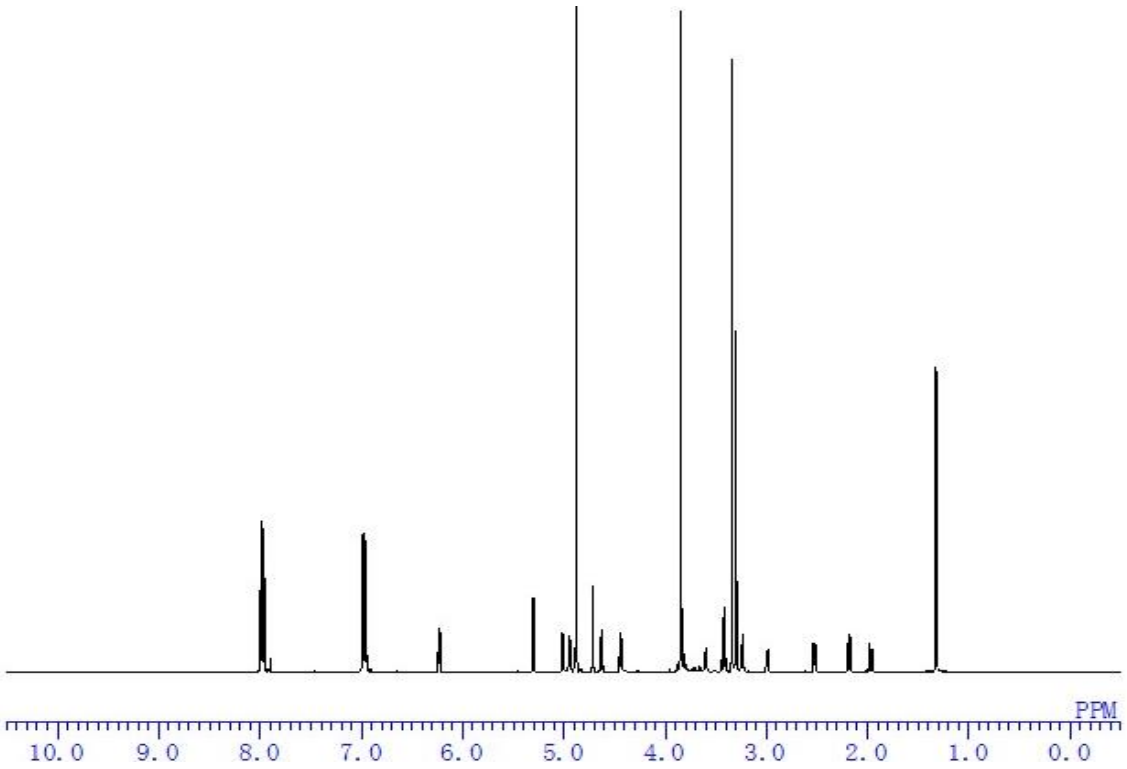

^{1}H NMR spectrum of **10** in CD_3OD

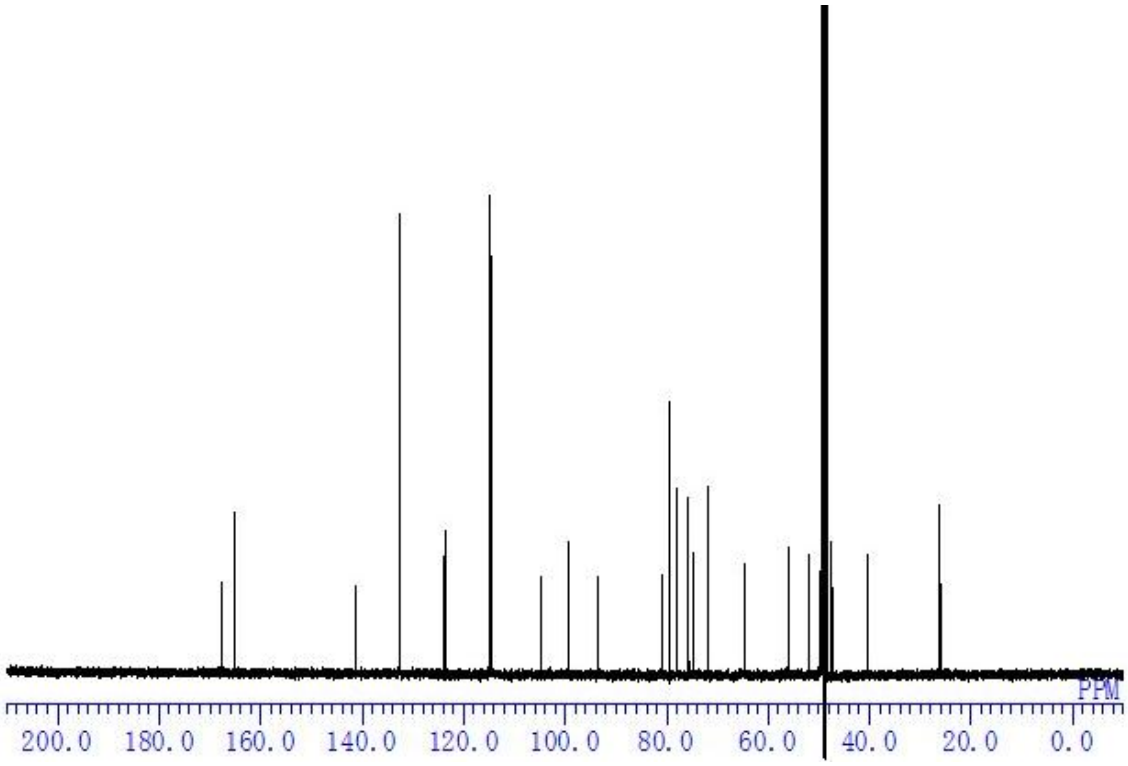

^{13}C NMR spectrum of **10** in CD_3OD

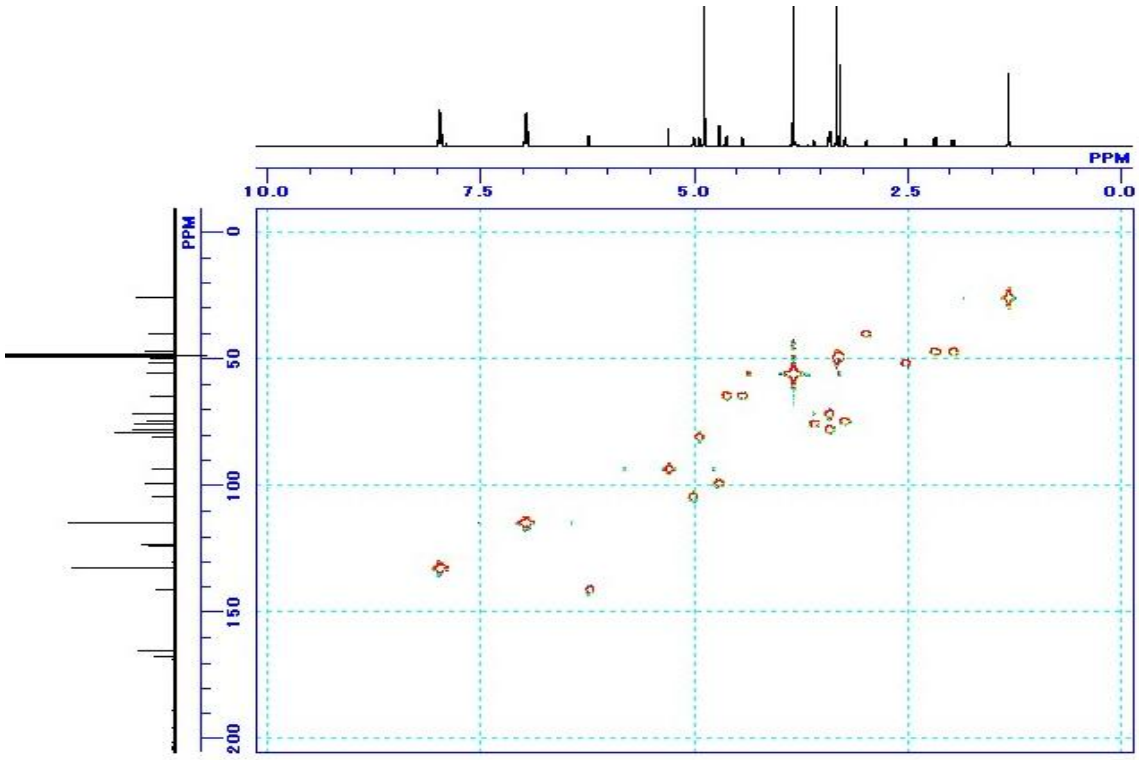

HMQC spectrum of **10** in CD_3OD

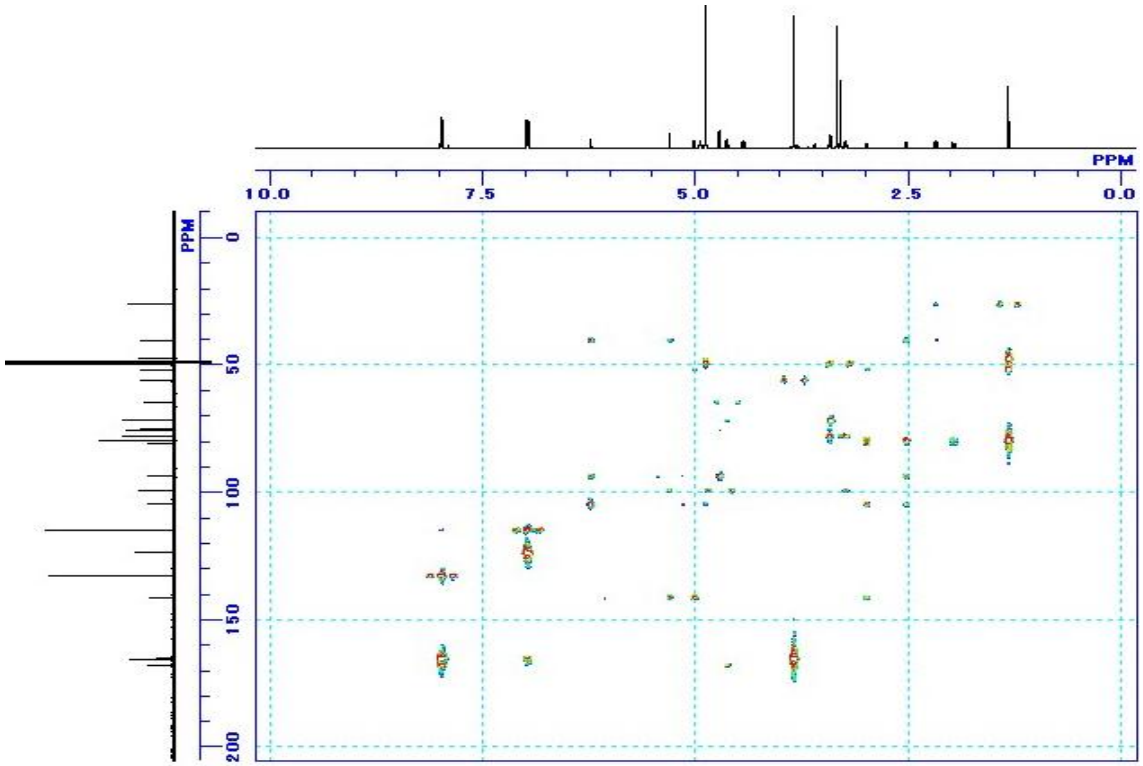

HMBC spectrum of **10** in CD_3OD

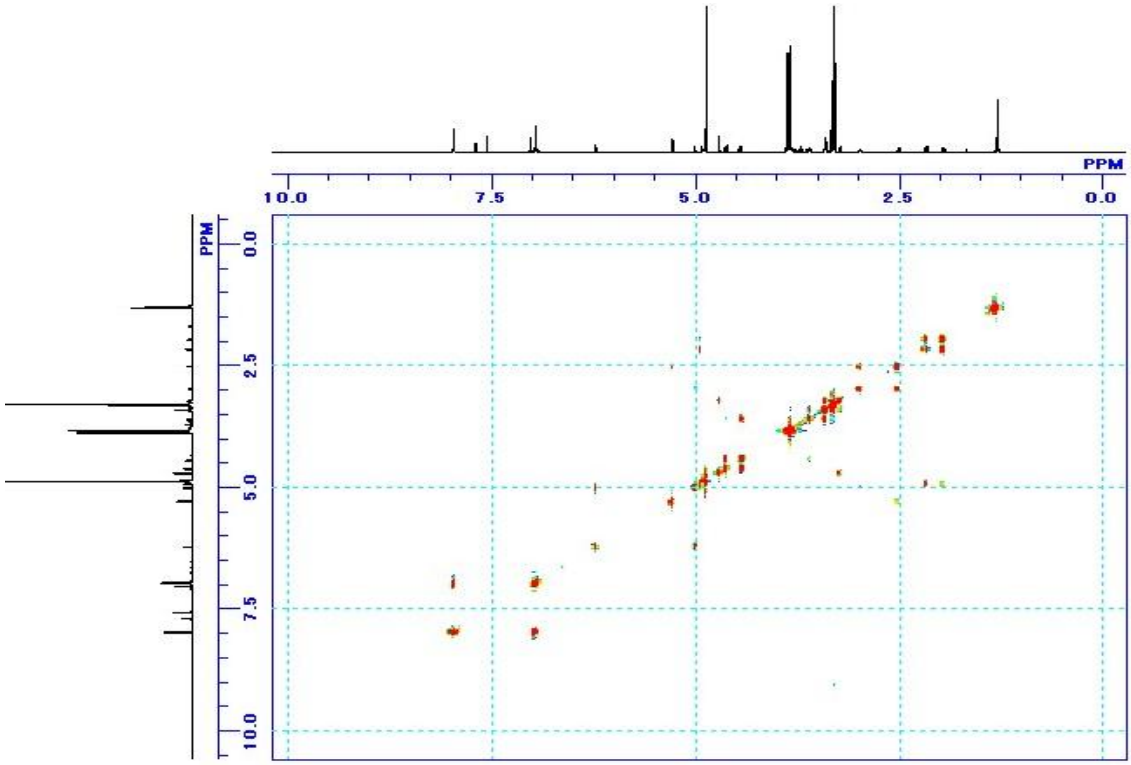

^{1}H-^{1}H COSY spectrum of **10** in CD_3OD

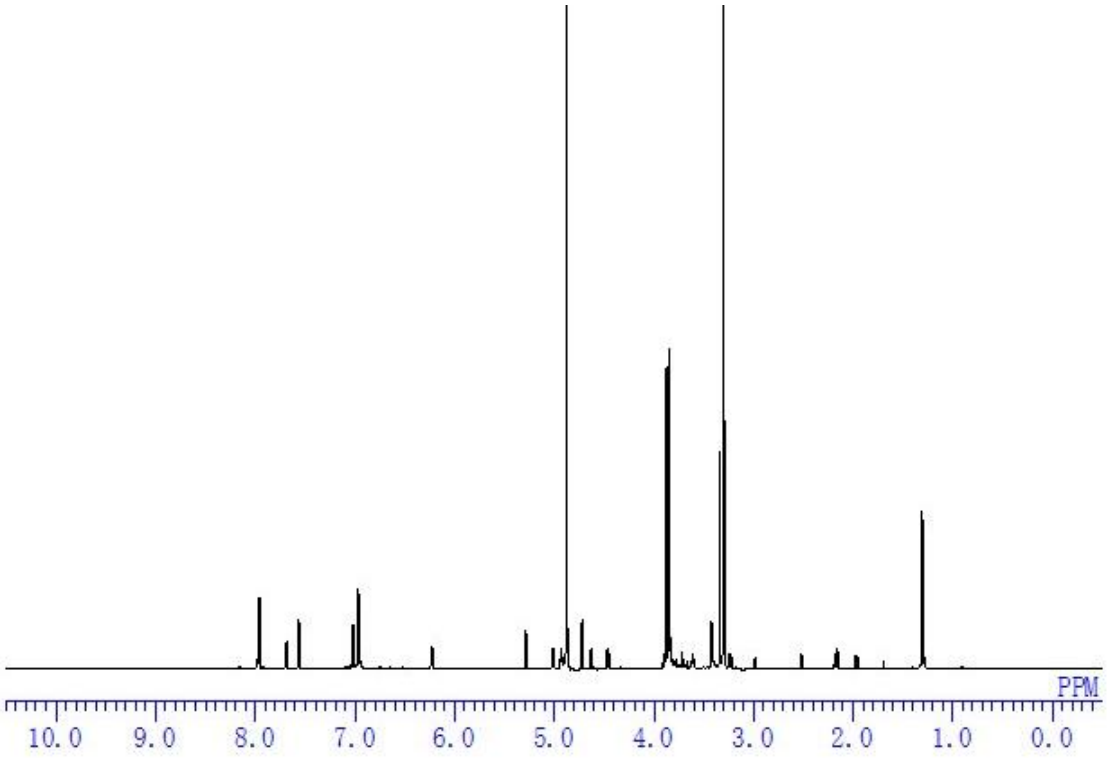

^{1}H NMR spectrum of **11** in CD_3OD

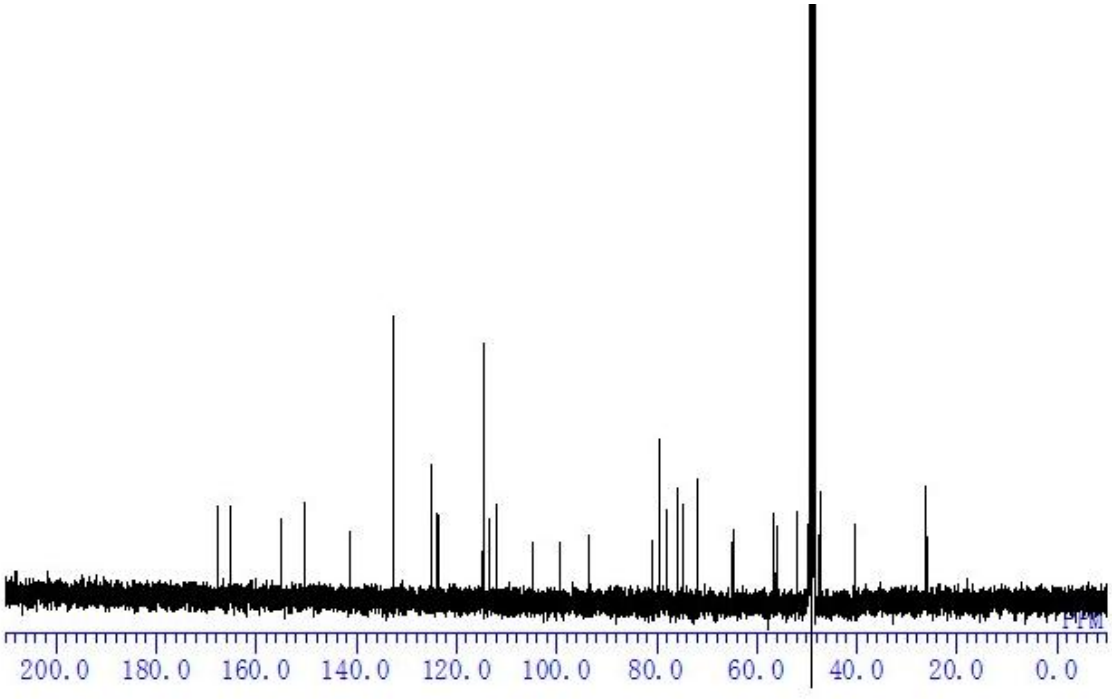

^{13}C NMR spectrum of **11** in CD_3OD

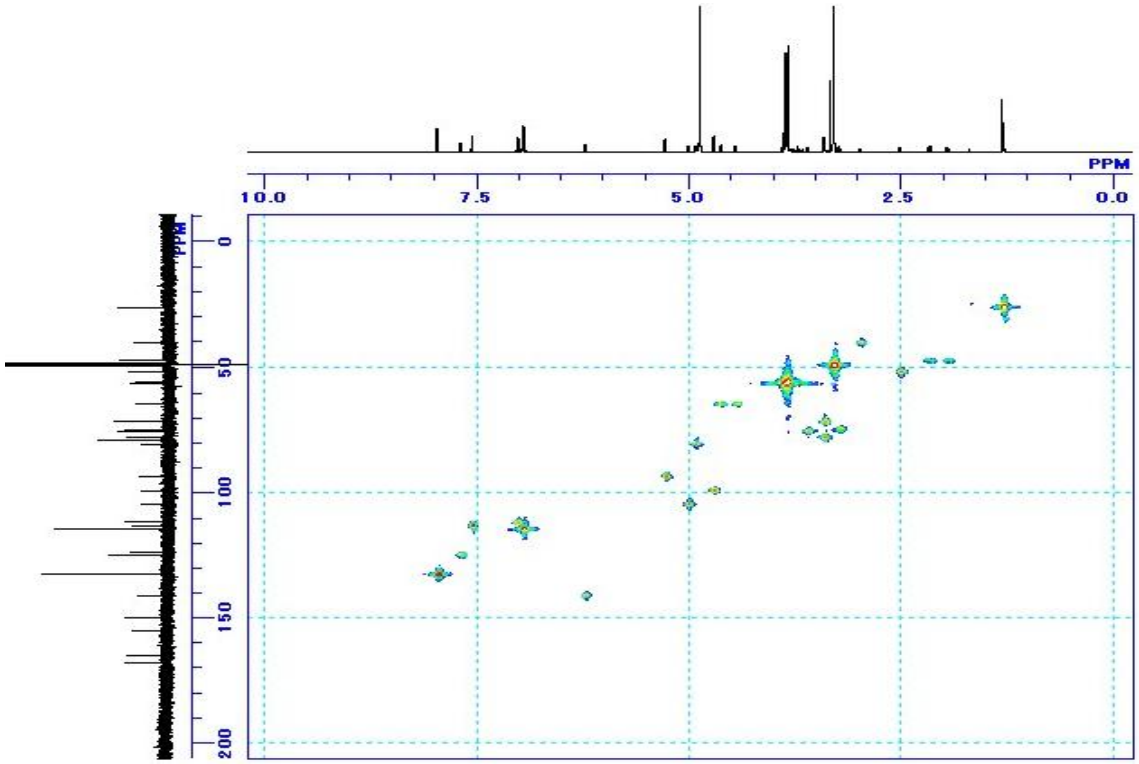

HMQC spectrum of **11** in CD_3OD

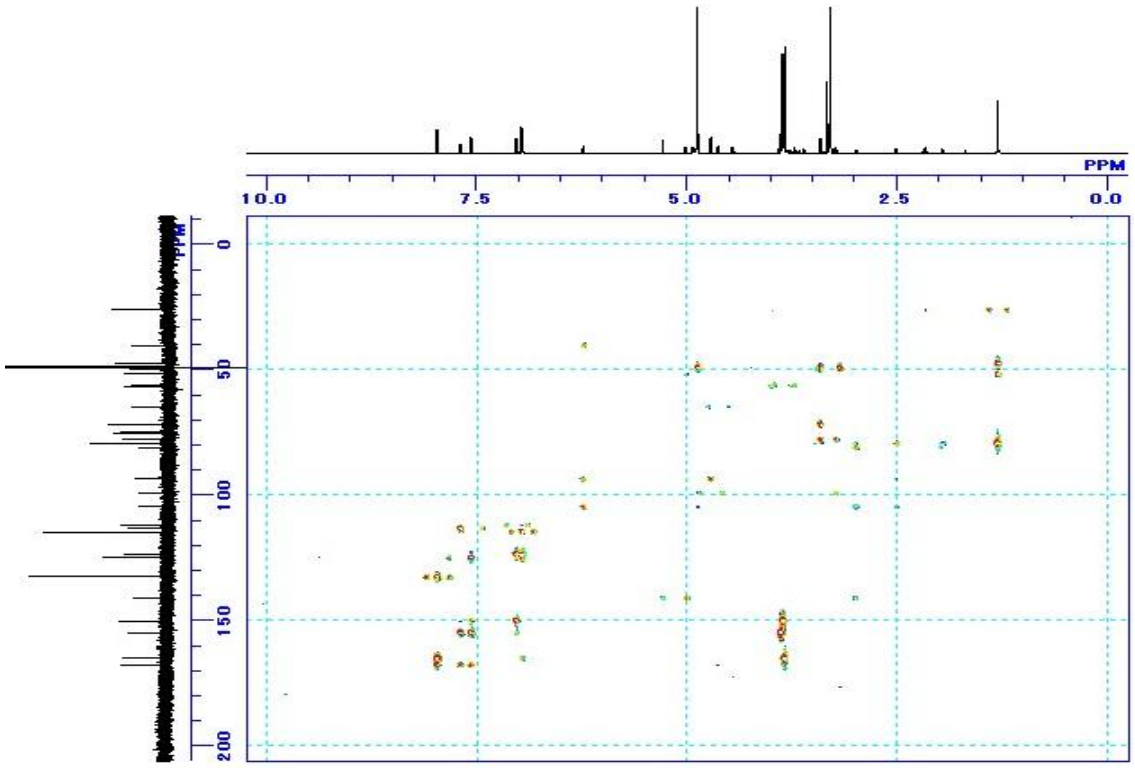

HMBC spectrum of **11** in CD_3OD

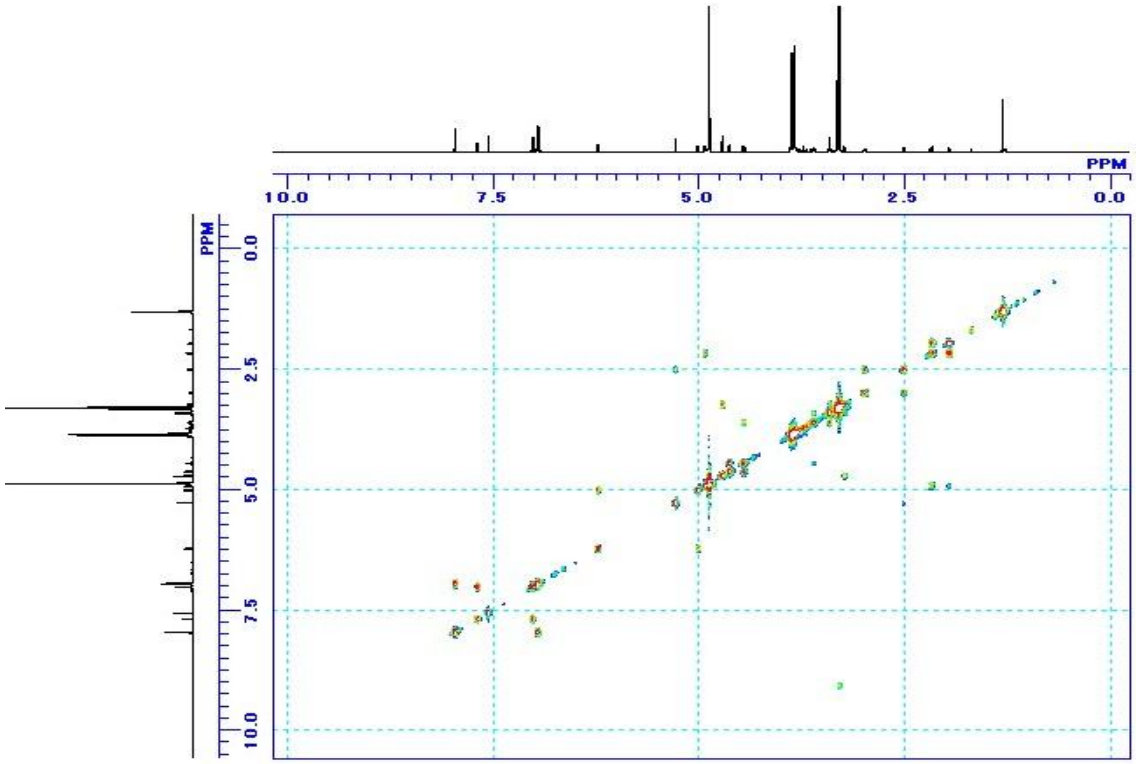

^{1}H-^{1}H COSY spectrum of **11** in CD_3OD

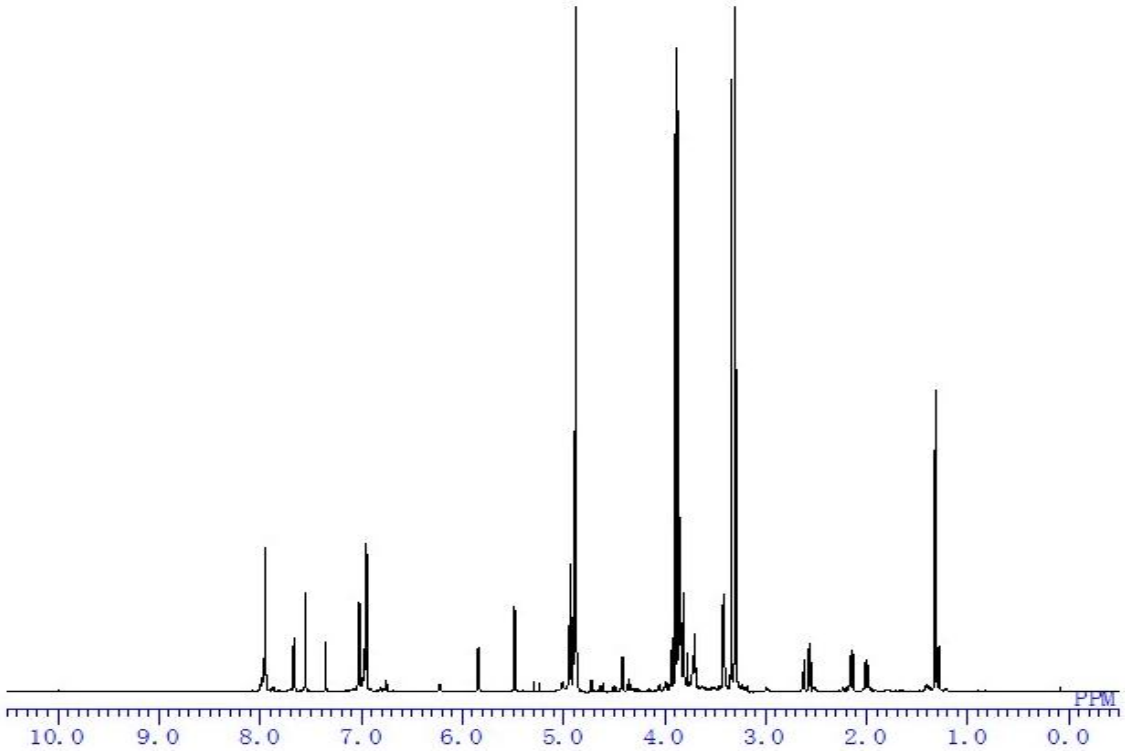

^{1}H NMR spectrum of **12** in CD_3OD

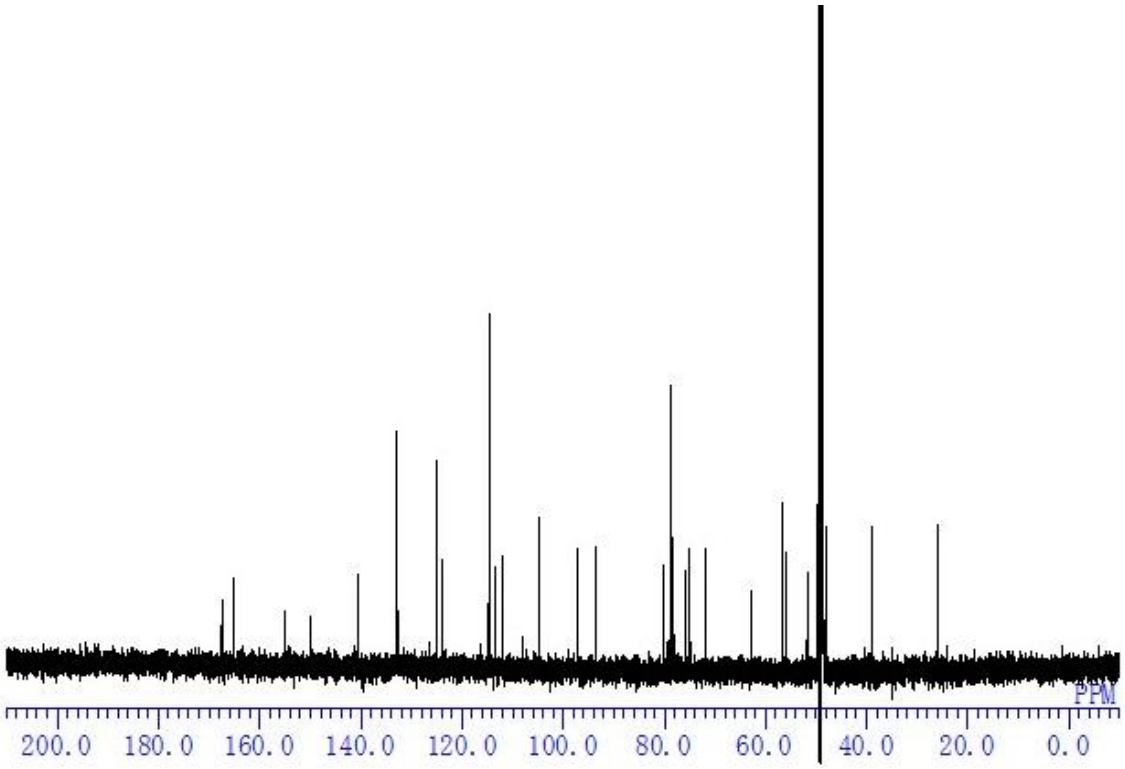

^{13}C NMR spectrum of **12** in CD_3OD

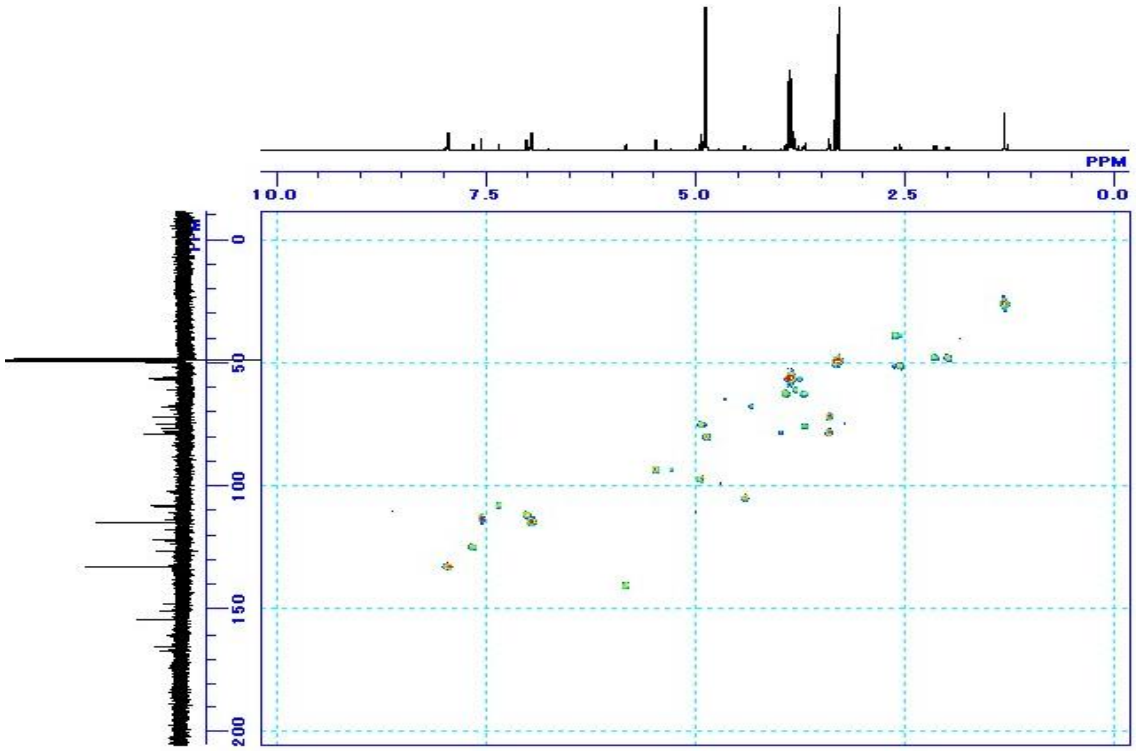

HMQC spectrum of **12** in CD_3OD

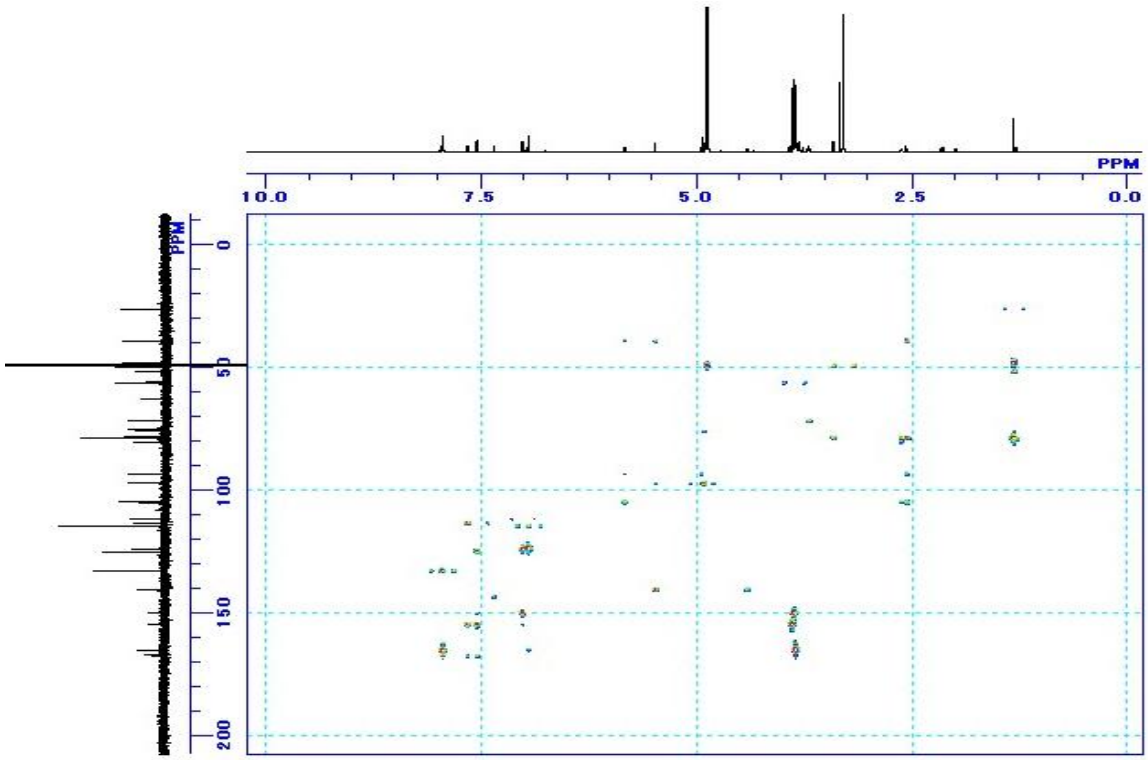

HMBC spectrum of **12** in CD_3OD

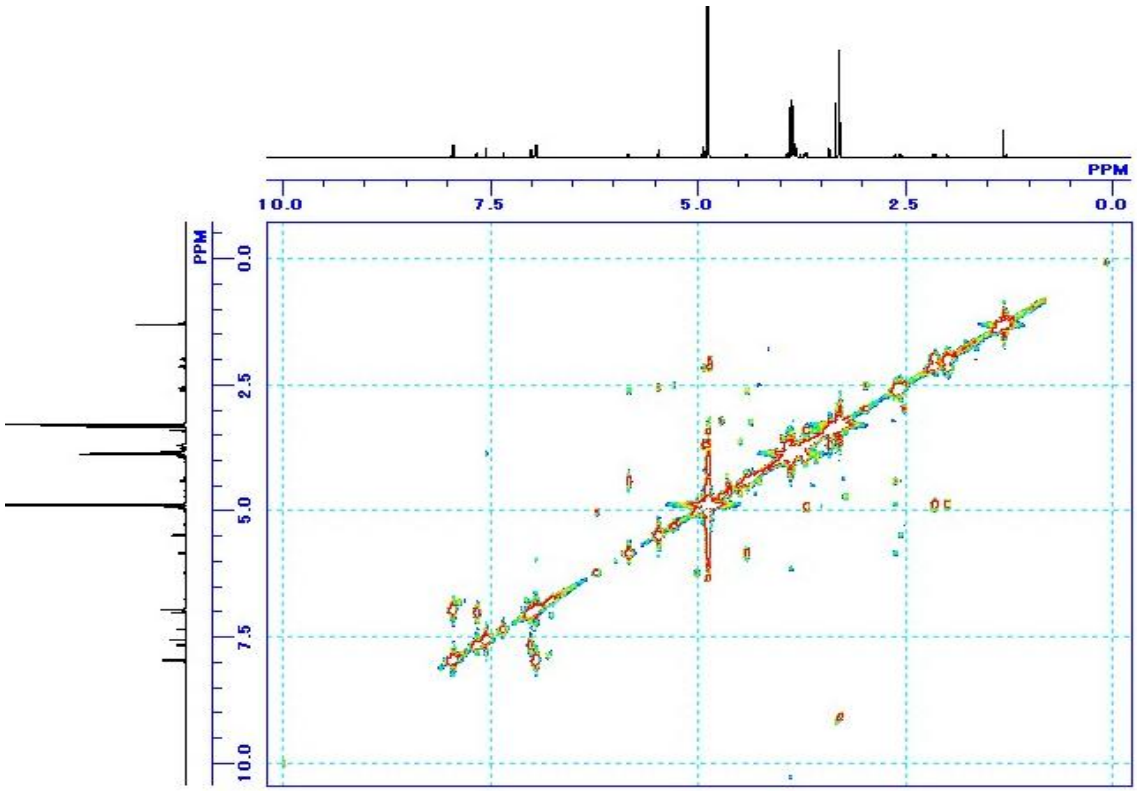

^{1}H-^{1}H COSY spectrum of **12** in CD_3OD

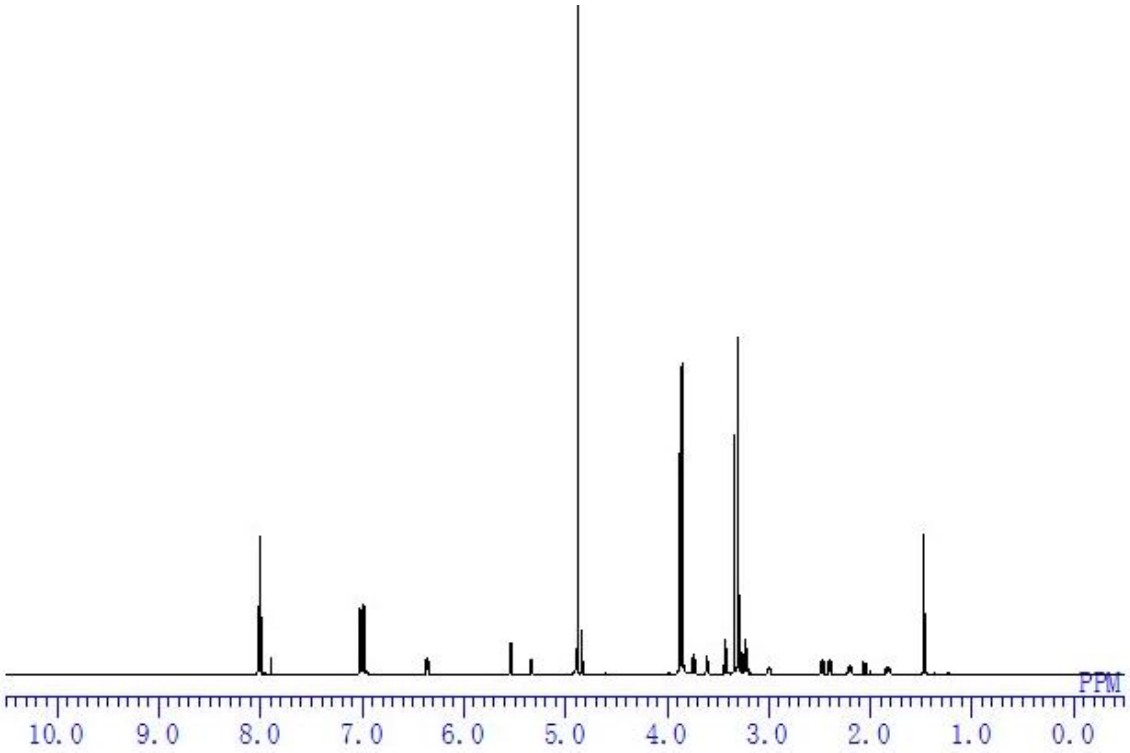

^{1}H NMR spectrum of **13** in CD_3OD

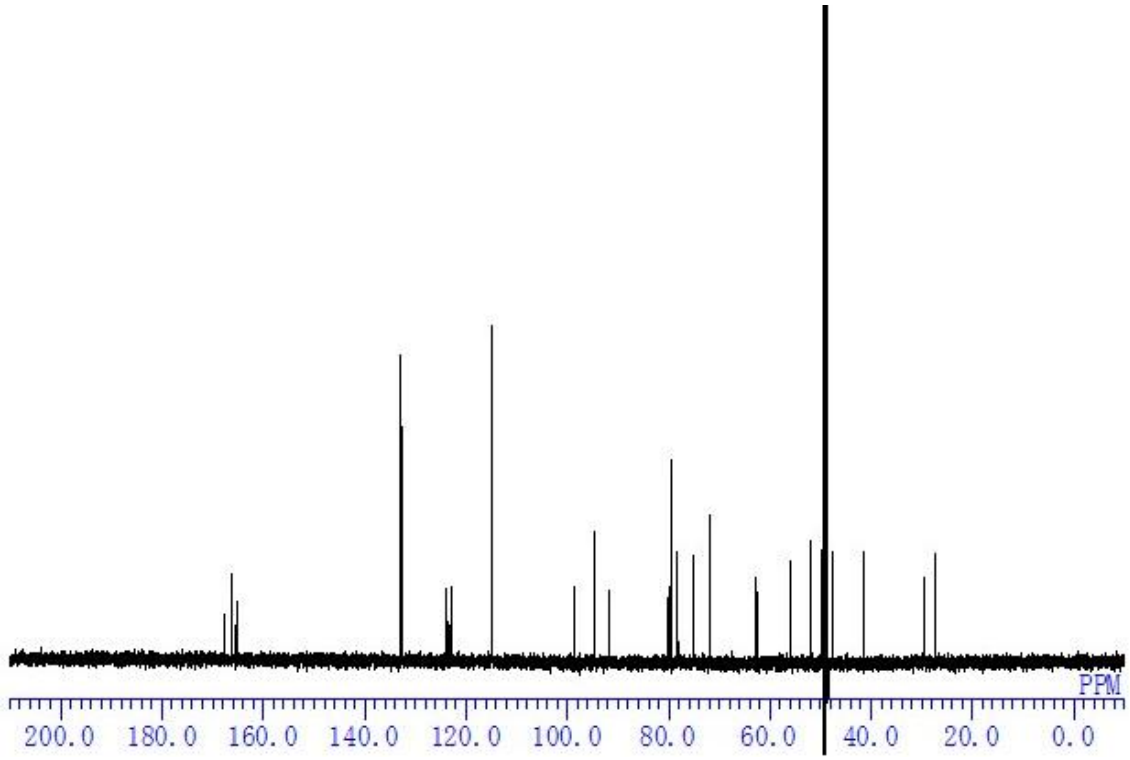

^{13}C NMR spectrum of **13** in CD_3OD

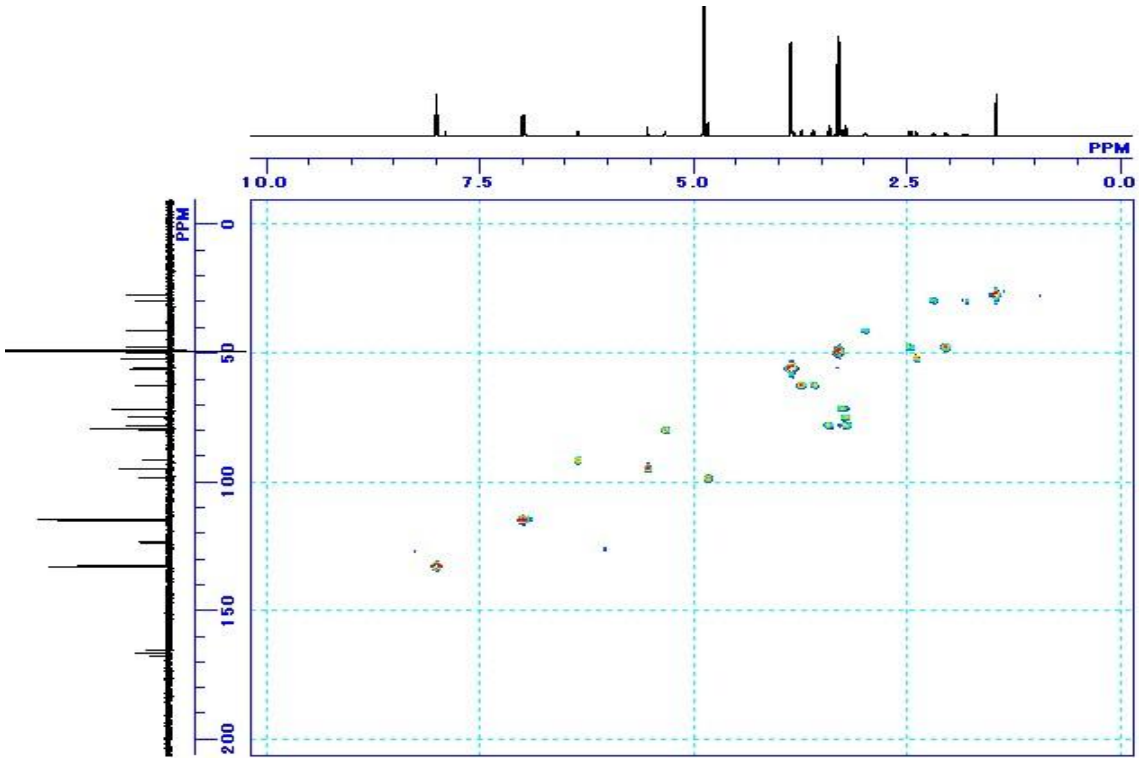

HMQC spectrum of **13** in CD_3OD

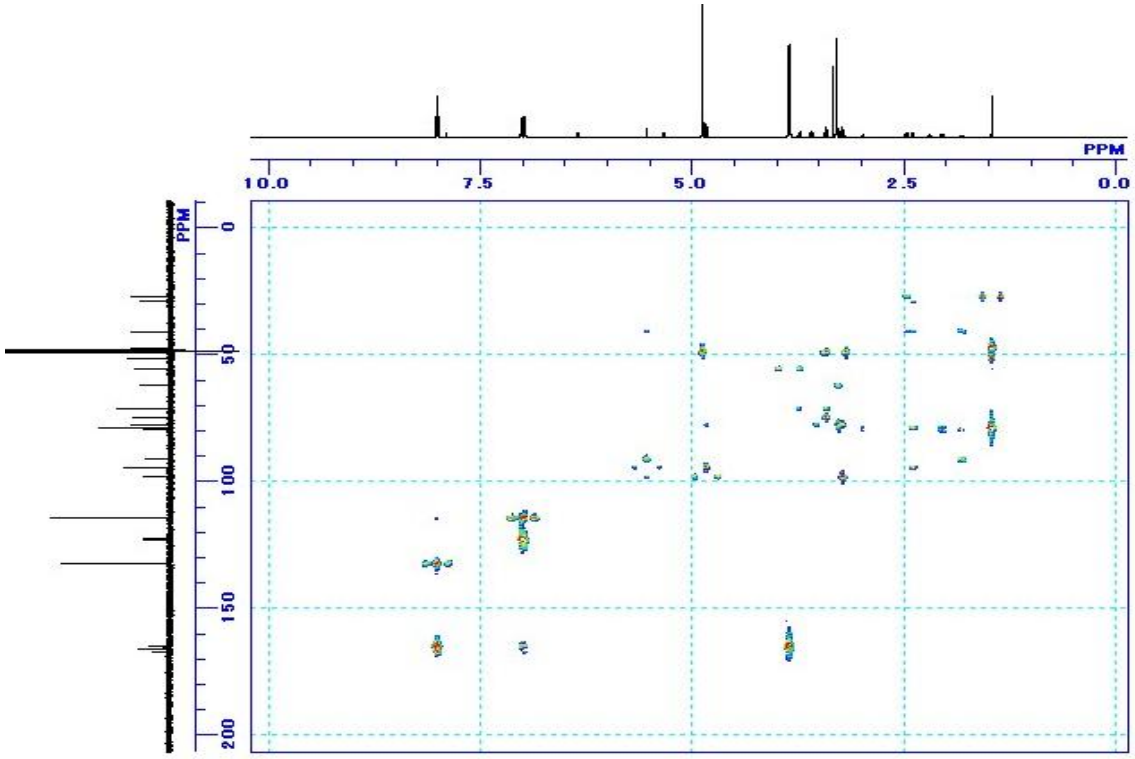

HMBC spectrum of **13** in CD_3OD

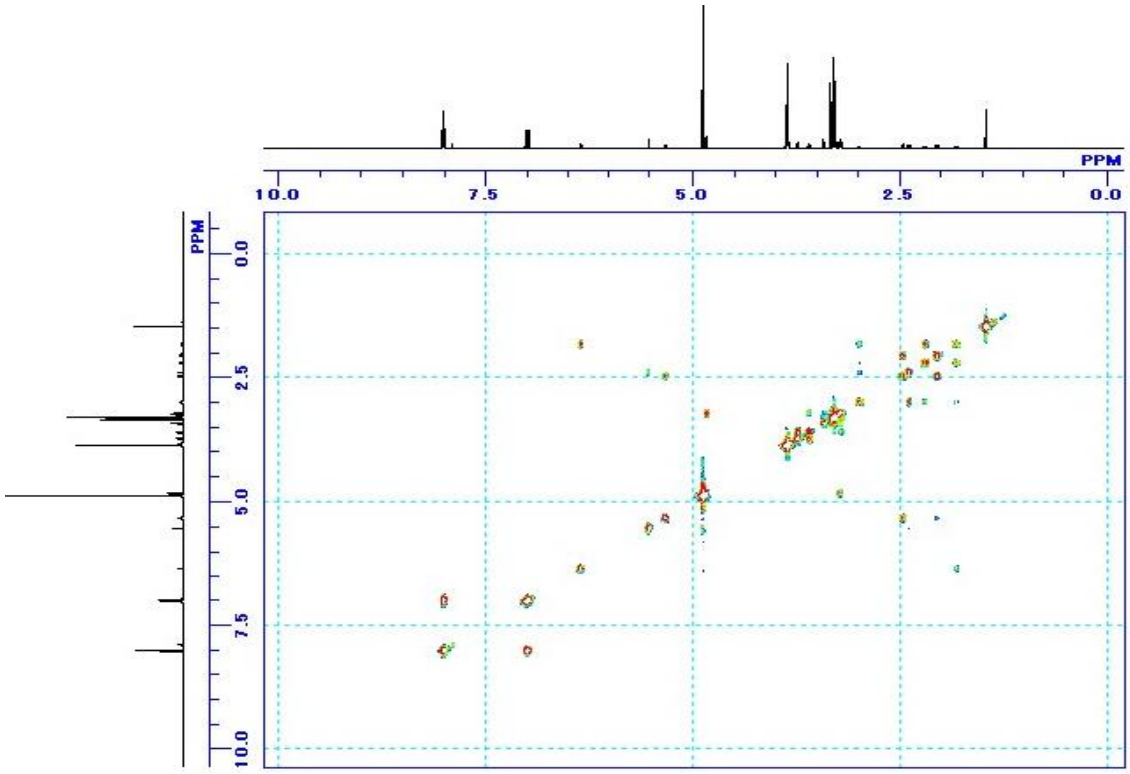

^{1}H-^{1}H COSY spectrum of **13** in CD_3OD

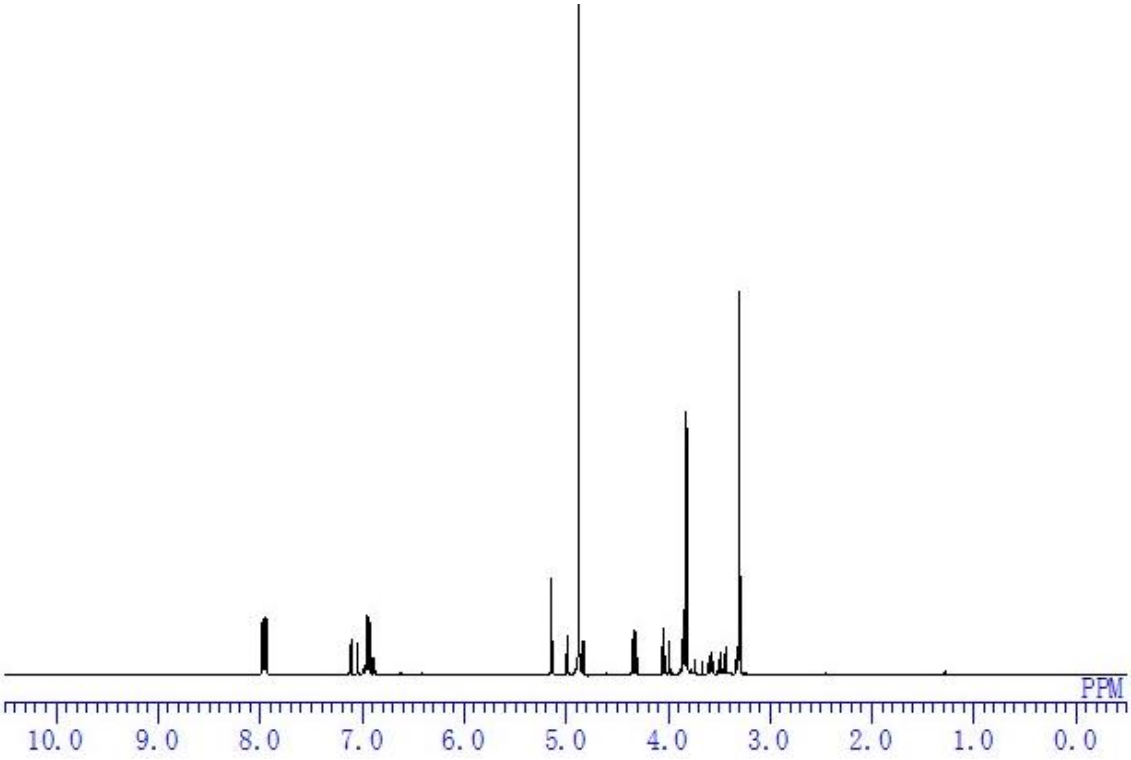

^{1}H NMR spectrum of **14** in CD_3OD

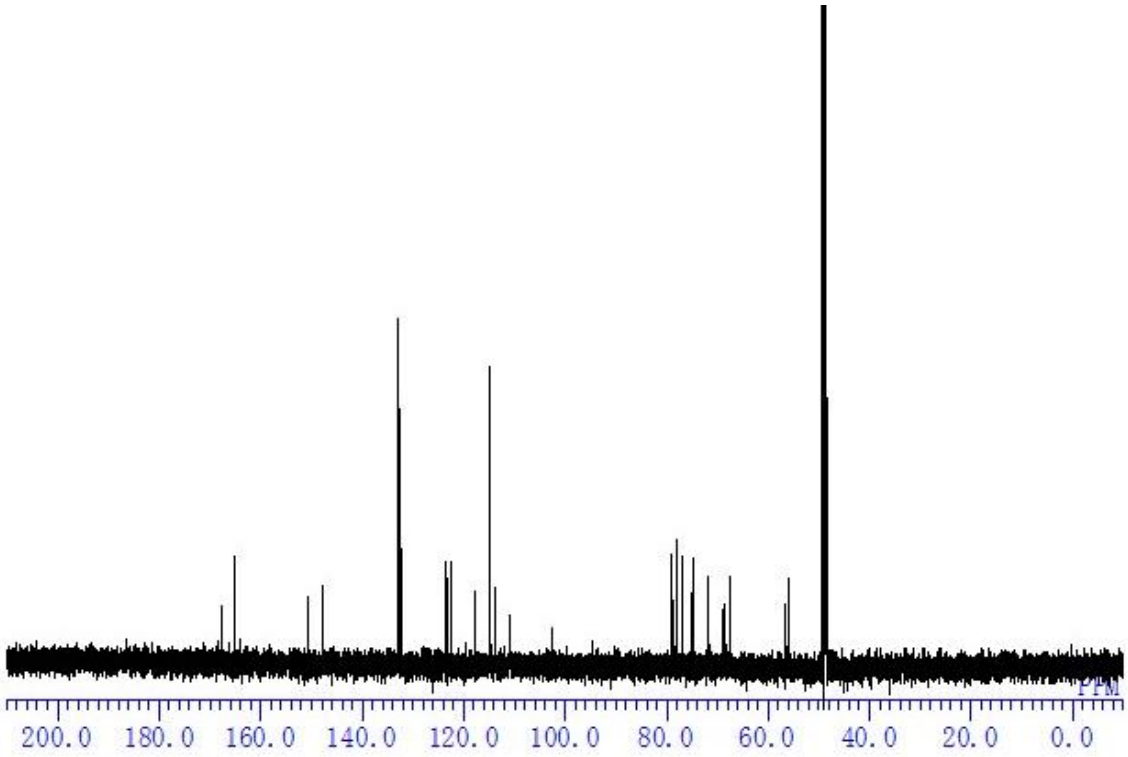

^{13}C NMR spectrum of **14** in CD_3OD

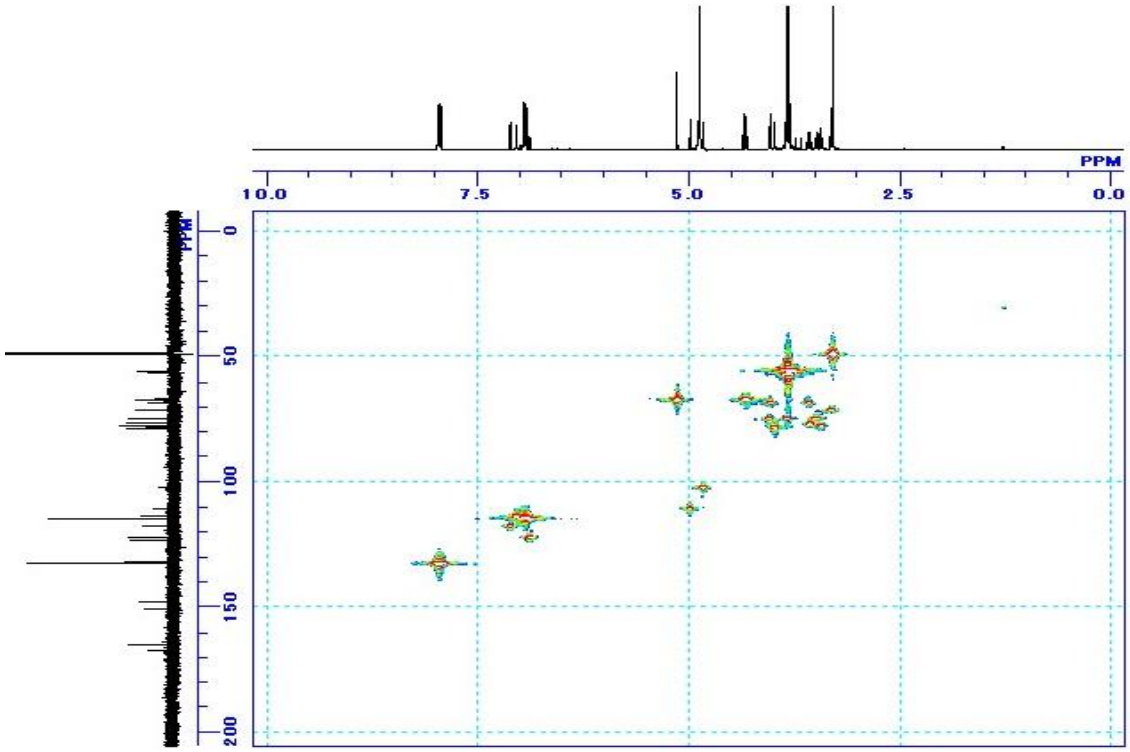

HMQC spectrum of **14** in CD_3OD

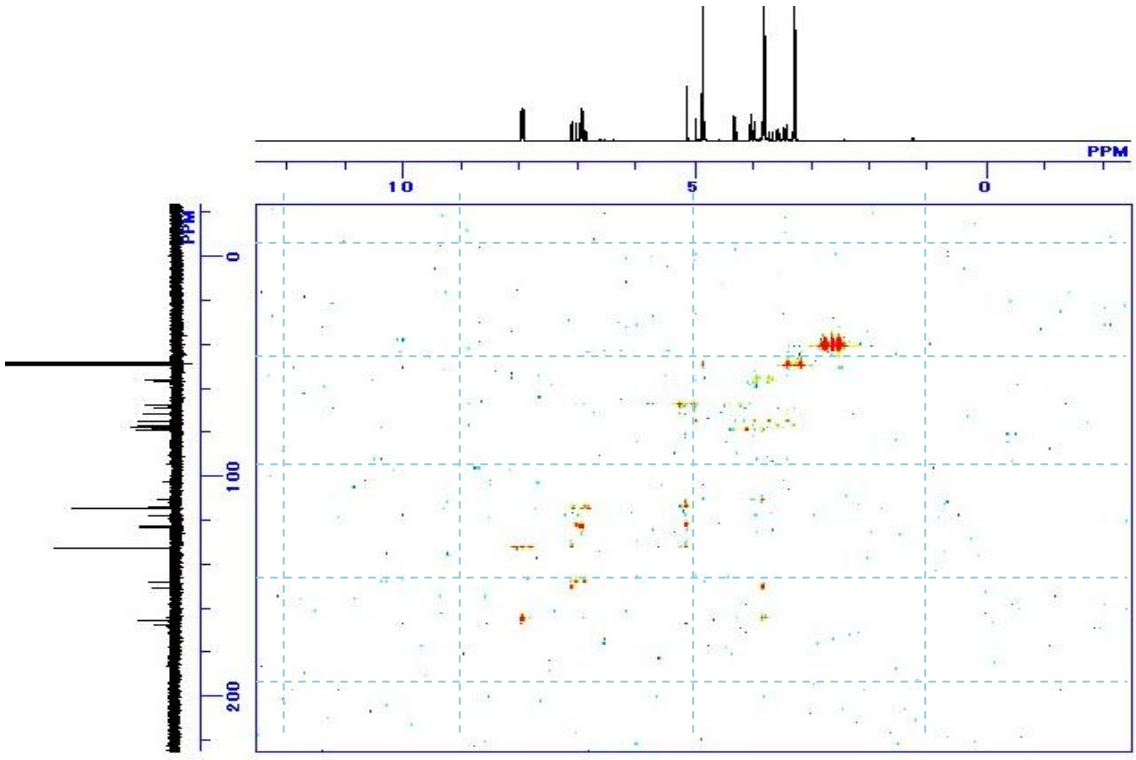

HMBC spectrum of **14** in CD_3OD

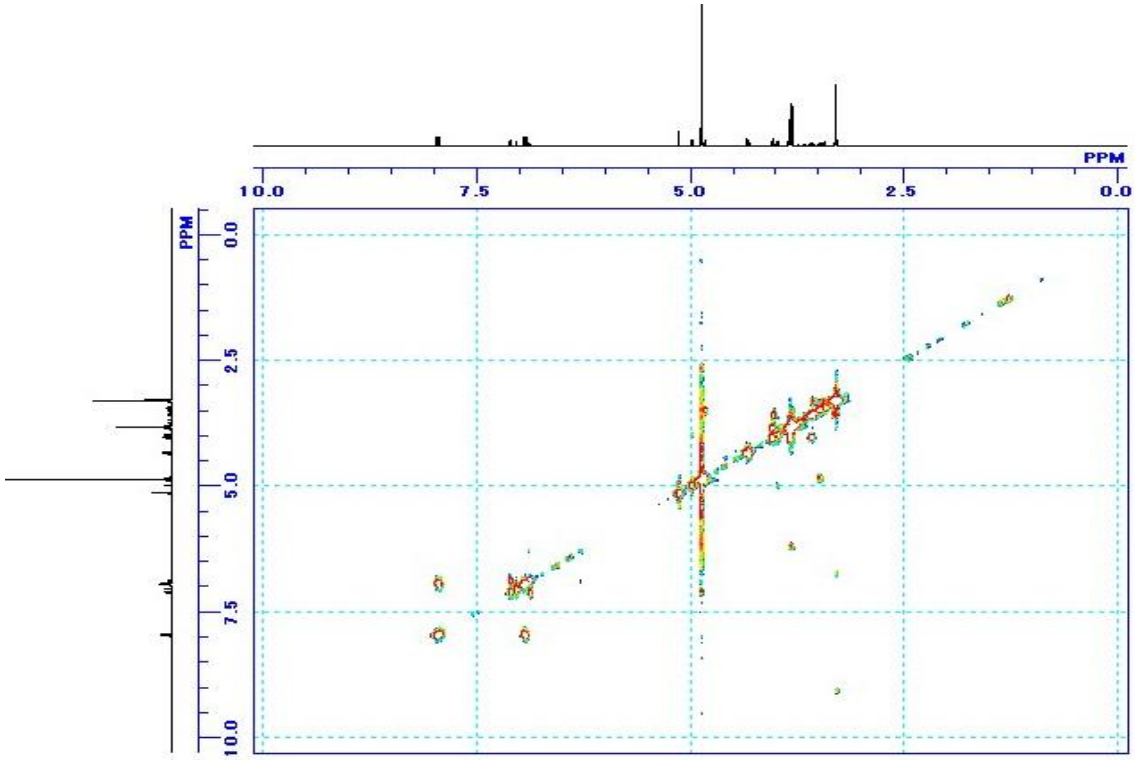

^{1}H-^{1}H COSY spectrum of **14** in CD_3OD

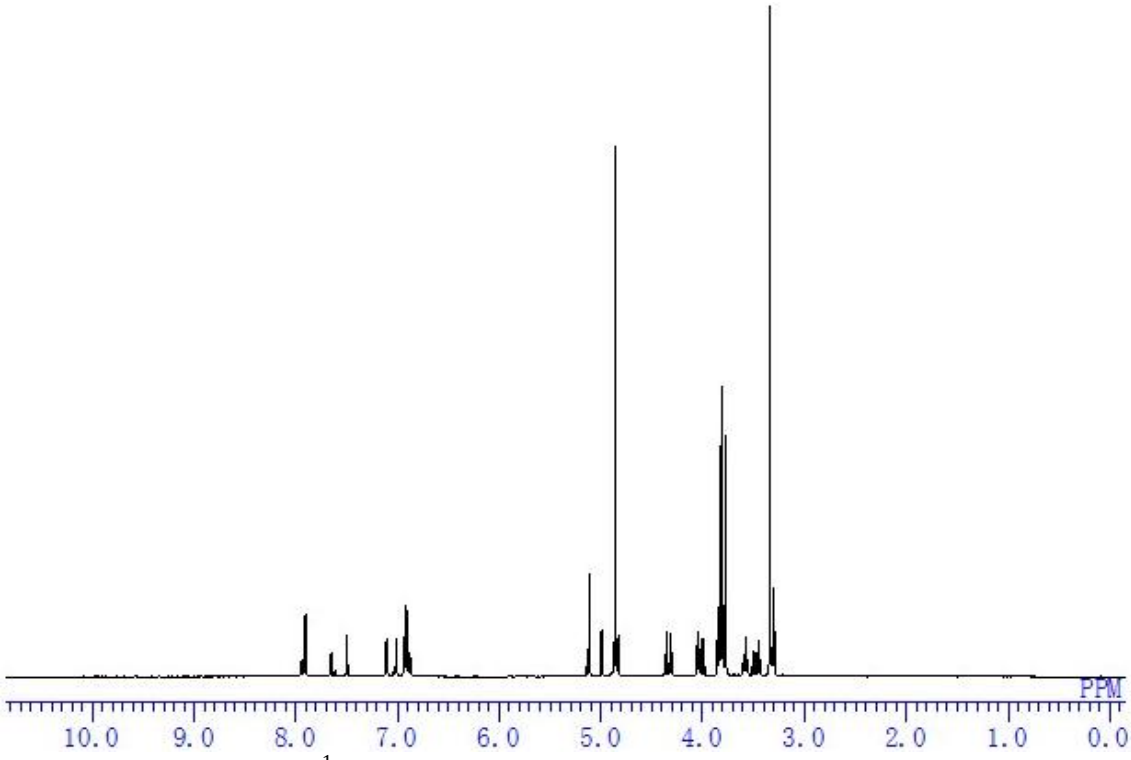

^{1}H NMR spectrum of **15** in CD_3OD

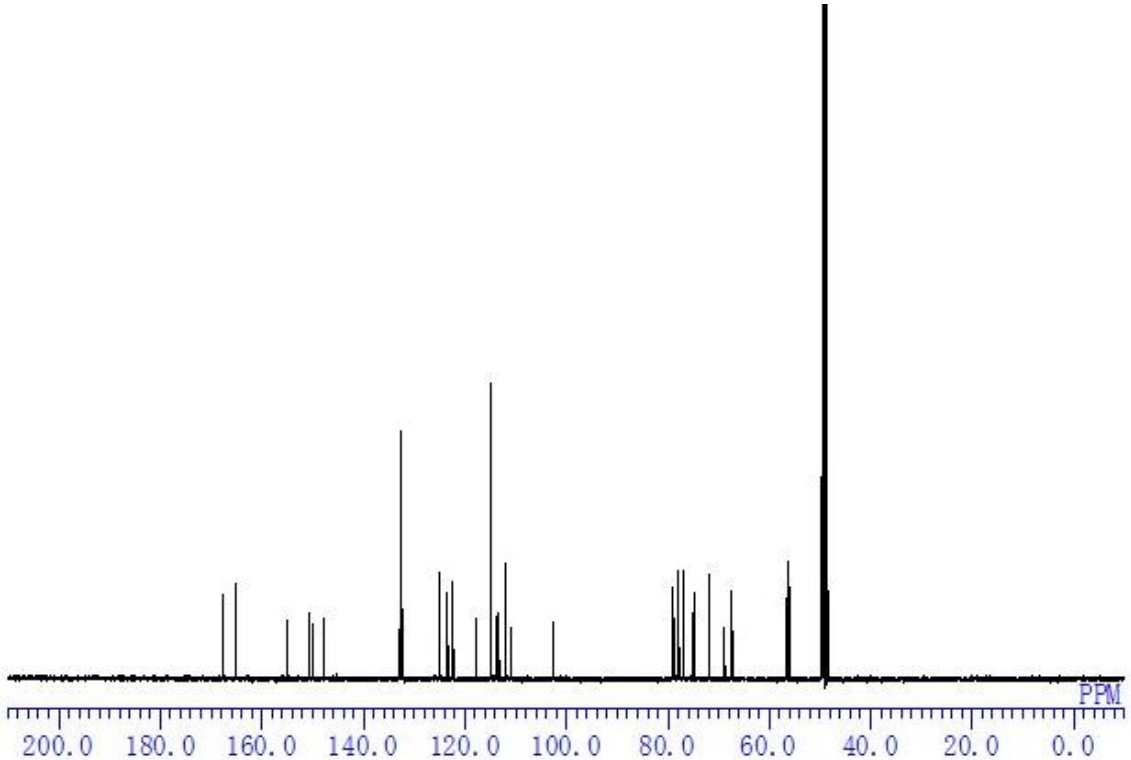

^{13}C NMR spectrum of **15** in CD_3OD

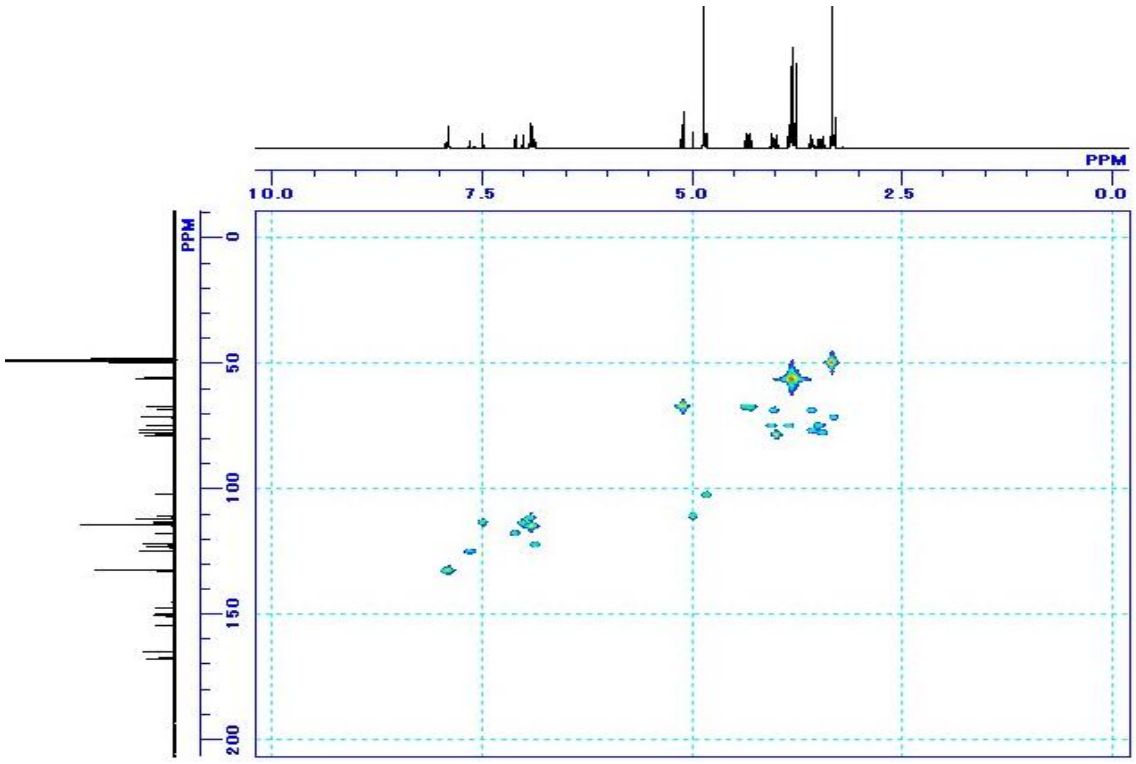

HMQC spectrum of **15** in CD_3OD

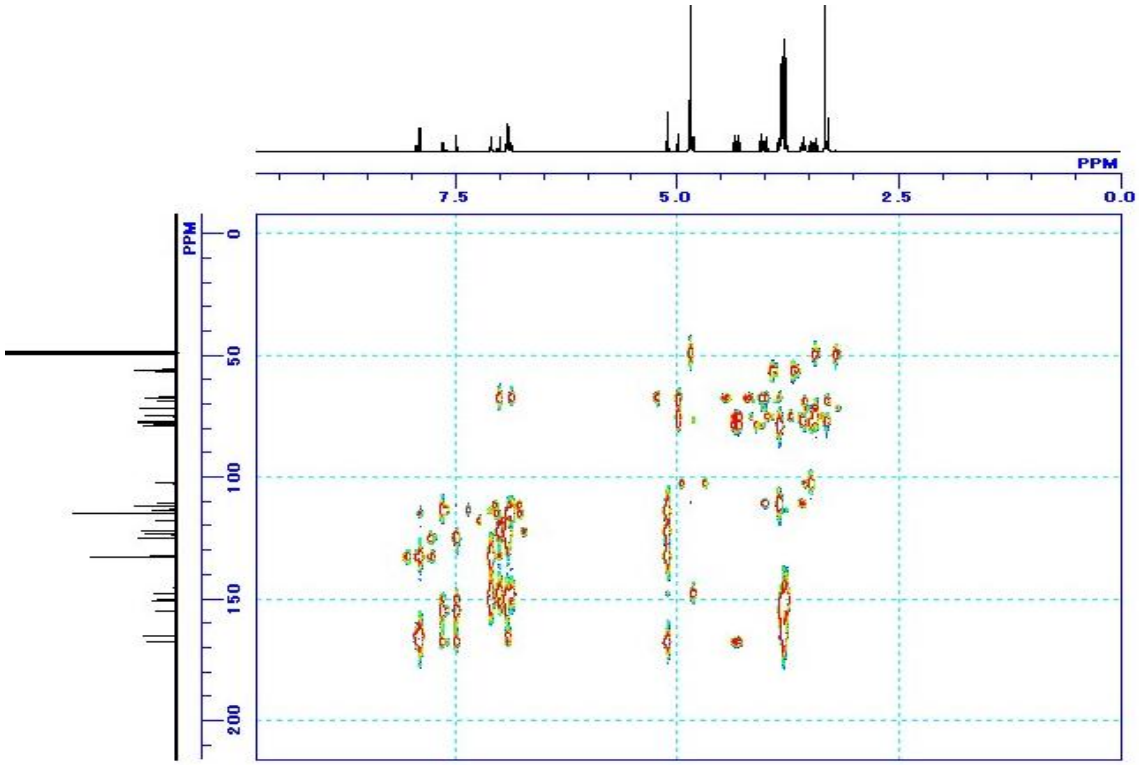

HMBC spectrum of **15** in CD_3OD

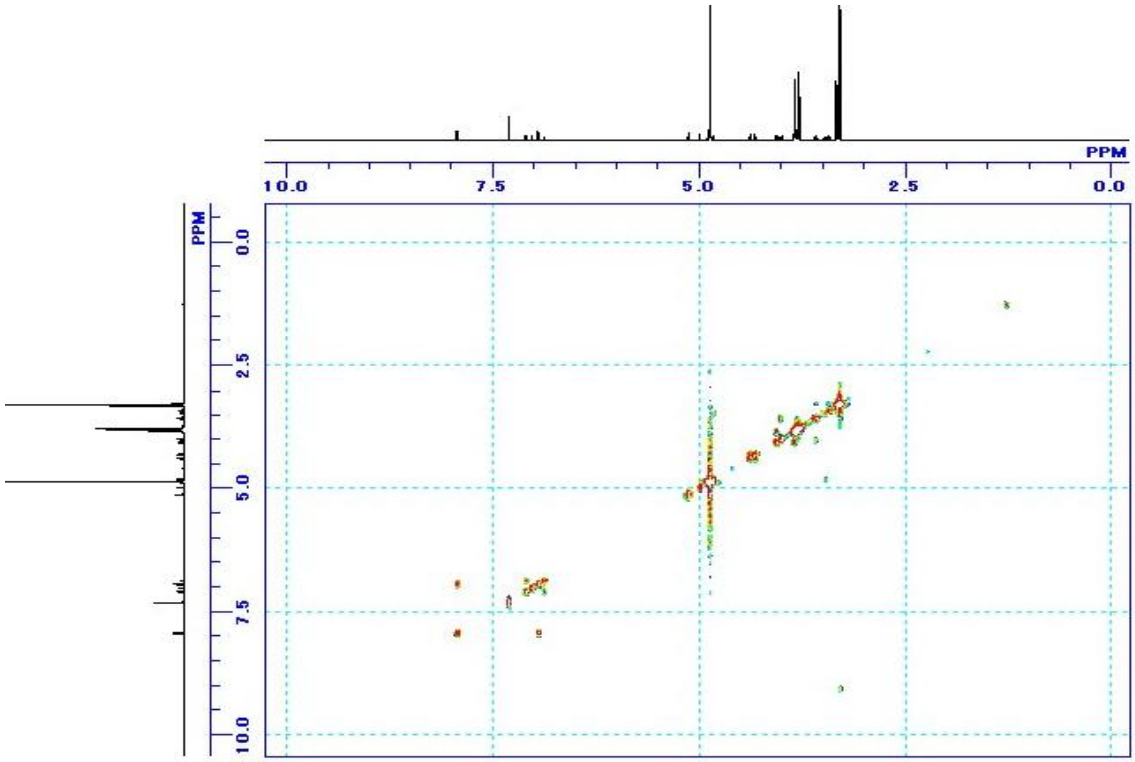

^{1}H-^{1}H COSY spectrum of **15** in CD_3OD

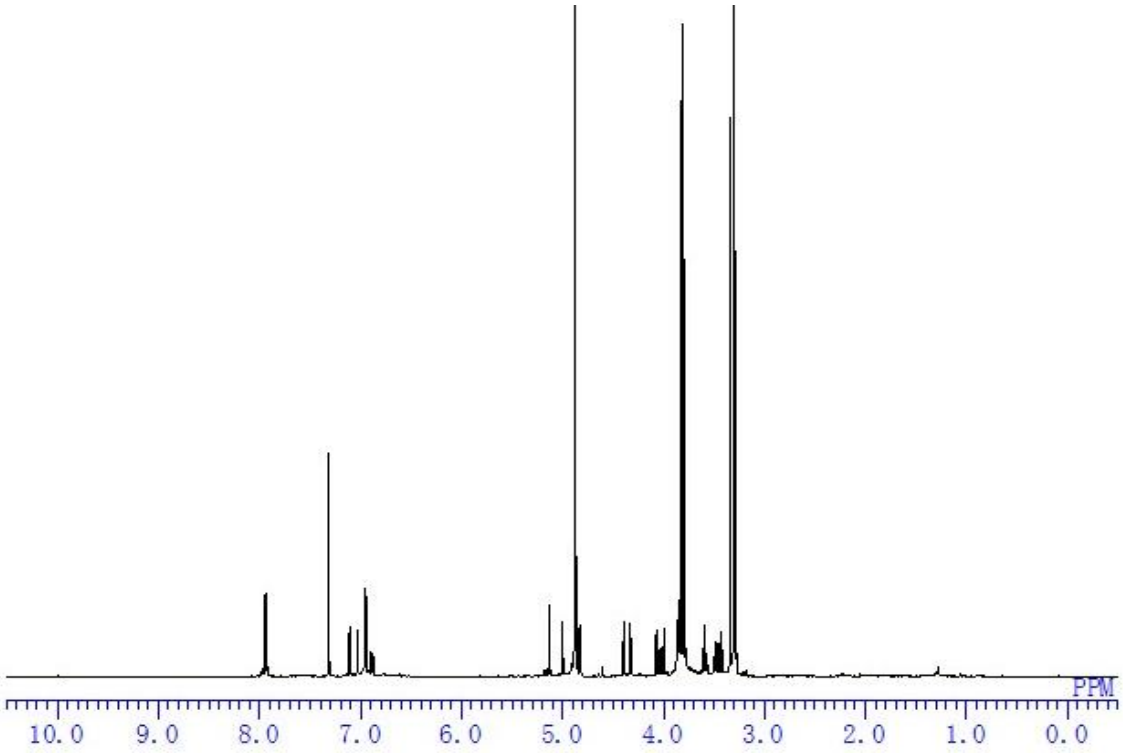

^{1}H NMR spectrum of **16** in CD_3OD

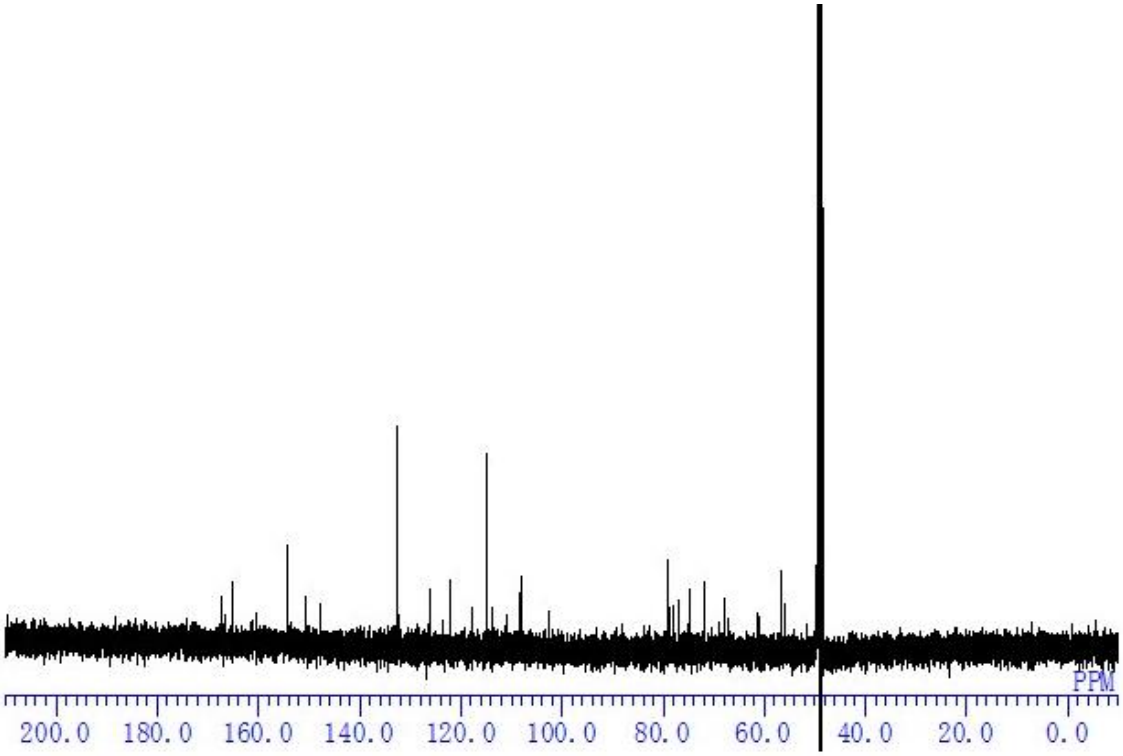

^{13}C NMR spectrum of **16** in CD_3OD

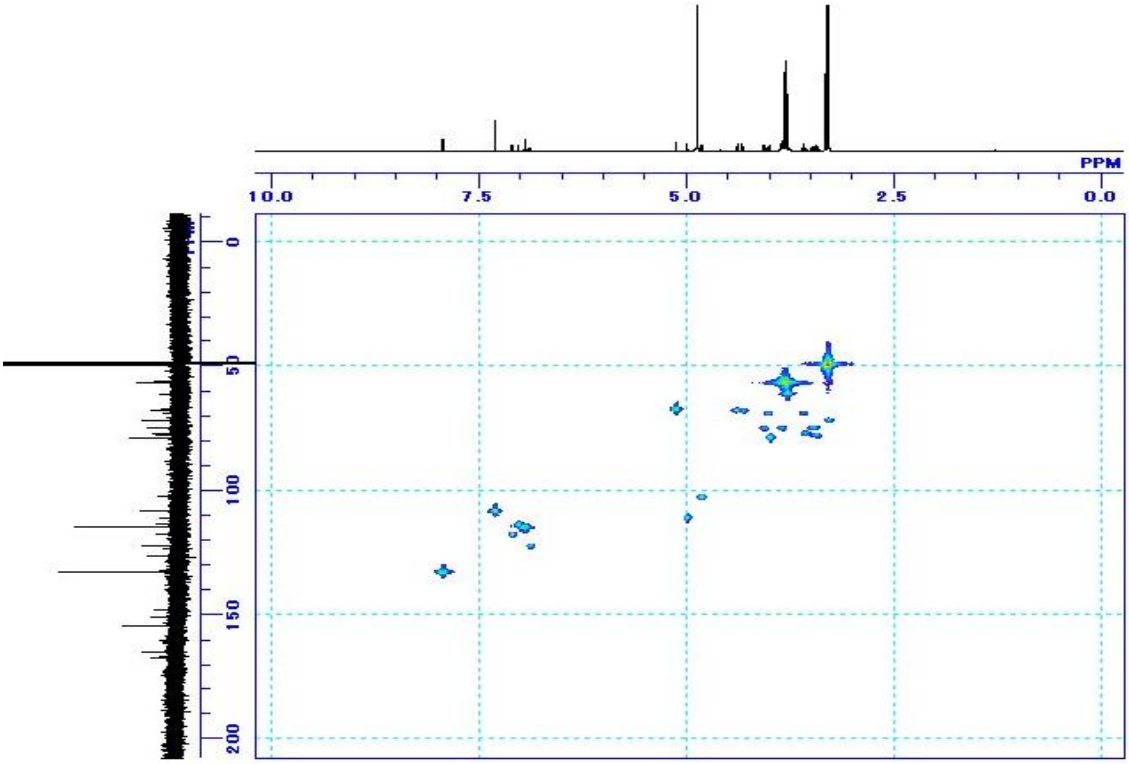

HMQC spectrum of **16** in CD_3OD

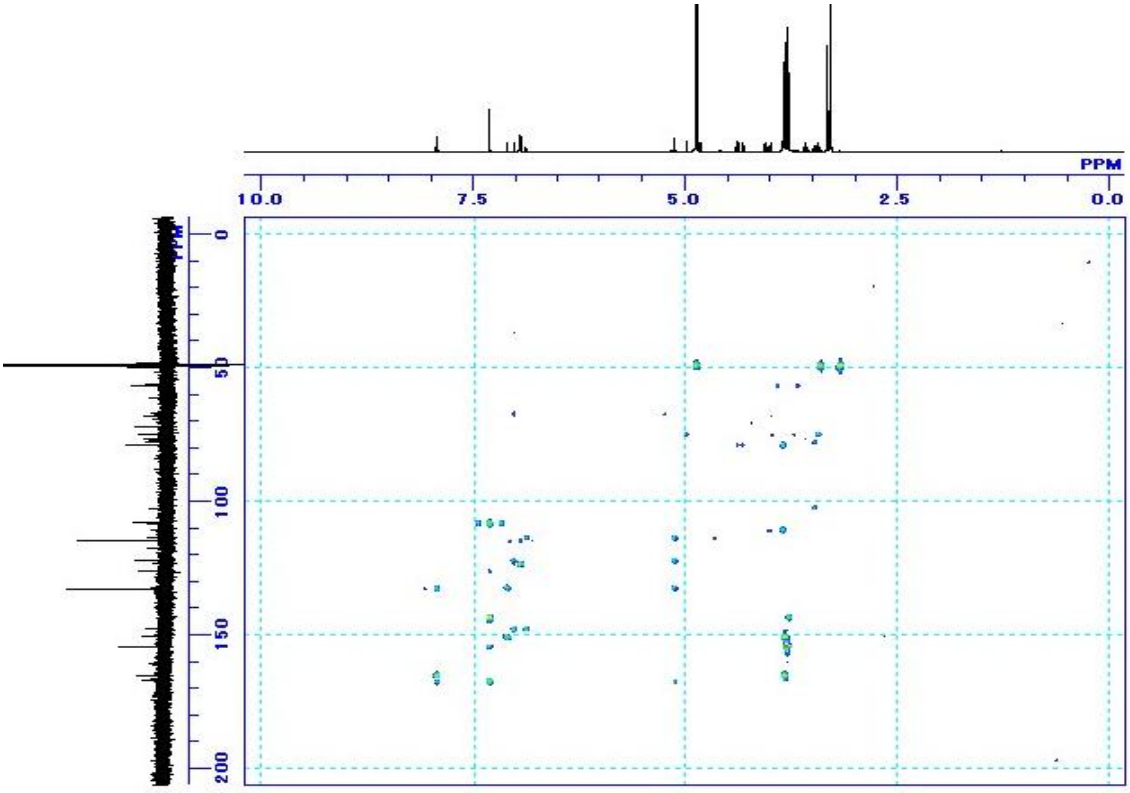

HMBC spectrum of **16** in CD_3OD

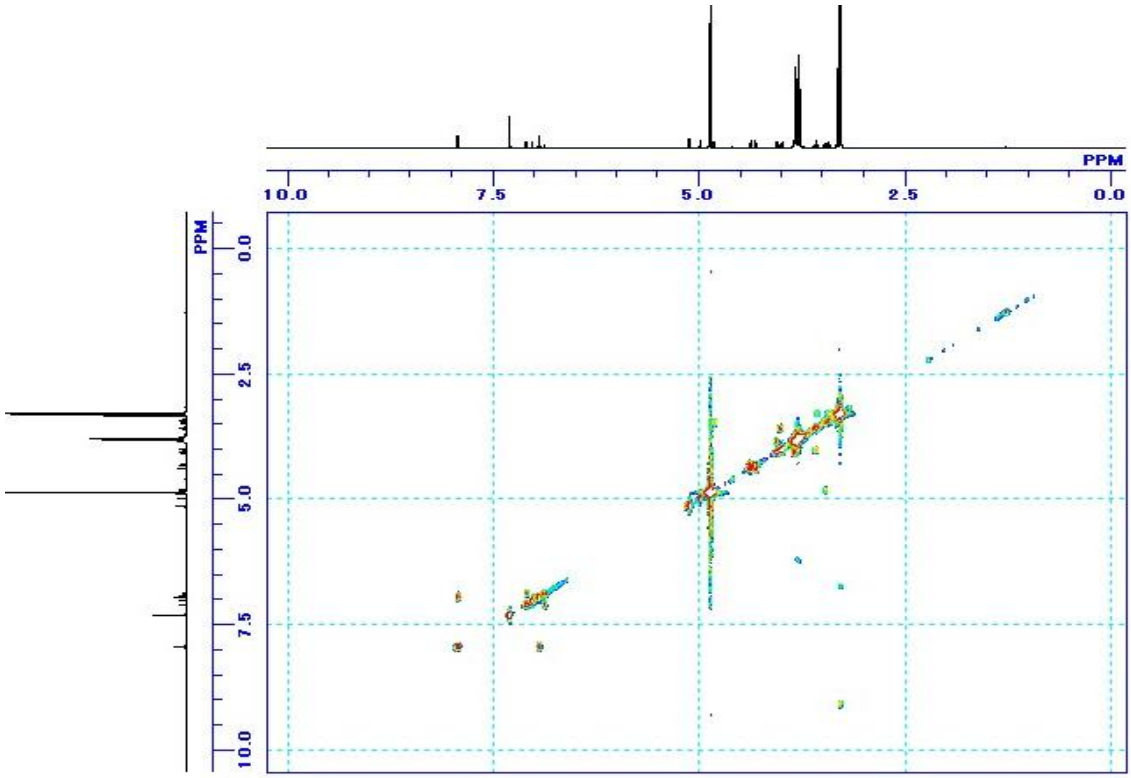

^{1}H-^{1}H COSY spectrum of **16** in CD_3OD

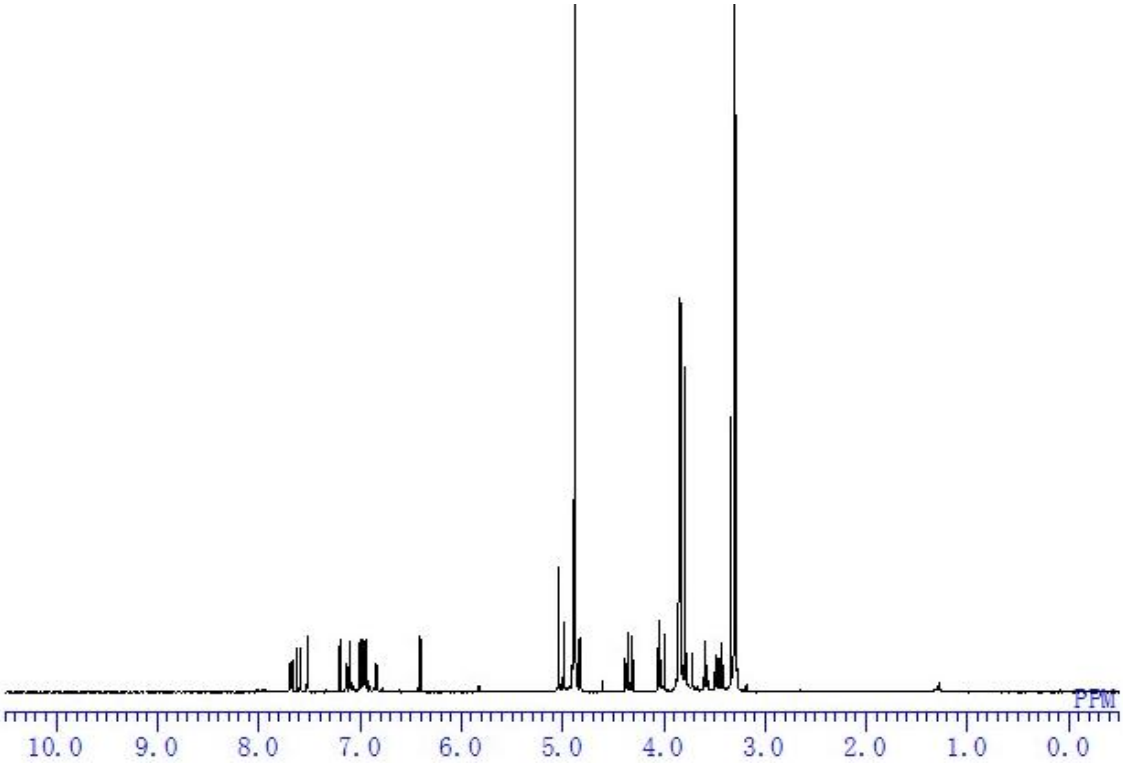

^{1}H NMR spectrum of **17** in CD_3OD

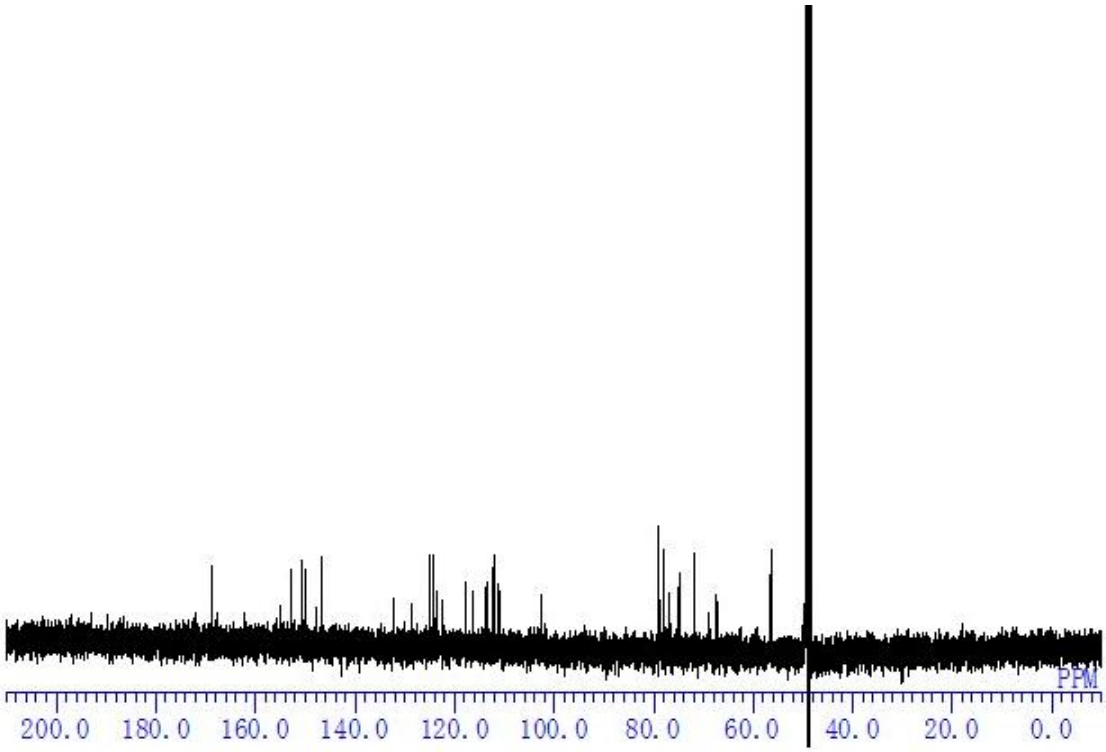

^{13}C NMR spectrum of **17** in CD_3OD

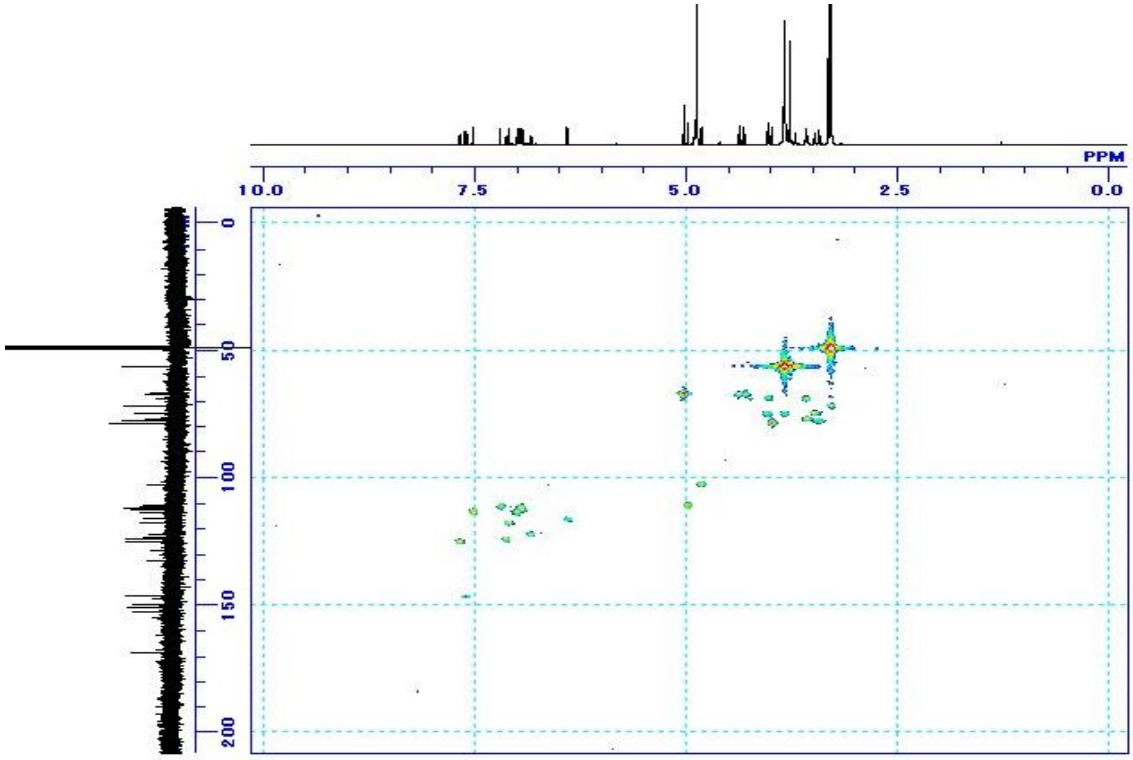

HMQC spectrum of **17** in CD_3OD

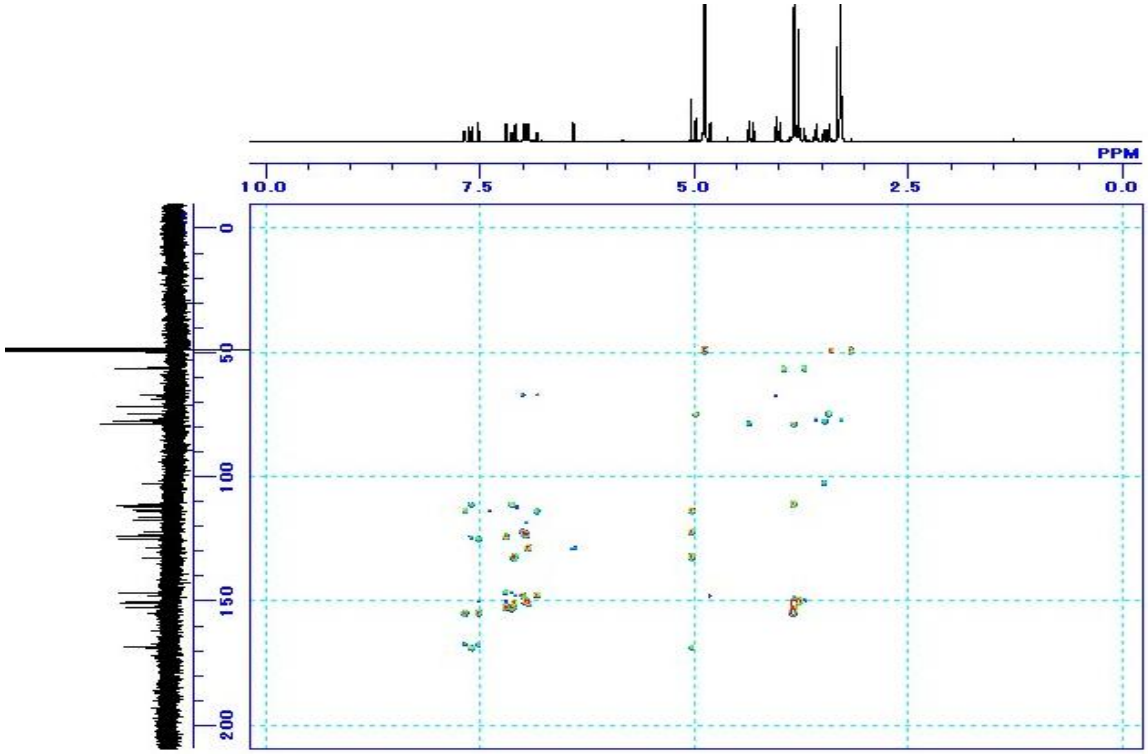

HMBC spectrum of **17** in CD_3OD

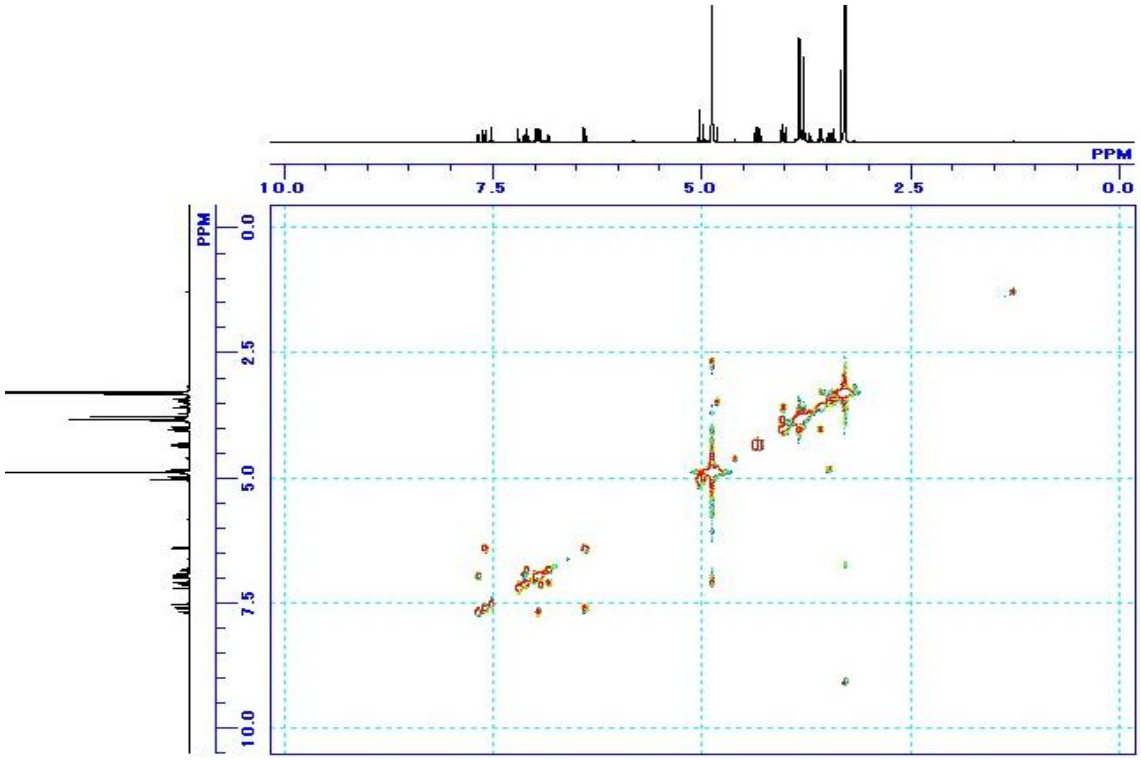

^{1}H-^{1}H COSY spectrum of **17** in CD_3OD

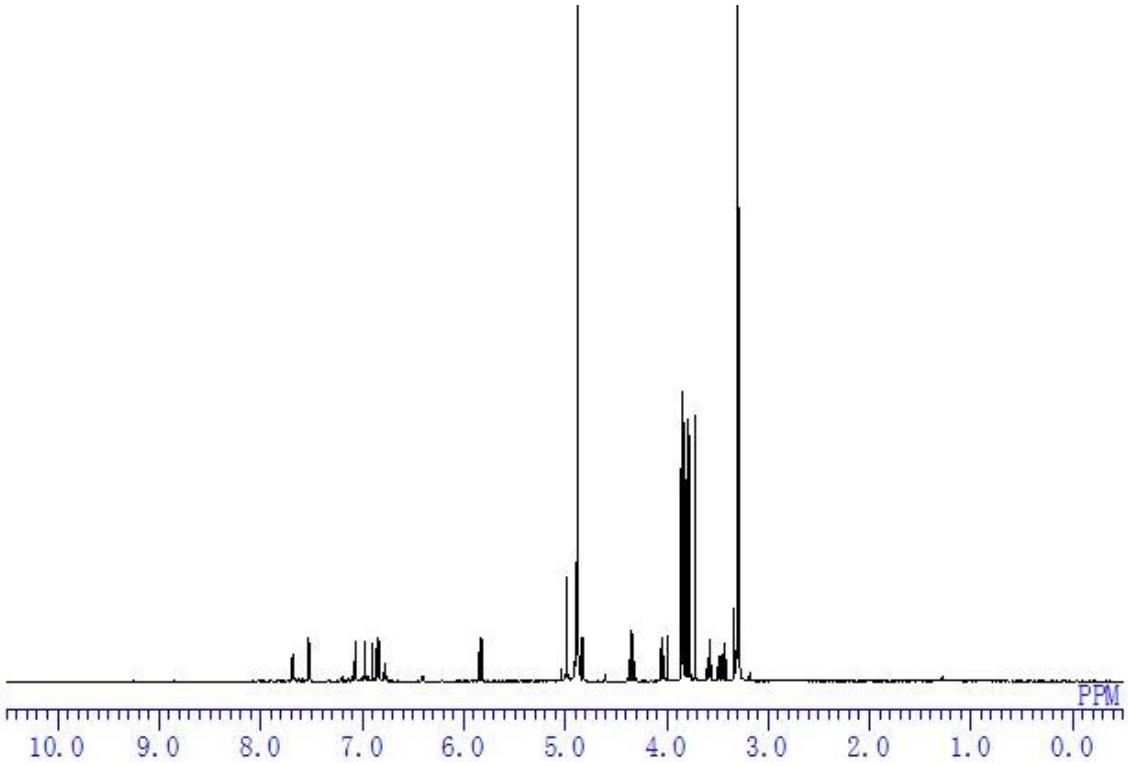

^{1}H NMR spectrum of **18** in CD_3OD

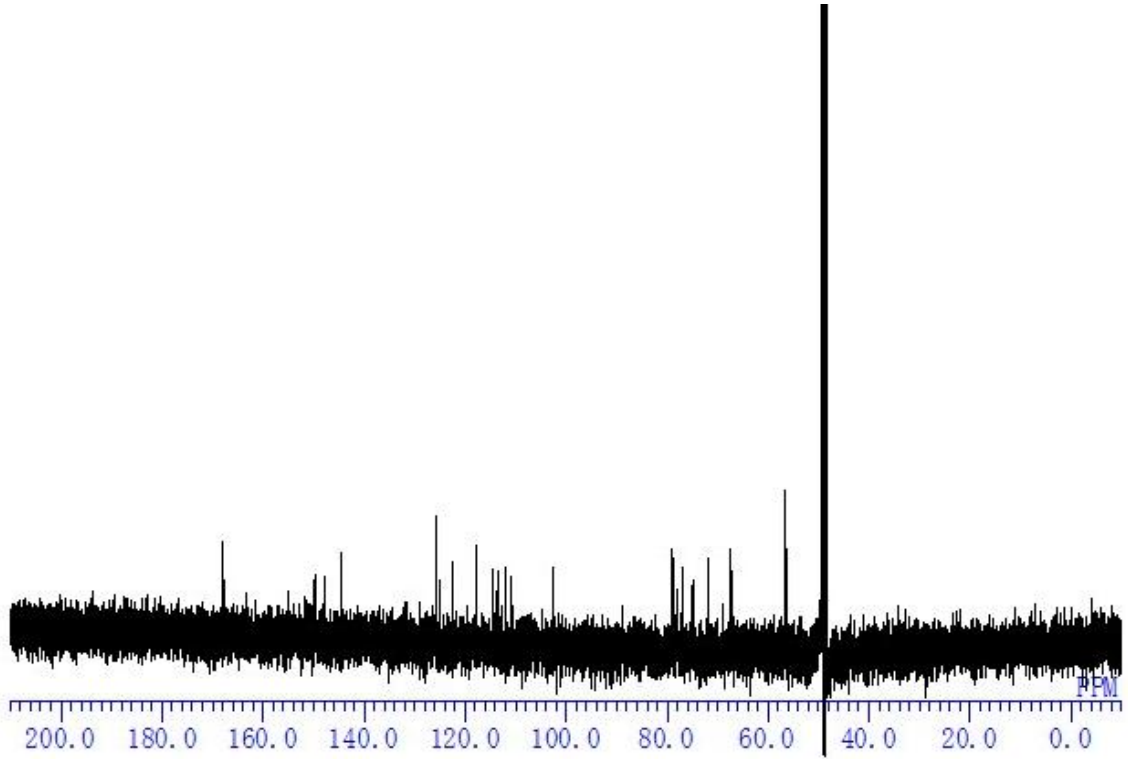

^{13}C NMR spectrum of **18** in CD_3OD

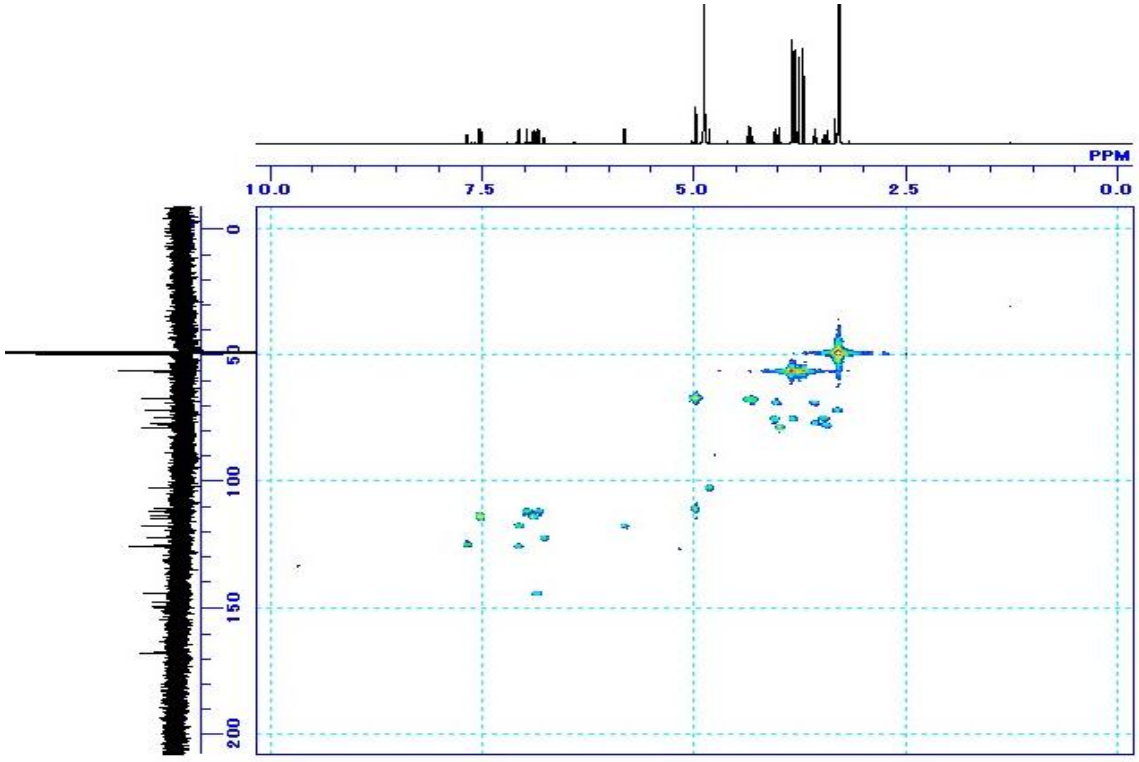

HMQC spectrum of **18** in CD_3OD

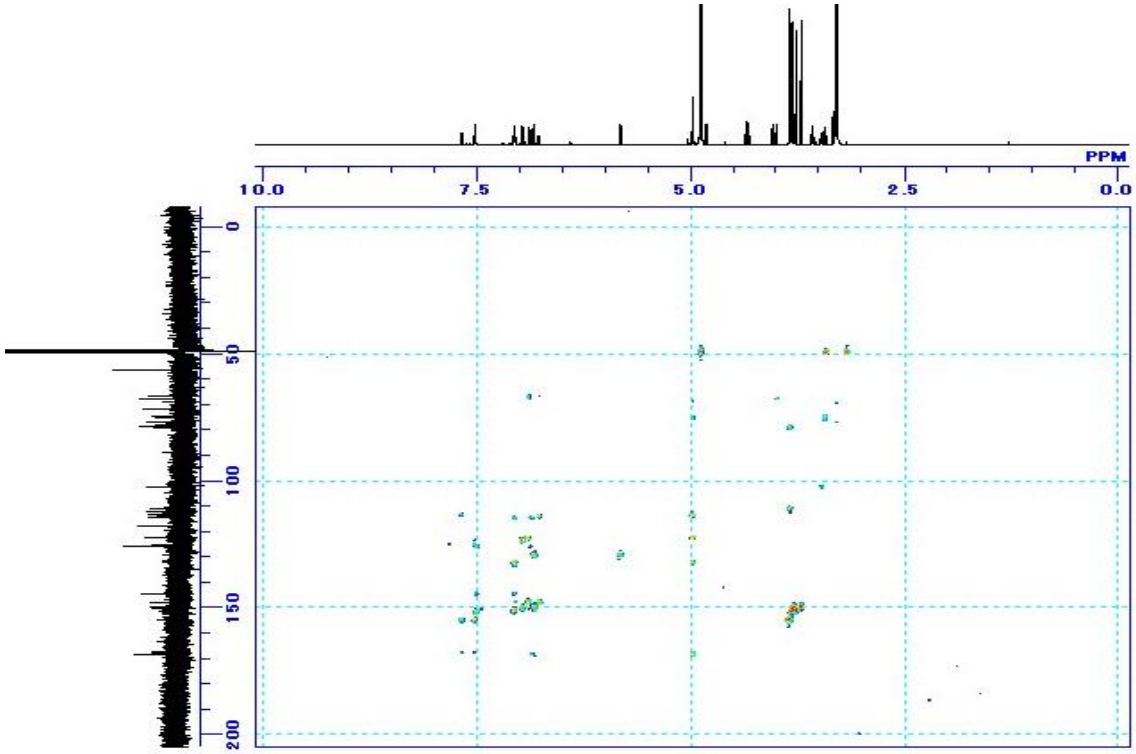

HMBC spectrum of **18** in CD_3OD

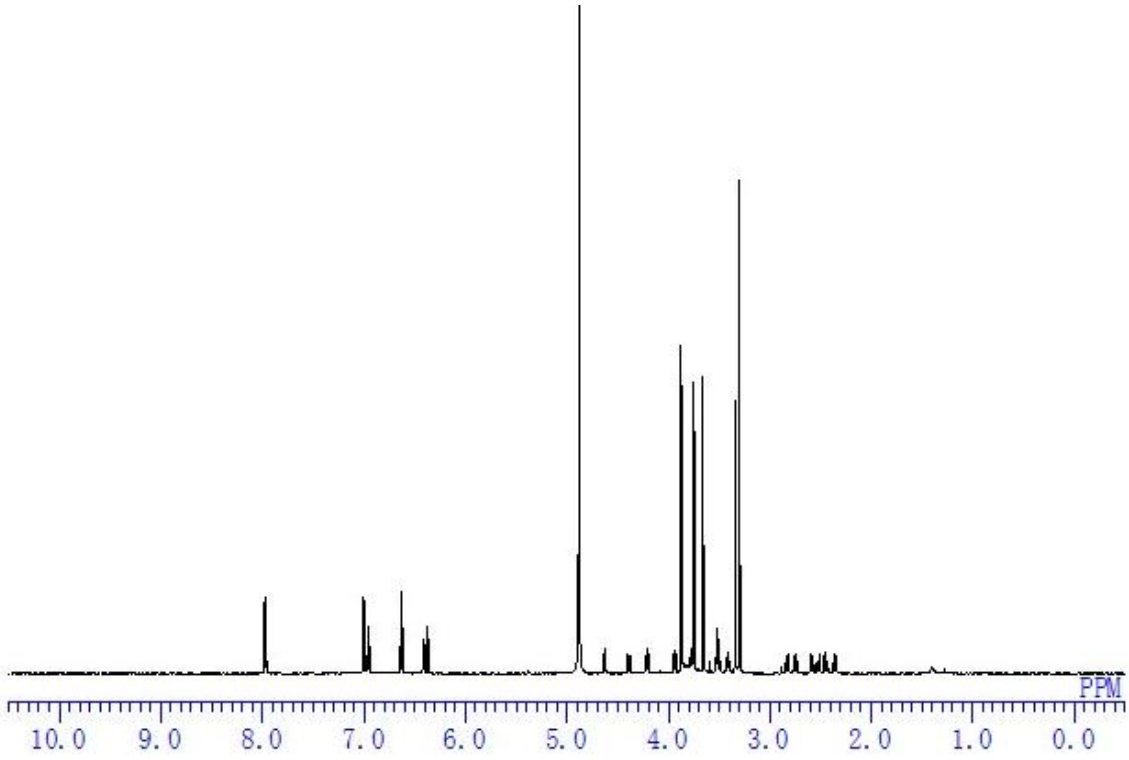

^{1}H NMR spectrum of **19** in CD_3OD

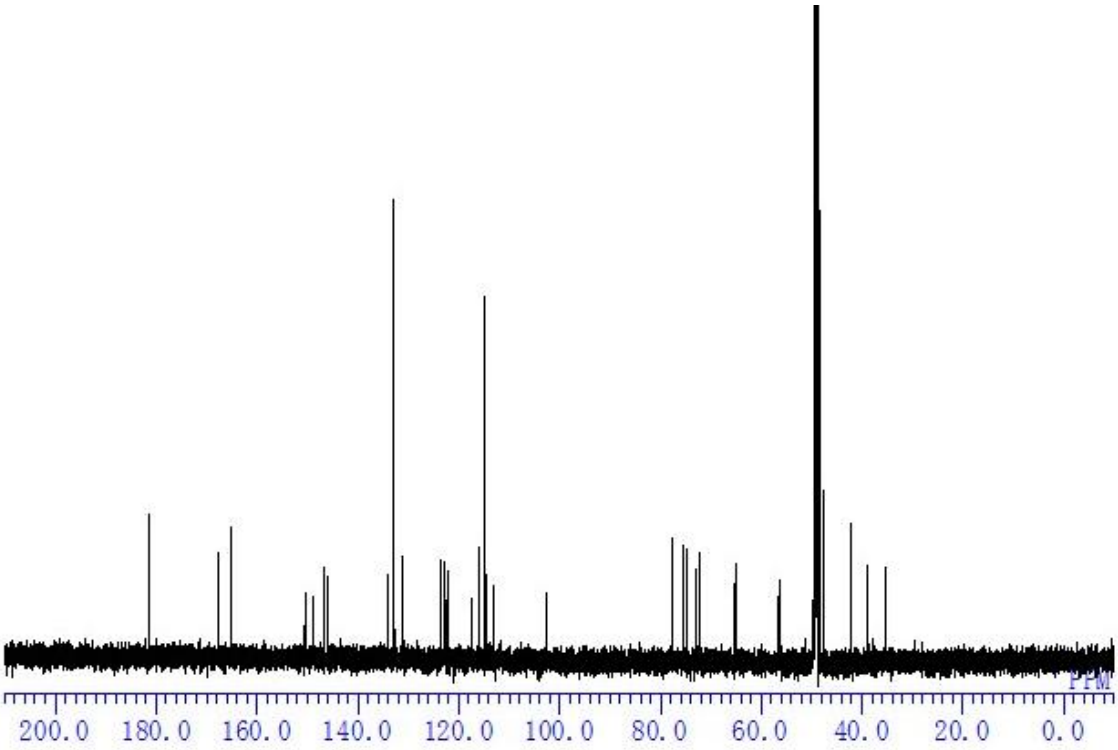

^{13}C NMR spectrum of **19** in CD_3OD

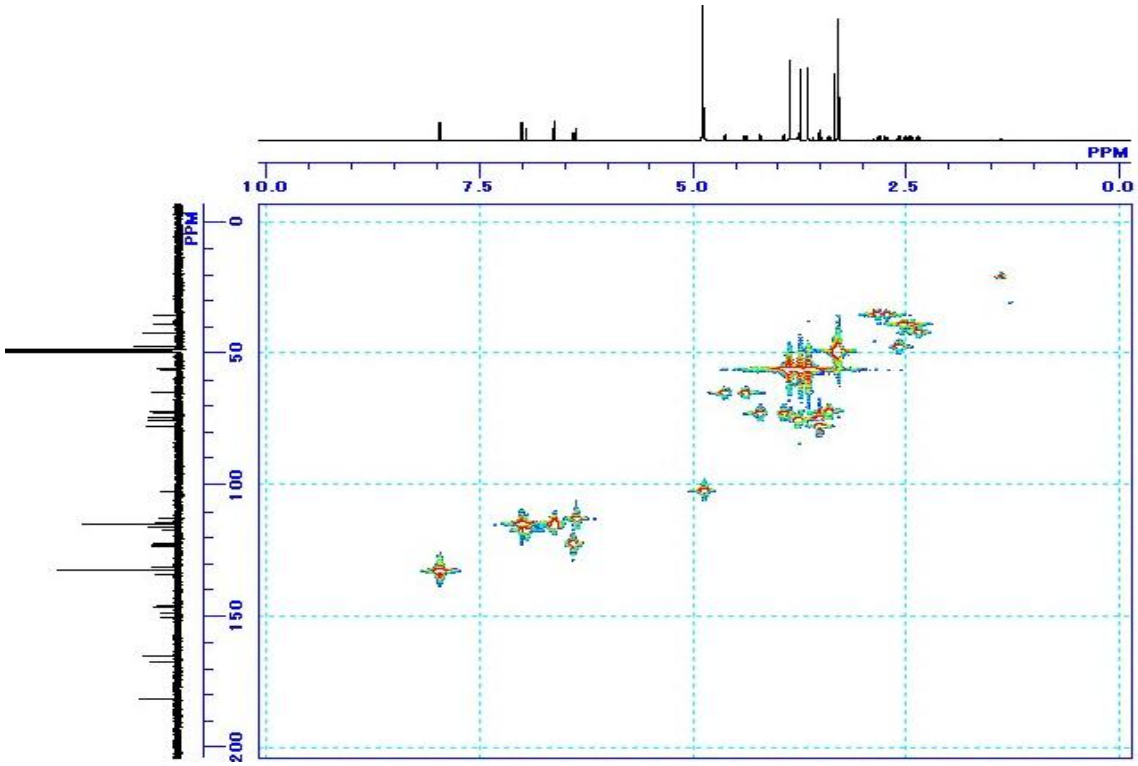

HMQC spectrum of **19** in CD_3OD

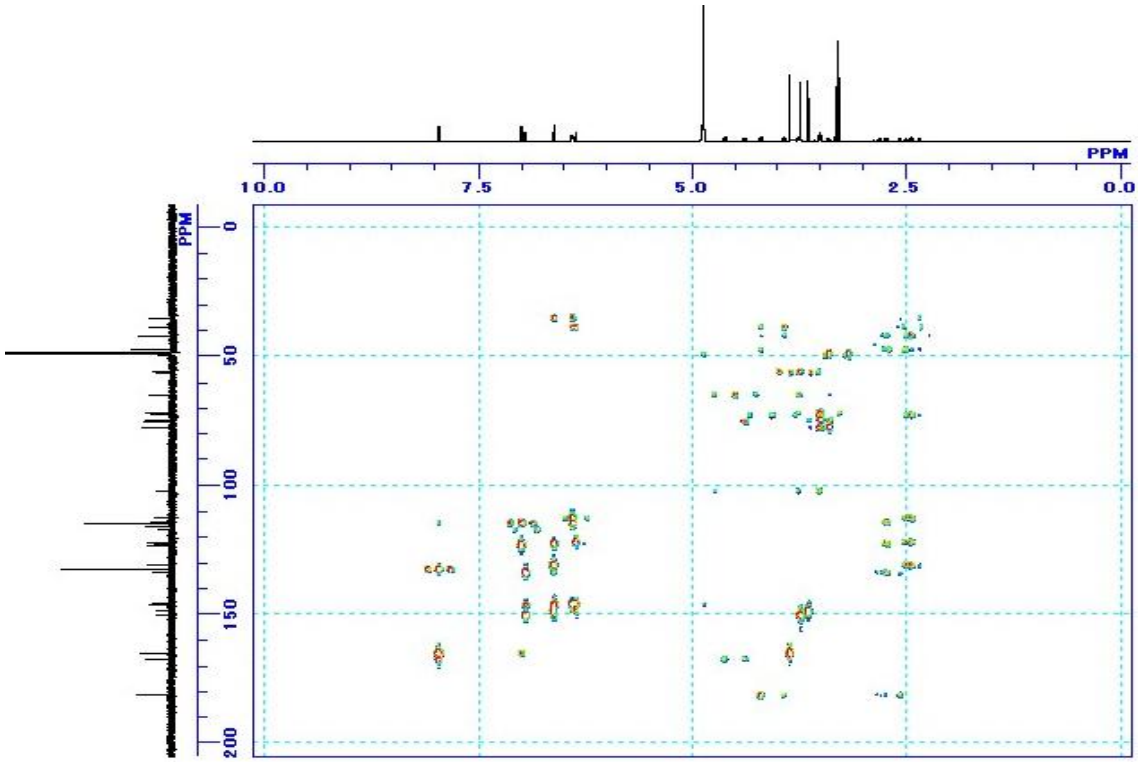

HMBC spectrum of **19** in CD_3OD

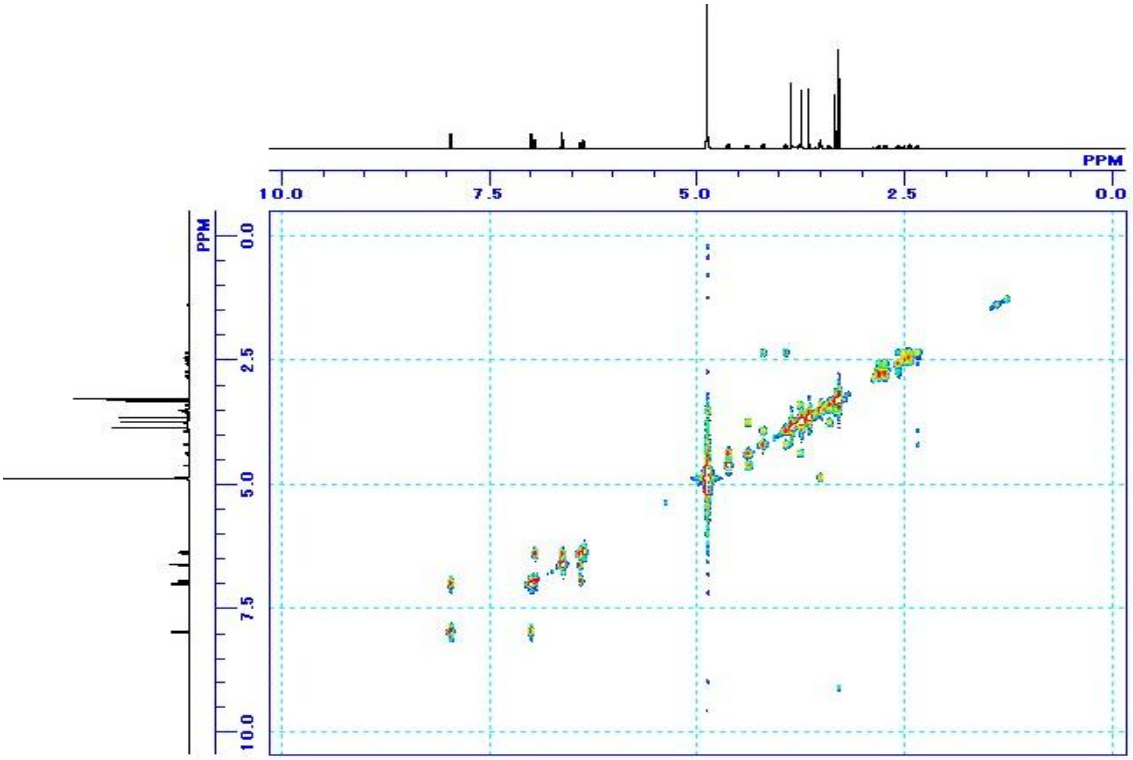

^{1}H-^{1}H COSY spectrum of **19** in CD_3OD

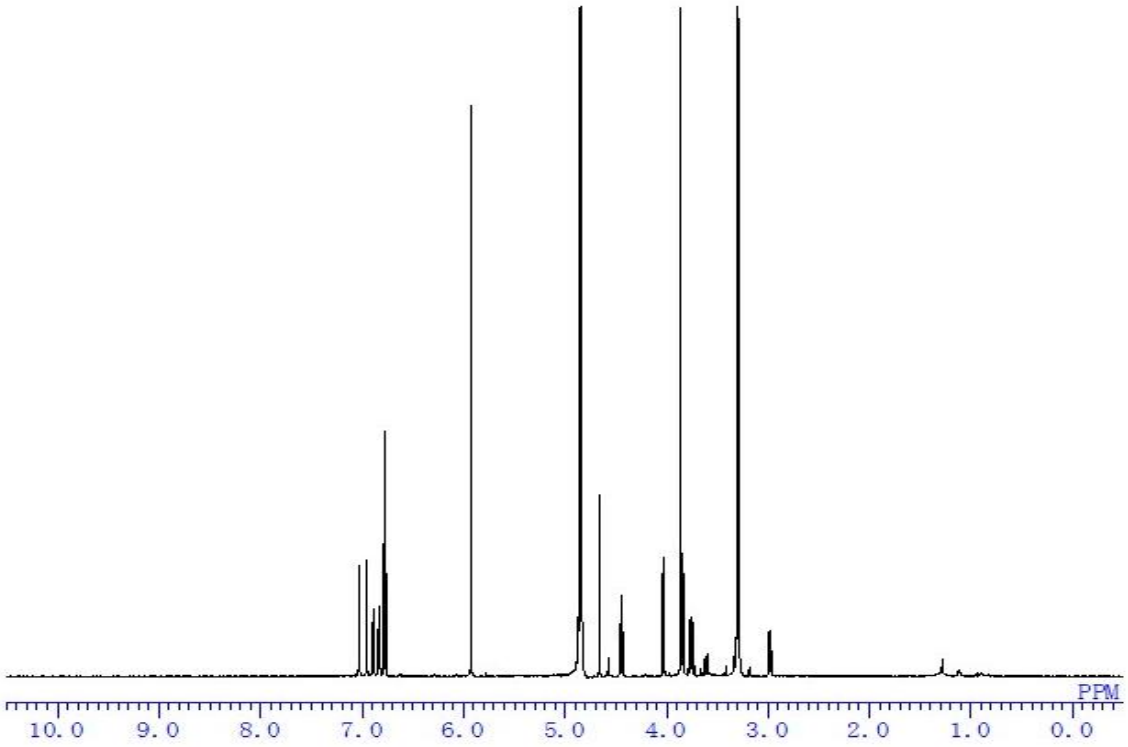

^{1}H NMR spectrum of **20** in CD_3OD

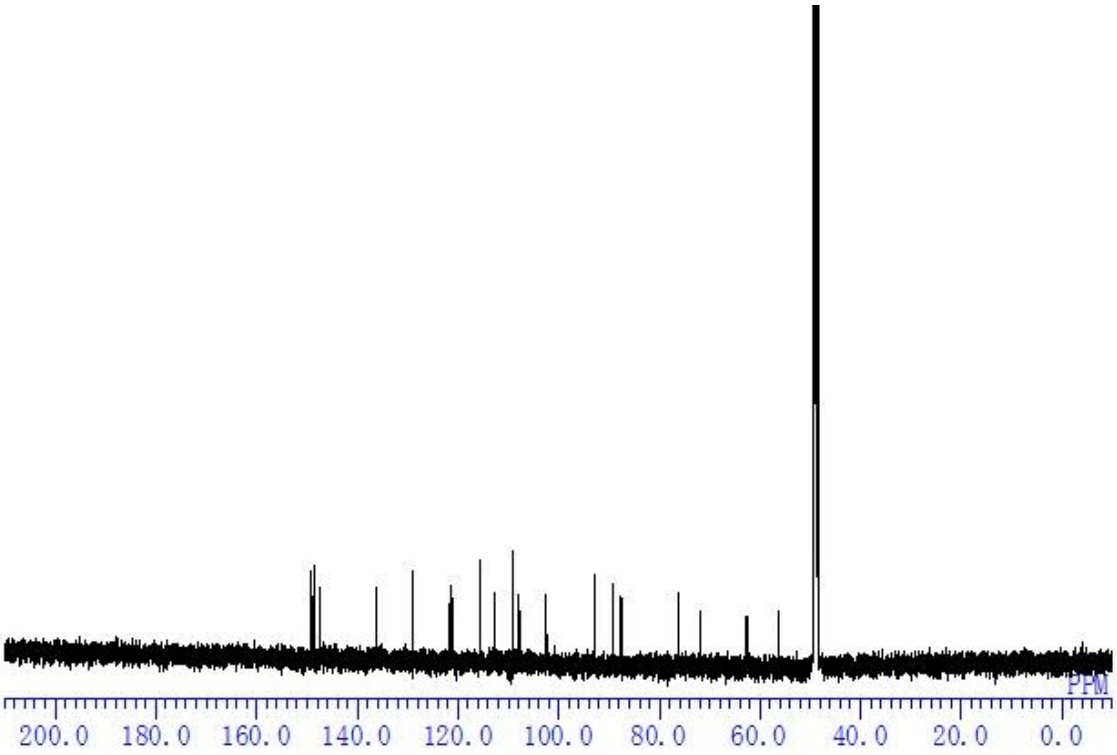

^{13}C NMR spectrum of **20** in CD_3OD

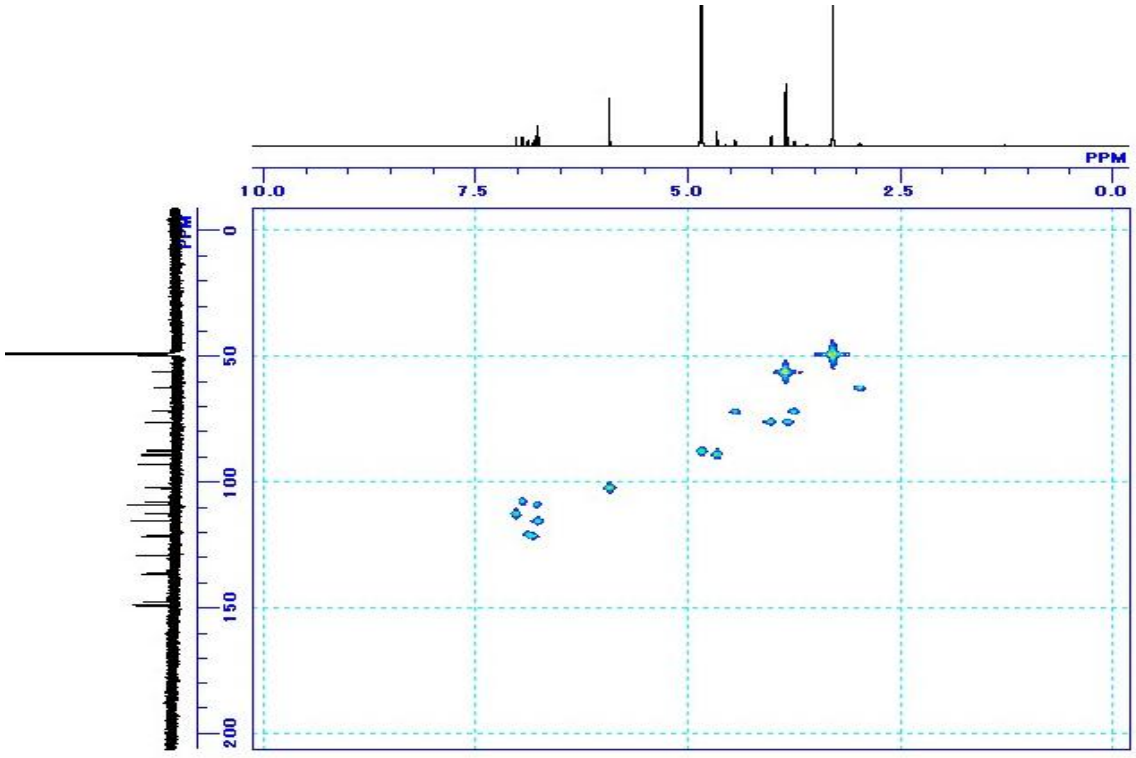

HMQC spectrum of **20** in CD_3OD

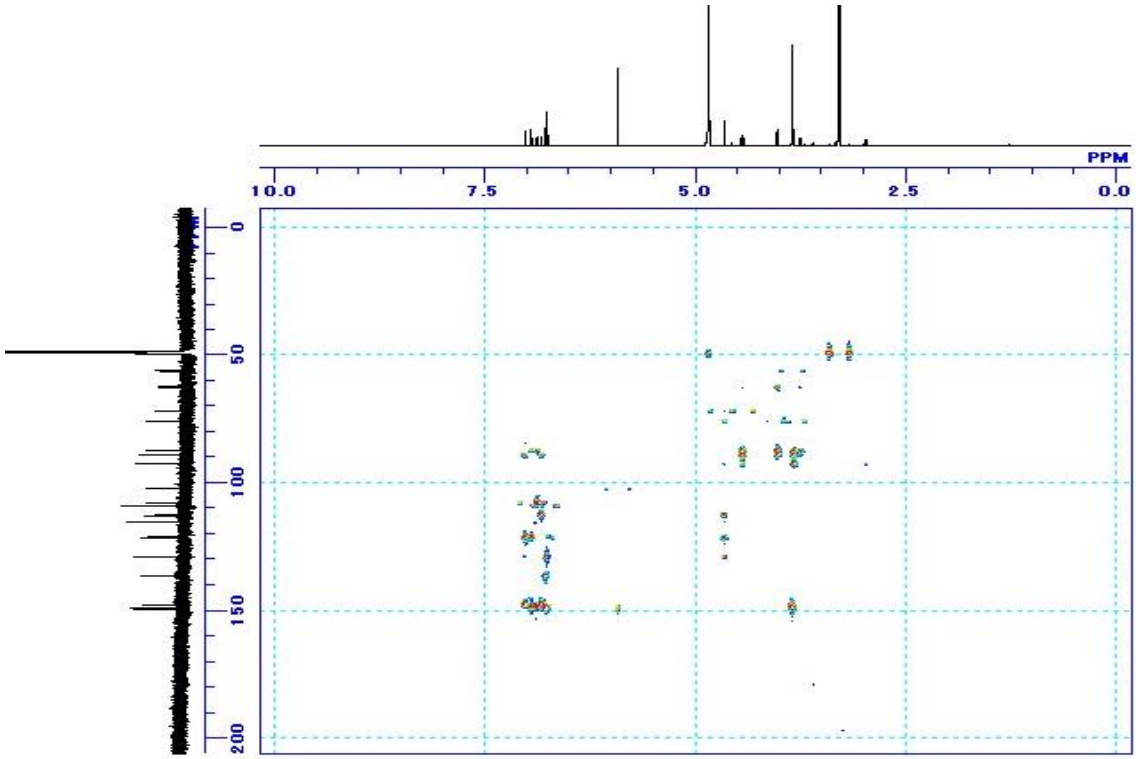

HMBC spectrum of **20** in CD_3OD

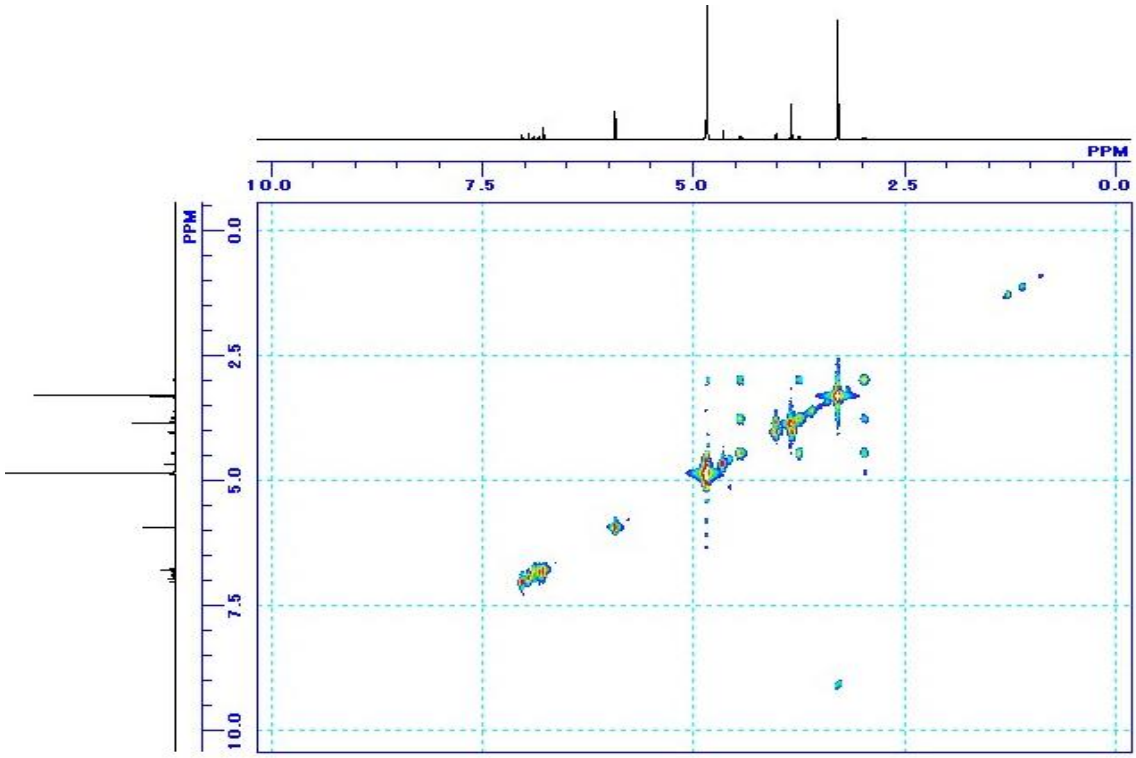

^{1}H-^{1}H COSY spectrum of **20** in CD_3OD

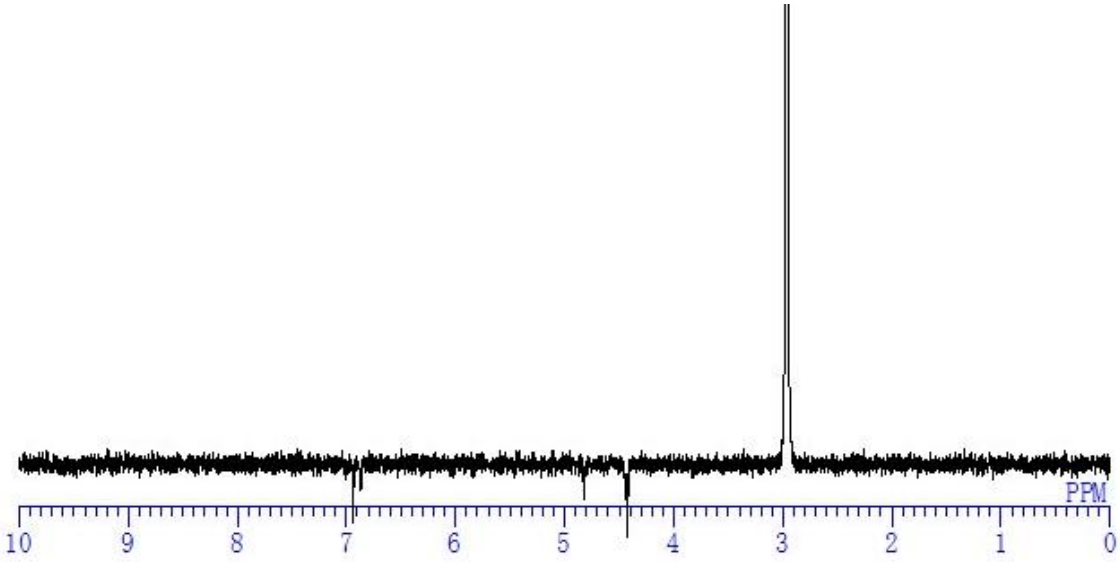

NOE spectrum of **20** in CD_3OD (δ_H 3.00)

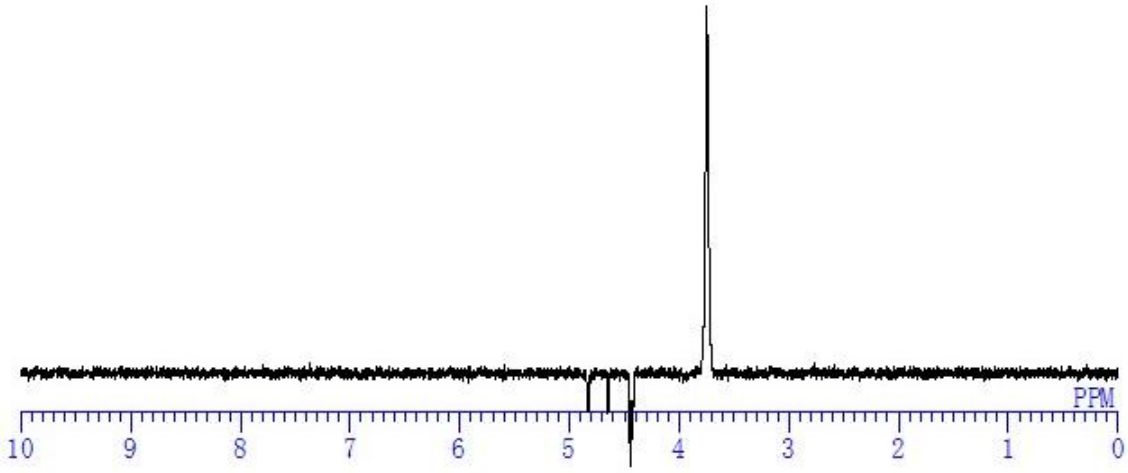

NOE spectrum of **20** in CD_3OD (δ_H 3.77)

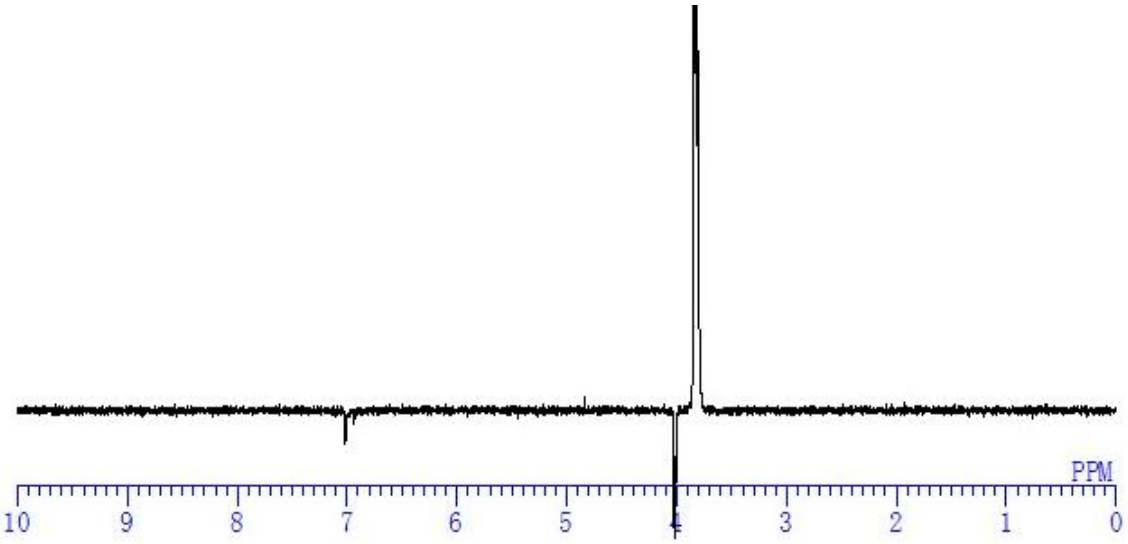

NOE spectrum of **20** in CD_3OD (δ_H 3.84)

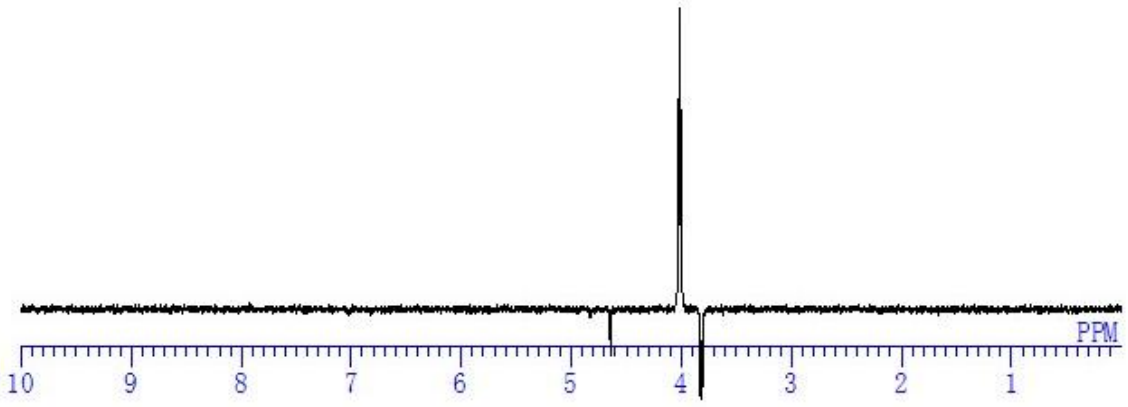

NOE spectrum of **20** in CD_3OD (δ_H 4.04)

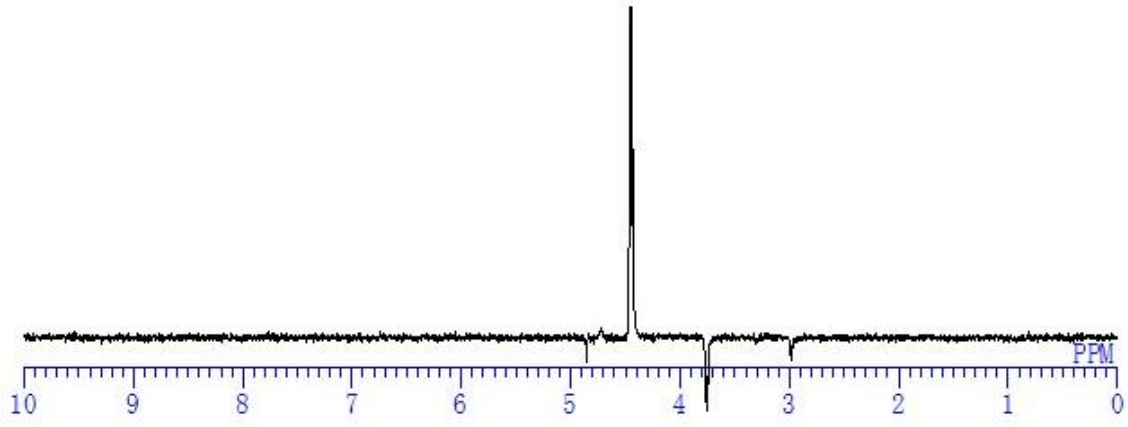

NOE spectrum of **20** in CD_3OD (δ_H 4.45)

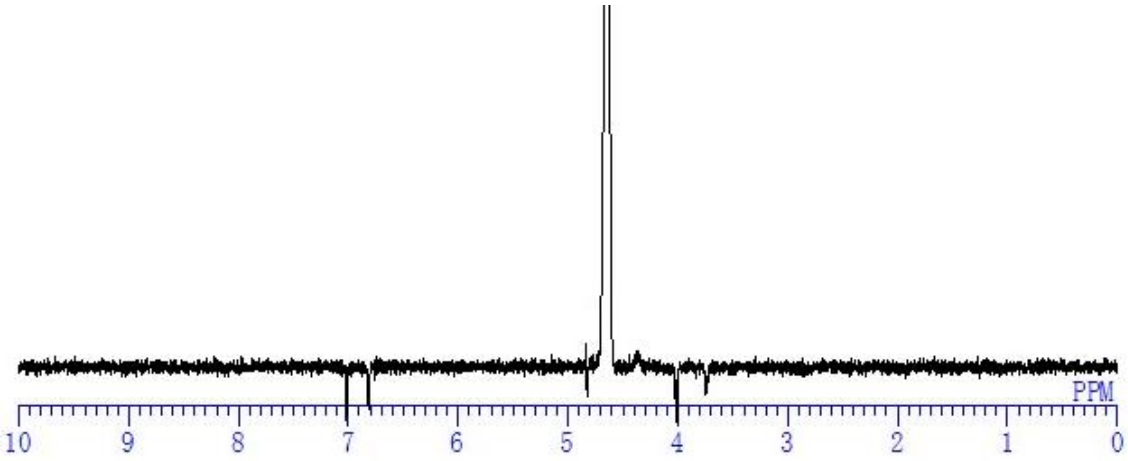

NOE spectrum of **20** in CD_3OD (δ_H 4.66)

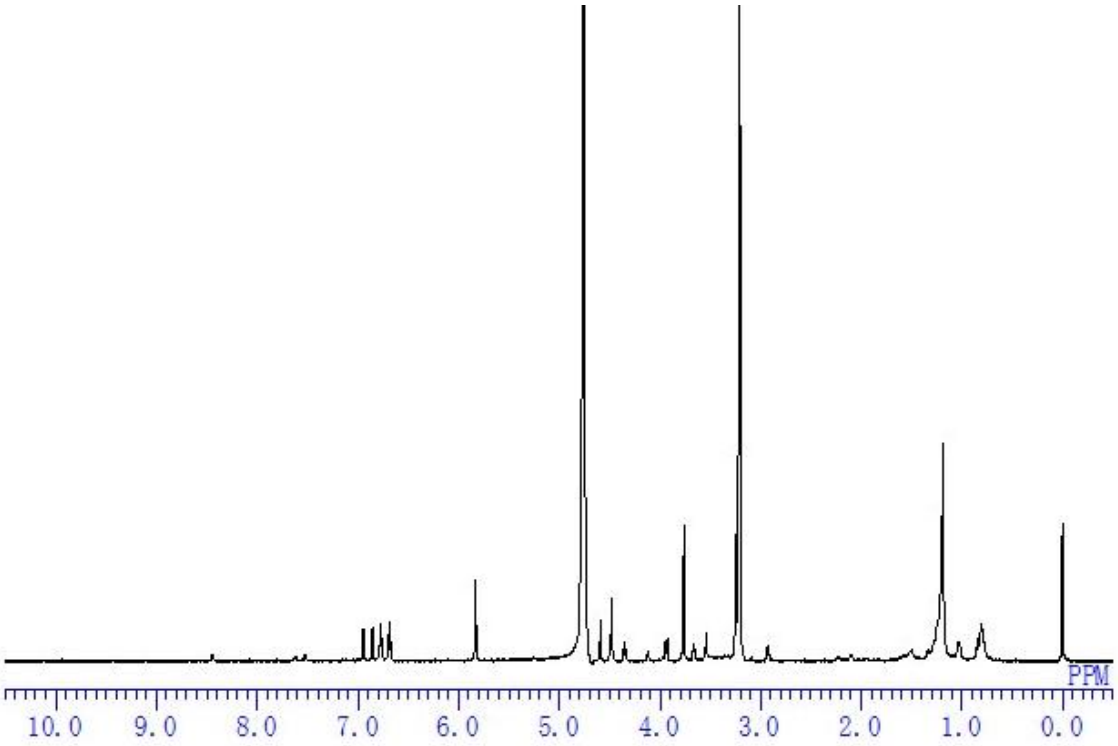

^{1}H NMR spectrum of **21** in CD_3OD

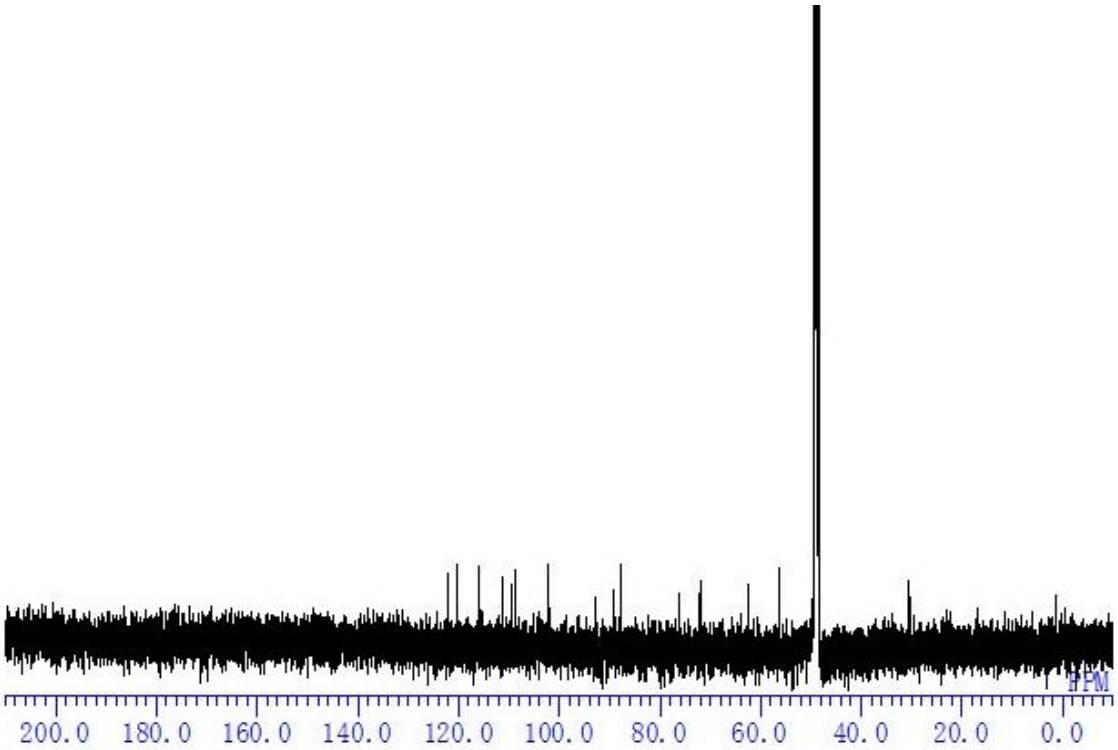

^{13}C NMR spectrum of **21** in CD_3OD

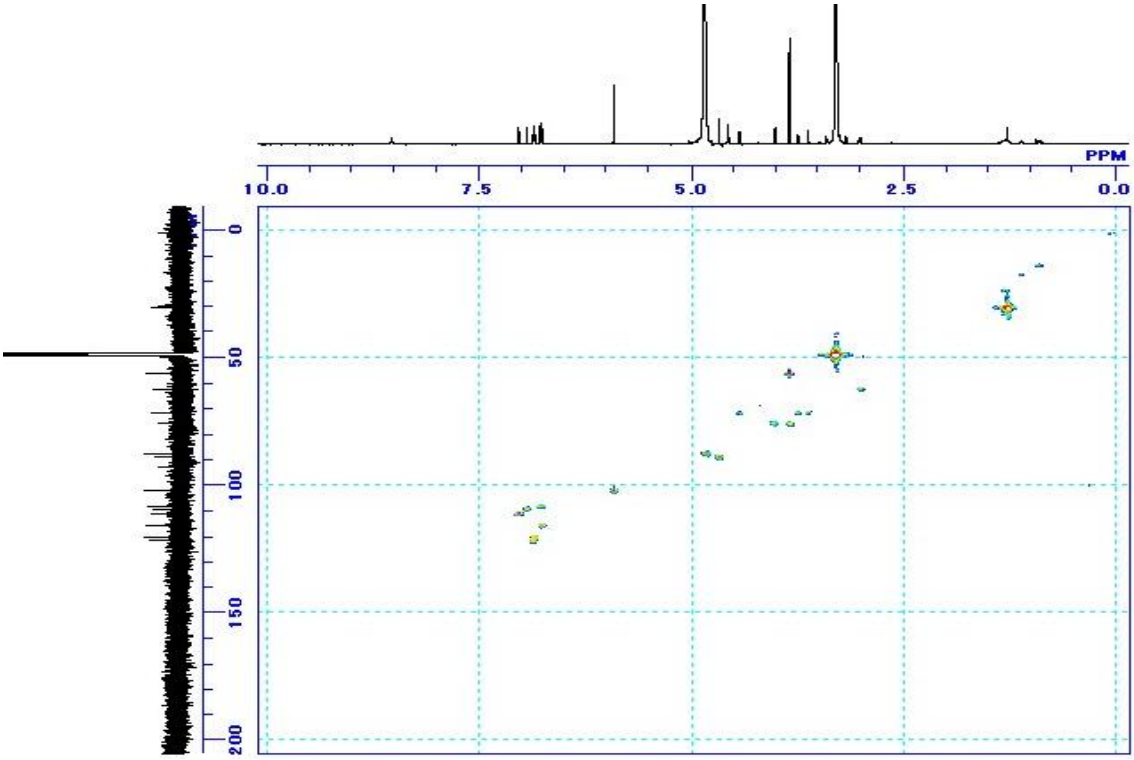

HMQC spectrum of **21** in CD_3OD

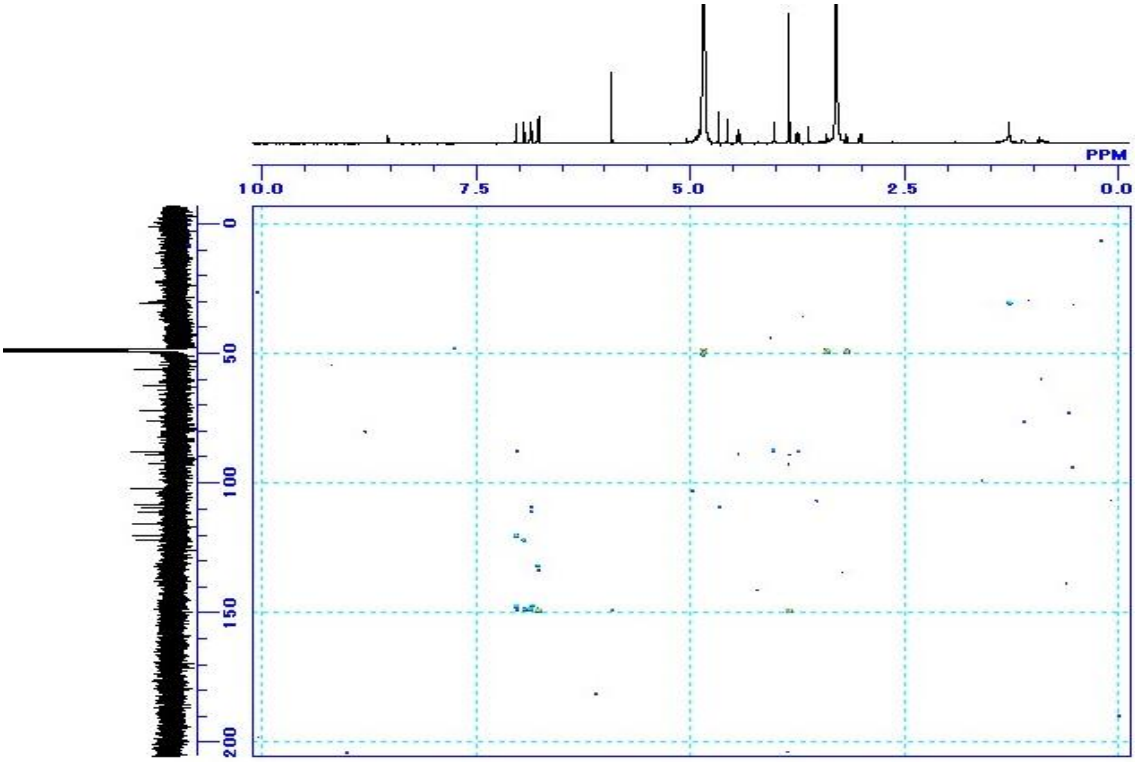

HMBC spectrum of **21** in CD_3OD

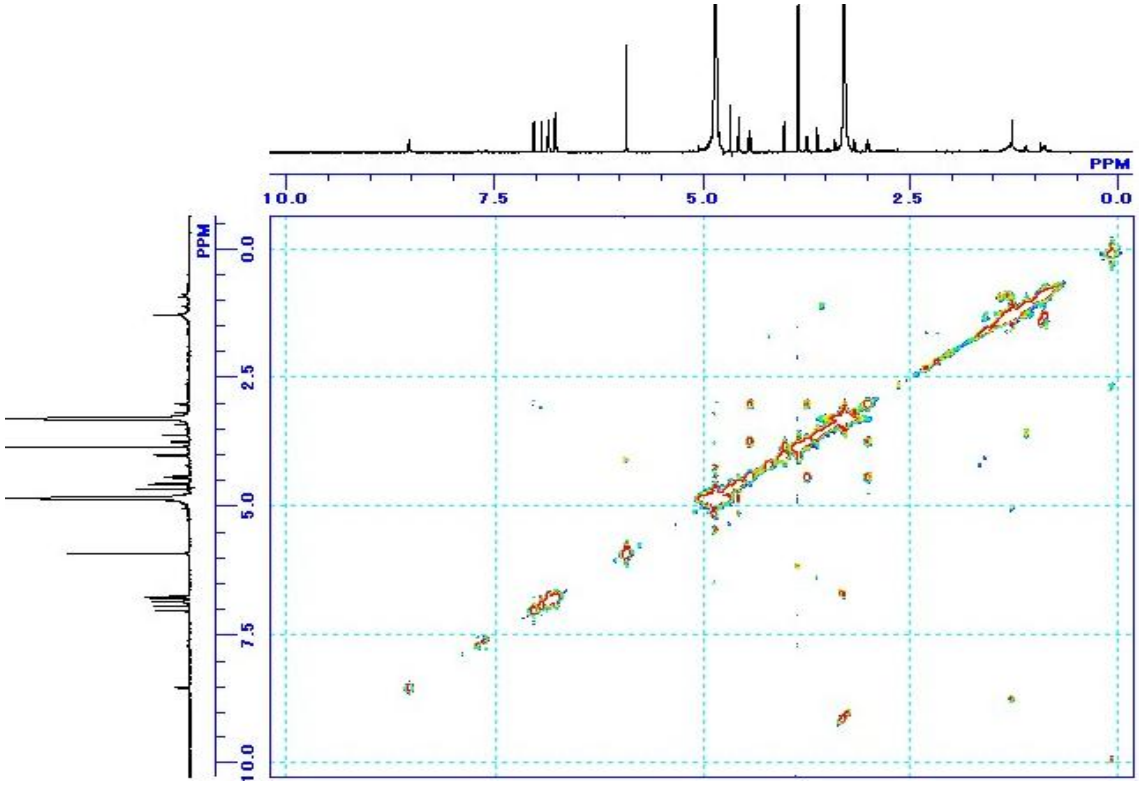

^{1}H-^{1}H COSY spectrum of **21** in CD_3OD

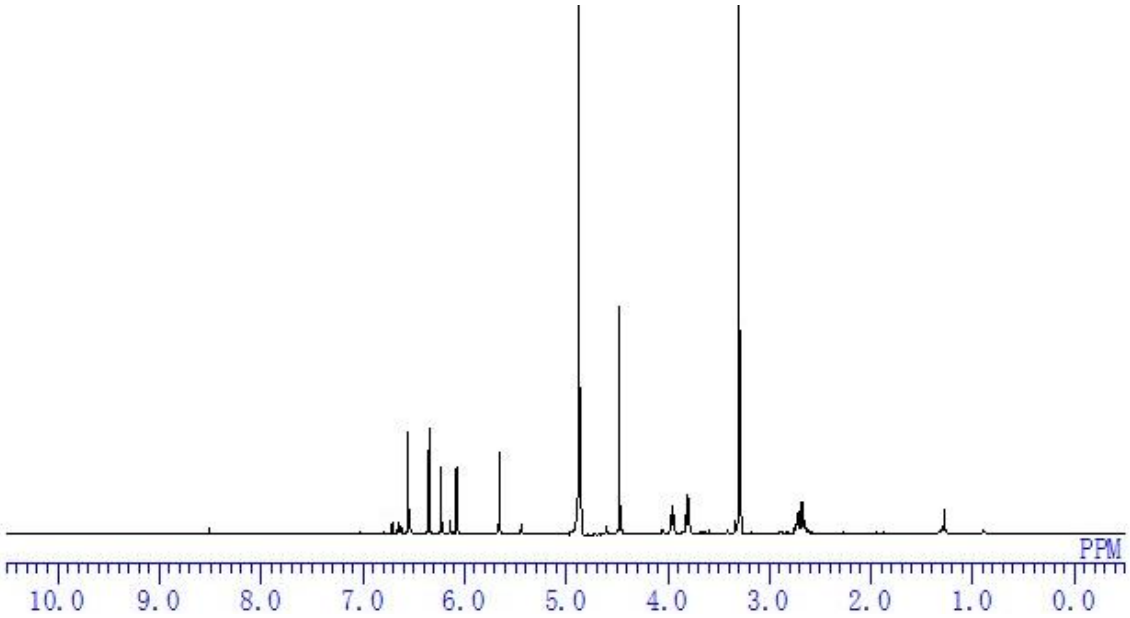

^{1}H NMR spectrum of **27** in CD_3OD

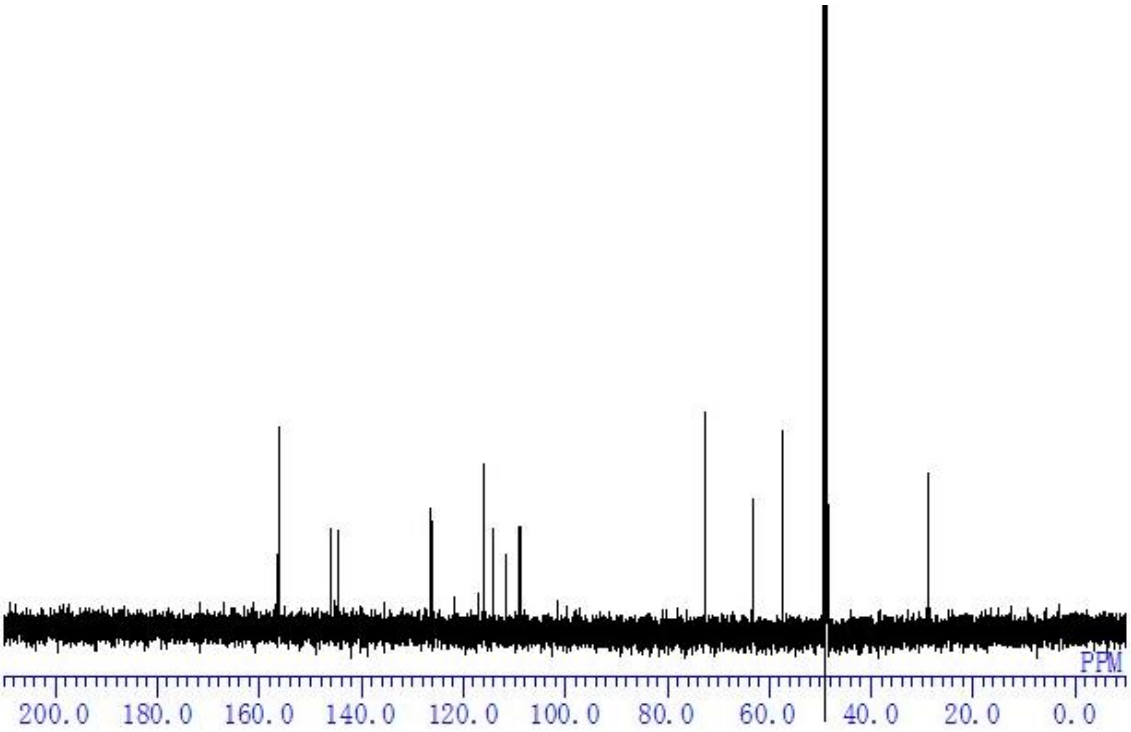

^{13}C NMR spectrum of **27** in CD_3OD

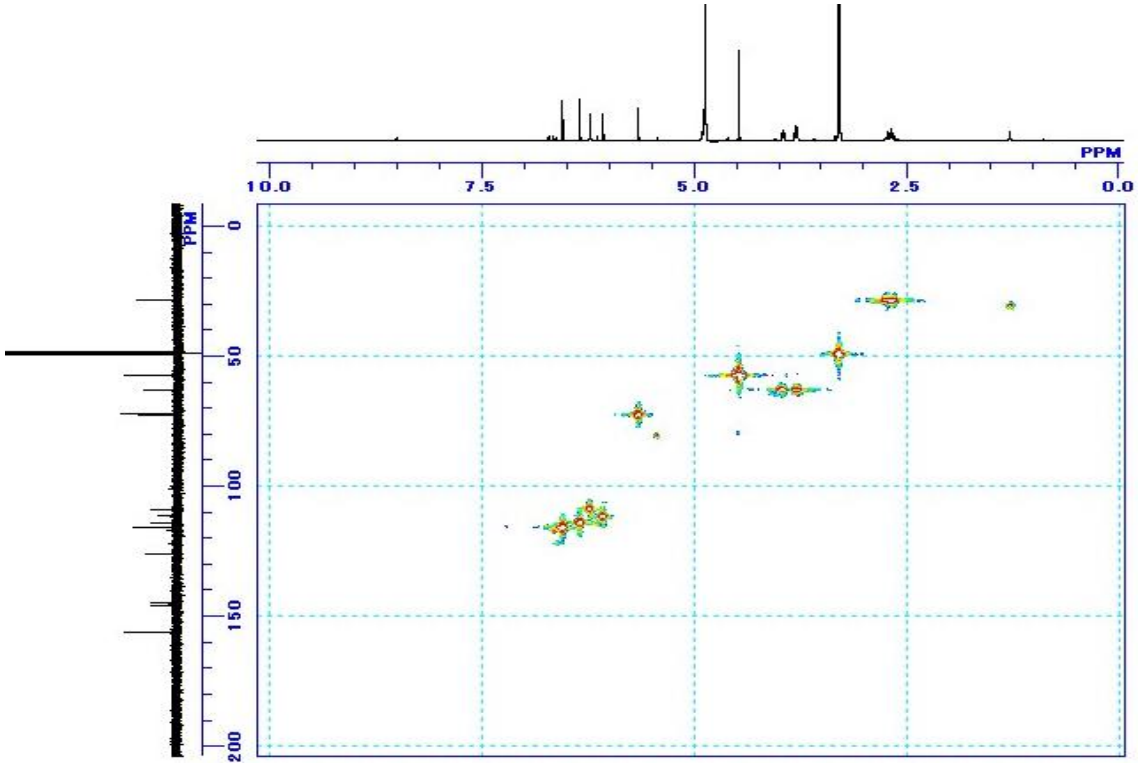

HMQC spectrum of **27** in CD_3OD

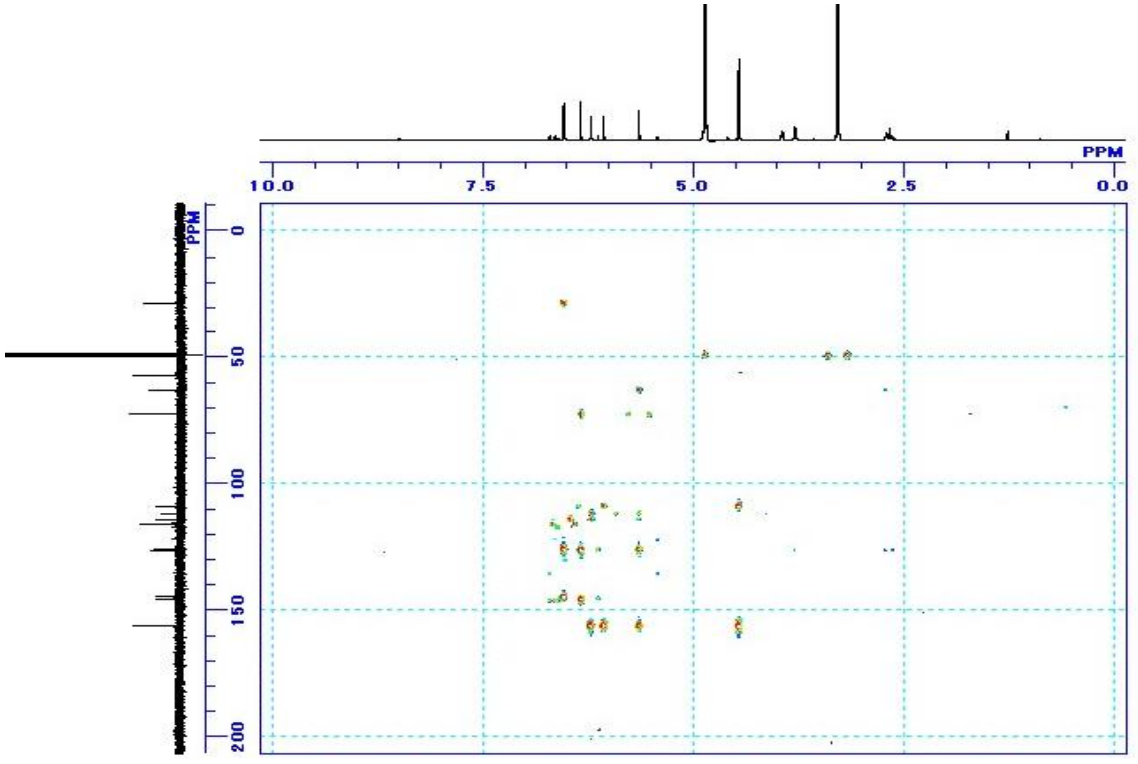

HMBC spectrum of **27** in CD_3OD

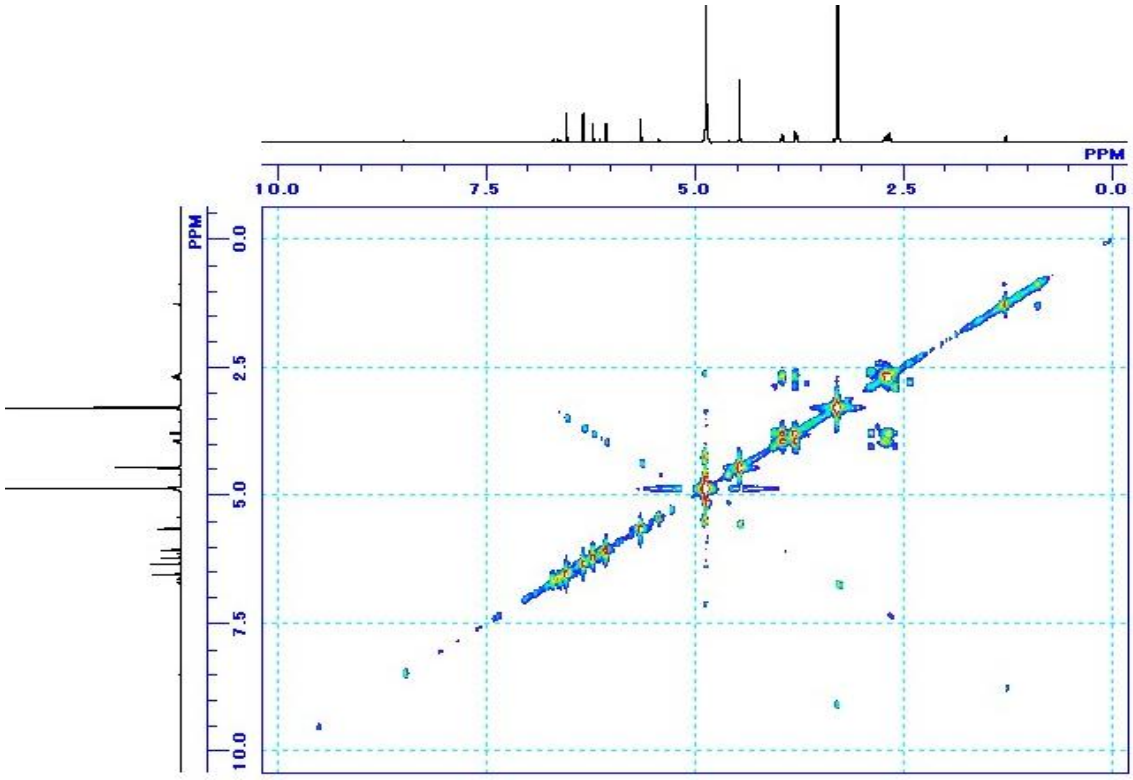

^{1}H-^{1}H COSY spectrum of **27** in CD_3OD

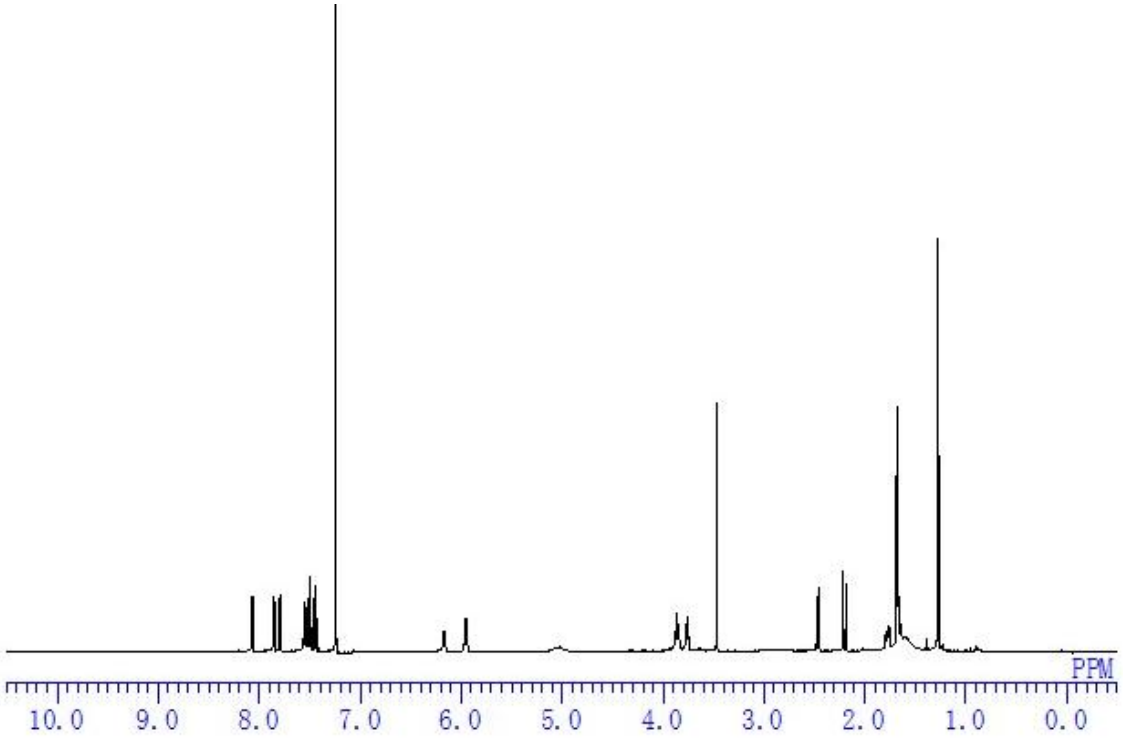

^{1}H NMR spectrum of **28** in $CDCl_3$

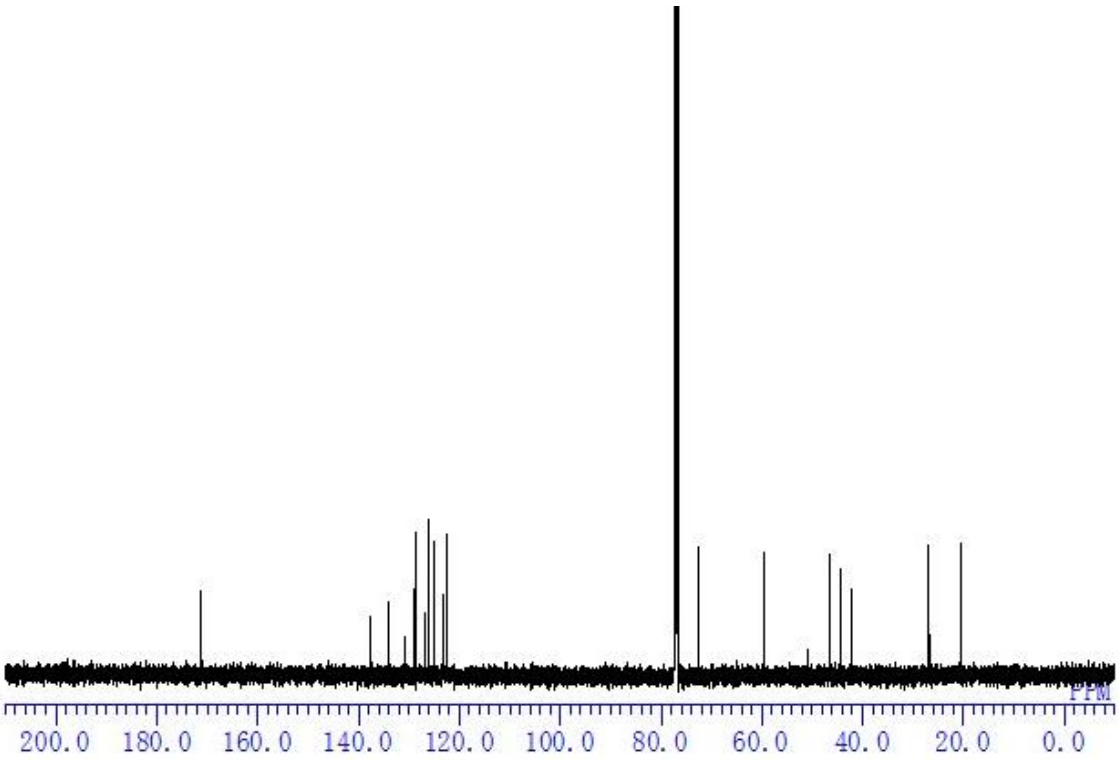

^{13}C NMR spectrum of **28** in $CDCl_3$

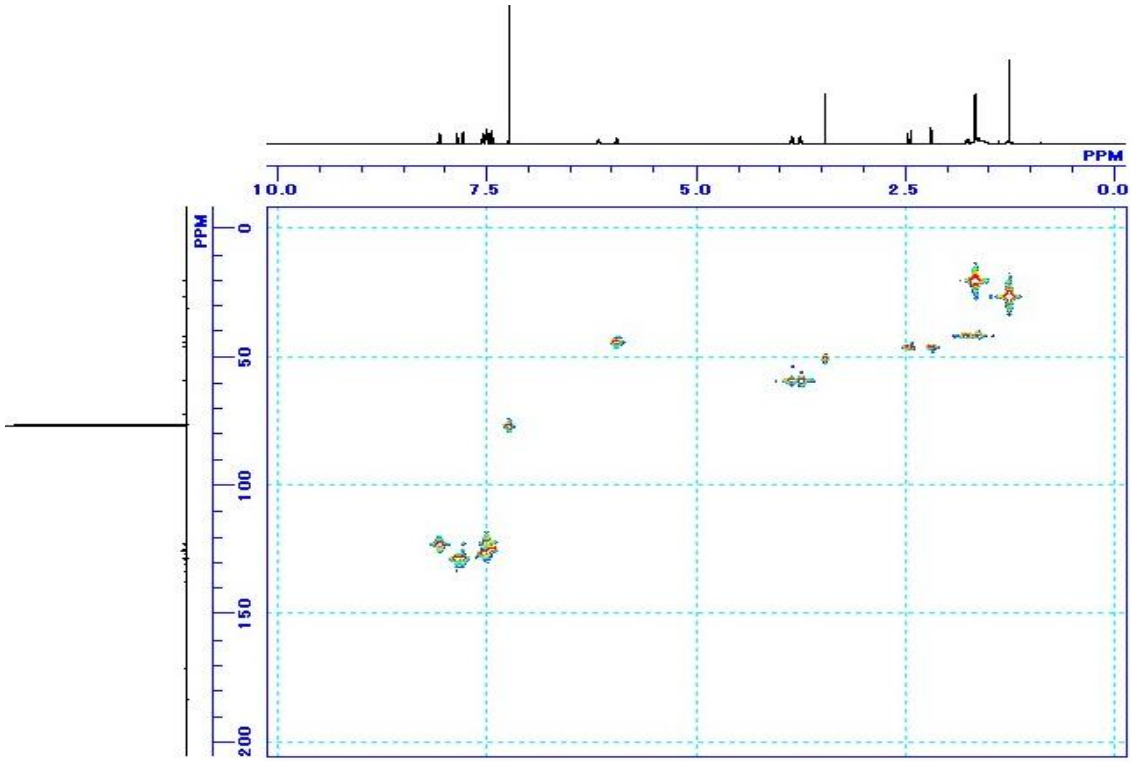

HMQC spectrum of **28** in $CDCl_3$

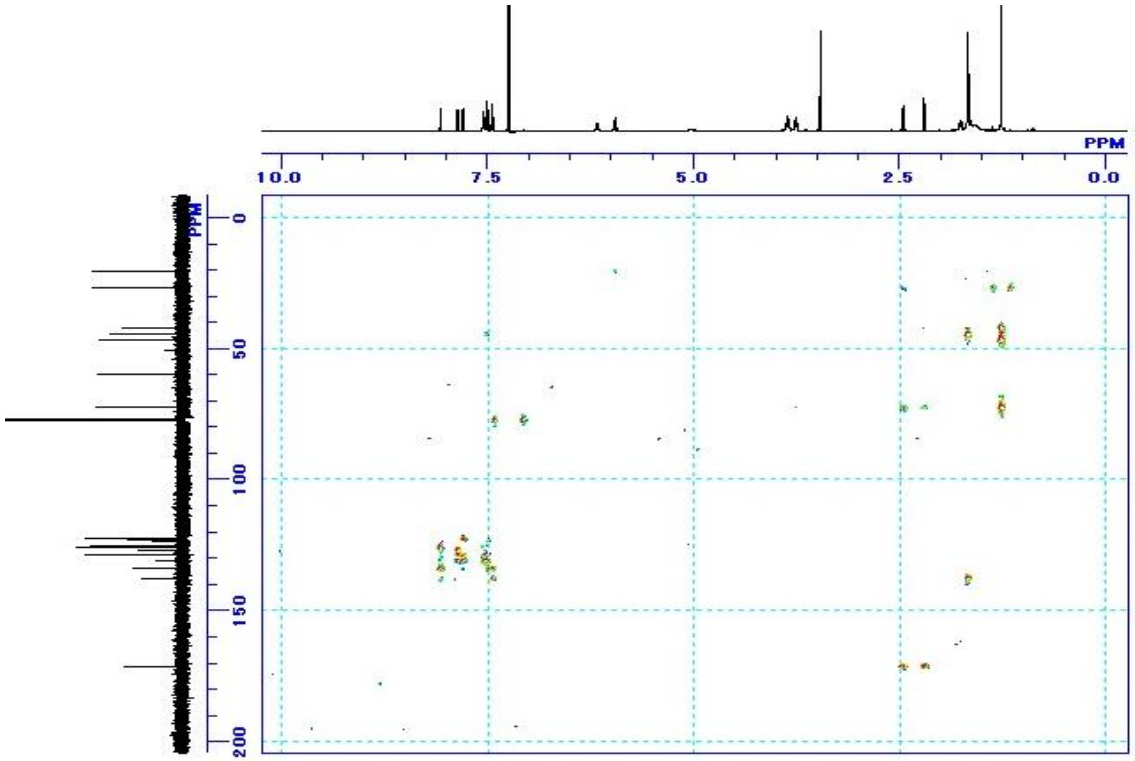

HMBC spectrum of **28** in $CDCl_3$

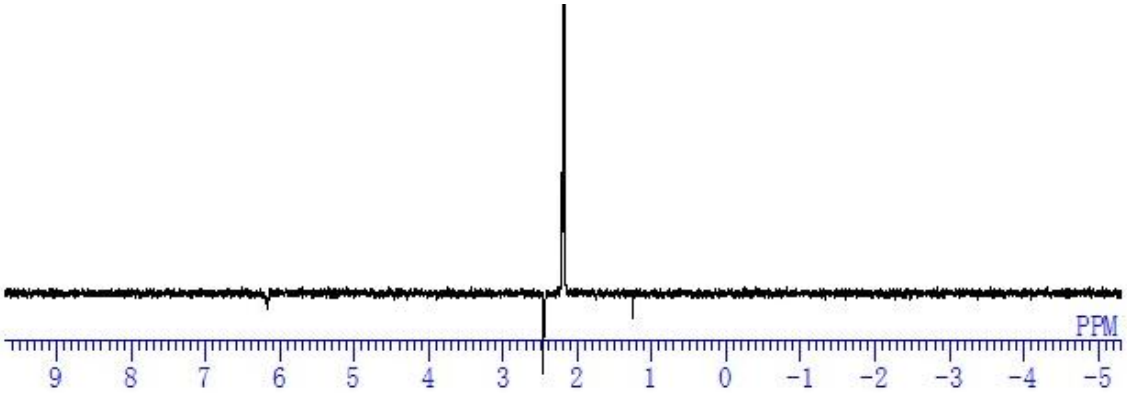

NOE spectrum of **28** in $CDCl_3$ 2.2

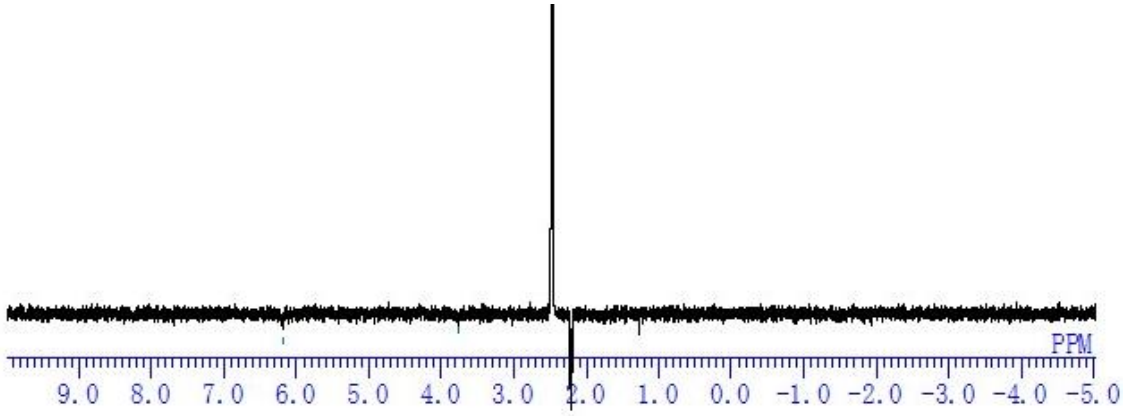

NOE spectrum of **28** in $CDCl_3$ 2.46

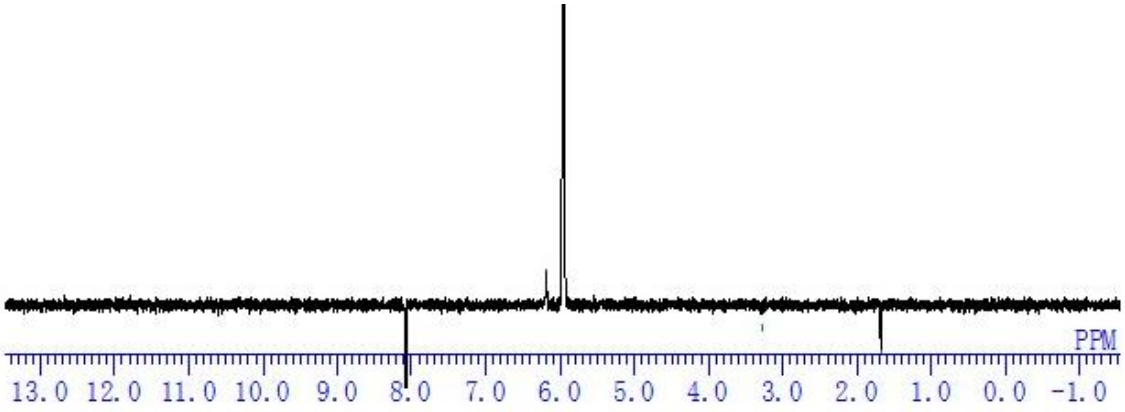

NOE spectrum of **28** in $CDCl_3$ 5.96

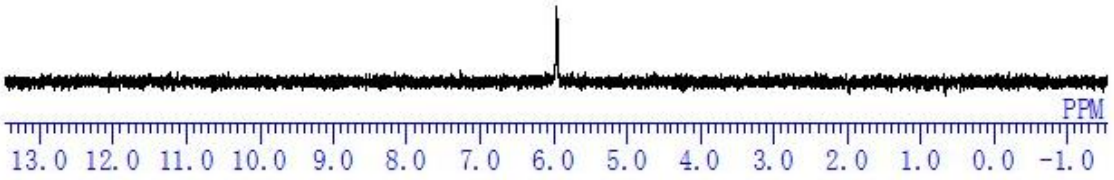

NOE spectrum of **28** in $CDCl_3$ 6.16

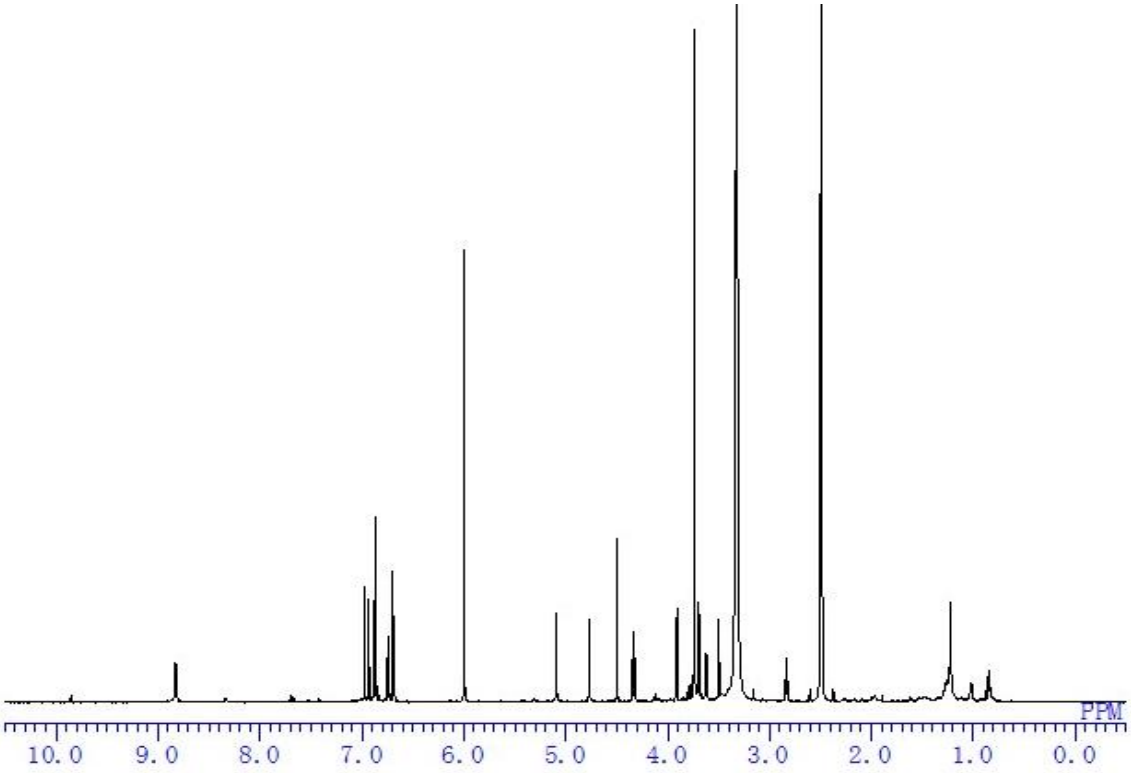

^{1}H NMR spectrum of **28** in DMSO

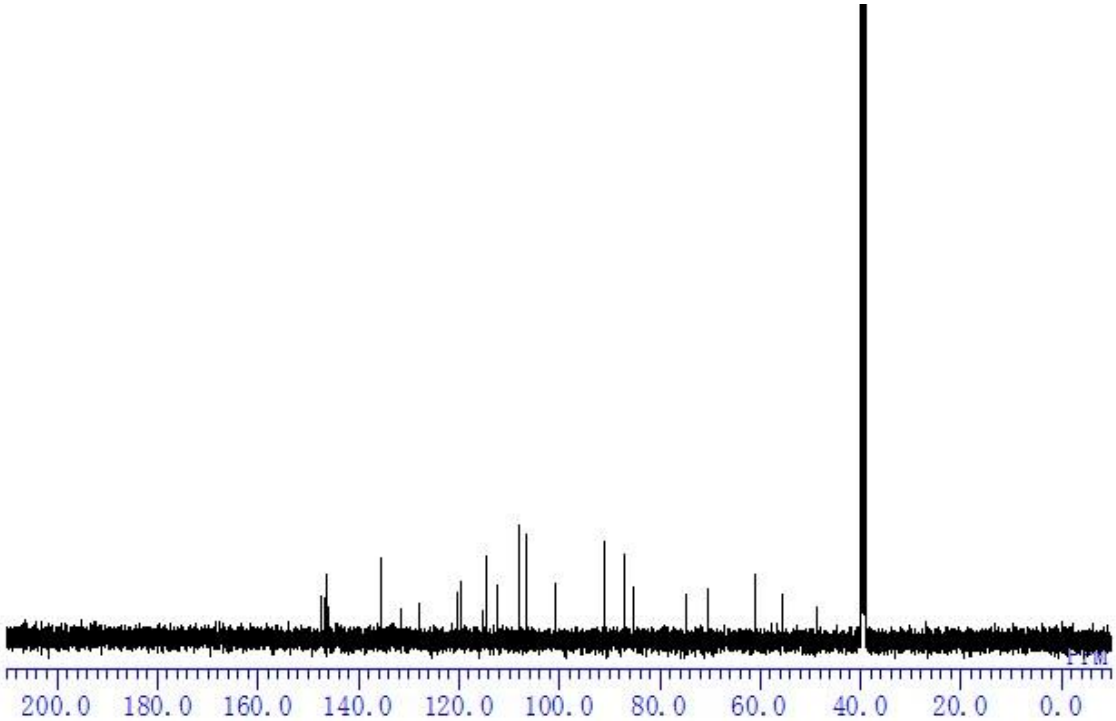

^{13}C NMR spectrum of **28** in DMSO

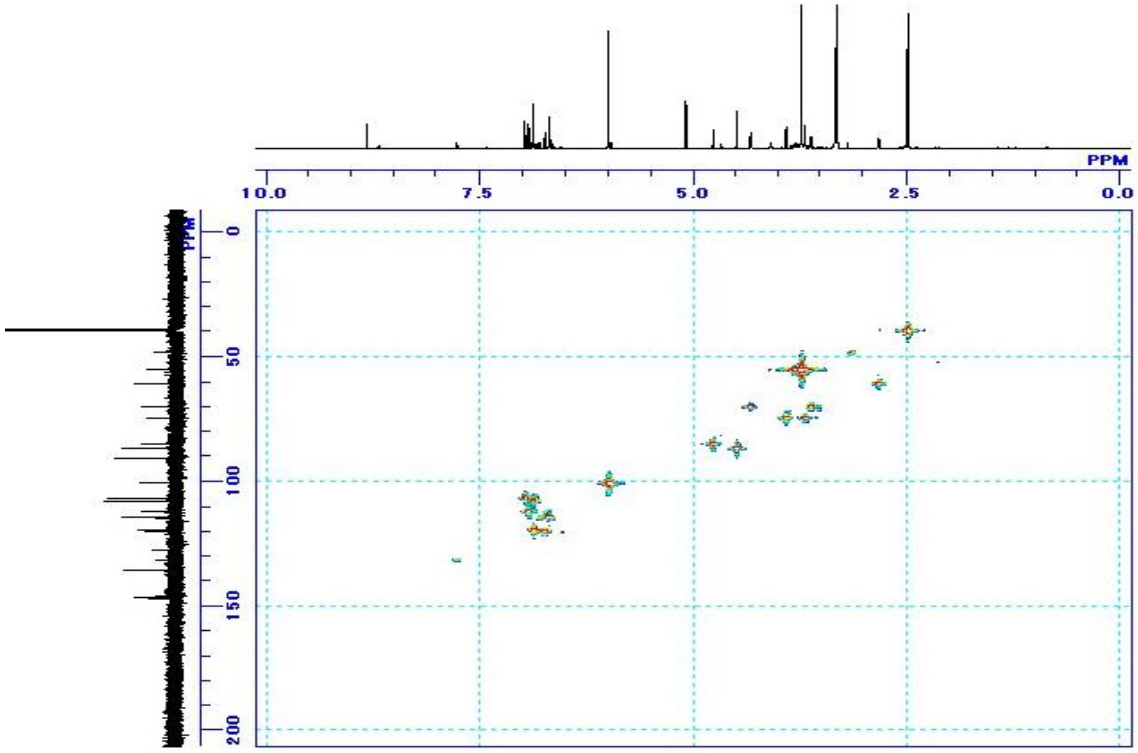

HMQC spectrum of **28** in DMSO

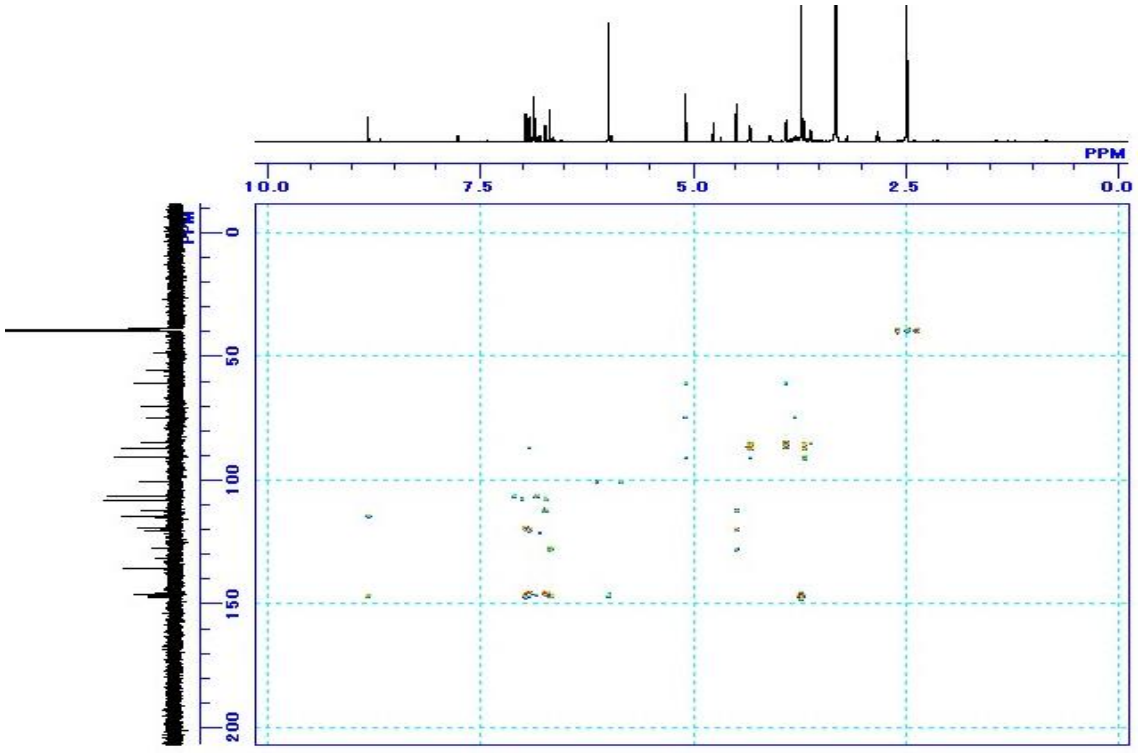

HMBC spectrum of **28** in DMSO

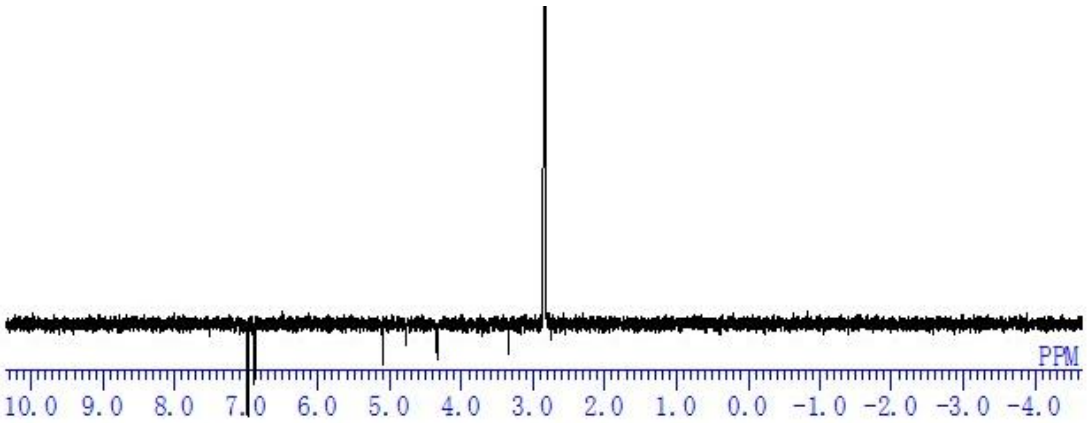

NOE spectrum of **28** in DMSO 2.85

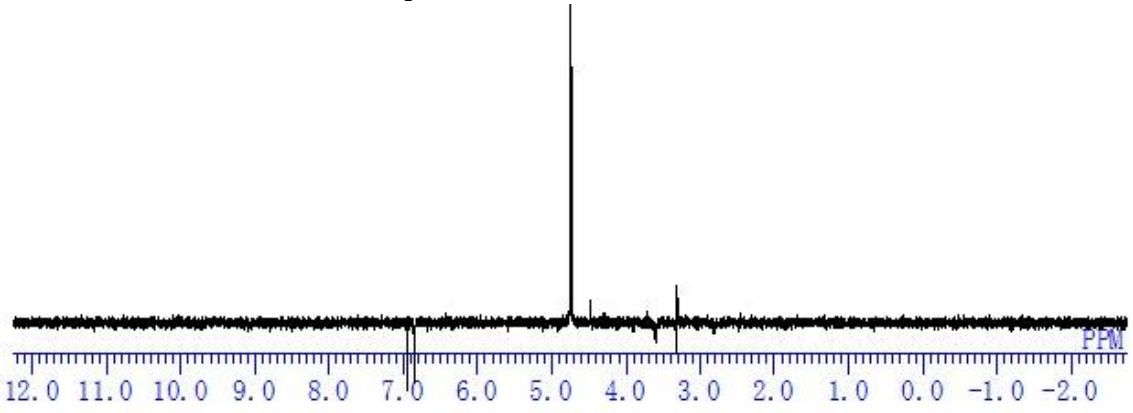

NOE spectrum of **28** in DMSO 4.77

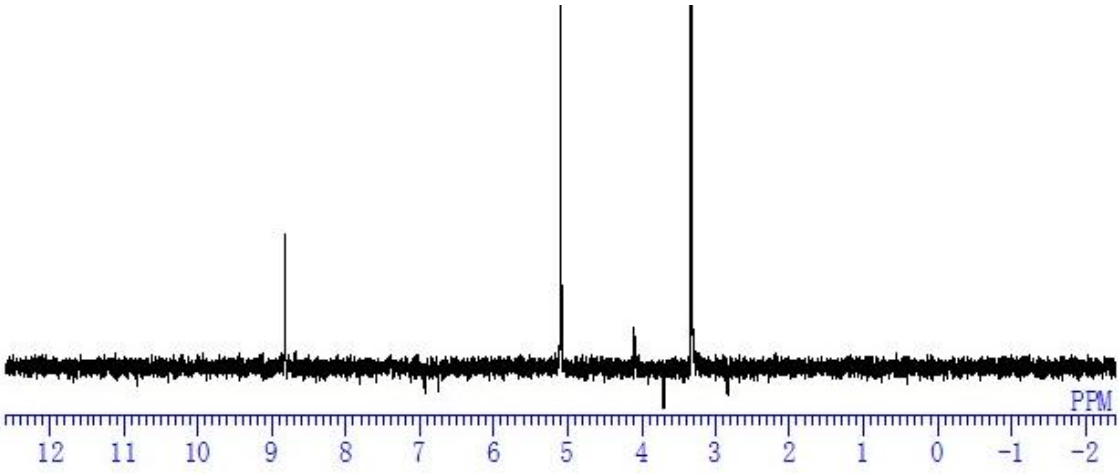

NOE spectrum of **28** in DMSO 5.6

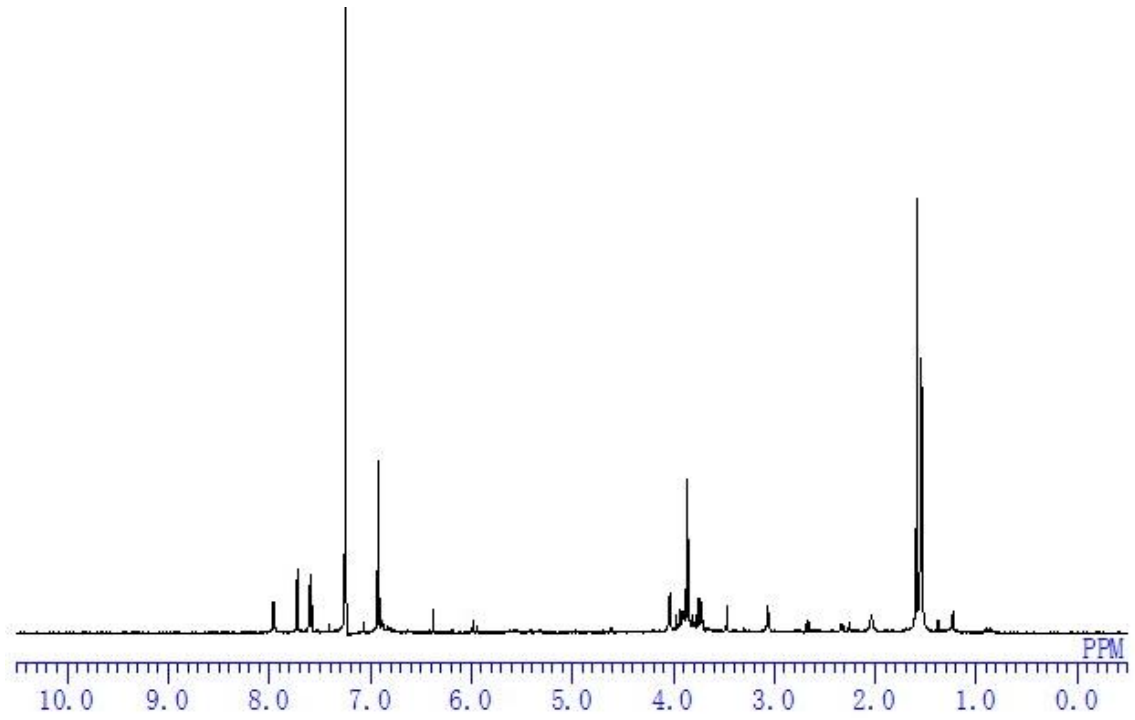

^{1}H NMR spectrum of **31** in $CDCl_3$

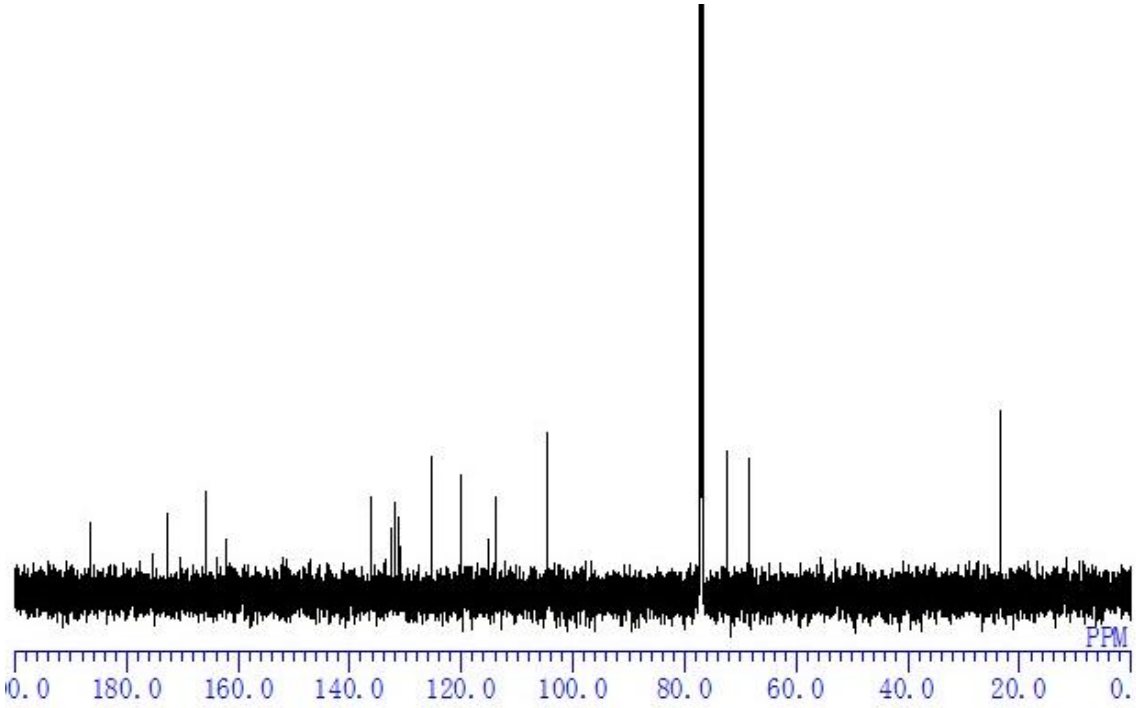

^{13}C NMR spectrum of **31** in $CDCl_3$

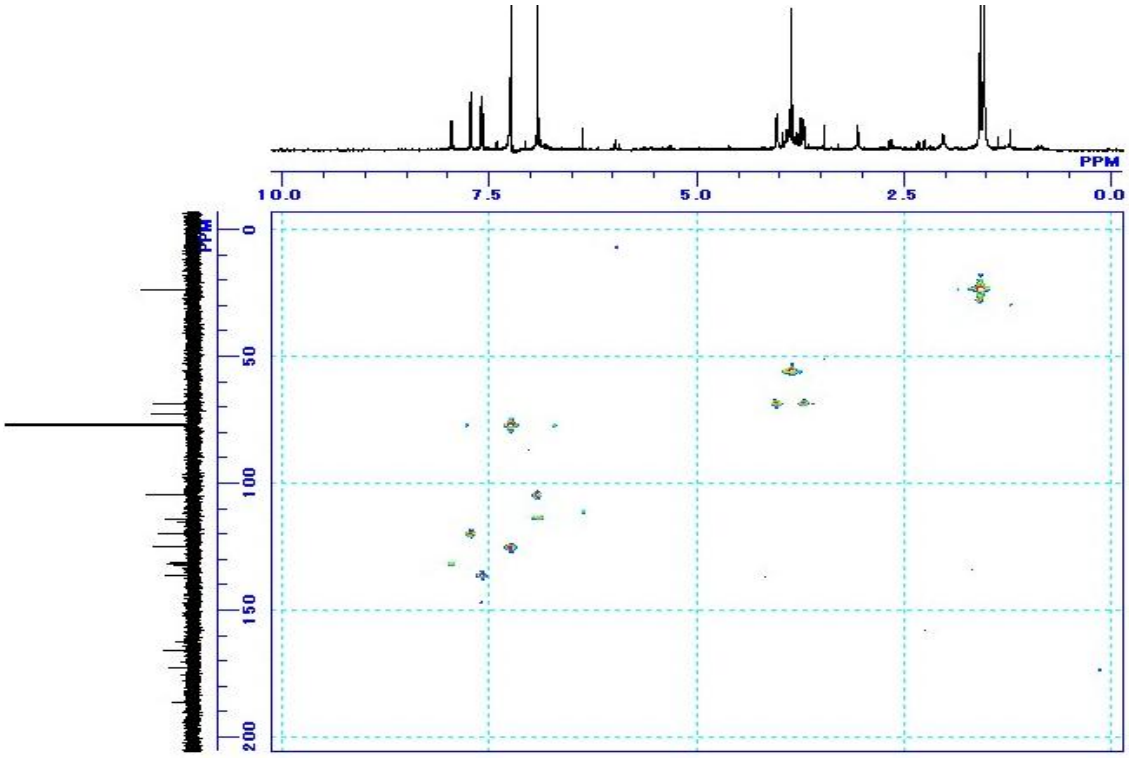

HMQC spectrum of **31** in $CDCl_3$

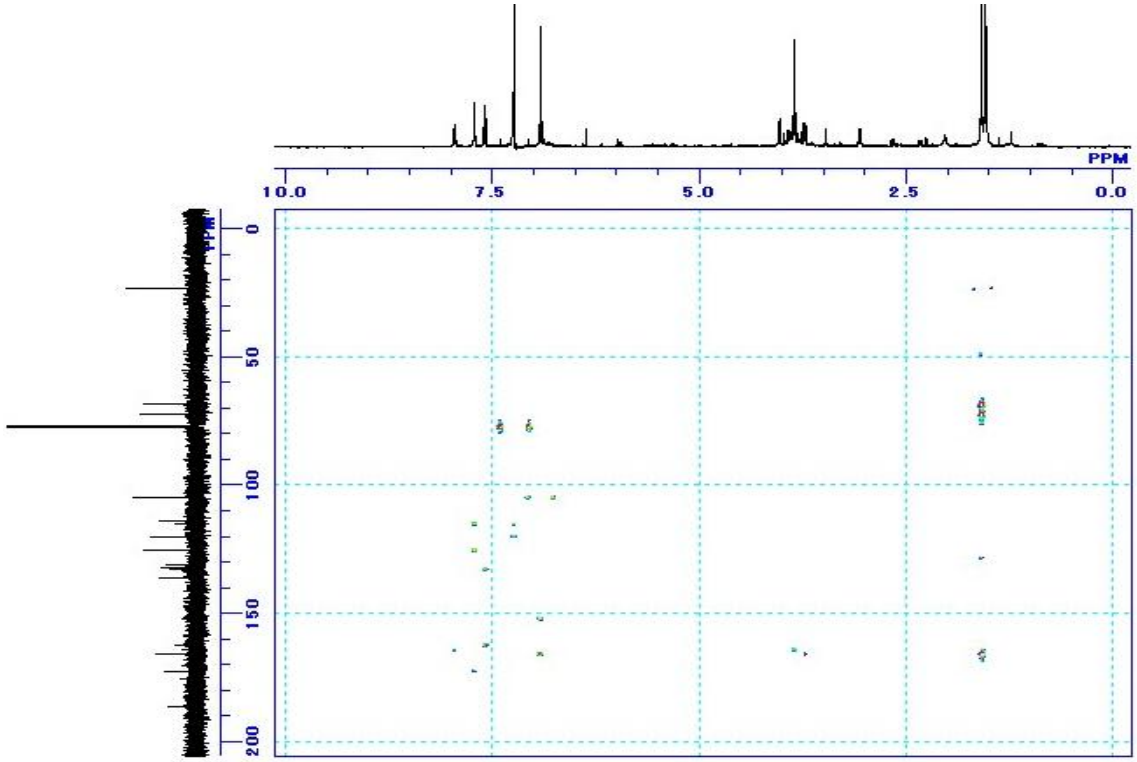

HMBC spectrum of **31** in $CDCl_3$

5 REFERENCES

1 Lubeck, W. *Healing Power of Pau D'Arco*. (Lotus Press, 1998).

2 Pinto, C. N. *et al.* Chemical reactivity studies with naphthoquinones from Tabebuia with anti-trypanosomal efficacy. *Arzneimittelforschung* **50**, 1120-1128 (2000).

3 Pereira, I. T. *et al.* Antiulcer effect of bark extract of Tabebuia avellanedae: activation of cell proliferation in gastric mucosa during the healing process. *Phytotherapy Research* **27**, 1067-1073 (2013).

4 Hashimoto, G. *Illustrated Cyclopedia of Brazilian Medicinal Plants*. (Aboc-sha, 1996).

5 Gómez Castellanos, J. R., Prieto, J. M. & Heinrich, M. Red Lapacho (*Tabebuia impetiginosa*)—A global ethnopharmacological commodity? *Journal of Ethnopharmacology* **121**, 1-13 (2009).

6 de Montmorency, A. Ancient South American Cancer Cure Blacked Our in America. *Spotlight, January* **5**, 10-11 (1981).

7 Jones, K. *Pau d'Arco: Immune power from the rain forest*. (Inner Traditions/Bear & Co, 1995).

8 Byeon, S. E. *et al. In vitro* and *in vivo* anti-inflammatory effects of taheebo, a water extract from the inner bark of *Tabebuia avellanedae*. *Journal of Ethnopharmacology* **119**, 145-152 (2008).

9 Jiménez-González, F. J., Veloza, L. A. & Sepúlveda-Arias, J. C. Anti-infectious activity in plants of the genus Tabebuia. *Universitas Scientiarum* **18**, 257 (2013).

10 Pardee, A. B., Li, Y. & Li, C. J. Cancer therapy with ß-lapachone. *Current Cancer Drug Targets* **2**, 227-242 (2002).

11 Ueda, S. *et al.* Production of anti-tumour-promoting furano-naphthoquinones in *Tabebuia avellanedae* cell cultures. *Phytochemistry* **36**, 323-325 (1994).

12 de Miranda, F. G., Vilar, J. C., Alves, I. A., Cavalcanti, S. C. & Antoniolli, Â. R. Antinociceptive and antiedematogenic properties and acute toxicity of Tabebuia avellanedae Lor. ex Griseb. inner bark aqueous extract. *BMC Pharmacology* **1**, 6 (2001).

13 Pereira, E. M. *et al.* Tabebuia avellanedae naphthoquinones: activity against methicillin-resistant staphylococcal strains, cytotoxic activity and in vivo dermal irritability analysis. *Annals of Clinical Microbiology and Antimicrobials* **5**, 5 (2006).

14 Riffel, A. *et al.* In vitro antimicrobial activity of a new series of 1, 4-naphthoquinones. *Brazilian Journal of Medical and Biological Research* **35**, 811-818 (2002).

15 Portillo, A., Vila, R., Freixa, B., Adzet, T. & Cañigueral, S. Antifungal activity of Paraguayan plants used in traditional medicine. *Journal of Ethnopharmacology* **76**, 93-98 (2001).

16 Freitas, A. E. *et al.* Antidepressant-like action of the ethanolic extract from *Tabebuia avellanedae* in mice: Evidence for the involvement of the monoaminergic system. *Progress in Neuro-Psychopharmacology and Biological Psychiatry* **34**, 335-343 (2010).

17 Freitas, A. E. *et al.* Antidepressant-like action of the bark ethanolic extract from *Tabebuia avellanedae* in the olfactory bulbectomized mice. *Journal of Ethnopharmacology* **145**, 737-745 (2013).

18 Twardowschy, A. *et al.* Antiulcerogenic activity of bark extract of *Tabebuia avellanedae*, Lorentz ex Griseb. *Journal of Ethnopharmacology* **118**, 455-459 (2008).

19 Kung, H. N. *et al.* Involvement of NO/cGMP signaling in the apoptotic and anti‐angiogenic effects of β‐lapachone on endothelial cells in vitro. *Journal of Cellular Physiology* **211**, 522-532 (2007).

20 Yamashita, M. *et al.* Synthesis and evaluation of bioactive naphthoquinones from the Brazilian medicinal plant, *Tabebuia avellanedae*. *Bioorganic & Medicinal Chemistry* **17**, 6286-6291 (2009).

21 Suo, M., Isao, H., Kato, H., Takano, F. & Ohta, T. Anti-inflammatory constituents from *Tabebuia avellanedae*. *Fitoterapia* **83**, 1484-1488 (2012).

22 de Santana, C. F., de Lima, O., d'Albuquerque, I., Lacerda, A. & Martins, D. Antitumoral and toxicological properties of extracts of bark and various wood components of Pau d'arco (Tabebuia avellanedae). *Revista do Instituto de Antibioticos, Universidade Federal de Pernambuco* **8**, 89 (1968).

23 Machado, T. *et al.* In vitro activity of Brazilian medicinal plants, naturally occurring naphthoquinones and their analogues, against methicillin-resistant *Staphylococcus aureus*. *International Journal of Antimicrobial Agents* **21**, 279-284 (2003).

24 Wagner, H., Kreher, B., Lotter, H., Hamburger, M. O. & Cordell, G. A. Structure Determination of New Isomeric Naphtho [2, 3‐b] furan‐4, 9‐diones from Tabebuia avellanedae by the selective‐INEPT technique. *Helvetica Chimica Acta* **72**, 659-667 (1989).

25 Alonso, J. R. *Tratado de Fitofármacosy Nutracéuticos*. (Corpus, 2004).

26 Rao, M. M. & Kingston, D. G. Plant anticancer agents. XII. Isolation and structure elucidation of new cytotoxic quinones from Tabebuia cassinoides. *Journal of Natural Products* **45**, 600-604 (1982).

27 Mukherjee, B., Telang, N. & Wong, G. Growth inhibition of estrogen receptor positive human breast cancer cells by Taheebo from the inner bark of Tabebuia avellandae tree. *International Journal of Molecular Medicine* **24**, 253 (2009).

28 Gosalvez, M., Garcia-Canero, R., Blanco, M. & Gurucharri-Lloyd, C. Effects and specificity of anticancer agents on the respiration and energy metabolism of tumor cells. *Cancer Treatment Reports* **60**, 1-8 (1976).

29 Linardi, M. d. C. F., De Oliveira, M. & Sampaio, M. Lapachol derivative active against mouse lymphocytic leukemia P-388. *Journal of Medicinal Chemistry* **18**, 1159-1161 (1975).

30 Subramanian, S., Ferreira, M. & Trsic, M. A structure-activity relationship study of lapachol and some derivatives of 1, 4-naphthoquinones against carcinosarcoma Walker 256. *Structural Chemistry* **9**, 47-57 (1998).

31 Block, J., Serpick, A., Miller, W. & Wiernik, P. Early clinical studies with lapachol (NSC-11905). *Cancer Chemotherapy Reports. Part 2* **4**, 27 (1974).

32 Choi, Y. H., Kang, H. S. & Yoo, M.-A. Suppression of Human Prostate Cancer Cell Growth by beta-Lapachone via Down-regulation of pRB Phosphorylation and Induction of Cdk Inhibitor p21W A F 1/ C I P 1. *Journal of Biochemistry and Molecular Biology* **36**, 223-229 (2003).

33 Lee, J. H., Cheong, J., Park, Y. M. & Choi, Y. H. Down-regulation of cyclooxygenase-2 and telomerase activity by β-lapachone in human prostate carcinoma cells. *Pharmacological Research* **51**, 553-560 (2005).

34 Lee, J. *et al.* beta-lapachone induces growth inhibition and apoptosis in bladder cancer cells by modulation of Bcl-2 family and activation of caspases. *Experimental oncology* **28**, 30-35 (2006).

35 Woo, H. J. *et al.* β-lapachone, a quinone isolated from Tabebuia avellanedae, induces apoptosis in HepG2 hepatoma cell line through induction of Bax and activation of caspase. *Journal of Medicinal Food* **9**, 161-168 (2006).

36 Queiroz, M. L. *et al.* Comparative studies of the effects of *Tabebuia avellanedae* bark extract and β-lapachone on the hematopoietic response of tumour-bearing mice. *Journal of Ethnopharmacology* **117**, 228-235 (2008).

37 Yamashita, M., Kaneko, M., Iida, A., Tokuda, H. & Nishimura, K. Stereoselective synthesis and cytotoxicity of a cancer chemopreventive naphthoquinone from *Tabebuia avellanedae*. *Bioorganic & Medicinal Chemistry Letters* **17**, 6417-6420 (2007).

38 Casinovi, C., MARINI, B. G., Limaog, D., Daliamaia, M. & D albuquerque, I. ON Quinones isolated from the wood of *Tabebuia avellanedae* lor. ex griseb. *Rendiconti-Istituto Superiore di Sanità* **26**, 5 (1963).

39 Awale, S. *et al.* Nitric oxide (NO) production inhibitory constituents of Tabebuia avellanedae from Brazil. *Chemical and Pharmaceutical Bulletin* **53**, 710-713 (2005).

40 Böhler, T. *et al. Tabebuia avellanedae* extracts inhibit IL-2-independent T-lymphocyte activation and proliferation. *Transplant Immunology* **18**, 319-323 (2008).

41 Oga, S. & Sekino, T. Toxicity and antiinflammatory activity of Tabebuia avellanedae extracts. *Revista de farmácia e bioquímica da Universidade de São Paulo* **7**, 47-53 (1969).

42 Koyama, J., Morita, I., Tagahara, K. & Hirai, K.-I. Cyclopentene dialdehydes from *Tabebuia impetiginosa*. *Phytochemistry* **53**, 869-872 (2000).

43 Garcez, F. R., Garcez, W. S., Mahmoud, T. S., Figueiredo, P. d. O. & Resende, U. M. New constituents from the trunk bark of Tabebuia heptaphylla. *Química Nova* **30**, 1887-1891 (2007).

44 Nakano, K., Maruyama, K., Murakami, K., Takaishi, Y. & Tomimatsu, T. Iridoids from *Tabebuia avellanedae*. *Phytochemistry* **32**, 371-373 (1993).

45 Warashina, T., Nagatani, Y. & Noro, T. Constituents from the bark of Tabebuia impetiginosa. *Chemical and Pharmaceutical Bulletin* **54**, 14-20 (2006).

46 Mori, K. & Okada, K. Synthesis of mevalonolactone (hiochic acid lactone) employing asymmetric epoxidation as the key-step. *Tetrahedron* **41**, 557-559 (1985).

47 Williams, R. B. *et al.* Two new cytotoxic naphthoquinones from Mendoncia cowanii from the rainforest of Madagascar. *Planta Medica* **72**, 564 (2006).

48 Katayama, T., Davin, L. B., Chu, A. & Lewis, N. G. Novel benzylic ether reductions in lignan biogenesis in *Forsythia intermedia*. *Phytochemistry* **33**, 581-591 (1993).

49 Falah, S., Katayama, T. & Suzuki, T. Chemical constituents from Gmelina arborea bark and their antioxidant activity. *Journal of Wood Science* **54**, 483-489 (2008).

50 González, A. G., Estévez-Reyes, R. & Mato, C. Salicifoliol, a new furolactone-type lignan from Bupleurum salicifolium. *Journal of Natural Products* **52**, 1139-1142 (1989).

51 Gao, G. *et al.* Minor compounds from the stem bark of Chinese mangrove associate Catunaregam spinosa. *Die Pharmazie-An International Journal of Pharmaceutical Sciences* **63**, 542-544 (2008).

52 Braga de Oliveira, A., Raslan, D. S., G de Oliveira, G. & Maia, J. G. S. Lignans and naphthoquinones from *Tabebuia incana*. *Phytochemistry* **34**, 1409-1412 (1993).

53 Schwartz, G. K. & Shah, M. A. Targeting the cell cycle: a new approach to cancer therapy. *Journal of Clinical Oncology* **23**, 9408-9421 (2005).

54 Foster, I. Cancer: A cell cycle defect. *Radiography* **14**, 144-149 (2008).
55 Kawabe, T. G2 checkpoint abrogators as anticancer drugs. *Molecular Cancer Therapeutics* **3**, 513-519 (2004).
56 Zhang, M. & Yang, H. Negative growth regulators of the cell cycle machinery and cancer. *Pathophysiology* **16**, 305-309 (2009).
57 Johnson, D. & Walker, C. Cyclins and cell cycle checkpoints. *Annual Review of Pharmacology and Toxicology* **39**, 295-312 (1999).
58 Jacobson, M. D., Weil, M. & Raff, M. C. Programmed cell death in animal development. *Cell* **88**, 347-354 (1997).
59 Maximov, G. & Maximov, K. The role of p53 tumor-suppressor protein in apoptosis and cancerogenesis. *Biotechnology and Biotechnological Equipment* **22**, 664 (2008).
60 Adams, J. M. & Cory, S. The Bcl-2 protein family: arbiters of cell survival. *Science* **281**, 1322-1326 (1998).
61 Hemann, M. & Lowe, S. The p53–Bcl-2 connection. *Cell Death & Differentiation* **13**, 1256-1259 (2006).
62 Hengartner, M. O. The biochemistry of apoptosis. *Nature* **407**, 770-776 (2000).
63 Gross, A., McDonnell, J. M. & Korsmeyer, S. J. BCL-2 family members and the mitochondria in apoptosis. *Genes & Development* **13**, 1899-1911 (1999).
64 Ghobrial, I. M., Witzig, T. E. & Adjei, A. A. Targeting apoptosis pathways in cancer therapy. *CA: A Cancer Journal for Clinicians* **55**, 178-194 (2005).
65 Vaux, D. L. & Korsmeyer, S. J. Cell death in development. *Cell* **96**, 245-254 (1999).
66 Oeckinghaus, A., Hayden, M. S. & Ghosh, S. Crosstalk in NF-κ B signaling pathways. *Nature Immunology* **12**, 695-708 (2011).
67 Shuai, K. & Liu, B. Regulation of JAK–STAT signalling in the immune system. *Nature Reviews Immunology* **3**, 900-911 (2003).
68 Karin, M. & Greten, F. R. NF-κB: linking inflammation and immunity to cancer development and progression. *Nature Reviews Immunology* **5**, 749-759 (2005).
69 Ito, K., Caramori, G. & Adcock, I. M. Therapeutic potential of phosphatidylinositol 3-kinase inhibitors in inflammatory respiratory disease. *Journal of Pharmacology and Experimental Therapeutics* **321**, 1-8 (2007).
70 Wellen, K. E. & Hotamisligil, G. S. Inflammation, stress, and diabetes. *Journal of Clinical Investigation* **115**, 1111-1119 (2005).
71 Yu, H., Pardoll, D. & Jove, R. STATs in cancer inflammation and immunity: a leading role for STAT3. *Nature Reviews Cancer* **9**, 798-809 (2009).
72 Xie, Q. W., Whisnant, R. & Nathan, C. Promoter of the mouse gene encoding calcium-independent nitric oxide synthase confers inducibility by interferon gamma and bacterial lipopolysaccharide. *The Journal of Experimental Medicine* **177**, 1779-1784 (1993).
73 Zhang, G. & Ghosh, S. Molecular mechanisms of NF-κB activation induced by bacterial lipopolysaccharide through Toll-like receptors. *Journal of Endotoxin Research* **6**, 453-457 (2000).
74 Guha, M. & Mackman, N. LPS induction of gene expression in human monocytes. *Cellular Signalling* **13**, 85-94 (2001).
75 Hald, A., Rønø, B., Lund, L. R. & Egerod, K. L. LPS counter regulates RNA expression of extracellular proteases and their inhibitors in murine macrophages. *Mediators of Inflammation*

2012 (2012).

76 Pan, C.-H., Kim, E. S., Jung, S. H., Nho, C. W. & Lee, J. K. Tectorigenin inhibits IFN-γ/LPS-induced inflammatory responses in murine macrophage RAW 264.7 cells. *Archives of Pharmacal Research* **31**, 1447-1456 (2008).

77 Laskin, D. L. & Pendino, K. J. Macrophages and inflammatory mediators in tissue injury. *Annual Review of Pharmacology and Toxicology* **35**, 655-677 (1995).

78 Minghetti, L. & Pocchiari, M. Cyclooxygenase‐2, Prostaglandin E_2, and Microglial Activation in Prion Diseases. *International Review of Neurobiology* **82**, 265-275 (2007).

79 Tsatsanis, C., Androulidaki, A., Venihaki, M. & Margioris, A. N. Signalling networks regulating cyclooxygenase-2. *The International Journal of Biochemistry & Cell Biology* **38**, 1654-1661 (2006).

80 Hofseth, L. J. Nitric oxide as a target of complementary and alternative medicines to prevent and treat inflammation and cancer. *Cancer Letters* **268**, 10-30 (2008).

81 Korhonen, R., Lahti, A., Kankaanranta, H. & Moilanen, E. Nitric oxide production and signaling in inflammation. *Current Drug Targets-Inflammation & Allergy* **4**, 471-479 (2005).

82 Zamora, R., Vodovotz, Y. & Billiar, T. R. Inducible nitric oxide synthase and inflammatory diseases. *Molecular Medicine* **6**, 347 (2000).

83 Shin, J.-H. *et al.* Short-term heating reduces the anti-inflammatory effects of fresh raw garlic extracts on the LPS-induced production of NO and pro-inflammatory cytokines by downregulating allicin activity in RAW 264.7 macrophages. *Food and Chemical Toxicology* **58**, 545-551 (2013).

84 Guadagni, F. *et al.* TNF/VEGF cross-talk in chronic inflammation-related cancer initiation and progression: an early target in anticancer therapeutic strategy. *In Vivo* **21**, 147-161 (2007).

85 Parameswaran, N. & Patial, S. Tumor necrosis factor-α signaling in macrophages. *Critical Reviews™ in Eukaryotic Gene Expression* **20** (2010).

86 Mackaness, G. The mechanism of macrophage activation. *Infectious Agents and Host Reactions. Stuart Mudd, editor. WB Saunders Company, Philadelphia, Pa* **62** (1970).